BLANK PAGES
IN THIS
DOCUMENT
WERE NOT
FILMED

Bulletin No. 33

SHOCK, VIBRATION and ASSOCIATED ENVIRONMENTS

PART IV

MARCH 1964

Office of
The Director of Defense
Research and Engineering

Washington, D.C.

Published by
U. S. Naval Research Laboratory
Washington, D. C.

Bulletin No. 33

SHOCK, VIBRATION and ASSOCIATED ENVIRONMENTS

PART IV.

MARCH 1964

Office of
The Director of Defense
Research and Engineering

The 33rd Symposium on Shock, Vibration and Associated Environments was held in Washington, D. C. on 3-5 December 1963. The Navy was host.

Washington, D.C.

DISTRIBUTION

Aberdeen Proving Ground, Md.
- Att: Ballistic Research Lab. 1
- Att: Development & Proof Services 1
- Att: Physical Test Lab. 1

Advisory Group on Electron Tubes
- Att: Secretary 1

Aeronautical Standards Group, DC 1

Aeronautical Systems Division, WPAFB
- Att: FDFE, C. A. Golueke 1
- Att: FDD, H. A. Magrath 1
- Att: ASNDSV, R. F. Wilkus 1
- Att: ASTEVS, C. W. Gerhardt 1
- Att: AFML(MAMD), J. R. Henderson 1

Air Defense Command, Ent AFB
- Att: Deputy for Civil Engineering 1
- Att: ADIRP 1

Air Proving Ground Center, Elgin AFB
- Att: PGTRI, Technical Library 1

Air Force Flight Test Center, Edwards AFB
- Att: FTRLC, A. J. Davies 1

Air Force Headquarters, DC
- Att: AFCIN-3K2 1
- Att: AFDRD-GW 1
- Att: Opers. Analysis Off., Off VCOS, Library 2

Air Force Logistics Command, WPAFB
- Att: MCTEP, G. P. Civille 1

Air Force Missile Development Center, Holloman AFB
- Att: MDSGL-2, Mr. H. Dunbar 3

Air Force Missile Test Center, Patrick AFB
- Att: Chief, Tech. Systems Lab. 2

Air Force Office of Scientific Research, DC
- Att: Library 1

Air Force Regional Civil Engineer
- Att: North Atlantic Region, AFRCE-NA-A 1
- Att: South Atlantic Region, AFRCE-SA-E 1

Air Force Systems Command, Andrews AFB
- Att: Technical Library 2

Air Force Weapons Lab., Kirtland AFB
- Att: Development Test Division 1
- Att: WLRS, Dr. W. E. Fisher 1
- Att: SWOI 631-276 1

Army Air Defense Center, Ft. Bliss
- Att: Technical Library 1

Army Chemical Center, Md.
- Att: Library 1

Army Electronics R&D Lab., Ft. Monmouth
- Att: SELRA/SL-ADT 1
- Att: SELRA/SL-PEE 1
- Att: SELRA/SL-PRT 1
- Att: SELRA/SL-G 1
- Att: SELRA/SL-GTF 1
- Att: J. J. Oliveri 1

Army Engineer District, NY
- Att: NANGD 1

Army Engineer R&D Labs., Ft. Belvoir
- Att: Director of Research 1
- Att: Package Development Br. 1
- Att: Mr. A. Carolla 1
- Att: Chief, Spec. Proj. Branch 4

Army Engineer Waterways Exp. Sta., Vicksburg
- Att: Mr. J. M. Strange 1

Army Erie Ordnance Depot, Ohio
- Att: Chief Materiel Testing Div. 1

Army Materiel Command, DC
- Att: AMCRD-RS-CM 1

Army Materiel Command, Redstone Arsenal
- Att: Technical Library 4

Army Missile Command, Redstone Arsenal
- Att: AMSMI-RB 1
- Att: AMSMI-RG 1
- Att: AMSMI-RL 1
- Att: AMSMI-RS 1
- Att: AMSMI-RT 1
- Att: AMSMI-RTR, J. M. Taylor 1

Army Mobility Command, Centerline
- Att: Otto Renius 1

Army, Office Chief of Engineers, DC
- Att: ENGMC-EM 2

Army, Office Quartermaster General, DC
- Att: Military Planning Division 1

Army, Office Chief of Res. & Dev., Arlington
- Att: A. L. Tarr 1

Army, Office Chief Signal Officer, DC
- Att: R&D Division 1

Army, Office Chief of Transportation
- Att: Dir of Transportation Engrg. 1

Army Ordnance Ammunition Command, Joliet
- Att: ORDLY-T 1
- Att: NNSC/A 1

Army Ordnance Arsenal, Detroit, Mich.
Att: Tech. Library 2
Att: Engrg. Standards Unit 1
Att: Engrg. Design Div. ORDMX-N 1

Army Security Agency, Md. 1

Army Transportation Engrg. Agency, Ft. Eustis
Att: Library 1
Att: L. J. Pursifull 1

Arnold Engineering Dev. Ctr., Tenn.
Att: AEOIM 1

Atomic Energy Commission, Oak Ridge 6

Atomic Energy Commission, DC
Att: Library 1
Att: Div. of Reactor Development, Tech. Evaluation Branch (Army Reactors) 1

Aviation Supply Office, Phila.
Att: TEP-1 1

Ballistic Systems Div., AFSC, Norton AFB
Att: Technical Data Division 3

Boston Naval Shipyard
Att: Library 1

Bureau of Medicine & Surgery, DC
Att: Research Division 1

Bureau of Naval Weapons, DC
Att: DLI-3 2
Att: FWAA, C. H. Barr 1
Att: PREN-5 5
Att: RRMA 1
Att: RAAE-2 1
Att: RM-3 2
Att: RM-2 1
Att: RSSH 2
Att: FWAE 1
Att: RREN-8 1

Bureau of Naval Weapons Rep., E. Hartford 2

Bureau of Naval Weapons Rep., Pomona
Att: Chief Engineer 1
Att: Metrology Dept., Code 60 1

Bureau of Naval Weapons Rep., Sunnyvale 1

Bureau of Ships, DC
Att: Code 423 20

Bureau of Supplies & Accounts, DC
Att: Library 1

Bureau of Yards & Docks, DC
Att: Code D-440 1
Att: Code D-220 1
Att: Code D-220 (Unclassified Parts) 6

Coast Guard Headquarters, DC 1

David Taylor Model Basin, Portsmouth
Att: Code 281A 1

David Taylor Model Basin, DC
Att: Library 3
Att: Harry Rich 1
Att: Contract Research Administrator, 513 1
Att: J. A. Luistra, Code 591L 1

Dayton Air Force Depot, Gentile AFB
Att: MDMG 1

Defense Atomic Support Agency, DC
Att: Technical Director 1
Att: Weapons Development Div. 1
Att: John G. Lewis 1

Defense Atomic Support Agency, Livermore
Att: Administrative Officer 1

Defense Documentation Center, Alexandria 20

District Public Works Office, 14th ND 1

Electronic Systems Div., L. G. Hanscom Field
Att: Library 1

Electronics Supply Office, Great Lakes 1

Federal Aviation Agency, DC
Att: Emergency Readiness Division Off. of Plans & Requirements 2

Frankfort Arsenal, Phila.
Att: Library Branch, CC 0270/40 1
Att: David Askin, CC 1730-230 1

Harry Diamond Laboratories, DC
Att: B. M. Horton 1
Att: Chief, Lab. 700 1
Att: Branch 320, Miss Johnson 1
Att: Chief, Branch 850 1
Att: Ben Reznek 1

Inspector of Naval Material, San Francisco 1

Library of Congress, DC
Att: Exchange & Gift Div (Unclassified Only) 1

Long Beach Naval Shipyard, Calif.
Att: Code 240 1

Los Angeles Air Procurement District, Calif.
Att: Quality Control Division 1

Los Angeles Ordnance District, USA, Calif.
Att: ORDEV 1

Mare Island Naval Shipyard, Calif.
Att: Library 1

Marine Corps Equipment Board, Quantico 2

Marine Corps Headquarters, DC
Att: Res & Dev Section 1
Att: Code A04E 1

Maxwell Air Force Base, Ala.
Att: Air University Library 1

Mobile Air Materiel Area, Brookley AFB
Att: MONRPPR 1
Att: MONE 1

NASA, Ames Research Ctr., Moffett Field
Att: S. J. DeFrance, Dir. 1

NASA, High Speed Flight Sta., Edwards AFB 1

NASA, Goddard Space Flight Ctr., Greenbelt
Att: J. C. New, Code 320 1
Att: G. Hinshelwood, Code 623.3 1
Att: Elias Klein 1
Att: K. M. Carr, Code 321.2 1
Att: F. Lindner, Code 321.2 1

NASA, Langley Research Ctr., Va.
Att: Library 2
Att: S. A. Clevenson, Dynamic Loads Div. 1

NASA, Lewis Flight Propulsion Lab., Cleveland
Att: Library 1

NASA, Manned Spacecraft Center, Houston
Att: G. A. Watts 1

NASA, Marshall Space Flight Center, Huntsville
Att: Mr. R. M. Hunt, M-P&VE-S 1
Att: Mr. James Farrow, M-P&VE-ST 1
Att: AMSMI-RBLD 1

NASA, Scientific & Tech. Info. Facility, Bethesda
Att: S-AK/DL 1

National Bureau of Standards, DC
Att: B. L. Wilson 1
Att: S. Edelman, Mech. Div. 1

National Security Agency, DC
Att: Engineering 1

Naval Air Development Center, Johnsville
Att: E. R. Mullen 1
Att: Aeronautical Instruments Lab. 1
Att: NADC Library 2

Naval Air Engineering Center, Phila.
Att: Library 1

Naval Air Station, Patuxent River
Att: Weapons Systems Test (E. B. Hamblett) 2

Naval Air Test Center, Patuxent River
Att: Electronics Test Div. 1
Att: VTOL/STOL Br. 1

Naval Ammunition Depot, Crane
Att: Code 3540 1
Att: Code 3400 1

Naval Ammunition Depot, Earle
Att: Chief Engr., Materials Handling Lab. 1

Naval Ammunition Depot, Oahu
Att: Weapons Tech. Library 1

Naval Applied Science Laboratory, Brooklyn
Att: Library 1

Naval Attache, Navy 100
Att: Logistics Division 1

Naval Civil Engineering Lab., Pt. Hueneme
Att: Library 2

Naval Construction Battalion Ctr., Pt. Hueneme
Att: OIC, USN School, Civil Engineer Corps Officers 1

Naval Medical Field Research Lab., Camp Lejeune
Att: Commanding Officer 1

Naval Mine Engrg. Facility, Yorktown
Att: Library 1

Naval Missile Center, Pt. Mugu
Att: Library, N-03022 1
Att: Environment Div., N314 2

Naval Operations, Office Chief of, DC
Att: Op 31 1
Att: Op 34 1
Att: Op 75 1
Att: Op 07T6, T. Soo-Hoo 1
Att: Op 725 1

Naval Ordnance Lab., Corona
Att: Quality Eval. Lab 1
Att: Code 56, Sys. Eval. Div. 1

Naval Ordnance Lab., White Oak
Att: Technical Director 1
Att: Library 3
Att: Environmental Simulation Div. 6
Att: G. Stathopoulos 1

Naval Ordnance Test Sta., China Lake
Att: Technical Library 1
Att: Code 3023 1
Att: Code 3073 1
Att: Code 4062 1

Naval Ordnance Test Sta., Pasadena
Att: P8087 3
Att: P8092 1
Att: P8073 1
Att: P80962 1

Naval Postgraduate School, Monterey
Att: Library 1

Naval Propellant Plant, Indian Head
Att: Library 1

Naval Radiological Def. Lab., San Fran.
Att: Library 1

Naval Research Laboratory, DC
Att: Code 6250 1
Att: Code 6260 1
Att: Code 6201 1
Att: Code 4021 2

Naval Security Engrg. Facility, DC
Att: R&D Branch 1

Naval Supply R&D Facility, Bayonne
Att: Library 1

Naval Torpedo Station, Keyport
Att: QEL, Technical Library 1

Naval Training Device Ctr., NY
Att: Library Branch 1
Att: Code 4211 1

Naval Underwater Ord. Sta., Newport
Att: Tech. Documents Library 1

Naval Weapons Evaluation Facility, Albuquerque
Att: Library, Code 42 1

Naval Weapons Laboratory, Dahlgren
Att: Technical Library 1

Navy Central Torpedo Office, Newport
Att: Quality Evaluation Lab. 1

Navy Electronics Lab., San Diego
Att: Library 1

Navy Marine Engineering Lab., Annapolis
Att: Code 705 1

Navy Mine Defense Lab., Panama City
Att: Library 1

Navy ROTC & Admin. Unit, MIT, Cambridge 1

Navy Underwater Sound Lab., New London
Att: Technical Director 1
Att: J. G. Powell, Engrg & Eval. Div. 1

Navy Underwater Sound Ref. Lab., Orlando
Att: J. M. Taylor, Code 120 1

Norfolk Naval Shipyard, Va.
Att: Design Superintendent 1

Norton AFB, Calif.
Att: AFIMS-2-A 1

Off. Director of Defense R&E, DC
Att: Technical Library 3
Att: Mr. Melvin Bell 1
Att: Mr. Walter M. Carlson 1

Off. of Naval Material, DC 1

Off. Naval Research, DC
Att: Code 439 6
Att: Code 104 1

Off. Naval Research Branch Office, Boston 1

Off. Naval Research Branch Office, Pasadena 1

Off. Naval Research Branch Office, San Fran. 1

Ogden Air Materiel Area, Hill AFB
Att: Service Engr. Dept., OONEW 1

Oklahoma City Air Materiel Area
Att: Engineering Division 1

Pearl Harbor Naval Shipyard
Att: Code 264 1

Philadelphia Naval Shipyard
Att: Ship Design Section 1
Att: Naval Boiler & Turbine Lab. 1

Picatinny Arsenal, Dover
Att: Library SMUPA-VA6 1
Att: SMUPA-VP7, R. G. Leonardi 1
Att: SMUPA-T, R. J. Klem 1
Att: SMUPA-D, E. Newstead 1
Att: SMUPA-VP3, A. H. Landrock 1

Portsmouth Naval Shipyard
Att: Code 246 1
Att: E. C. Taylor 1

Puget Sound Naval Shipyard
Att: Code 251 1
Att: Material Labs. 1
Att: K. G. Johnson, Code 242 1

Quartermaster Food & Container Inst., Chicago
Att: Dir., Container Lab. 1
Att: Technical Library 1

Quartermaster R&E Airborne Test Activity, Yuma
Att: QMATA 1

Quartermaster Res. & Engrg. Ctr., Natick
Att: Technical Library 2
Att: Dr. W. B. Brierly 1

Randolph AFB, Texas
Att: USAF School of Aviation Medicine 1

Rome Air Development Center, NY
Att: Dana Benson, RASSM 1

Rossford Ordnance Depot, Ohio
Att: Ordnance Packaging Agency 1

San Francisco Naval Shipyard
Att: Design Division 1

Savanna Ordnance Depot, Illinois
Att: OASMS 1

Sheppard AFB, Texas
Att: 3750th Tech. School (TC) 1

6511 Test Group (Parachute), El Centro
Att: E. C. Myers, Tech. Dir. 1

6570 Aerospace Med. Res. Labs., WPAFB
Att: MRMAE 1

Special Projects, USN, DC
Att: SP Tech. Library 1

Springfield Armory, Mass.
Att: Library 2

Strategic Air Command, Offutt AFB
Att: Operations Analysis Office 1

Supervisor of Shipbuilding, USN, Camden, NJ
Att: Code 299 2

Watertown Arsenal, Mass.
Att: R. Beeuwkes, Jr., Ord. Matls, Res. Off. 2
Att: Technical Information Sec. 1
Att: ORDBE-LE 1

Watervliet Arsenal, NY
Att: ORDBF-RR 2

White Sands Missile Range, NM
Att: Electro-Mechanical Div. 1
Att: ORDBS-TS-TIB 3

ERRATUM

The following correction should be noted to the paper "The Shock Environment of Submarine Pressure-Hull Penetrations Under Explosion Attack," by E. W. Palmer appearing in the 33rd Bulletin, Part I. Equation (7) should read:

$$\frac{\dot{u}}{V_m} = \frac{\cos \omega_{eo} t}{\pi} + \frac{1}{4}(1 + \cos \omega_{el} t) \cos \theta + \sum_{n=2,4,6\cdots}^{\infty} \frac{2(-1)^{n/2}}{\pi(1-n^4)} (n^2 \cos \omega_{fn} t + \cos \omega_{en} t) \cos n\theta.$$

CONTENTS

PART IV

PAPERS APPEARING IN PART I
Part I - Confidential
(Titles Unclassified)

PAPERS APPEARING IN PART III

Instrumentation

Shock Testing

Vibration Testing

Combined Temperature-Vibration Tests

Section 1
MECHANICAL IMPEDANCE

THE APPLICATION OF IMPEDANCE TECHNIQUES TO A SHIPBOARD VIBRATION ABSORBER*

R. M. Mains
General Electric Company
Schenectady, New York

This paper compares the results of vibration absorption achieved in a full-size test with the absorption predicted by impedance methods. Criteria for placement and effectiveness of the absorber are developed, and the measured results are compared to the calculated results.

INTRODUCTION

In the design, construction, and measurement of the effectiveness of a shipboard vibration absorber, the following steps were necessary:

1. To devise a mathematical model for the turbine-generator-support complex which would produce calculated impedances similar to available measured data.

2. To devise criteria for the selection of the best place to locate a passive vibration absorber, and for predicting its effectiveness.

3. To apply these criteria to the model, design a vibration absorber, and predict its effectiveness.

4. To build and apply the vibration absorber to the actual structure and compare its measured effectiveness with that predicted.

The various hardware components in the problem were individually complex enough to tax the capacity of the 32,000-word computer available, so it was necessary to treat each component separately and then put them together by impedance techniques. Figure 1 shows the components used and their relative size.

The displacement mobilities, $x(i\omega)/f(i\omega)$, were calculated since a program for doing this (rather than impedance) was already available. Successive applications of the series addition principal for mobilities then gave the mobilities at each interface, B through D with E assumed zero.

The criterion devised for the best location for a vibration absorber was: the interface for which the sum of the mobilities looking each way from the interface is greatest is the optimum location. The attenuation factor for the absorber was: the sum of the impedances looking both ways from the interface divided by this sum plus the impedance of the absorber. In other words, the recipe was: find the most mobile interface and attach the largest impedance absorber possible at that interface.

Since the absorber impedance for a single-degree-of-freedom mass at resonance was the product of absorber mass and Q (the magnification factor at resonance), a large mass-high Q absorber was designed for resonance at the frequency for which attenuation was desired. Four 750-pound, 830-Q, 60-cycle absorbers were built and applied at the corners of the subbase near the rubber mounts. The effectiveness criterion mentioned above predicted about 25-db attenuation at 60 cycles, and attenuations of this

*The work reported herein was performed under Navy Contract NObs-86829, Project Serial No. SF-013-11-05, Task 3680.

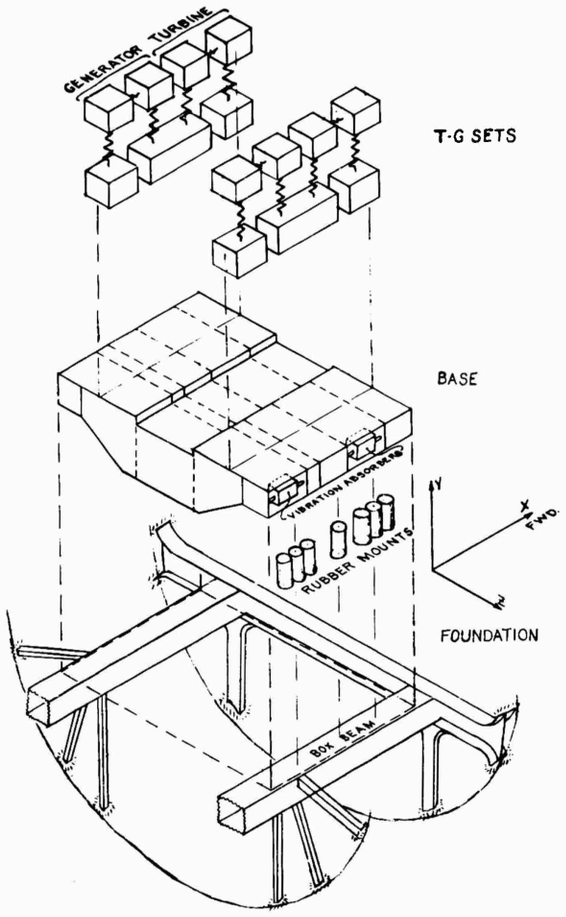

Fig. 1 - Exploded view of assembly

magnitude were measured. As might have been expected, measurements showed that while vibration at the absorbers was reduced appreciably, vibration at other parts of the system between the absorbers and the rotors increased appreciably.

STATEMENT OF PROBLEM

It was desired to determine: (1) where in the turbine-generator-support complex illustrated in Fig. 2 would be the best location for a passive vibration absorber, (2) what the optimum characteristics of the passive absorber should be, (3) to design and apply an absorber to the system, and (4) to compare measured effectiveness of the absorber with that predicted by calculation. To fulfill these desires, it was necessary first to devise a mathematical description of the system, and then devise some criteria for optimum location and absorber characteristics compatible with the mathematical description of the system.

DEVELOPMENT OF MATHEMATICAL MODEL

Because of the nature of the problem, the complexity of some parts of the system, and because of the limitations of a 32,000-word storage computer, it was decided to describe the system in terms of the mobility of a series of "black boxes." Figure 3 shows the black box diagram used for the system. The black box between terminals A and B was the turbine-generator, shown schematically in Fig. 4. The

black box between terminals B and C was the sub-base, for which the mass-spring representation is shown in Fig. 5. The sub-base black box was in turn supported by the rubber mounts, which were in three sets along each side of the sub-base, and each mount was represented by a single spring-mass system as shown in Fig. 6. The next support elements were the two box beams, one of which is shown in Fig. 7. In keeping with Navy practice, the hull and bulkheads were taken as fixed.

The computer program available for compiling stiffness matrices for the black boxes was limited (by machine storage) to 25 masses, 50 springs, 6-degrees-of-freedom per mass.[1] This would be enough to compile the stiffness for each separate subsystem, but the resulting matrices for the box beam and the sub-base would be too large to carry the problem further. Fortunately, the two turbine-generators were identical and symmetrically disposed with regard to the X-Y plane. Also the sub-base and

[1]For a discussion of the principles involved in stiffness compilation and some practical problems, see R. M. Mains, "The Practical Problems of Generating Large Stiffness or Flexibility Matrices," ASME Mach. Des. paper, 63WA268.

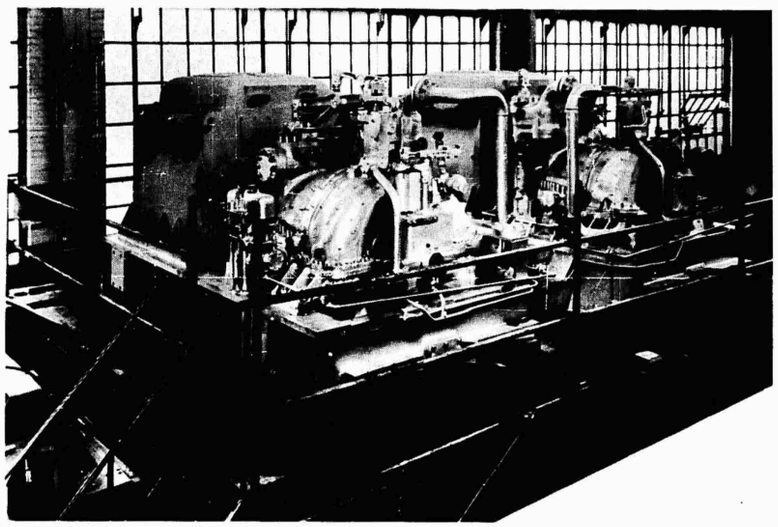

Fig. 2 - Turbine-generator-support complex ready for test (FTD-673, 2000 kw, 3600 rpm, SS(B)N 616)

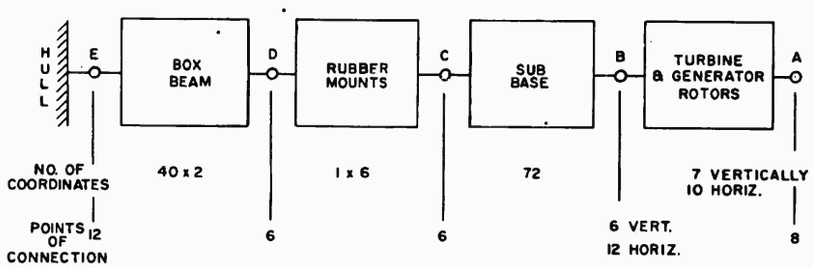

Fig. 3 - System "black box" diagram

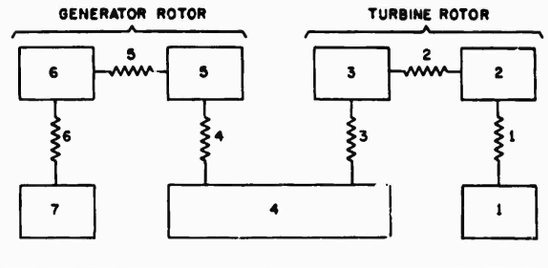

$$M = \begin{bmatrix} 1 & 2 & 3 & 4 & 5 & 6 & 7 \\ 21.2 & & & & & & \\ & 5.31 & & & & & \\ & & 5.31 & & & & \\ & & & 41.2 & & & \\ & & & & 3.5 & & \\ & & & & & 3.5 & \\ & & & & & & 20.0 \end{bmatrix} \text{ LB. SEC.}^2/\text{IN.}$$

$$K = 10^6 \times \begin{bmatrix} 1 & 2 & 3 & 4 & 5 & 6 & 7 \\ +0.588 & -0.588 & & & & & \\ -0.588 & +1.46 & -0.872 & & & & \\ & -0.872 & +1.46 & -0.588 & & & \\ & & -0.588 & +1.296 & -0.708 & & \\ & & & -0.708 & +1.55 & -0.842 & \\ & & & & -0.842 & +1.55 & -0.708 \\ & & & & & -0.708 & +0.708 \end{bmatrix} \text{ LB./IN.}$$

Fig. 4 - Mass-spring representation of turbine-generator (vertical)

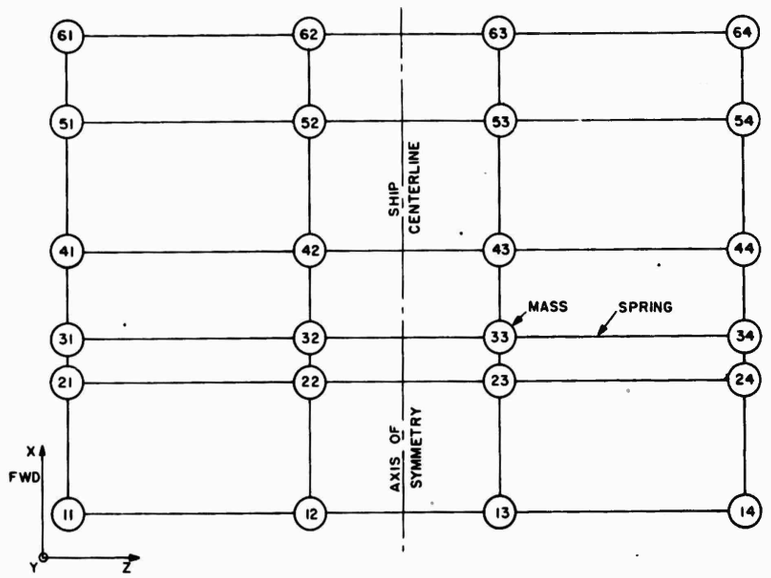

Fig. 5 - Mass-spring diagram of sub-base

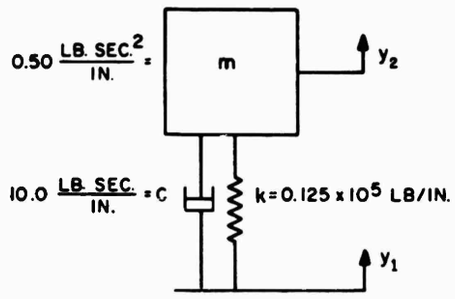

Fig. 6 - Mass-spring diagram for rubber mounts

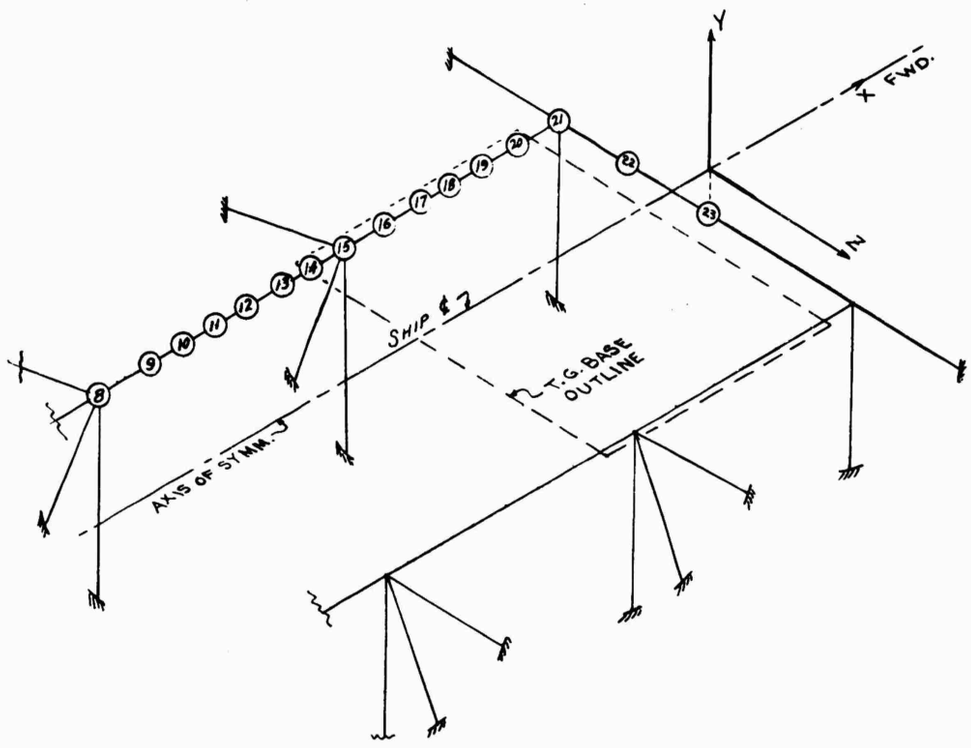

Fig. 7 - Mass-spring diagram for box beam

box beams were symmetric about the X-Y plane. By taking advantage of this symmetry and dealing with the vertical direction and the athwartship direction separately, it was possible to reduce the size of the matrices to the 40×40 limit of the computer program available for calculating mobilities.

CALCULATION OF MOBILITIES

The various stiffness and mass matrices were compiled and are on file, but their complete reporting herein would require too much space and would not be particularly helpful. Instead, one of the smaller sets, for the turbine generator in the vertical direction is reproduced in Fig. 4. It should be noted that these matrices were adjusted to give the correct first two critical frequencies of the rotors and shaft.

The equation from which mobilities were calculated was:

$$M\ddot{x} + C\dot{x} + Kx = f(t), \qquad (1)$$

in which

M = mass matrix (diagonal),

C = damping matrix,

K = stiffness matrix,

x, $\dot{x}$, $\ddot{x}$ the displacement vector and its time derivatives, and $f(t)$ = the forcing function.

If the substitution

$$x = a \cos \omega t + b \sin \omega t$$
$$f(t) = f_1 \cos \omega t + f_2 \sin \omega t \qquad (2)$$

is made in Eq. (1), we get

$$\begin{bmatrix} (-\omega^2 M + K) & (+\omega c) \\ (-\omega c) & (-\omega^2 M + K) \end{bmatrix} \begin{bmatrix} a \\ b \end{bmatrix} = \begin{bmatrix} f_1 \\ f_2 \end{bmatrix}. \qquad (3)$$

In Eq. (3) a is the in-phase (or real) vector of response to the steady state forcing function, and b is the out-of-phase (or imaginery) vector. Similarly, f_1 is the real part of the forcing vector, and f_2 is the imaginary part. For a real forcing function, f_2 is zero, and if f_1 then has unit value on a particular coordinate and zero on the other coordinates, then a and b are the real and imaginary components of the displacement mobility. In practice, instead of solving Eq. (3) separately for each forcing vector at each value of ω, we recognized that the mobility matrix was the inverse of the displacement impedance matrix on the left side of Eq. (3). Hence it was only necessary to invert the impedance matrix for a particular frequency and post-multiply it by a rectangular matrix made up of unit-zero vectors with the 1's in the appropriate places to get the direct and transfer mobilities that were desired.

Displacement mobilities were calculated then for each black box for a range of frequencies from 50 to 200 cps. The reporting in detail of all of these calculations would require too many pages, so a sample mobility matrix for the turbine-generator in the athwartship direction at 60 cps in given in Table 1.

CRITERION FOR ABSORBER LOCATION AND IMPEDANCE

Once the mobility matrices were available, it was necessary to combine them in such a way that a criterion for absorber location could be devised. To do this, the various series combinations of mobilities across black boxes in Fig. 3 were calculated: AB vs BE, AC vs CE, and AD vs DE. This was accomplished by successive application of the series addition principle for mobilities (see Fig. 8). In the sketch the displacement mobilities can be written as:

$$\begin{bmatrix} x_3 \\ x_2 \end{bmatrix} = \begin{bmatrix} m_{332} & m_{32} \\ m_{23} & m_{223} \end{bmatrix} \begin{bmatrix} f_{32} \\ f_{23} \end{bmatrix},$$
$$\begin{bmatrix} x_2 \\ x_1 \end{bmatrix} = \begin{bmatrix} m_{221} & m_{21} \\ m_{12} & m_{112} \end{bmatrix} \begin{bmatrix} f_{21} \\ f_{12} \end{bmatrix}, \qquad (4)$$

and they combine to

$$\begin{bmatrix} x_3 \\ x_1 \end{bmatrix} = \begin{bmatrix} (m_{332} - m_{32} B_2^{-1} m_{23}) & (m_{32} B_2^{-1} m_{21}) \\ (m_{12} B_2^{-1} m_{23}) & (m_{112} - m_{12} B_2^{-1} m_{21}) \end{bmatrix} \begin{bmatrix} f_{32} \\ f_{12} \end{bmatrix}, \qquad (5)$$

in which

$$B_2 = (m_{223} + m_{221}).$$

Note that the m's can be matrices and the x's vectors, i.e., there can be many terminals at 1, 2, and 3. Furthermore the matrices and vectors can be complex, as was true in this problem.

To get at the vibration absorber problem more easily, consider the displacement impedance (inverse of mobility) for the system shown in the sketch:

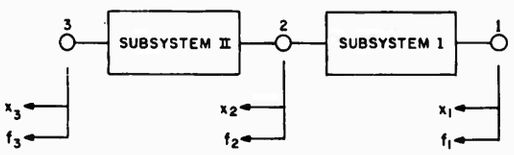

Fig. 8 - Series addition of mobilities

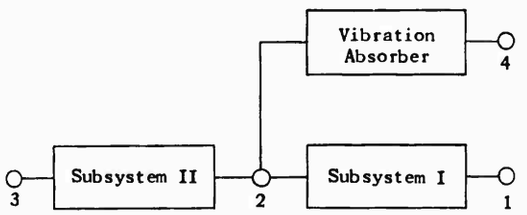

TABLE 1
Mobility Matrix for T-G at 50 cps (Athwartship) (Omega = 50.00* 2PI)

No. of Coordinate Corresponding to Mass in Fig. 3	A = a in Eq. (3) (in./lb except 2, 6, 10 are rad/in. lb)	B = b in Eq. (3)	C = $(A^2+B^2)^{1/2}$	Omega* C = Velocity	PHI = Phase Angle of C Relative to Driving Force	Case No. = No. of Coordinate Being Driven
I	A	B	C	Omega* C	PHI	Case No.
1	-0.49851E-06	-0.19718E-08	0.49851E-06	0.15661E-03	-0.22663E-00	1
2	-0.76979E-10	0.55764E-10	0.95055E-10	0.29862E-07	0.35920E 02	1
3	-0.52063E-06	-0.10423E-07	0.52074E-06	0.16359E-03	-0.11469E 01	1
4	-0.32605E-06	-0.23927E-08	0.32606E-06	0.10244E-03	-0.42045E-00	1
5	0.58942E-07	0.59814E-08	0.59245E-07	0.18612E-04	-0.57945E 01	1
6	-0.57095E-09	-0.85435E-10	0.57731E-09	0.18137E-06	-0.85104E 01	1
7	0.12627E-06	0.55213E-06	0.12639E-06	0.39705E-04	-0.25036E 01	1
8	0.92064E-07	0.41051E-09	0.92065E-07	0.28923E-04	-0.25548E-00	1
9	-0.37182E-07	-0.44126E-08	0.37443E-07	0.11763E-04	-0.67679E 01	1
10	0.36116E-09	0.62301E-10	0.36650E-09	0.11514E-06	-0.97672E 01	1
1	-0.76979E-10	0.55764E-10	0.95055E-10	0.29862E+07	0.35920E 02	2
2	-0.48877E-09	0.20205E-11	0.48876E-09	0.15355E-06	0.23665E-00	2
3	0.50414E-08	0.32708E-09	0.50520E-08	0.15871E-05	-0.37121E 01	2
4	0.31590E-06	0.16476E-09	0.31633E-06	0.99378E-06	-0.29857E 01	2
5	-0.56866E-09	-0.83563E-10	0.57476E-09	0.18057E-06	-0.83597E 01	2
6	0.54965E-11	0.10759E-11	0.56008E-11	0.17595E-08	-0.11076E 02	2
7	-0.12213E-08	-0.10834E-09	0.12261E-08	0.38520E-06	-0.50691E 01	2
6	-0.89209E-09	-0.43953E-10	0.89317E-09	0.28060E-06	-0.26207E 01	2
9	0.35844E-09	0.56910E-10	0.36325E-09	0.11412E-06	-0.93331E 01	2
10	-0.34733E-11	-0.76063E-12	0.35556E-11	0.11170E-06	-0.12352E 02	2
1	-0.52063E-06	-0.10423E-07	0.52074E-06	0.16359E-03	-0.11469E 01	3
2	0.50414E-08	0.32708E-09	0.50520E-08	0.15871E-05	-0.37121E 01	3
3	0.87737E-06	-0.82961E-07	0.88128E-06	0.27686E-03	0.54016E 01	3
4	0.54866E-06	-0.58907E-07	0.55182E-06	0.17336E-03	0.61281E 01	3
5	-0.10026E-06	0.13195E-08	0.10026E-06	0.31499E-04	0.75407E 00	3
6	0.97645E-09	0.33447E-10	0.97702E-09	0.30694E-06	-0.19618E 01	3
7	-0.21336E-06	0.15087E-07	0.21389E-06	0.67196E-04	0.40447E 01	3
8	-0.15487E-06	0.17079E-07	0.15581E-06	0.48948E-04	0.62931E 01	3
9	0.63367E-07	0.24261E-09	0.63387E-07	0.19907E-04	-0.21936E-00	3
10	-0.61926E-09	-0.35041E-10	0.62025E-09	0.19486E-06	-0.32386E 01	3
1	-0.32605E-06	-0.23927E-08	0.32606E-06	0.10244E-03	-0.42045E-00	4
2	0.31590E-08	0.16476E-09	0.31633E-08	0.99378E-06	-0.29857E 01	4
3	0.54866E-06	-0.56907E-07	0.55182E-06	0.17336E-03	0.61281E 01	4
4	0.10856E-05	-0.74446E-07	0.10881E-05	0.34184E-03	0.39231E 01	4
5	-0.19765E-06	-0.50063E-08	0.19771E-06	0.62112E-04	-0.14510E 01	4
6	0.19215E-08	0.13999E-09	0.19266E-06	0.60525E-06	-0.41669E 01	4
7	-0.42156E-06	0.13540E-07	0.42177E-06	0.13250E-03	0.18397E 01	4
6	-0.30645E-06	0.21903E-07	0.30724E-06	0.96521E-04	0.40680E 01	4
9	0.12484E-06	0.52656E-08	0.12495E-06	0.39255E-04	-0.24244E 01	4
10	-0.12176E-08	-0.11603E-09	0.12231E-08	0.38424E-06	-0.54436E 01	4
1	0.56942E-07	0.59814E-08	0.59245E-07	0.18612E-04	-0.57945E 01	5
2	-0.56866E-09	-0.63563E-10	0.57476E-09	0.16057E-06	-0.83597E 01	5
3	-0.10026E-06	0.13195E-08	0.10026E-06	0.31499E-04	0.75407E 00	5
4	-0.19765E-06	-0.50063E-08	0.19771E-06	0.62112E-04	-0.14510E 01	5
5	-0.21949E-06	-0.24006E-06	0.21950E-06	0.68959E-04	-0.62662E 00	5
6	-0.25843E-09	0.17954E-10	0.25906E-09	0.81385E-07	0.39741E 01	5
7	-0.42091E-06	0.23549E-07	0.42157E-06	0.13244E-03	0.32023E 01	5
8	-0.30570E-06	0.29170E-07	0.30709E-06	0.96474E-04	0.54506E 01	5
9	0.12487E-06	0.23144E-08	0.12489E-06	0.39236E-04	-0.10616E 01	5
10	-0.12194E-08	-0.87001E-10	0.12225E-08	0.38405E-06	-0.40611E 01	5
1	-0.57095E-09	-0.85435E-10	0.57731E-09	0.16137E-06	-0.85104E 01	6
2	0.54965E-11	0.10759E-11	0.56006E-11	0.17595E-08	-0.11076E 02	6
3	0.97645E-09	0.33447E-10	0.97702E-09	0.30694E-06	-0.19618E 01	6
4	0.19215E-08	0.13999E-09	0.19266E-08	0.60525E-06	-0.41669E 01	6
5	-0.25843E-09	0.17954E-10	0.25906E-09	0.81385E-07	0.39741E 01	6
6	-0.23601E-09	0.12244E-11	0.23602E-09	0.74146E-07	0.29724E-00	6
7	0.41186E-08	0.14543E-10	0.41187E-08	0.12939E-05	-0.20232E-00	6
6	0.29983E-08	-0.10711E-09	0.30002E-08	0.94254E-06	0.20460E 01	6
9	-0.12165E-08	-0.95021E-10	0.12202E-08	0.38333E-06	-0.44664E 01	6
10	0.11842E-10	0.15560E-11	0.11943E-10	0.37521E-06	-0.74856E 01	6
1	0.12627E-06	0.55213E-08	0.12639E-06	0.39705E-04	-0.25036E 01	7
2	-0.12213E-06	-0.10834E-09	0.12261E-06	0.38520E-06	-0.50691E 01	7
3	-0.21336E-06	0.15067E-07	0.21389E-06	0.67196E-04	0.40447E 01	7
4	-0.42156E-06	0.13540E-07	0.42177E-06	0.13250E-03	0.16397E 01	7
5	-0.42091E-06	0.23549E-07	0.42157E-06	0.13244E-03	0.32023E 01	7
6	0.41186E-06	0.14543E-10	0.41187E-06	0.12939E-05	-0.20232E-00	7
7	0.23666E-05	-0.37765E-06	0.23966E-05	0.75290E-03	0.90663E 01	7
8	0.17116E-05	-0.34251E-06	0.17458E-05	0.54844E-03	0.11315E 02	7
9	-0.70751E-06	0.59439E-07	0.71000E-06	0.22305E-03	0.46023E 01	7
10	0.69463E-08	-0.21623E-09	0.69496E-08	0.21833E-05	0.17830E 01	7
1	0.92064E-07	0.41051E-09	0.92065E-07	0.28923E-04	-0.25548E-00	8
2	-0.89209E-09	-0.43953E-10	0.89317E-09	0.28060E-06	-0.26207E 01	8
3	-0.15467E-06	0.17079E-07	0.15581E-06	0.48948E-04	0.62931E 01	6
4	-0.30645E-06	0.21903E-07	0.30724E-06	0.96521E-04	0.40880E 01	8
5	-0.30570E-06	0.29170E-07	0.30709E-06	0.96474E-04	0.54506E 01	6
6	0.29983E-08	-0.10711E-09	0.30002E-08	0.94254E-06	0.20460E 01	6
7	0.17116E-05	-0.34251E-06	0.17458E-05	0.54644E-03	0.11315E 02	6
6	0.20684E-05	-0.36326E-06	0.21001E-05	0.65976E-03	0.99606E 01	8
9	-0.85256E-06	0.51373E-07	0.85410E-06	0.26832E-03	0.34484E 01	6
10	0.83599E-06	-0.62610E-10	0.83601E-08	0.26264E-05	0.42910E-00	8
1	-0.37182E-07	-0.44126E-08	0.37443E-07	0.11763E-04	-0.67679E 01	9
2	0.35844E-09	0.58910E-10	0.36325E-09	0.11412E-06	-0.93331E 01	9
3	0.63367E-07	0.24261E-09	0.63367E-07	0.19907E-04	-0.21936E-00	9
4	0.12484E-06	0.52856E-08	0.12495E-06	0.39255E-04	-0.24244E 01	9
5	0.12487E-06	0.23144E-08	0.12489E-06	0.39236E-04	-0.10618E 01	9
6	-0.12165E-08	-0.95021E-10	0.12202E-06	0.38333E-06	-0.44664E 01	9
7	-0.70751E-06	0.59439E-07	0.71000E-06	0.22305E-03	0.48023E 01	9
6	-0.85256E-06	0.51373E-07	0.85410E-06	0.26832E-03	0.34484E 01	9
9	-0.32391E-06	-0.69381E-08	0.32404E-06	0.10180E-03	-0.15806E 01	9
10	-0.15081E-06	0.35907E-10	0.15085E-08	0.47390E-06	0.13640E 01	9
1	0.36116E-09	0.62301E-10	0.36650E-09	0.11514E-06	-0.97872E 01	10
2	-0.34733E-11	-0.76063E-12	0.35556E-11	0.11170E-08	-0.12352E 02	10
3	-0.61926E-09	-0.35041E-10	0.62025E-09	0.19486E-06	-0.32386E 01	10
4	-0.12176E-08	-0.11603E-09	0.12231E-06	0.38424E-06	-0.54436E 01	10
5	-0.12194E-08	-0.67001E-10	0.12225E-06	0.38405E-06	-0.40611E 01	10
6	0.11842E-10	0.15560E-11	0.11943E-10	0.37521E-08	-0.74856E 01	10
7	0.69463E-08	-0.21623E-09	0.69496E-08	0.21833E-05	0.17630E 01	10
8	0.83599E-08	-0.62610E-10	0.83601E-06	0.26264E-05	0.42910E-00	10
9	-0.15081E-08	0.35907E-10	0.15085E-08	0.47390E-06	0.13640E 01	10
10	-0.45046E-09	0.26264E-11	0.45049E-09	0.14153E-06	0.33404E-00	10

for which

$$\begin{bmatrix} f_3 \\ f_2 \end{bmatrix} = \begin{bmatrix} Z_{332} & Z_{32} \\ Z_{23} & Z_{223} \end{bmatrix} \begin{bmatrix} x_3 \\ x_2 \end{bmatrix},$$

$$\begin{bmatrix} f_4 \\ f_2 \end{bmatrix} = \begin{bmatrix} Z_{442} & Z_{42} \\ Z_{24} & Z_{224} \end{bmatrix} \begin{bmatrix} x_4 \\ x_2 \end{bmatrix},$$

$$\begin{bmatrix} f_2 \\ f_1 \end{bmatrix} = \begin{bmatrix} Z_{221} & Z_{21} \\ Z_{12} & Z_{112} \end{bmatrix} \begin{bmatrix} x_2 \\ x_1 \end{bmatrix}. \quad (6)$$

If we consider 1-2-3 the original system, with 2-3 not yet attached, then the combination of 1-2-4 with $f_4 = 0$ (as it would be if 2-4 were the vibration absorber), gives:

$$\begin{bmatrix} f_2 \\ f_1 \end{bmatrix} = \begin{bmatrix} (Z_{221} + Z_{224} - Z_{24} Z_{442}^{-1} Z_{42}) & Z_{21} \\ Z_{12} & Z_{112} \end{bmatrix} \begin{bmatrix} x_2 \\ x_1 \end{bmatrix}, \quad (7)$$

and we observe that only the Z_{221} term is affected by the 2-4 system. If we let

$$Z_a = Z_{224} - Z_{24} Z_{442}^{-1} Z_{42} \quad (8)$$

then Eq. (7) becomes

$$\begin{bmatrix} f_2 \\ f_1 \end{bmatrix} = \begin{bmatrix} (Z_{221} + Z_a) & Z_{21} \\ Z_{12} & Z_{112} \end{bmatrix} \begin{bmatrix} x_2 \\ x_1 \end{bmatrix}. \quad (9)$$

Now if we add 1-2 (without 2-4) and 2-3 in series, we get

$$\begin{bmatrix} f_3 \\ f_1 \end{bmatrix} = \begin{bmatrix} (Z_{332} - Z_{32} \beta_2^{-1} Z_{23}) & -(Z_{32} \beta_2^{-1} Z_{21}) \\ -(Z_{12} \beta_2^{-1} Z_{23}) & (Z_{112} - Z_{12} \beta_2^{-1} Z_{21}) \end{bmatrix} \times \begin{bmatrix} x_3 \\ x_1 \end{bmatrix}, \quad (10)$$

in which

$$\beta_2 = (Z_{223} + Z_{221}). \quad (11)$$

Examination of Eqs. (9), (10), and (11) shows that only β_2 is affected by the addition of the absorber, system 2-4, and that by this addition, β_2 becomes:

$$\beta_{2a} = (Z_{223} + Z_{221} + Z_a). \quad (12)$$

Now we introduce a shorter notation for Eq. (10):

$$\begin{bmatrix} f_3 \\ f_1 \end{bmatrix} = \begin{bmatrix} Z_{331} & Z_{31} \\ Z_{13} & Z_{113} \end{bmatrix} \begin{bmatrix} x_3 \\ x_1 \end{bmatrix}, \quad (10^1)$$

and consider the magnitude of f_3 and x_3 as functions of f_1 for two different cases, one without the absorber system attached, and one with it attached. If we solve Eq. (10^1) for f_3, we can get:

$$f_3 - \left(Z_{331} - Z_{31} Z_{113}^{-1} Z_{13}\right) x_3 = Z_{31} Z_{113}^{-1} f_1. \quad (13)$$

When the impedance to which interface 3 is attached is large, x_3 tends to be small and

$$f_3 \approx Z_{31} Z_{113}^{-1} f_1. \quad (14)$$

A return to the expanded notation of Eq. (10) gives

$$f_3 = -\left(Z_{32} \beta_2^{-1} Z_{21}\right) \left(Z_{112} - Z_{12} \beta_2^{-1} Z_{21}\right)^{-1} f_1 \quad (14^1)$$

for Eq. (14^1), and we can examine conditions which make f_1 a minimum. The first term in parentheses needs to be a minimum, which results from making β_2 large compared to $Z_{32} Z_{21}$. The second term needs to be a maximum before inversion, which results from making β_2 large compared to $(Z_{12} Z_{21})$. This is so because Z_{112} is positive, so also is the product $(Z_{12} Z_{21})$ and so is β_2, hence for the term to be as large as possible it is necessary for $(Z_{12} \beta_2^{-1} Z_{21})$ to be as small as possible, and this is accomplished by making β_2 large compared to $(Z_{12} Z_{21})$. If β_2 is large compared to $(Z_{12} Z_{21})$, then the first term of Eq. (14^1) dominates in controlling f_3 as a function of f_1. For the comparison of f_3 with no absorber to f_{3a} with an absorber, we then have:

$$f_{3a} \approx -\left(Z_{32} \beta_{2a}^{-1} Z_{21}\right) \left(Z_{112} - Z_{12} \beta_{2a}^{-1} Z_{21}\right)^{-1} f_1, \quad (15)$$

and the reduction factor for f_{3a} vs f_3 is essentially

$$f_{3a} \approx (\beta_{2a}^{-1} \beta_2) f_3. \quad (16)$$

So far we know that we want β_{2a} to be large, which means to make Z_a as large as possible in comparison to $(Z_{223} + Z_{221})$. We further

have an approximation to the improvement factor for the vibration absorber in Eq. (16). To answer the question of where best to put the absorber, consider Eq. (5) in which

$$x_3 - \left(m_{332} - m_{32}B_2^{-1}m_{23}\right) f_3 = \left(m_{32}B_2^{-1}m_{21}\right) f_1 . \quad (17)$$

To make either x_3 or f_3 small, B_2 must be large, and $B_2 = m_{223} + m_{221}$. Thus, on the basis of the limits of the problem (large impedance to which interface 3 attaches so $x_3 \rightarrow 0$, or small impedance to which interface 3 attaches so $f_3 \rightarrow 0$), we can establish a set of rules for absorber location and impedance which at least fits these limiting conditions and at the same time agrees with a common sense consideration of the problem:

1. Find the interface, 2, for which $(m_{223} + m_{221})$ is the largest available or for which the displacement impedance $(Z_{221} + Z_{223})$ is the smallest available.

2. Design the vibration absorber so that Z_a is large compared to $(Z_{223} + Z_{221})$.

3. Expect a reduction in f_3 of the order of $(Z_{223} + Z_{221} + Z_a)^{-1} (Z_{223} + Z_{221})$.

VIBRATION ABSORBER DESIGN

In accordance with the foregoing rules, the values of $(Z_{223} + Z_{221})$ were calculated at each interface, B, C, and D, for a range of frequencies. The results are shown in Table 2. Since 60 cps was a frequency for which a large noise transmission to the hull occurred, it was agreed with the Navy to design an absorber for that particular frequency and see how the rules worked.

Interface C had the smallest set of values for $(Z_{223} + Z_{221})$ at 60 cycles, as shown in Table 2, so it was chosen as the absorber location. Since interface C was the connection between the sub-base and the rubber mounts, the sub-base was examined for a suitable location in which to put a vibration absorber. There were rectangular openings in the box-beamlike edge of the sub-base, next to the recesses for the rubber mounts. These openings were 18 × 17 × 18 inches in size, so the problem became the one of designing a simple spring-mass system to be resonant at 60 cycles, to fit the available space, with as large a mass as possible and as large a Q as possible. The design used is shown in Fig. 9, with the weight approximately 750 lb. Two of these absorbers were set up back-to-back and tuned to 60 cps by adding small weights. The Q (magnification factor) at resonance for the pair was measured as 832. Since the displacement impedance for a single-mass absorber at resonance is

$$Z_a = -\omega^2 MQ \quad (18)$$

this absorber should have an impedance at 60 cps of 0.23×10^8 lb/in.

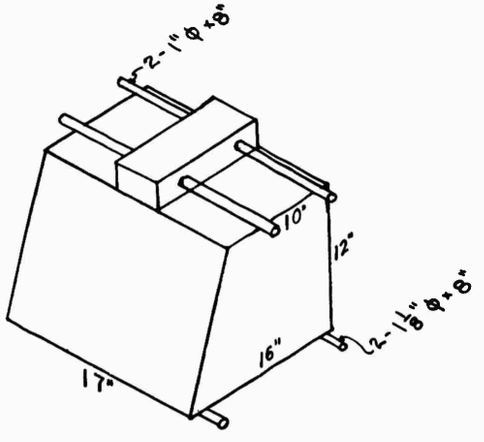

Fig. 9 - Configuration of vibration absorber

Examination of the 60-cps impedances for interface C shows a total impedance for all three connection points of about 0.26×10^7 lb/in. For two of these vibration absorbers at the three connection points, the reduction factor should then be (per Eq. 16):

$$\frac{0.26 \times 10^7}{2 \times 0.23 \times 10^8 + 0.26 \times 10^7} = 0.053$$

or approximately 27 db.

COMPARISON OF MEASURED AND CALCULATED RESULTS

A set of measurements of direct impedance at the four corners of the T-G base were available from unpublished data. These measurements were made in 1960 on the test stand at Fitchburg with the SSN593 T-G set, and are plotted in Fig. 10. In making the measurements, an accelerometer and force gage were used for one set of data, while a commercial impedance head was used for the second set of points. As

TABLE 2
Impedance at Interfaces B, C, D

	$(Z_{BBA} + Z_{BBE})$			$(Z_{CCA} + Z_{CCE})$			$(Z_{DDA} + Z_{DDE})$			(cps)
	000001	000002	000003	000001	000002	000003	000001	000002	000001	
000001 R	-27660968 07[a]	-56812401 06	-13721972 03	-57499778 06	-53639480 02	-54322920 02	41659933 11	-12752121 11	-46415247 10	50
000001 1M	-82772290 04	-51052987 05	13383536 04	-97975732 04	81878798 02	12037021 03	22237596 10	-10614653 10	-18271825 10	
000002 R	-56812410 06	-70551213 07	-25909904 07	-53629817 02	-65068032 06	38555607 03	-12752121 11	46376570 11	13498503 11	
000002 1M	-51053874 05	11663593 05	35512372 05	78442797 02	-44099376 04	17220647 03	-10614653 10	16339618 10	42847332 09	
000003 R	-13720510 03	-25909904 07	-49677721 07	-54310919 02	38556076 03	-57698402 06	-46415248 10	13498503 11	34352438 11	
000003 1M	13383644 04	35513038 05	10288906 06	11830385 03	17326762 03	-10898304 05	-18271825 10	42847334 09	18634007 10	
000001 R	-35026484 07	-73642069 06	-85540627 02	-68803421 06	-54904565 02	-42385209 02	83286097 10	-73030246 10	25751708 11	55
000001 1M	-18847134 05	-66679313 05	15424345 04	-10791758 05	42788377 02	78917795 02	44238053 11	22123689 10	-40763167 11	
000002 R	-73642077 06	-21727365 07	34926050 07	-54812120 02	-78509078 06	55251917 03	-73030245 10	37257279 11	90284731 10	
000002 1M	-66680247 05	14569694 07	14162789 07	38894240 02	-51155893 04	21830344 03	22123692 10	11751722 10	-28975983 10	
000003 R	-85536865 02	34926050 07	53173870 06	-42472335 02	55248887 03	-69066816 06	25751707 11	90284731 10	30204567 10	
000003 1M	15423272 04	14162794 07	14078981 07	76923772 02	22022889 03	-12253546 05	-40763167 11	-28975983 10	38440014 11	
000001 R	-44470878 07	-10571407 07	71633810 02	-81177088 06	-75240937 02	-44176383 02	49550756 11	-49221295 10	-11994340 11	60
000001 1M	-33034872 05	-86939085 05	18219461 04	-11798469 05	-46138632 02	-20476477 02	31275144 10	64127118 09	-34447151 10	
000002 R	-10571408 07	-59734306 07	11208907 07	-75183307 02	-93292635 06	95961765 03	-49221296 10	30555172 11	11492954 11	
000002 1M	-86939341 05	25562163 06	26841759 06	-51866956 02	-61334050 04	45199445 03	64127118 09	30107643 10	-37208324 10	
000003 R	71635991 02	11208907 07	-25071430 07	-44251861 02	95982287 03	-81580138 06	-11994340 11	11492954 11	30452938 11	
000003 1M	18216581 04	26841743 06	29365523 06	-21337374 02	45563557 03	-13883148 05	-34447153 10	-37208324 10	71435104 10	
000001 R	-59457369 07	-18758829 07	43036777 03	-94628971 06	-16977785 03	-12124062 03	44764117 11	34025208 10	-17118704 11	65
000001 1M	-23811381 05	-85119992 05	20465925 04	-12844645 05	-23707202 03	-22828612 03	22326687 10	21974516 08	-17112823 10	
000002 R	-18758825 07	-84476374 07	69001206 06	-16967267 03	-10955980 07	27901840 04	34025208 10	35971048 11	-19240438 10	
000002 1M	-85113915 05	12011928 06	15145187 06	-24925581 03	-89105338 04	23290481 04	21974498 08	45790531 10	-56243280 10	
000003 R	43034837 03	69001194 06	-36540397 07	-12133657 03	27903139 04	-95432507 06	-17118704 11	-19240438 10	46826393 11	
000003 1M	20458283 04	15145021 06	18444173 06	-22489013 03	23419972 04	-16749611 05	-17112823 10	-56243280 10	83979964 10	
000001 R	-11849396 08	-71268901 07	17173001 04	-10485406 07	-43102200 03	-62536721 03	41632248 11	28064584 09	-10622502 11	70
000001 1M	19867224 07	18321144 07	16332649 04	-15042141 05	-60221268 03	-64044582 03	80642652 10	-12604259 11	11139373 11	
000002 R	-71268884 07	-15187080 08	52070345 06	-43084450 03	-12348305 07	-16371902 05	28064584 09	35224321 11	-21884960 09	
000002 1M	18321407 07	19276474 07	11091851 06	-60938720 03	-12247207 05	72648613 04	-12604259 11	21751419 11	-20222696 11	
000003 R	17163196 04	52070389 06	-46006184 07	-62566325 03	-16372822 05	-10430739 07	-10622502 11	-21884970 09	39276538 11	
000003 1M	16166888 04	11092642 06	14804741 06	-64293366 03	73156812 04	-23754166 05	11139372 11	-20222696 11	19455019 11	

[a] -27660968 07 = -0.2766×10^7

000001 R	-20956325 07	34680907 07	23406999 04	-12027905 07	-12445525 04	-12993276 04	41432877 11	-34061288 10	-54311217 10	75
000001 1M	13577434 07	13550544 07	46276123 03	-16117157 05	95560287 03	78372436 03	20371254 10	-23181793 10	17925103 10	
000002 R	34680904 07	-61101311 07	43919158 06	-12499723 04	-14251619 07	-44042484 04	-34061288 10	40231775 11	-52326168 10	
000002 1M	13550505 07	15996816 07	88967687 05	94838537 03	-21282642 04	30483433 04	-23181792 10	35611230 10	-33098369 10	
000003 R	23405442 04	43919135 06	-55246894 07	-12994034 04	-43949085 04	-12003956 07	-54311216 10	-52326167 10	41638666 11	
000003 1M	45989373 03	88963755 05	13176906 06	77597520 03	30603617 04	-14449648 05	17925103 10	-33098368 10	35606211 10	
000001 R	-48837284 07	15413000 07	10764682 04	-13665073 07	-54644404 03	-67315419 03	36951796 11	76235634 09	-82816216 10	80
000001 1M	44499220 06	41084567 06	14458349 03	-16668511 05	92650784 03	85931645 03	61221466 10	-58544942 10	47932856 10	
000002 R	15412999 07	-96107678 07	40042806 06	-54653960 03	-16233224 07	-23608392 04	76235634 09	33539175 11	80930988 09	
000002 1M	41084528 06	61552554 06	77117545 05	92594289 03	-35196224 04	27737703 04	-58544941 10	64142714 10	-57515730 10	
000003 R	10764350 04	40042792 06	-64731934 07	-67317746 03	-23607560 04	-13648498 07	-82816217 10	80930988 09	34348570 11	
000003 1M	14380483 03	77114939 05	12519750 06	85697540 03	27759312 04	-14777399 05	47932856 10	-57515730 10	57043162 10	
000001 R	-63108052 07	10222671 07	57771944 03	-15412951 07	-36656886 03	-49392803 03	40868205 11	-25715680 10	-53861092 10	85
000001 1M	28814620 06	24428007 06	31794508 03	-17591943 05	83984361 03	81737054 03	65141286 10	-78882757 10	79111445 10	
000002 R	10222739 07	-11803606 08	39434251 06	-36660411 03	-44270859 06	-15795679 04	-25715680 10	34262562 11	99309134 09	
000002 1M	24430682 06	43719135 06	68155969 05	83975301 03	-76695220 06	24293488 04	-78882758 10	11046234 11	-11920520 11	
000003 R	58557906 03	39435964 06	-74688104 07	-49388886 03	-41728305 07	-15396467 07	-53861093 10	99299700 09	31954166 11	
000003 1M	32788046 03	68151925 05	12434767 06	81583006 03	22895258 07	-16012366 05	79111444 10	-11920450 11	13602951 11	
000001 R	-75061961 07	79321273 06	33150167 03	-17270160 07	-51712223 07	-40042568 03	45280507 11	-11035863 11	56977893 10	90
000001 1M	22946862 06	17998960 06	50862799 03	-18539830 05	29445915 07	77963287 03	58810845 10	-59202796 10	52757606 10	
000002 R	79321655 06	-13820397 08	42310366 06	-27837622 03	-33174463 06	-11928354 04	-11035786 11	47553754 11	-15623812 11	
000002 1M	18000290 06	37363349 06	55724472 05	79111237 03	-98663816 06	22374260 04	-59203617 10	90508978 10	-10062607 11	
000003 R	34570415 03	42311758 06	-85310041 07	-40046161 03	-51721369 07	-17251394 07	56977895 10	-15623889 11	51185022 11	
000003 1M	50834130 03	55723260 05	13208914 06	77813345 03	29460382 07	-17260669 05	52757606 10	-10062525 11	12425829 11	
000001 R	-86541155 07	67415730 06	19863340 03	-19238883 07	-21890338 03	-34062226 03	43645392 11	-76564262 10	18945760 10	95
000001 1M	20094909 06	14692488 06	66182645 03	-19477942 05	75287717 03	72733797 03	23783715 10	-19139756 10	10378586 10	
000002 R	67415732 06	-15874445 08	50869641 06	-21891382 03	-22902343 07	-97298672 03	-76564262 10	43095603 11	-11675196 11	
000002 1M	14692534 06	36738845 06	21006734 05	75271889 03	-60111677 04	21411970 04	-19139756 10	28298940 10	-26154387 10	
000003 R	19864712 03	50869639 06	-96894690 07	-34063550 03	-97299474 03	-19213116 07	18945760 10	-11675196 11	47399673 11	
000003 1M	66197144 03	21006119 05	16608589 06	72592858 03	21414475 04	-18451343 05	10378586 10	-26154388 10	33246480 10	
000001 R	-11006124 08	58900877 06	51053576 02	-23544823 07	-90901700 07	-23918726 03	40331784 11	-42009578 10	-22973970 07	105
000001 1M	17917985 06	11220328 06	91636669 03	-20943922 05	57775968 07	27907105 03	29640571 10	-27314180 10	78158194 09	
000002 R	58900873 06	-20027418 08	54714372 06	-58461481 02	23212928 06	-72726713 03	-42009262 10	37445326 11	-74411465 10	
000002 1M	11220372 06	13026208 07	-94661047 06	54037872 03	-19327624 07	21047598 04	-27314971 10	34974107 10	-14224407 10	
000003 R	52262761 02	54714874 06	-11990137 08	-23925149 03	-90908388 07	-23458570 07	-22973758 07	-74411779 10	42234305 11	
000003 1M	90933762 03	-94661242 06	11307833 07	27745440 03	57791611 07	-20693999 05	78158192 09	-14223615 10	10531480 10	

TABLE 2--Continued

	$(Z_{BBA} + Z_{BBE})$			$(Z_{CCA} + Z_{CCE})$			$(Z_{DDA} + Z_{DDE})$			(cps)
	000001	000002	000003	000001	000002	000003	000001	000002	000003	
000001 R	-12254636 08	60076901 06	-32443777 03	-26777838 07	-49195134 03	-45289180 04	40369674 11	-43354290 10	16150554 08	110
000001 1M	18059293 06	97825742 05	12071322 04	49191872 05	-42663754 04	-80831697 04	46362336 10	-55451169 10	15928577 10	
000002 R	60076913 06	-21372751 08	-26671766 06	-49199991 03	-30706168 07	-27641772 03	-43354290 10	37359628 11	-70396168 10	
000002 1M	97829404 05	90648984 06	-53425721 06	-42669215 04	-74729263 04	21498780 04	-55451169 10	81451295 10	-27747157 10	
000003 R	-32432898 03	-26671761 06	-12406481 08	-45289598 04	-27640851 03	-25736210 07	16150571 08	-70396168 10	41248453 11	
000003 1M	12102034 04	-53425621 06	70024399 06	-80842984 04	21494240 04	-22004236 05	15928577 10	-27747157 10	13202711 10	
000001 R	-15008990 08	78322718 06	15158900 02	-30568472 07	-32340654 03	-34696818 03	39970471 11	-62584936 10	11019759 10	120
000001 1M	25636517 06	12648353 05	11980990 04	-24532212 05	11295405 04	15439208 04	43830411 10	-37835469 10	26159443 09	
000002 R	78322717 06	-26211803 08	-13675246 06	-32339323 03	-36547713 07	-60883990 03	-62584935 10	41897840 11	-83699810 10	
000002 1M	12648599 05	54767262 06	-11656968 06	11292465 04	-84930908 04	21625787 04	-37835469 10	39485459 10	-65860138 09	
000003 R	15163637 02	-13675246 06	-15137877 08	-34697279 03	-60884056 03	-30635500 07	11019760 10	-83699811 10	40587855 11	
000003 1M	11981882 04	-11656976 06	29173078 06	15431915 04	21626008 04	-23929557 05	26159446 09	-65860138 09	46269859 09	
000001 R	-26249615 08	-10518944 06	-65840158 02	-55435590 07	-20407911 03	-24924916 03	43095888 11	-79611506 10	-17407128 07	160
000001 1M	32807492 06	-81153856 05	17887422 04	-31486135 05	12050826 04	15152676 04	29747309 09	-21641953 09	97990385 07	
000002 R	-10518944 06	-47010920 08	-17551087 05	-20408010 03	-65311445 07	-44748013 03	-79611505 10	40674754 11	-60236007 10	
000002 1M	-81153740 05	57733445 06	-11527901 05	12047588 04	-11523588 05	26739683 04	-21641953 09	22864881 09	-62474910 08	
000003 R	-65838282 02	-17551081 05	-27775853 08	-24924276 03	-44748026 03	-55460261 07	-17407075 07	-60236007 10	38326715 11	
000003 1M	17888135 04	-11527891 05	21915644 06	15145405 04	26739760 04	-31200069 05	97990378 07	-62474910 08	94836486 08	
000001 R	-29824609 08	-66229968 05	-74820210 02	57440995 07	-19697588 03	-24208585 03	42578402 11	-75848940 10	-11911522 08	170
000001 1M	30349988 06	-49148761 05	19224193 04	-21934897 07	12604644 04	15827528 04	20399796 09	-14460222 09	87101564 07	
000002 R	-66229794 05	-53360857 08	-12437994 05	-19697680 03	-33723181 07	-42743165 03	-75848940 10	40216126 11	-58830838 10	
000002 1M	-49149620 05	55378173 06	-78077902 04	12601985 04	-73234091 06	28206003 04	-14460222 09	16241539 09	-52148816 08	
000003 R	-74726822 02	-12437998 05	-31456805 08	-24209424 03	-42743175 03	57415836 07	-11911502 08	-58830838 10	38097529 11	
000003 1M	19217790 04	-78080887 04	22435911 06	15820610 04	28206104 04	-21932594 07	87101563 07	-52148817 08	79950025 08	
000001 R	-33590085 08	-44594951 05	-78164306 02	-70068253 07	-19117380 03	-23621194 03	42221540 11	-73322417 10	-18163307 08	180
000001 1M	29504141 06	-32823958 05	20540052 04	-35432191 05	13192403 04	16552794 04	15518107 09	-10686319 09	71710951 07	
000002 R	-44594950 05	-60063434 08	-91113373 04	-19117462 03	-82625872 07	-40998959 03	-73322417 10	39892300 11	-57753475 10	
000002 1M	-32823866 05	54926802 06	-53012824 04	13189837 04	-13132803 05	29709433 04	-10686319 09	12612637 09	-44635663 08	
000003 R	-78162933 02	-91113367 04	-35358130 08	-23621369 03	-40998967 03	-70091968 07	-18163320 08	-57753475 10	37916616 11	
000003 1M	20540647 04	-53012625 04	23107369 06	16546218 04	29709556 04	-35249483 05	71710950 07	-44635663 08	69549929 08	

000001 R	-37555615 08	-31481074 05	-82172214 02	-78027824 07	-18646575 03	-23131837 03	41959507 11	-71508952 10	-21797316 08	190
000001 1M	29379908 06	-23262730 05	21835268 04	-37403271 05	13797017 04	17308928 04	12611485 09	-84325309 08	57906017 07	
000002 R	-31481072 05	-67133930 08	-68567686 04	-18645667 03	-92048560 07	-39460338 03	-71508952 10	39649604 11	-56903068 10	
000002 1M	-23262648 05	55376656 06	-35157303 04	13794545 04	-13928612 05	31237691 04	-84325308 08	10373828 09	-39096988 08	
000003 R	-82172008 02	-68567682 04	-39478339 08	-23132969 03	-39460343 03	-78057264 07	-21797324 08	-56903067 10	37771144 11	
000003 1M	21835814 04	-35157082 04	23871337 06	17302678 04	31237834 04	-37262918 05	57906016 07	-39096988 08	61906357 08	
000001 R	-10974055 08	14625905 02	-82248844 02	-86424061 07	-18250662 03	-22710064 03	41759100 11	-70140950 10	-23770172 08	200
000001 1M	-33387767 04	15722653 04	23118267 04	-39379219 05	14417364 04	18088868 04	10725114 09	-69669171 08	46580046 07	
000002 R	13624569 02	-10975017 08	-27453410 03	-18256786 03	13037484 08	-38063443 03	-70140948 10	39459093 11	-56218520 10	
000002 1M	15724217 04	-36340885 04	27226518 04	14414388 04	-24935578 08	32784110 04	-69669171 08	88784537 08	-34926862 08	
000003 R	-84465302 02	-27543792 03	-10975498 08	-22670540 03	-69707565 08	-86446953 07	-23770171 08	-56218598 10	37652315 11	
000003 1M	23117906 04	27225229 04	-33195715 04	18086827 04	74765846 08	-39275678 05	46580043 07	-34901745 08	56111734 08	

may be seen, the two methods of measurement show somewhat the same shape of curve, but displaced by a factor of from 2 to 5. This was considered to be as good agreement between the two methods as could be expected at that time.

On the same plot, Fig. 10, is shown the set of calculated impedances for the nearest analytical point. It may be noted that the calculated data lie between the two sets of measured data from about 110 to 50 cps. Thus the analysis was considered to give results of the right general magnitude and trend.

In the foregoing section, the criterion for effectiveness of vibration absorber gave an attenuation factor of approximately 0.05 or 27 db at 60 cps at the absorber location. Measurements of the 60 cps component of vibration at the 4 absorber locations before the absorbers were applied averaged 84 vdb, while measurements after the absorbers were applied average 66 vdb. The attenuation factor was therefore an average of 18 db. This attenuation figure was considered to be in satisfactory agreement with the predicted value of 27 db, since a pair of vibration absorbers tested back to back would be expected to show a higher Q than they would when installed separately in the T-G base. (The 60-cps component was in both cases separated from the complex signal by the filter of the vibration analyzer. The vibration analyzer used was a General Radio 762B.)

CONCLUSIONS

Impedance techniques can be applied to a problem of this size and complexity with some success, as shown by Fig. 10 and by the agreement between predicted and measured attenuation. At this time, we see no alternative to using impedance methods for such problems except to over-simplify the problem. These methods, however, are far from being quick and easy; they are instead tedious and lengthy, even with nearly everything done by machine. The single greatest need in this kind of analysis is a good routine method for reducing a large size system to a smaller size system without modifying the dynamic characteristics over a specific frequency range.

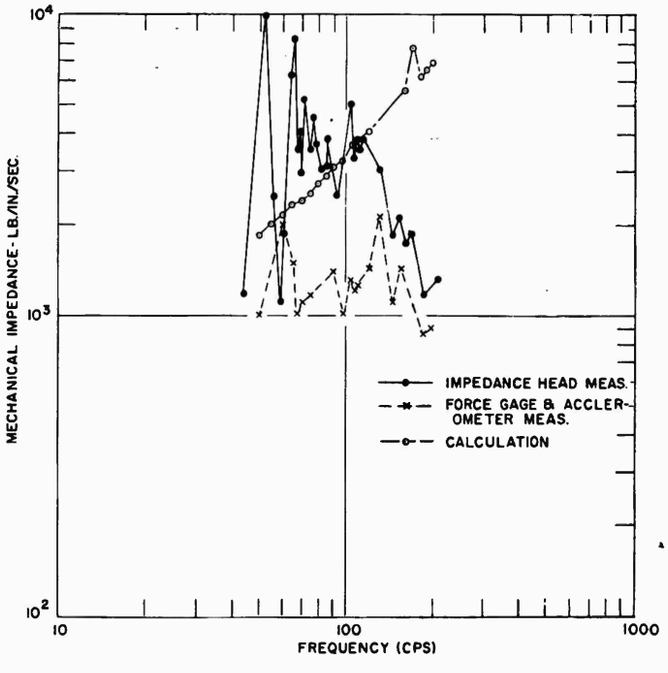

Fig. 10 - Measured vs calculated impedance, generator-corner of base

Mr. Otts (Sandia Corp.): In your phase measurements, what accuracy do you shoot for?

Dr. Mains: Well, first of all, I don't know how to measure phase properly in the presence of a noisy signal. It's something that we would like to be able to do, but we don't know how to do. It is best handled by the technique you Sandia people like very much — filtering out all but the fundamental. In this case we didn't have to measure phase.

Mr. Otts: I have found that phase measurements are hard to obtain to a really good accuracy, even to about 5 percent. Have you found this in general?

Dr. Mains: Yes. I also find a very large misunderstanding of what phase means in a complex system. If you look for resonances in terms of a phase shift of a complex system, you're kidding yourself, because only by accident do you get a phase shift at a resonance in such a system. The phase is the summation of many mathematical terms in the numerator, over a bunch of terms in the denominator. One of those terms may go to zero in a complex system, but not all of them.

Mr. Otts: Thank you.

Dr. Franken (Bolt, Beranek, and Newman): Will the converse recipe work if you find two elements that have a very high impedance and put a very soft impedance mount between them?

Dr. Mains: I don't know. I'd have to try it and see. It may be that it was a happy accident that our rule worked here. I would think it would apply in more general cases, but I can't be sure.

* * *

VIBRATION ANALYSIS OF AN IDEAL MOTOR USING MECHANICAL IMPEDANCE TECHNIQUES

J. I. Schwartz
U.S. Navy Marine Engineering Laboratory

This paper compares the theoretical response of a machine to its actual response when the machine is considered as a rigid body. The investigation shows that it is possible to predict rigid body vibration modes from theoretical considerations alone. It also shows that the ball bearing spring rates are obtainable directly from existing theory.

INTRODUCTION

The need for quiet machinery aboard Navy ships has reached the point where a designer must consider the vibration characteristics of the machine to be equally as important as the rest of its design. For example, the Navy specification for dynamic balance is 10 to 100 times more stringent than commercial specifications; but a commercial motor is as mechanically reliable as a Navy motor. This extreme specification is necessary to obtain quiet operation.

There are several ways available for a machine designer to obtain a quiet machine. He can build and test any machine and then modify it to obtain quiet performance; he can install the machine on vibration isolation mounts; or in the design stage he can consider the machine's vibration characteristics and design an inherently quiet machine from the beginning. In actual practice, these methods have been, or are being, used simultaneously, but this paper will deal only with the last method, inherently quiet design.

Vibrations generated within and by a machine can be classified into two categories. First, there are those vibrations that occur when the machine is considered as a series of rigid parts connected by springs and dashpots. This type of vibration can be described by standard rigid-body vibration theory. The second type of vibration occurs because of the continuous nature of all materials. That is, no machine can be completely described using rigid-body mathematics. Any mass-elastic body which can be deformed will possess resonant frequencies which defy analysis using standard techniques. The vibrations executed by a cylinder or a flat plate are good examples. If a designer is to make a comprehensive analysis of a machine, he must consider both types of vibration. This paper, while it acknowledges the existence of continuous body phenomena, will concentrate on the rigid-body analysis of a system.

THEORETICAL ANALYSIS

For the purposes of analysis, let us assume that the machine under consideration may be represented as shown in Fig. 1. The transducers have been added to the system to allow the measurement of bearing forces and accelerations. The following assumptions have been made in this analysis:

1. All masses are rigid bodies,

2. The bearings and transducers are springs,

3. Damping is assumed to be negligible, and

4. The system is assumed to be a linear bilateral system.

The system shown in Fig. 2 has four-degrees-of-freedom and hence has four resonant frequencies. By the symmetry of the system, it may be reduced to Fig. 3. This system could be analyzed by writing and solving simultaneously four second-order linear differential equations or by using the fourth assumption

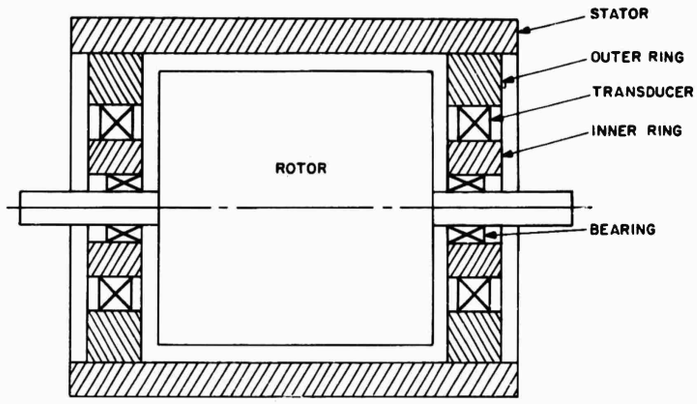

Fig. 1 - Section view of ideal motor

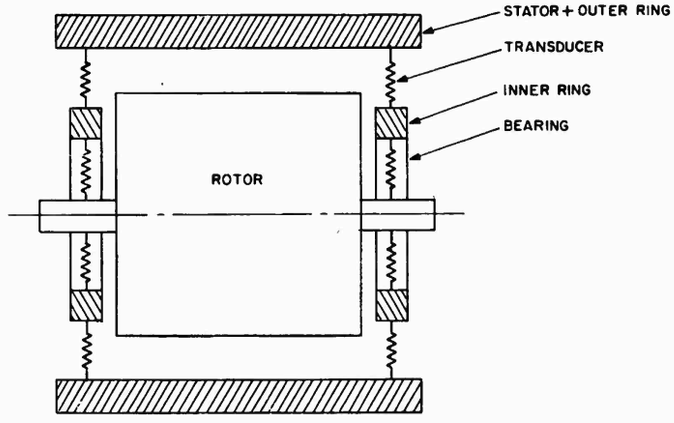

Fig. 2 - Motor representation for vibration analysis

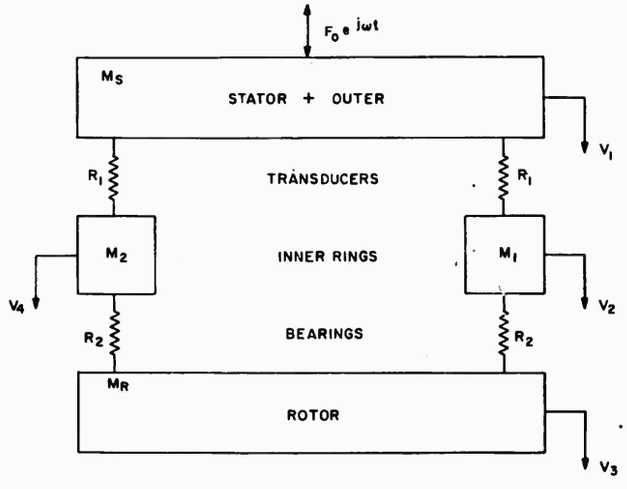

Fig. 3 - Motor block diagram

through the use of mechanical impedance techniques. It should be pointed out here that by using the reciprocity theorem and exciting the stator rather than the rotor, the experimental results are more easily verified.

The mechanical circuit shown in Fig. 4 may be obtained from Fig. 3. (The symbols used are defined at the end of the paper.) The loop velocity circuit equations from Fig. 4 are:

$$F = V_1(Z_1 + 2Z_3) - V_2 Z_3 + 0 - V_4 Z_3 ,$$

$$0 = -V_1 Z_3 + V_2(Z_2 + Z_3 + Z_4) - V_3 Z_4 + 0 ,$$

$$0 = -V_1 Z_3 + 0 - V_3 Z_4 + V_4(Z_2 + Z_3 + Z_4) ,$$

and

$$0 = 0 - V_2 Z_4 + V_3(2Z_4 + Z_5) - V_4 Z_4 . \qquad (1)$$

Notice at this point that if the rotor is allowed only translatory motion, $V_2 = V_4$. Making this substitution we find:

$$F = V_1(Z_1 + 2Z_3) - 2V_2 Z_3 ,$$

$$0 = -V_1 Z_3 + V_2(Z_2 + Z_3 + Z_4) - V_3 Z_4 ,$$

$$0 = -V_1 Z_3 + V_2(Z_2 + Z_3 + Z_4) - V_3 Z_4 ,$$

and

$$0 = -2V_2 Z_4 + V_3(2Z_4 + Z_5) . \qquad (2)$$

Since two of these equations are now identical, we actually have only three equations in the three unknowns

$$F = V_1(Z_1 + 2Z_3) - 2V_2 Z_3$$

$$0 = -V_1 Z_3 + V_2(Z_2 + Z_3 + Z_4) - Z_4 V_3$$

and

$$0 = -2V_2 Z_4 + V_3(2Z_4 + Z_5) . \qquad (3)$$

Equation (3) represents a system with three-degrees-of-freedom represented by the mechanical circuit in Item (a), Fig. 5 and the

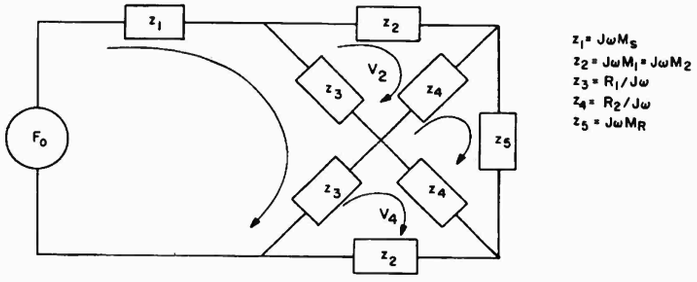

Fig. 4 - Motor mechanical circuit

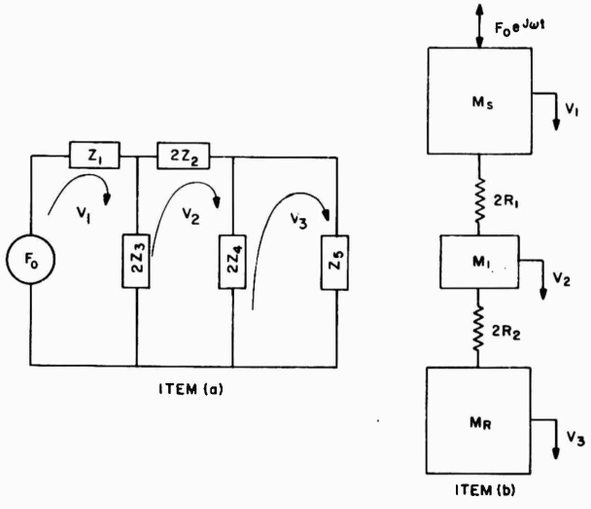

Fig. 5 - Simplified motor mechanical circuit

system in Item (b), Fig. 5. It may be pointed out here that the same three equations could have been obtained directly from the assumptions by combining k_1, k_2, M_1, and M_2, using the formula for parallel impedances and remembering that $M_1 = M_2$.

If one sets the determinant of the velocities equal to zero and substitutes the values of the various impedances in the expression, the resonant frequencies of the system are directly obtained and are found to be

$$\omega_1^2 = \frac{2k_1}{M_S} \; ; \quad \omega_2^2 = \frac{2k_2}{M_R} \; ; \quad \omega_3^2 = \frac{k_1 + k_2}{M_1} \; . \qquad (4)$$

Solving Eq. (3) for the velocities, one obtains

$$V_1 = \frac{F_o\left[2(Z_2 + Z_3 + Z_4)(2Z_4 + Z_5) - 4Z_4^2\right]}{(Z_1 + 2Z_3)\left[2(Z_2 + Z_3 + Z_4)(2Z_4 + Z_5) - 4Z_4^2\right] - 4Z_3^2(2Z_4 + Z_5)} \; ,$$

$$V_2 = \frac{F_o\left[2Z_3(2Z_4 + Z_5)\right]}{(Z_1 + 2Z_3)\left[2(Z_2 + Z_3 + Z_4)(2Z_4 + Z_5) - 4Z_4^2\right] - 4Z_3^2(2Z_4 + Z_5)} \; ,$$

and

$$V_3 = \frac{F_o\left[4Z_3 Z_4\right]}{(Z_1 + 2Z_3)\left[2(Z_2 + Z_3 + Z_4)(2Z_4 + Z_5) - 4Z_4^2\right] - 4Z_3^2(2Z_4 + Z_5)} \; . \qquad (5)$$

Remembering that an impedance is defined as the ratio of force to velocity and substituting values we obtain:

$$Z_D = \frac{F_o}{V_1} = \frac{M_S}{j\omega}(\omega_1^2 - \omega^2) + \frac{2k_1^2\left[M_R(\omega_2^2 - \omega^2)\right]}{j\omega\left[2k_2^2 - 2M_1 M_R(\omega_2^2 - \omega^2)(\omega_3^2 - \omega^2)\right]} \; ,$$

$$Z_{T1} = \frac{F_o}{V_2} = \frac{M_S(\omega_1^2 - \omega^2)\left[M_1 M_R(\omega_2^2 - \omega^2)(\omega_3^2 - \omega^2) - 2k_2^2\right]}{j\omega k_1 M_1(\omega_2^2 - \omega^2)} - \frac{2k_1}{j\omega} \; ,$$

and

$$Z_{T2} = \frac{F_o}{V_3} = \frac{M_S(\omega_1^2 - \omega^2)\left[M_1 M_R(\omega_2^2 - \omega^2)(\omega_3^2 - \omega^2) - 2k_2^2\right] - 2k_1^2 M_R(\omega_2^2 - \omega^2)}{j2\omega k_1 k_2} \; . \qquad (6)$$

The three expressions for the magnitude of the impedance of the structure with the information shown in Table 1 were programmed for an IBM (1401) computer. The resultant curves are shown in Figs. 6, 7, and 8.

TABLE 1

	Mass (lb-sec^2/in.)	Spring Constant (lb/in.)
M_S	1.310	Infinite
M_R	0.785	Infinite
M_1, M_2	0.0934	Infinite
k_1	0	2×10^7
k_2	0	6.5×10^5

EXPERIMENTAL VERIFICATION

Figure 9 shows schematically the instrumentation used to determine the various mechanical impedances required. The impedance curves which correspond to the theory are shown in Figs. 10 through 14. In comparing theory and experiment, the corresponding curves are as follows:

1. Fig. 6 - Figs. 10 and 11
2. Fig. 7 - Figs. 13 and 14
3. Fig. 8 - Fig. 12

If the presence of the stator and rotor cylinder frequencies is ignored, correlation between theory and experiment is quite good.

Figures 10 and 11 are driving point impedances measured at the stator mass center. In each figure there is a predominant resonance between 100 and 200 cps. The only difference between the two curves was the method of structure excitation. For the data in Fig. 10, the shaker drove into a small aluminum cone

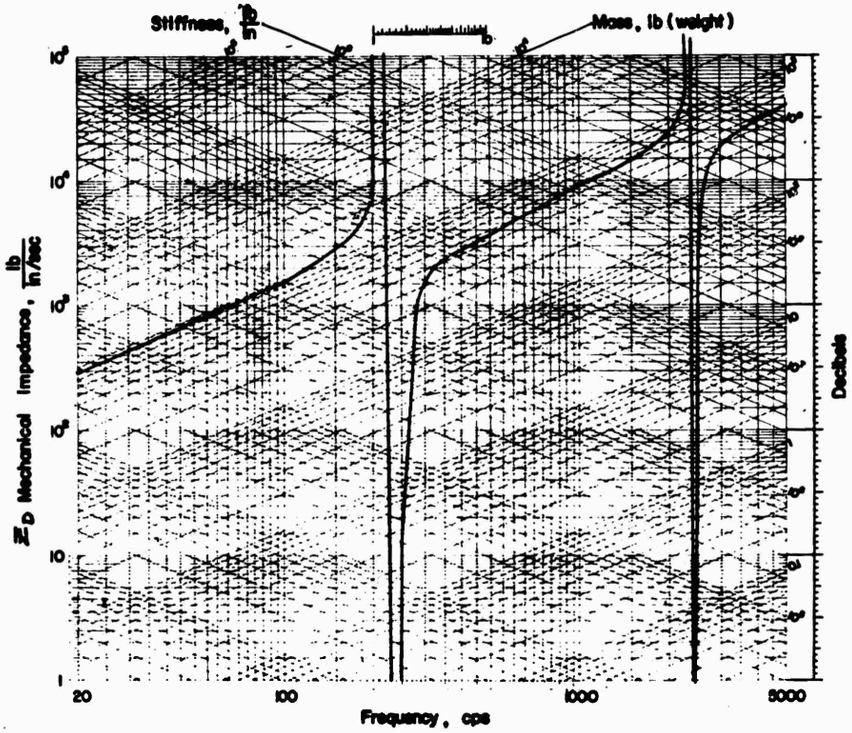

Fig. 6 - Theoretical driving point impedance

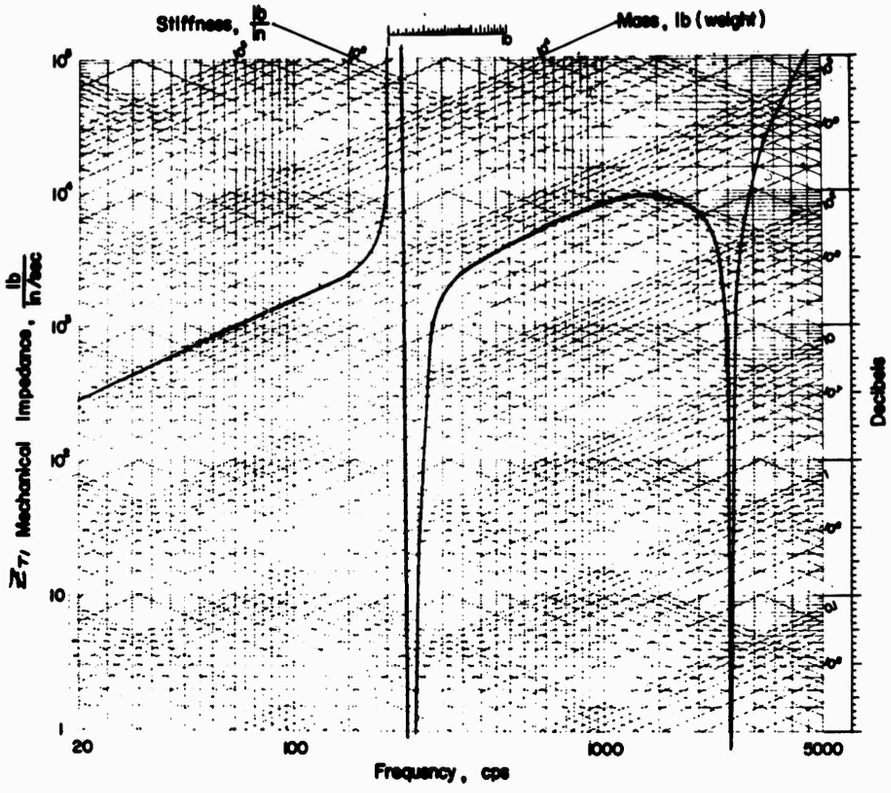

Fig. 7 - Theoretical transfer impedance

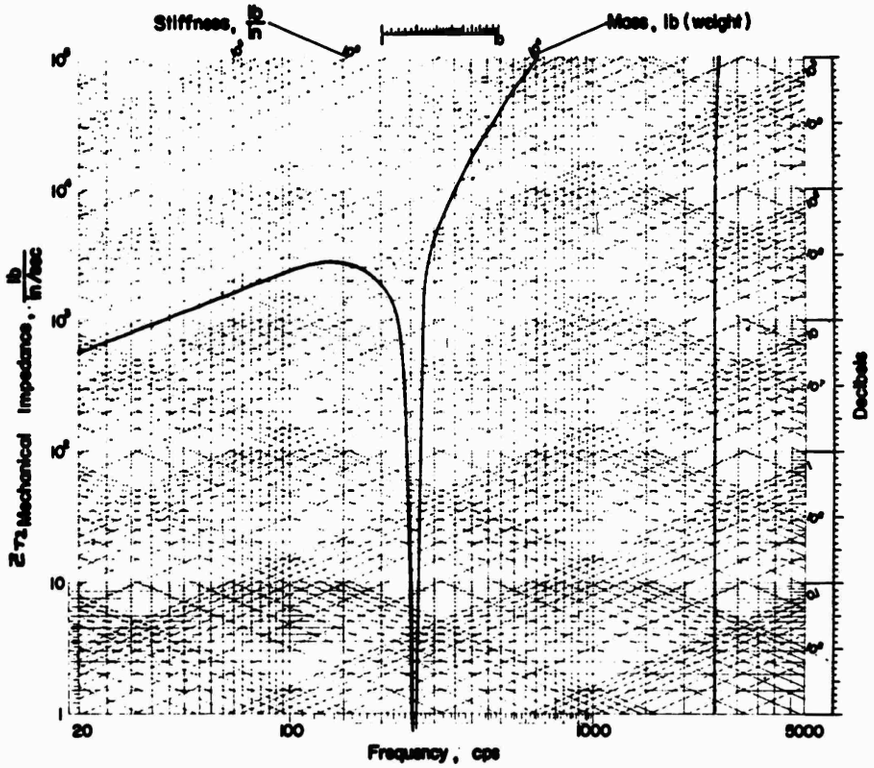

Fig. 8 - Theoretical transfer impedance

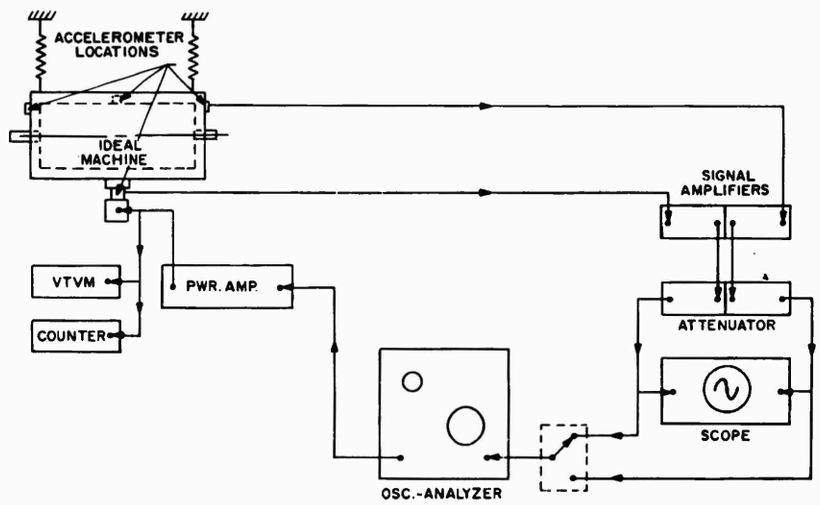

Fig. 9 - Experimental arrangements

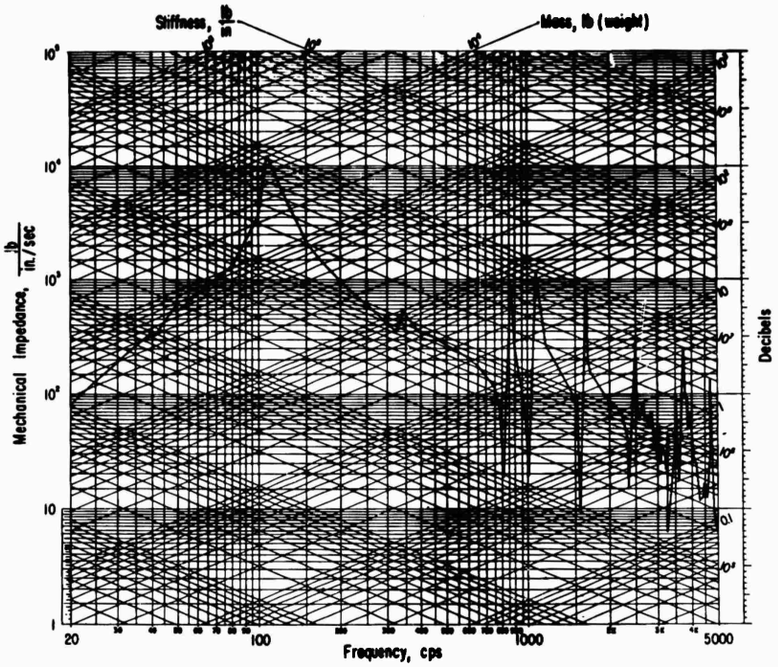

Fig. 10 - Driving point impedance measured at the stator mass center

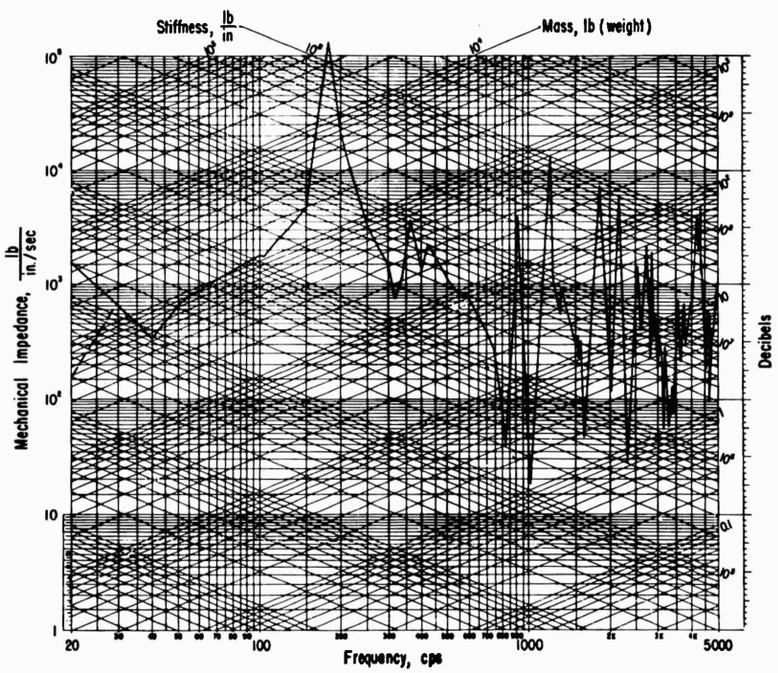

Fig. 11 - Driving point impedance measured at the stator mass center

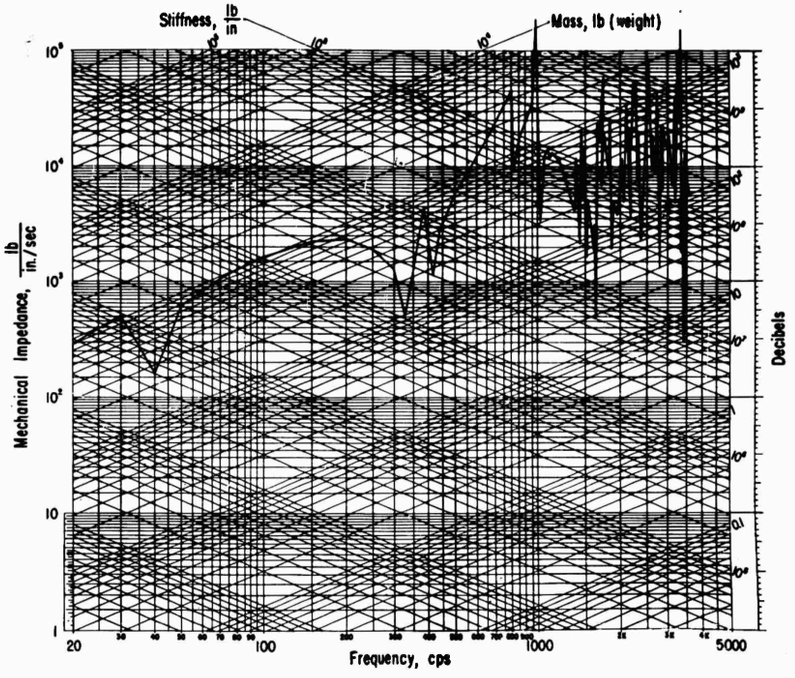

Fig. 12 - Measured transfer impedance

adaptor, while for the data in Fig. 11 a steel block, epoxied to the stator, was used. The shift in frequency obtained by different excitation methods indicates that the resonance is a function of the method of excitation and not a legitimate machine resonance. Verification of this local effect is the only reason for both sets of data and future remarks will pertain to Fig. 11 only.

The next frequencies of interest are 332, 357, and 420 cps. Detailed mode studies show that the first two are the theoretically predicted frequencies shown in Fig. 6. The 420-cps frequency was found to be one of the stator-cylinder mode frequencies corresponding to one axial half-wave and three circumferential node pairs. Further verification is obtained by comparing the remaining sets of corresponding graphs. If one compares Figs. 13 and 14, the transfer impedance to the inner rings on either end, surprisingly good agreement is obtained. The small variation in frequency can be attributed to manufacturing imperfections. It should be pointed out here that while in general the theoretical and experimental agree in shape and magnitude, many more resonances appear in the experimental data. These resonances can be attributed to the many stator and rotor natural frequencies which were ignored in the theoretical study. If these modes were sufficiently damped, it is probable that even better agreement could be obtained.

CONCLUSIONS

The principal conclusion that may be drawn from the portion of the program thus far completed is that mechanical impedance techniques can be used successfully to predict the rigid body resonances of a machine if a correct mathematical model is chosen.

ACKNOWLEDGMENT

The author wishes to publicly thank the U.S. Navy Marine Engineering Laboratory for permission to publish this work.

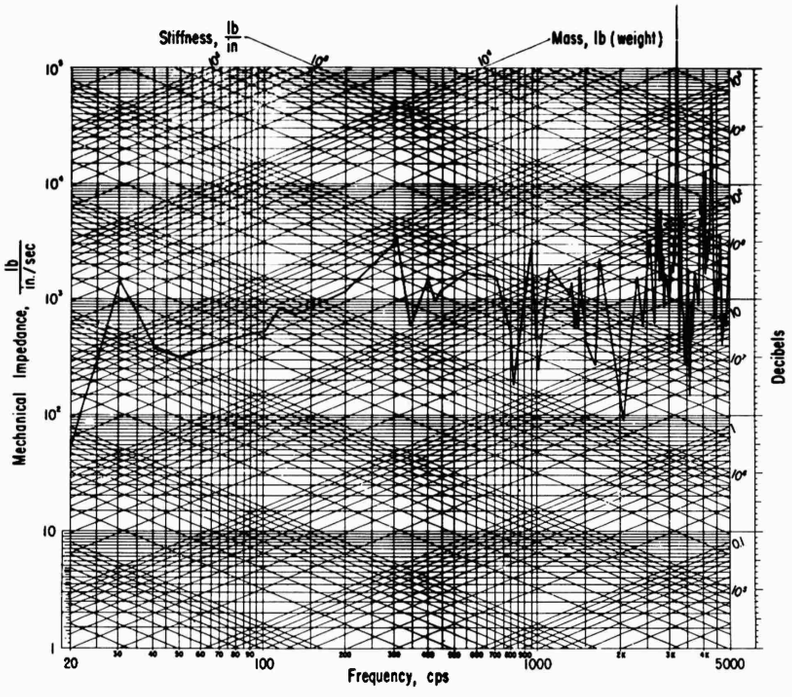

Fig. 13 - Measured transfer impedance

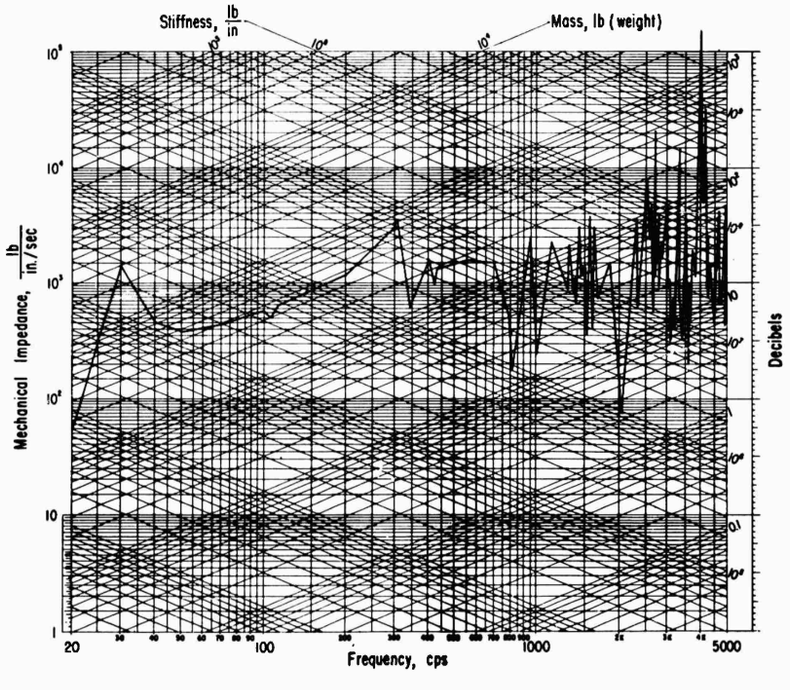

Fig. 14 - Measured transfer impedance

BIBLIOGRAPHY

Schwartz, J.I., U.S. Naval Engineering Experiment Station Report 85 498F, Phase Report I (July 25, 1963).

Schwartz, J.I., U.S. Naval Engineering Experiment Station Report 85 498 F, Phase Report II (to be published).

LIST OF SYMBOLS

M_S - Mass of Stator and Outer Ring

M_1, M_2 - Mass of Inner Ring

M_R - Mass of Rotor

k_1 - Spring Constant of Transducers

k_2 - Spring Constant of Bearings

V_1 - Stator Velocity

V_2 - Inner Ring Velocity

V_3 - Rotor Velocity

F_o - Force

Z - Mechanical Impedance

j - Complex Operator

ω - Circular Frequency

Z_D - Stator Driving Point Impedance

Z_{T1} - Stator to Inner Ring Transfer Impedance

Z_{T2} - Stator to Rotor Transfer Impedance

t - Time, seconds

$\omega_1, \omega_2, \omega_3$ - System Resonant Frequencies

DISCUSSION

Dr. Bouche (Endevco Corp.): I note that when you changed your fixture from aluminum to steel, your resonance frequency went up from about 100 cps to 200 cps. Do you think this means that you have to be very careful with the fixturing when trying to measure the impedance of a very large mass?

Mr. Schwartz: Yes, I would say so, especially when you have a rather large mass of relatively thin sections, as we had in this particular case. We were using a small aluminum cone with a total diameter of roughly one half inch, and it was driving into a 900-pound mass. I then shifted to using the impedance head to drive into a 3-inch square steel block, which of course, greatly stiffened the bottom portion of the stator. This caused the shift in resonance frequency.

Mr. Schloss (David Taylor Model Basin): This question brings out the age old problem that you want to measure something but the measuring attachments affect what you want to measure. In a sense, a change in the boundary conditions results by attaching impedance heads, and it really has nothing to do with the impedance test itself. The only way to get around this trouble is to use attachments which dynamically have as low an inertia as possible.

Mr. Schwartz: What you say is true. I don't think, however, that we had a low rotational impedance problem here. It was a case of local bending in the structure itself, and this local resonant effect was making what we were trying to find. I made the change in the method of attachment hoping to get rid of the resonance so that I could see what I was hunting for. It turned out that it did shift the frequency somewhat, but not enough.

* * *

LOW-FREQUENCY HULL MOBILITY

D. C. Robinson and J. T. Cummings
David Taylor Model Basin
Washington 7, D. C.

The significant natural frequencies of ship hulls usually occur below 25 cps. The David Taylor Model Basin uses vibration generators of various force capacities to measure the response of a hull at a natural frequency to a known force input. Also, underway trials are performed to determine the vibration response of a ship to wave, propulsion, and hydrodynamic force excitation. In addition, calculation techniques employing a digital computer are used to predict the response of a hull to either a constant or frequency-dependent force input.

The correlation between calculated prediction and experimental measurement of response is discussed. Current methods of approach to determine the hull damping values are presented.

INTRODUCTION

The subject of ship vibration is based on the elementary theory of beam vibrations. In the low frequency range, up to about 25 cps, a ship behaves like a free-free nonuniform beam. Hence, the theory of beam vibrations is useful in this frequency range. The beam theory, however, must be modified even within this frequency range due to the peculiarities which distinguish a ship from the classical uniform beam. The theory so developed must be verified and improved based on measurements. Two types of measurements presently made on ships are discussed; vibration generator tests on the NS SAVANNAH and underway vibration trials on the USS OKINAWA (LPH-3) are given as examples. Conclusions based on correlation of calculated and measured vibrations on these two ships are presented.

APPLICATION OF BEAM THEORY TO SHIP VIBRATION

The subject of this paper is "Low Frequency Hull Mobility," which is one of the many vibration disciplines in which the David Taylor Model Basin is engaged for the Navy. The Model Basin has developed over a number of years a rational theory of ship vibration, which is based on the elementary theory of the vibration of beams with important modifications. The theories of ship vibration are verified by correlating calculations with vibration measurements. One of the most valuable vibration measurements on a ship is performed with a vibration generator. The Model Basin uses vibration generators of various force capacities to measure the response of a hull at a natural frequency to a known force input. In addition, calculation techniques employing a digital computer are used to predict the response of a hull to either a constant or frequency-dependent force input. The correlation between calculation and experimental measurement of hull response will be discussed in this paper, but first some general background on ship hull vibration will be reviewed.

Elastic vibrations on a ship fall into two general categories: local vibrations and vibrations which are observed throughout the hull. The latter, in general, are of the type that may exist in a beam free in space and so are called "beamlike." Although the water surrounding a ship plays an important role in these vibrations, it does not destroy their beamlike characteristics. This analogy of ship vibration to beam vibration, however, is only valid for the low frequency hull modes. For high frequencies, the discontinuous mass and elastic properties of a ship become increasingly important, and the analogy of a vibrating ship to a beam loses significance. The significant or beamlike natural frequencies of ship hulls, that is, those of large amplitude, usually occur below 25 cps.

A beam free in space may undergo four principal types of elastic deformation designated as bending, twisting, shearing and longitudinal deformations. These may occur simultaneously. In the case of a ship, the elastic deformations that play a significant role in its vibration are limited to bending and shearing in both the vertical and horizontal planes through its neutral axes and to torsion about the longitudinal axis. It should be noted that a ship departs from the ideal beam usually considered in elementary vibration theory in that its cross section is large relative to its length. From a vibration standpoint, this means that the influence of shearing is much larger for a ship than for a thin beam and may influence considerably even the low frequency hull modes.

An important factor which distinguishes a vibrating ship from ordinary beam vibration is the influence of the water surrounding a ship. Water can actually exert only normal pressures and frictional forces on the hull, but these forces may be broken down into components. A component of the water force that is proportional to the acceleration of the hull at the point of interest and opposite to the acceleration in direction, produces the effect of increased ship inertia. The relatively high density of water makes this inertia effect of serious concern in the vibration of ships. This added mass concept is based on the assumption of incompressibility of the water, which is valid only for low frequencies. Figure 1 shows the magnitude of the added mass of water relative to the mass of a hull.

EXCITATION OF SHIP NATURAL FREQUENCIES

A hull is a much more complicated structure than a solid beam and, as has been mentioned, behaves like a free-free beam only in its lower modes of vibration. These beamlike modes may be excited by either transient or steady-state disturbances. The transient disturbances may be due to wave or slamming impacts which induce trains of damped vibrations in one or more of these modes simultaneously. Steady-state vibrations are caused by rotating unbalanced engine or machine elements, unbalanced propellers, or unbalanced shafting. Vibration may also be set up by nonuniformity of pitch among the blades of a propeller and by the variation in load on the individual blades as they rotate in the nonuniform velocity field in the propeller race. The propeller also causes pressure fluctuations on the surface of the hull and appendages in their immediate vicinity. Propeller blade excitation is the chief cause of steady-state ship vibration of most ships. Figure 2 shows a surface ship with the various forces which may act on the ship.

A common characteristic of the forced propeller-excited vibration of ships is that it is concentrated in the stern. Since all the beamlike modes of vibration involve large amplitudes at both ends of the hull, this phenomenon does not result from vibration in a single mode. It is due to the resultant of the nonresonant responses in several modes.

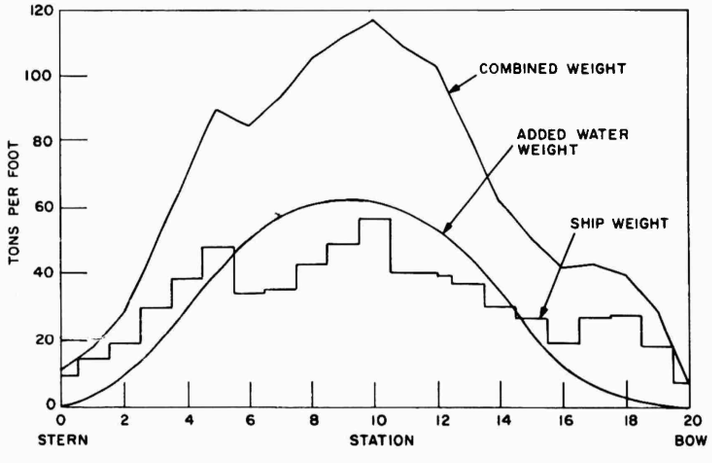

Fig. 1 - Typical weight curve used for calculation of mode shapes

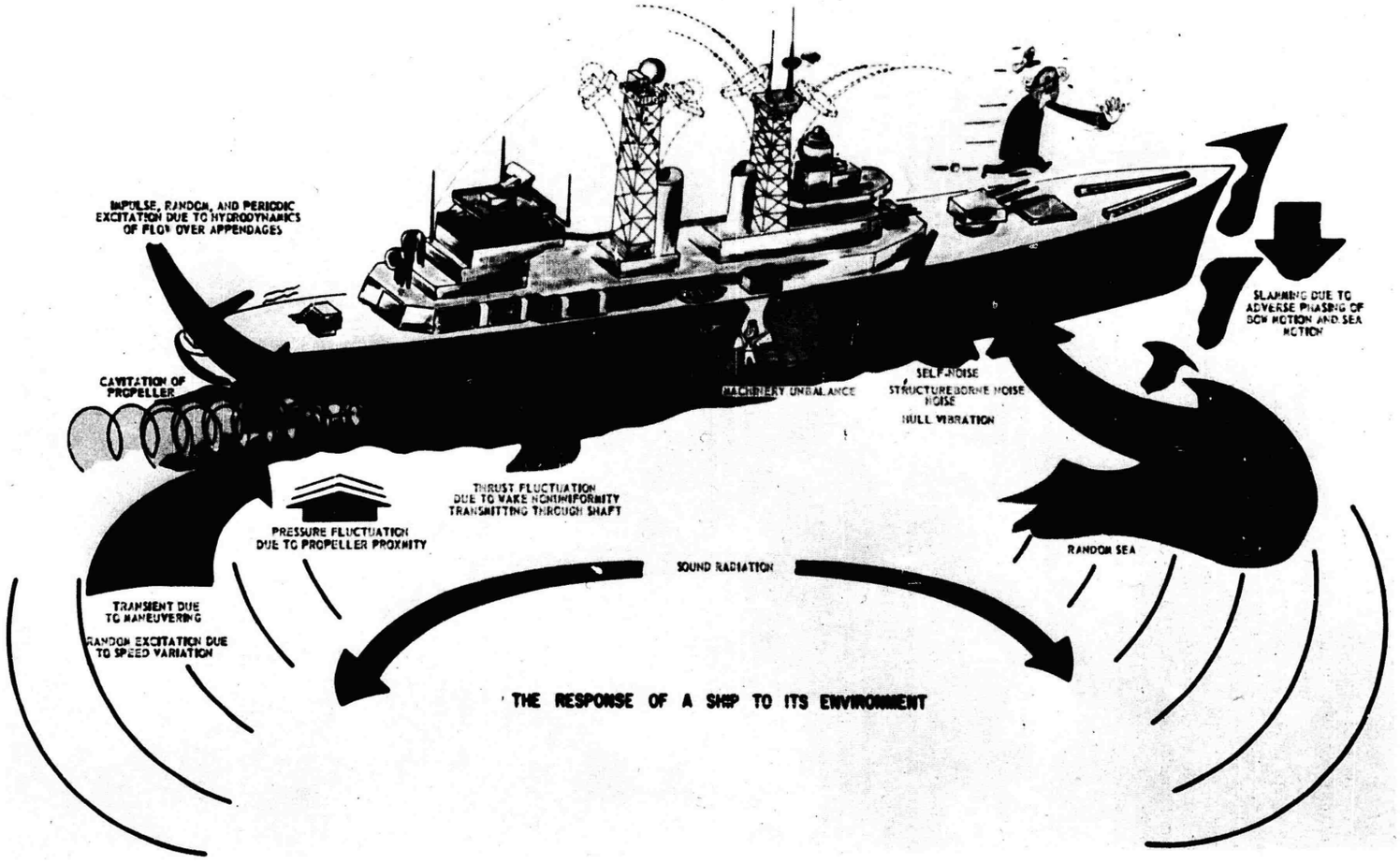

Fig. 2 - The response of a ship to its environment

One of the properties of the normal modes of ideal beams that is important for forced vibration is the influence function. The normal mode influence relation states that the normal mode pattern determines the influence of the point of application of a simple harmonic driving force on the magnitude of the amplitude excited in that mode. Thus, a given force will not excite a mode which has a nodal point at its point of application and will excite the maximum amplitude in the mode when applied at the point where the normal mode pattern is at a maximum. Use of this property arises in the performance of vibration generator tests on ships, as will be discussed later.

LOW FREQUENCY HULL MOBILITY CALCULATIONS

The normal modes of a vibrating body are the patterns in which the body can vibrate freely after the removal of external forces. The normal modes of vibration of the ideal free-free beam are independent of one another; and in general, exciting forces will cause the beam to vibrate in many of these modes simultaneously.

Patterns of typical flexural and torsional modes of a free-free uniform bar are shown in Fig. 3. The significant modes of a vibrating hull have mode shapes similar to those shown.

The partial differential equations of ship vibration, for reasons of brevity, will not be presented in this paper. An excellent discussion of these equations may be found in Refs. 1 and 2. Here it is only mentioned that these equations are similar to the equations of flexural and torsional motion for a uniform beam with the addition of terms for shear and rotary inertia.

The parameters in the differential equations cannot be expressed as continuous functions of the space variables, and hence, analytical solutions of these equations are not possible; graphical, analog, or digital methods must be used.

Digital calculations can be made on computers by converting the differential equations into equivalent finite difference equations and

[1] R. T. McGoldrick, "Ship Vibration," DTMB Report 1451 (Dec. 1960).

[2] R. C. Leibowitz and E. H. Kennard, "Theory of Freely Vibrating Nonuniform Beams, Including Methods of Solution and Application to Ships," DTMB Report 1317 (May 1961).

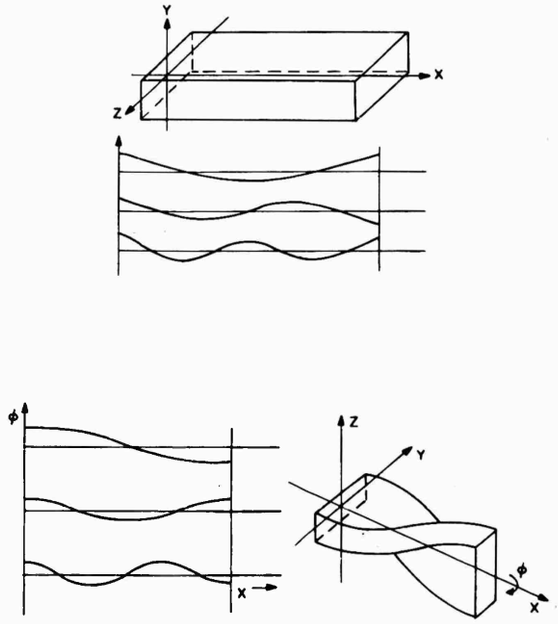

Fig. 3 - Flexural and torsional modes of a free-free uniform bar

following the general method suggested by Prohl and Myklestad.[3] The entire ship is assumed to be executing simple harmonic vibrations. The normal mode problem is to find those frequencies and the corresponding patterns or normal mode shapes for which, in the absence of damping, a steady free vibration is possible without external forces or moments. If the ship is subdivided into an equivalent "lumped" system, the relations between the internal forces and moments acting on adjacent lumps are given in terms of the motion of these lumps or elements by the finite difference equations. It has been found that if a ship is divided into 20 sections, as shown in Fig. 4, and the parameters evaluated for each of these stations, sufficient accuracy is obtained to calculate the significant hull modes.

linear system during the frequency range under discussion; experimental evidence supports this assumption. Hence, the principle of superposition applies, and the motion of a ship can be considered to be composed of independent normal modes. It is assumed, on the basis of experience, that under a simple harmonic driving force a hull can respond in only a limited number of normal mode components.

In harmony with the rational or semi-empirical beam theory of hull vibration developed at the Model Basin, a damping coefficient c is used which represents a damping force per unit velocity, per unit length.

This coefficient is restricted to either of two types: the Rayleigh type which is viscous

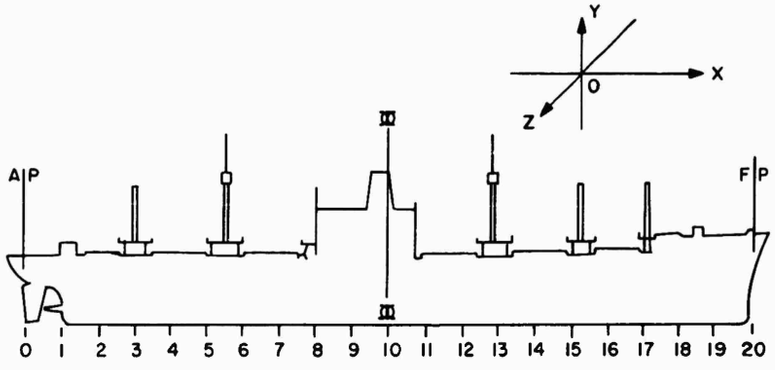

Fig. 4 - Illustration of breakdown of a ship and orientation of axes for digital calculation

The calculation of forced vibration by the use of finite difference equations is based on the general theory as used for free vibration with the addition of damping terms. The damping action is assumed to be represented in the lumped system by a series of ideal dashpots acting between the masses and a frame of reference fixed in space, each exerting a force proportional to the linear velocity but in the opposite direction.

For the beamlike modes of hull vibration, an analysis of forced vibration response of hulls, based on the normal mode method, is useful. It is assumed that a ship behaves as a

and proportional to mass, so that c/μ is constant (where μ is the mass per unit length of the hull including the allowance for added mass of the surrounding water),[4] or the type increasing with frequency so that $c/\mu\omega$ is constant, where ω is the circular frequency.[5] The assumption of viscous damping does not mean that the energy must be absorbed by the surrounding water. But the use of a viscous damping constant is based on the assumption that an equivalent viscous damping constant can be found and that its value is independent of frequency and amplitude. The data available

[3] A. W. Mathewson, "Preparations of Data for Computation of Vertical Flexural Modes of Hull Vibration by Digital Process," DTMB Report 632 (Sept. 1949).

[4] E. J. Adams, "The Steady-State Response of a Ship Hull to a Simple Harmonic Driving Force Computed by a Digital Process," DTMB Report 715 (May 1950).

[5] R. C. Leibowitz, "Effects of Damping on Modes of Vertical Vibration of Hull of USS THRESHER (SS(N)593)," DTMB Report 1384 (Mar. 1960).

suggest that the damping constant increases with both amplitude and frequency; and hence, the damping coefficient which increases with frequency is currently used in the calculations of the forced vibratory response of hulls.

From measurements of the decay of the first mode of vertical vibration excited by dropping and then snubbing the anchor of a ship, it has been found that the logarithmic decrement is approximately 0.1, which corresponds to a value of $c/\mu\omega$ of approximately 0.03[1], which for a system with viscous damping corresponds to a ratio of damping to critical damping of about 1.5 percent.

By assuming that the damping of the flexural vibration of the hull can be represented by a distributed viscous damping constant proportional to the mass per unit length, the ship can be treated as a "Rayleigh System," at least in dealing with vibration in its significant flexural modes. Under such assumptions, the forced vibrations of the hull may be treated in terms of normal mode responses.

The independent behavior of the normal modes of mass elastic systems permits the use of the convenient concept of effective systems of one-degree-of-freedom, each representing a normal mode. There are various ways of defining such effective systems. They may be defined with respect to a particular driving point or without this restriction. When the hull is represented by an equivalent lumped system, its effective mass at a driving point d in the i^{th} normal mode is

$$m_{di} = \frac{\Sigma m Y_i^2}{Y_{di}^2}, \tag{1}$$

where Y_i is the amplitude at any station in the i^{th} normal mode pattern, Y_{di} is the normal mode amplitude at the driving point, and the summation includes the total number of lumps into which the hull is subdivided.

The effective spring constant of the one-degree system is given by the equation

$$k_{di} = m_{di}\,\omega_i^2, \tag{2}$$

where ω_i is the circular frequency of the i^{th} normal mode, and the effective damping constant is given for Rayleigh damping by the equation

$$c_{di} = (\text{constant}) \times m_{di}. \tag{3}$$

The effective system can thus be visualized as the familiar one-degree-of-freedom system usually considered in vibration theory. The steady-state amplitude is

$$Y_{di} = \frac{P}{k_{di} - m_{di}\,\omega^2 + j c_{di}\,\omega}. \tag{4}$$

This gives not only the magnitude of the displacement amplitude in the i^{th} mode but also the phase of its rotating vector in relation to that of the driving force of circular frequency ω.

A mechanical mobility may be defined on the basis of either displacement amplitude or velocity amplitude. In naval architecture, the designer is much more familiar with levels of vibration expressed in terms of displacement amplitude than in terms of vibratory velocity amplitude. When the mechanical mobility is based on displacement, it is the ratio of the displacement amplitude at the driving point to the amplitude of the driving force. Thus

$$M = \frac{Y}{P}. \tag{5}$$

The mobilities in the various modes combine by direct addition to give the net driving point mobility; that is,

$$M_d = \sum_{i=1}^{n} M_{di}. \tag{6}$$

It is a common observation that, when the frequency of propeller exciting forces of a propulsion device is well above the range of significant hull mode frequencies, the forced vibration of the hull is concentrated in the stern of the ship and settles down to a fairly constant level regardless of the speed, unless a local resonance of some structure in the stern is encountered.

At high frequencies, the inertia component is the major component of mobility when the damping is of the Rayleigh type. If the elastic and damping components are then neglected, the mobility becomes

$$M = \frac{1}{m_{di}\,\omega^2}, \tag{7}$$

and the net mobility has the form

$$M_d = \sum \frac{1}{m_{di}\,\omega^2} = \frac{1}{\omega^2} \sum \frac{1}{m_{di}}. \tag{8}$$

This indicates that under forces increasing as the square of the frequency, the stern amplitude will remain constant at shaft speeds above the range of significant hull criticals.

In any calculations dealing with response in a single mode, experience has shown it feasible to assume that the logarithmic decrement remains constant; hence, it is expedient to assume

$$\frac{c_{di}}{m_{di}\omega_i} = \text{constant}. \tag{9}$$

In deriving hull damping values from vibration generator tests, use can be made of the fact that at resonance the mechanical mobility in the mode in question is solely the damping mobility $1/c_{di}\omega$, expressed in absolute terms. Hence, the hull damping, c_{di} can be computed from the equation

$$c_{di} = \frac{P}{Y_{di}\omega_i}, \tag{10}$$

where P is the maximum value of the alternating force applied by the vibration generator, Y_{di} is the measured resonant amplitude at the driving point, and ω_i is the hull resonance frequency.

The critical damping is

$$(c_c)\,d_i = 2m_{di}\omega_i \tag{11}$$

at the point of excitation, and the logarithmic decrement is

$$\delta \simeq 2\pi \left(\frac{c}{c_c}\right)_{di}. \tag{12}$$

The values of the logarithmic decrements and the percent of critical damping of various modes on a destroyer, calculated on the basis of vibration generator data,[6] are given in Table 1.

TABLE 1
Damping Characteristics of a Destroyer Calculated[a] on the Basis of Vibration Generator Data

Type of Vibration	Number of Nodes	Logarithmic Decrement	Percent of Critical Damping
Horizontal Flexural	2	0.024	0.37
	3	0.053	0.84
Vertical Flexural	2	0.055	0.88
	3	0.028	0.45
	4	0.040	0.63
	5	0.15	2.38
Torsional	1	0.11	1.75

[a]These calculations are made under the assumption that the damping is viscous in character.

PROCEDURE FOR CALCULATION OF HULL RESPONSE

The calculated hull responses for two ships, NS SAVANNAH and USS OKINAWA (LPH-3), are presented in this paper. The NS SAVANNAH (Fig. 5) is a P2-N1-MA40 nuclear-powered passenger-cargo ship, similar to the MARINER Class, designed by the U.S. Maritime Administration. Its principal characteristics are shown in Table 2. The USS OKINAWA (LPH-3), Fig. 6,

[6]N. H. Jasper, "Structural Vibration Problems of Ships: A Study of the DD694 Class Destroyers," DTMB Report C-36 (Feb. 1950).

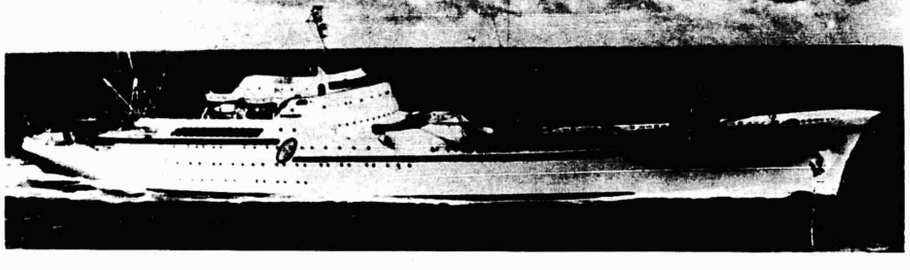

Fig. 5 - NS SAVANNAH

TABLE 2
Principal Characteristics of NS SAVANNAH and USS OKINAWA (LPH-3)

Characteristics	Ship	
	NS SAVANNAH	USS OKINAWA
Length between perpendiculars (ft)	539	556
Molded beam (ft)	78	84.2
Depth to main deck (ft)	50	47.2
Design draft (ft)	29.5	26.1
Length to beam ratio (L/B)	6.9	6.6
Length to depth ratio (L/D)	10.8	11.8
Beam to depth ratio (B/D)	1.6	1.8
Displacement (tons)		
Heavy load	21,840	18,482
Light load	11,850	15,691
Maximum shaft speed (rpm)	110	117
Number of propellers	1	1
Number of propeller blades	5	4

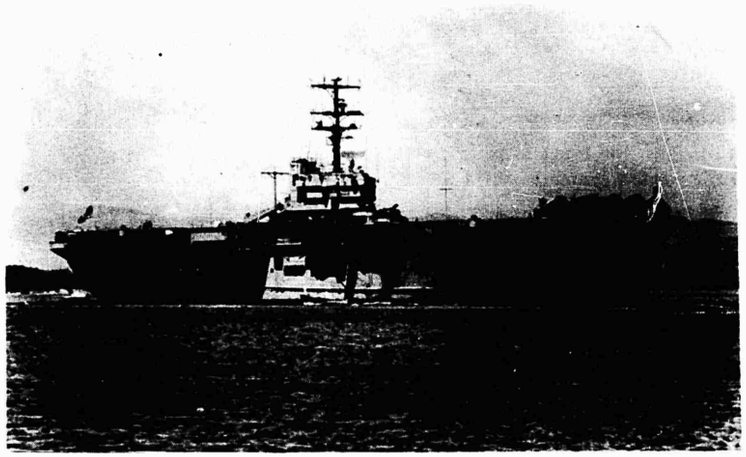

Fig. 6 - USS OKINAWA (LPH-3)

TABLE 3
Mass and Stiffness Data for Computing Vertical Flexural Vibration of NS SAVANNAH

($E = 13.4 \times 10^3$ (ton/in.^{2}); $G = 5.36 \times 10^6$ (lb/in.^{2}))

Station	Δx (ft)	$\mu \Delta x$ (ton-sec^2/ft)	$\Delta x/EI \times 10^8$ (1/ton-ft)	$\Delta x/KAG \times 10^6$ (ft/ton)
0	13.625			10.087
1/2	27.25	7.510	1.189	
1				7.211
1-1/2	27.25	14.20	0.4125	
2				5.290
2-1/2	27.25	27.73	0.2501	
3				4.833
3-1/2	27.25	40.01	0.1835	
4				4.622
4-1/2	27.25	54.91	0.1485	
5				4.483
5-1/2	27.25	59.04	0.1290	
6				4.491
6-1/2	27.25	62.18	0.1182	
7				4.588
7-1/2	27.25	71.99	0.1138	
8				4.584
8-1/2	27.25	75.69	0.1139	
9				4.475
9-1/2	27.25	101.48	0.1114	
10				4.429
10-1/2	27.25	101.63	0.1195	
11				4.656
11-1/2	27.25	60.09	0.1434	
12				5.172
12-1/2	27.25	54.88	0.1543	
13				5.556
13-1/2	27.25	54.03	0.1580	
14				5.643
14-1/2	27.25	47.15	0.1651	
15				5.386
15-1/2	27.25	35.95	0.1781	
16				5.064
16-1/2	27.25	25.20	0.2032	
17				4.805
17-1/2	27.25	14.55	0.2501	
18				4.580
18-1/2	27.25	8.235	0.3718	
19				5.274
19-1/2	27.25	7.647	1.0219	
20	13.625			6.707

is an amphibious assault ship, designed to carry personnel and helicopters. Its principal characteristics are also presented in Table 2.

For calculation purposes, each ship was divided into 20 sections of equal length, as explained previously. The mass and stiffness parameters were calculated for each station. The parameters for the NS SAVANNAH are given in Table 3; those for the USS OKINAWA are seen in Table 4. Calculations of vertical response were performed on a digital computer, using a damping factor $c/\mu\omega = 0.03$ and a driving force of 1 ton at station 0 (the stern). The

results of these calculations, which are reported in more detail in Refs. 7 and 8, are presented later in this paper in comparison with the experimentally determined hull response of each ship.

[7] J. T. Cummings, "Calculated Normal Modes and Natural Frequencies of NS SAVANNAH, Including Sprung Mass Considerations," DTMB Report 1787 (Dec. 1963).

[8] D. C. Robinson, "Calculated Natural Frequencies and Normal Modes of Vibration on the USS OKINAWA (LPH-3)," DTMB Report 1766 (Aug. 1963).

MEASUREMENT OF HULL RESPONSE ON NS SAVANNAH

As a part of the extensive safety and performance testing program planned for the NS SAVANNAH, the Maritime Administration

TABLE 4
Mass and Stiffness Data for Computing Vertical Flexural Vibration of USS OKINAWA (LPH-3)

Station	Ship Mass $\mu\Delta x$ (ton-sec^2/ft)	$\Delta x/KAG \times 10^6$ (ft/ton)	$\Delta x/EI \times 10^8$ (1/ton-ft)
0		7.07	
1/2	22.40		0.1183
1		9.42	
1-1/2	21.66		0.1455
2		9.55	
2-1/2	30.42		0.1280
3		9.23	
3-1/2	49.74		0.1083
4		8.08	
4-1/2	66.10		0.0881
5		6.58	
5-1/2	83.83		0.0707
6		5.40	
6-1/2	98.31		0.0586
7		4.94	
7-1/2	101.95		0.0521
8		4.74	
8-1/2	106.95		0.0506
9		4.82	
9-1/2	113.14		0.0522
10		4.88	
10-1/2	104.58		0.0540
11		4.82	
11-1/2	97.39		0.0548
12		4.74	
12-1/2	86.23		0.0552
13		4.80	
13-1/2	83.12		0.0588
14		4.95	
14-1/2	46.02		0.0655
15		5.12	
15-1/2	33.86		0.0734
16		4.36	
16-1/2	22.37		0.0955
17		5.66	
17-1/2	16.55		0.1499
18		6.01	
18-1/2	13.57		0.2301
19		6.50	
19-1/2	6.90		0.3317
20		7.16	

requested the David Taylor Model Basin to conduct a series of vibration trials on this ship. The first phases of these trials involved the DTMB 40,000-pound, three-mass, vibration generator, shown in Fig. 7.

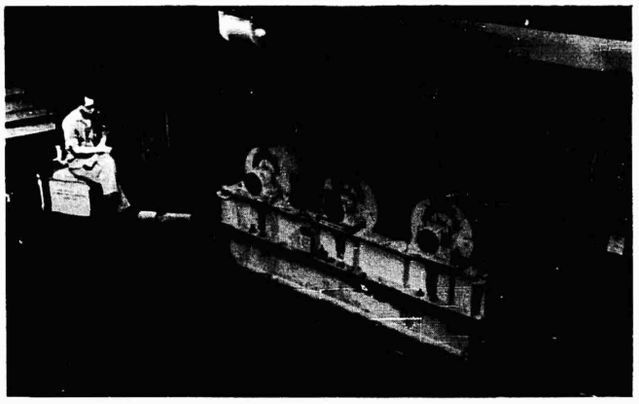

Fig. 7 - DTMB 40,000-pound, three-mass, vibration generator

The DTMB 40,000-pound, three-mass, vibration generator is a unique instrument designed to excite vibrations in large structures, such as ships. Forces up to 40,000 pounds in any direction perpendicular to the axis of rotation, and moments up to 120,000 ft-lb can be generated over a frequency range from 0.6 to 20 cps. Forces and moments are varied by adjusting the eccentricity of the three masses and changing the speed of rotation. The operation of the vibration generator is explained in Refs. 9 and 10.

For the conduct of these trials, the vibration generator was placed at the stern as close as possible to the plane of the propeller, as can be seen in Fig. 8. Temporary braces were installed under the vibration generator, as shown in Figs. 9 and 10, in order to reduce local vibration in the area of the generator and to transmit the force into the hull. The response of the hull was measured by velocity gages placed in various locations on "A" Deck (indicated by the dots in Fig. 8).

The response of the hull was measured on two occasions under different conditions. The first test was at dockside in Camden, New Jersey before the ship was completed; and the results of this test are reported in Ref. 11. The second test was conducted in deep water, while the ship was enroute to Yorktown, Virginia. The results of this trial are used in this paper and are reported in more detail in Ref. 12.

During both trials the vibration generator was operated over the range 90 to 900 rpm (1.5 to 15 cps). A 21-degree eccentricity setting was used from 90 to 550 rpm. Above this speed, as can be seen from Fig. 11, it was necessary to change the eccentricity setting to 6 degrees, in order not to exceed the force limit of the vibration generator.

Comparison of Calculated and Measured Response of NS SAVANNAH

Table 5 and Fig. 12 compare the calculated and measured response in the vertical direction of the NS SAVANNAH. The calculated response at station 0 and the measured response at Frame 226, which correspond to approximately

[9] Q. R. Robinson, "Vibration Machines at the David W. Taylor Model Basin," DTMB Report 821 (July 1952).

[10] R. L. Price, "The DTMB 40,000-Pound Vibration Generator: Its Description and Operation," DTMB Report 1771 (Nov. 1963).

[11] J. T. Birmingham, "Preliminary Results of Vibration Generator Tests on NS SAVANNAH at Dockside," DTMB Report 1527 (May 1961).

[12] C. J. Noonan and J. T. Cummings, "Vibration Generator Tests on NS SAVANNAH in Deep Water," DTMB Report 1784 (Nov. 1963).

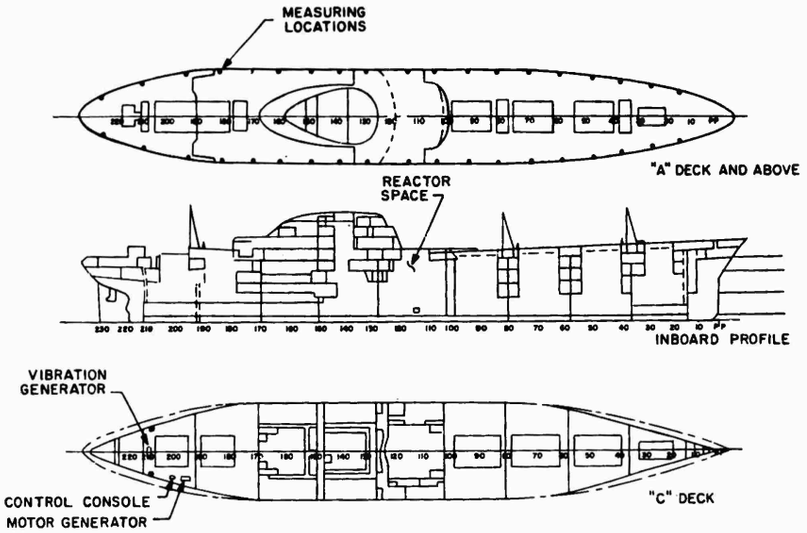

Fig. 8 - NS SAVANNAH inboard profile and plan view of "A" and "C" decks showing instrumentation positions and vibration generator location

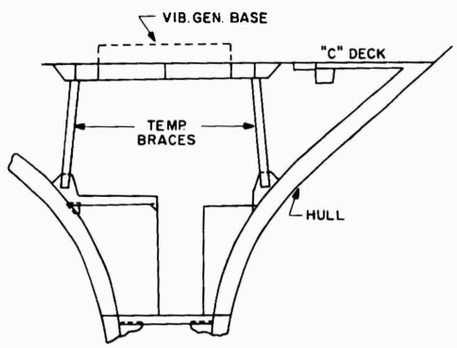

Fig. 9 - Bracing for vibration generator

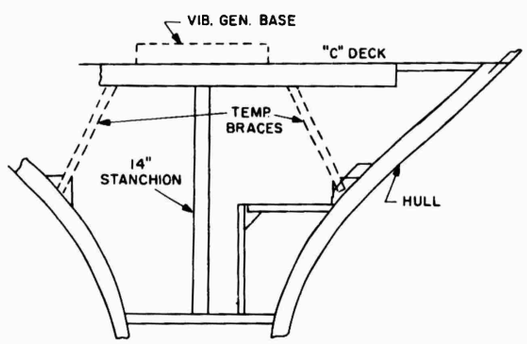

Fig. 10 - Bracing for vibration generator

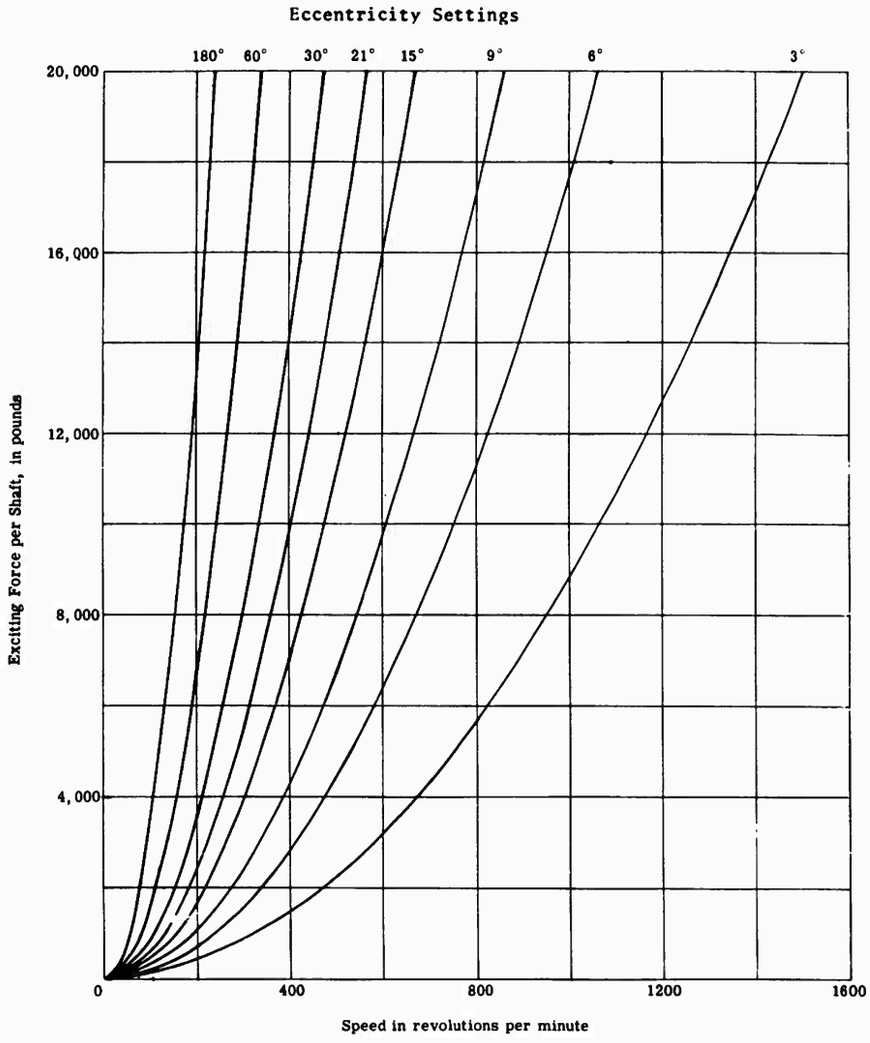

Fig. 11 - Vibration generator force -- speed curve

the same location, are presented. The measured response is normalized to a 1-ton driving force by dividing each measured amplitude response by the force in tons developed by the vibration generator at the generator speed at which each measurement was taken.

TABLE 5
Comparison of Calculated and Measured Resonant Frequencies, NS SAVANNAH

Mode	Calculated Frequencies (cps)	Measured Frequencies (cps)
1st	1.45	1.55
2nd	3.15	3.25
3rd	4.55	4.25
4th	6.25	6.00
5th	7.75	6.70

As can be seen from Table 5 and Fig. 12, the frequency correspondence between calculated and measured results is quite good for the first four modes. At higher frequencies, the ship bears less resemblance to a free-free beam; and as a result, the predicted frequency becomes less accurate. The amplitude correspondence suggests that a damping factor slightly higher than 0.03, which would result in slightly lower calculated amplitudes, might be appropriate. This conclusion is drawn despite the fact that the measured amplitude for the first mode is higher than the calculated. The measured amplitude at this frequency (1.5 cps) is somewhat questionable because of the nonlinear amplitude response at low frequencies of the velocity pickups used during the trials. The final phase of the vibration trials of the NS SAVANNAH, presently planned to be conducted after the completion of the overhaul now being carried out, is the determination of the response of the hull of propeller-excited vibration. It is hoped that a correlation of underway and vibration generator results will provide invaluable data regarding the amount of force exerted on the hull by the propeller.

The present lack of information regarding the magnitude of the hydrodynamic forces acting on the hull is sorely felt in the field of ship vibration. The NS SAVANNAH represents a unique opportunity to obtain this information because of the extensive calculation and vibration generator investigations already conducted.

MEASUREMENT OF HULL RESPONSE ON USS OKINAWA (LPH-3)

In addition to calculating the hull response of the USS OKINAWA, the Model Basin conducted underway vibration trials at sea during March, 1963. Velocity pickups were placed in several locations throughout the hull of the ship, which

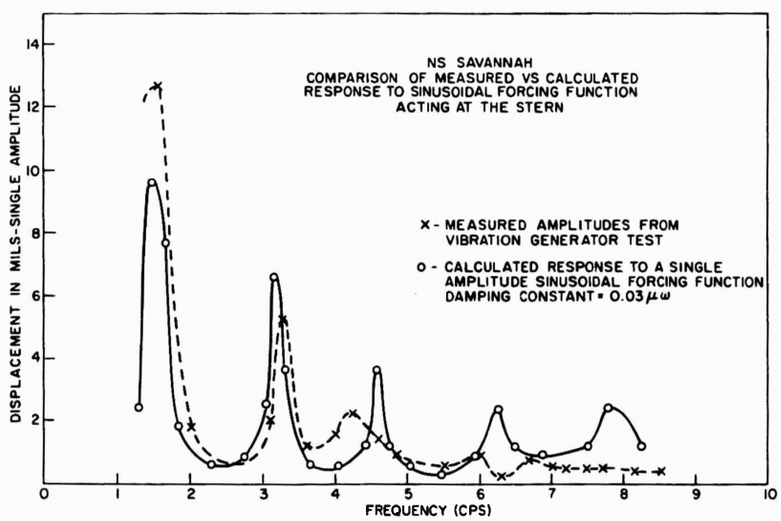

Fig. 12 - NS SAVANNAH hull response

is shown in outboard profile in Fig. 13. Measurements of propeller-induced vibration were made over a shaft speed range of 50 to 117 rpm, at approximately 5-rpm increments. This test is reported in more detail in Refs. 13 and 14.

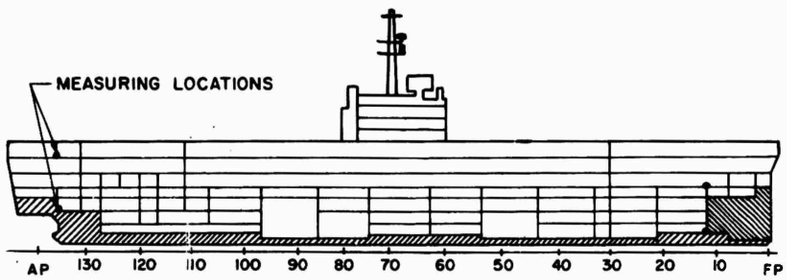

Fig. 13 - USS OKINAWA outboard profile

Comparison of Calculated and Measured Response of USS OKINAWA (LPH-3)

Table 6 and Fig. 14 compare the calculated and measured response in the vertical direction of the USS OKINAWA. The calculated response at station 0 and the measured response at Frame 135, which correspond to the same location, are presented.

TABLE 6
Comparison of Calculated and Measured Resonant Frequencies, USS OKINAWA (LPH-3)

Mode	Calculated Frequencies (cps)	Measured Frequencies (cps)
1st	1.9	1.8
2nd	3.3	3.3
3rd	4.75	4.7

The amplitudes of the measured response peaks were normalized relative to a constant driving force. For purposes of comparison to the calculated response in Fig. 14, the amplitude of the first measured peak was set equal to that of the first calculated peak; and then the following calculated peaks were adjusted accordingly.

From Fig. 14, it can be seen that the frequency correspondence between measured and calculated values is very good for the three measured peaks that can be identified. The amplitude correspondence suggests that a damping factor slightly lower than 0.03, which would result in slightly higher calculated peaks, might be appropriate. This inference can be drawn even though using a lower damping factor would increase the discrepancy between the amplitudes of the calculated and measured first mode, because, as in the case of the NS SAVANNAH, the frequency of the first mode lies in the range where the response of the velocity pickups used in the trial is nonlinear.

In the past, direct mobility measurements of hulls have not generally been made. The vibration response of ships is usually given in the form of curves showing displacement amplitude versus frequency. Data from vibration generator tests, however, can be presented to show the variation of mechanical mobility with frequency. In Fig. 15, there is shown the mechanical mobility versus frequency for the NS SAVANNAH. The calculated mobility, which is based on a damping constant of 0.03, is also given. As can be seen from the figure, there is a relatively large variation in the mobility for the low frequencies – the peaks corresponding to the low hull modes. The variation in mobility diminishes as the frequency increases, during which the inertial component becomes the predominant component of the mobility.

DAMPING

The damping factor of 0.03, which is presently used in the calculation of the forced

[13] D. C. Robinson, "Preliminary Report on Underway Vibration Trials of the USS OKINAWA (LPH-3), March 1963," DTMB Technical Note SML-760-54 (May 1963).

[14] D. C. Robinson, "Vibration Survey on USS OKINAWA (LPH-3)," DTMB Report (in preparation).

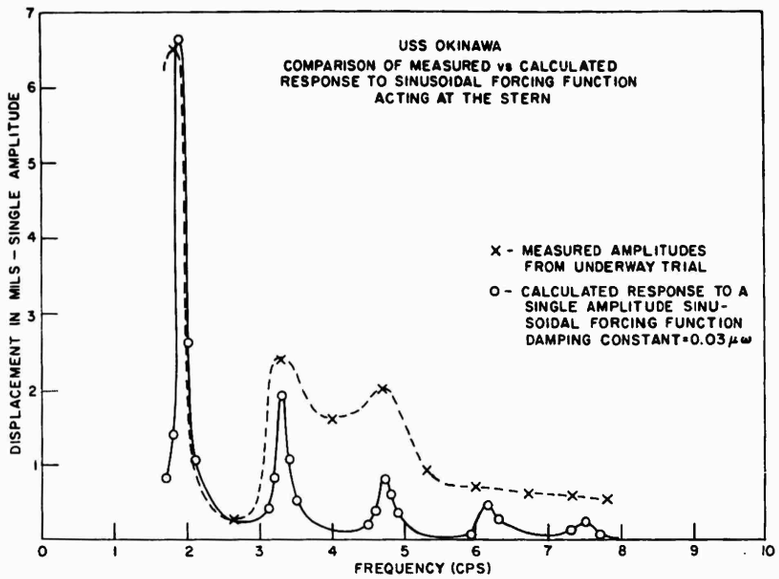

Fig. 14 - USS OKINAWA hull response

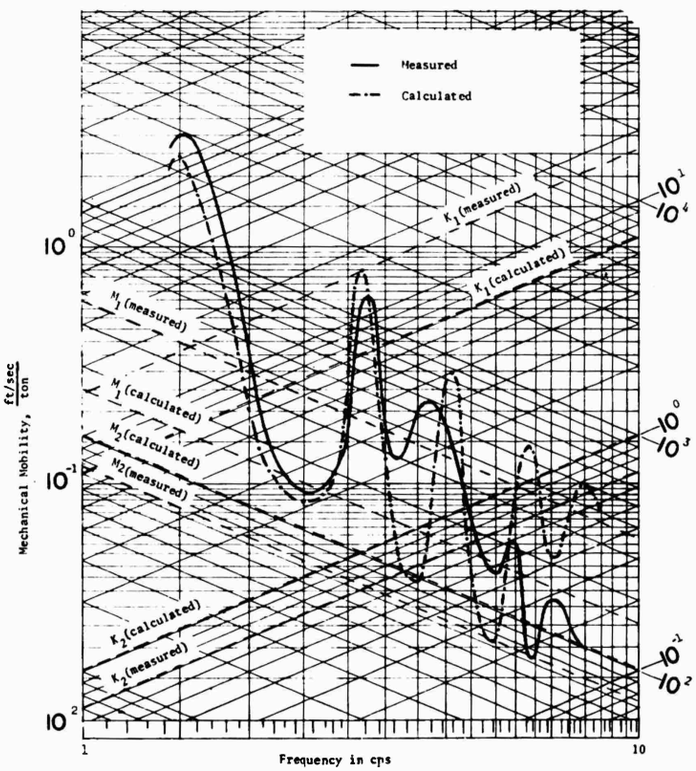

Fig. 15 - Mechanical mobility versus frequency NS SAVANNAH

vibration response of ships, was based on an average of the decrements obtained from various classes of ships such as those shown earlier in Table 1. Knowledge of the logarithmic decrement does not, of course, indicate the type of damping actually present for a given ship. The precise nature of the damping process in hull vibration is not well understood at the present time. Certain qualitative remarks, however, may be made.

The possible sources of damping are (1) the surrounding water, (2) internal friction in the hull structural material, and (3) friction between slipping or sliding surfaces within the hull, associated with equipment or cargo.

Recent work by Suetsugu and Fujii[15] has shown that the surrounding water may have effects on the hull response in addition to that of virtual mass. Model and full-scale tests showed induced local vibration of the double bottom introduced additional modes into the vibratory profile. This local vibration is similar in effect to that of sprung mass as discussed in Refs. 1, 7, and 16.

Experiments on the SS GOPHER MARINER show that the most important source of damping appears to be the cargo friction, if by "cargo" there is included everything movable inside the hull proper.

Reference 15 also discusses the effect of cargo loading on hull response. Figure 16 shows the difference in response of a cargo ship in ballast (9854 tons) and full-load (20,240 tons) conditions. As can be seen, not only are the hull frequencies affected, but the damping changes have decreased some amplitudes and increased others.

The damping source next in importance seems to be the hysteresis in the hull itself if the structure is welded. With a riveted construction, the working of the joints can cause a dissipation of energy which is chargeable to the hull although not to the material. The least

[15] I. Suetsugu and K. Fujii, "The Effects of the Bottom Vibration on Hull Natural Frequencies," Presentation to the Kansai Society of Naval Architects, Japan (May 1963).

[16] E. H. Kennard, "Forced Vibrations of Beams and the Effect of Sprung Masses," DTMB Report 955 (July 1955).

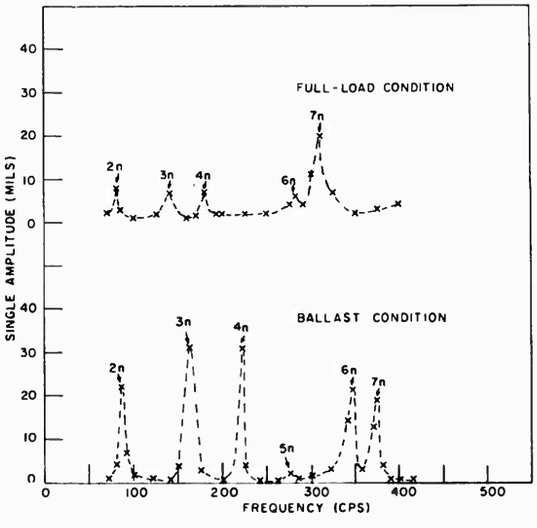

Fig. 16 - Hull response of Japanese cargo ship in ballast and full-load conditions

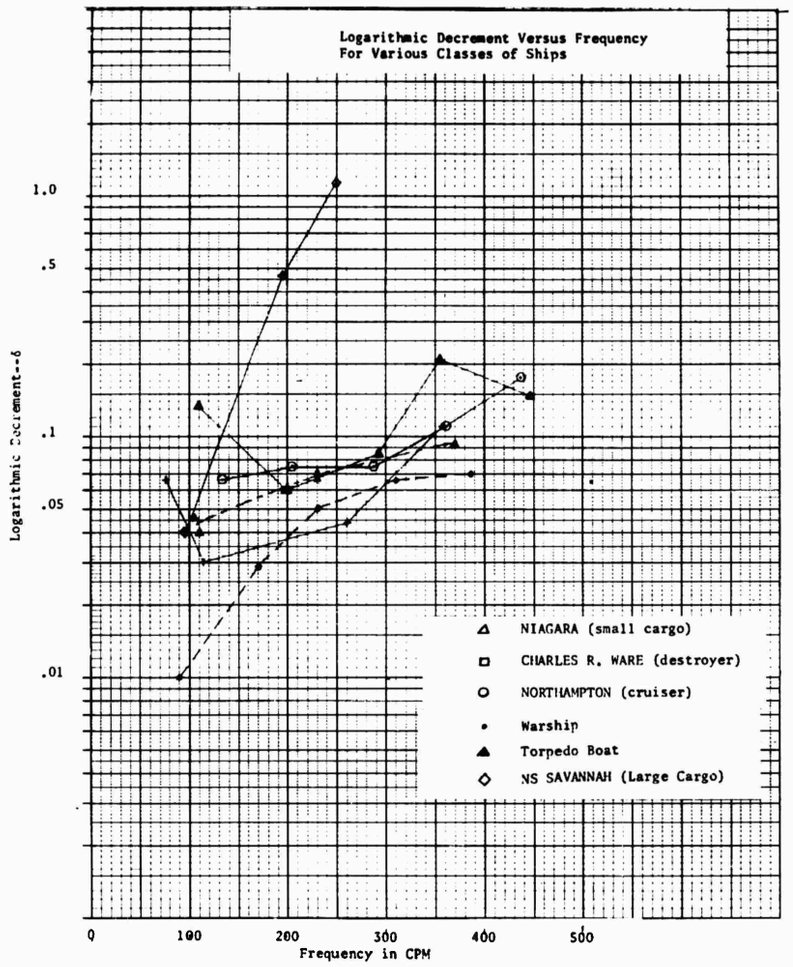

Fig. 17 - Logarithmic decrements

important source of damping for low frequency hull modes appears to be the water. Thus, the damping coefficients used in actual calculations cannot be determined analytically from given hull design data but must be based on values determined experimentally on other ships.

Figure 17 shows the values of the logarithmic decrement computed for the lower modes of several ships reported in Refs. 1 and 17 and the values computed for the lower modes of the NS SAVANNAH. As can be seen, the values for NS SAVANNAH are somewhat higher than the others. This gives further indication that the proper damping factor for NS SAVANNAH is higher than 0.03.

It is apparent that a damping factor of approximately 0.03, which had been empirically derived, is not to be used indiscriminately for all surface ships. Further experimental data are necessary to determine the proper damping factor for various classes of ships. Because of inherent difficulties in further pursuing the theoretical attack on the complex system damping problem, it is evident that further progress will rely in large part on obtaining reliable data from a wide variety of ships.

[17] F. H. Todd, Ship Hull Vibration (Edward Arnold, Ltd., London (Publisher) (1961).

* * *

A THEORETICAL BASIS FOR MECHANICAL IMPEDANCE SIMULATION IN SHOCK AND VIBRATION TESTING

F. J. On
Goddard Space Flight Center
Greenbelt, Maryland

Fundamental and useful mathematical relations for impedance are given for the analysis, control, and simulation in mechanical structures that can be considered as one-dimensional linear-passive systems. The validation of these expressions in the application to impedance control and simulation is approached primarily from analytical considerations, with general theories of application summarized.

INTRODUCTION

One of the most vexing problems confronting the environmental test engineer today is how to achieve a more realistic simulation of a shock and vibration environment in the test laboratory. Generally there are so many structural configurations and so many kinds of motions to which they are subjected that generalizations about the environment of one configuration from tests conducted on another, when two situations are different, are often incorrect.

The intent of this paper is to present some guidelines, based on theoretical considerations, whereby simulation in environmental shock and vibration testing can be optimized.

GENERAL THEORY

Mechanical Impedance Analysis

Consider a mechanical structure which vibrates about a stable equilibrium configuration. It follows that, in oscillation about this position, the complete set of force equilibrium equations may be given by

$$[M]\left\{\frac{d^2x}{dt^2}\right\} + [C]\left\{\frac{dx}{dt}\right\} + [K]\{x\} = \{f(t)\}, \quad (1)$$

where M, C and K are respectively the mass, damping, and stiffness coefficients of the structure. The Laplace Transform of this equation, in terms of transform velocities, can then be expressed by the transform equation

$$[Z(s)]\{V(s)\} = \{F(s)\}, \quad (2)$$

where the Z's represent the proportionality between a transform velocity and a transform force. Consequently, the matrix Z represents the mechanical impedances of the structure, while the column matrix V represents the transform velocities corresponding to the transform of input forces F. If the force matrix is partitioned in terms of an externally applied force and an internally applied force matrix, then Eq. (2) can be expressed in partitioned form as

$$\begin{bmatrix} [Z_{EE}(s)] & [Z_{EI}(s)] \\ [Z_{IE}(s)] & [Z_{II}(s)] \end{bmatrix} \begin{Bmatrix} \{V_E(s)\} \\ \{V_I(s)\} \end{Bmatrix} = \begin{Bmatrix} \{F_E(s)\} \\ \{F_I(s)\} \end{Bmatrix}, \quad (3)$$

where the subscripted Z matrices are the submatrices corresponding to the partition. The subscripts EE, II, and EI denote respectively the external, internal, and external-internal couplings. Because of symmetry in the impedance matrix Z of Eq. (2), the matrix Z_{EI} is the transpose of the matrix Z_{IE}, i.e., $[Z_{IE}] = [Z_{EI}]^T$.

The expanded form of this matrix equation provides a set of equations from which the matrices can be developed entirely in terms of quantities referred to the exterior coordinates only. This permits us to describe the performance of a structure completely without knowing the precise details of the system's interior makeup. Thus obtaining the matrix V_I from the second equation of the partitioned form, and substituting in the first equation, yields

$$[Z_E(s)]\,\{V_E(s)\} = \{F_E(s) - F_E^b(s)\}\,. \quad (4)$$

where

$$[Z_E(s)] \equiv [Z_{EE}(s)] - [Z_{EI}(s)] \times [Z_{II}(s)]^{-1}\,[Z_{IE}(s)] \quad (5)$$

$$\{F_E^b(s)\} \equiv [Z_{EI}(s)]\,[Z_{II}(s)]^{-1}\,\{F_I(s)\} \quad (6)$$

and $[Z_{II}]^{-1}$ is the inverse matrix of $[Z_{II}]$.

Equation (4) is termed the "external equation" of the system because all quantities now refer to exterior coordinates. The matrix Z_E in this equation then represents the internal mechanical impedances as seen from the exterior coordinates, and differs from the matrix Z in Eq. (2) only in the coordinates to which it is referred. The matrix F_E^b is defined as the "blocked force matrix" of the system, and it represents the internal excitations as observed at the exterior coordinates for exterior coordinates blocked so that no motion occurs. Thus the character of the matrix on the right hand side determines the "state" of the system. The system is considered "active" if the blocked forces are not zero and considered "passive" if they are zero.

Premultiplying thru Eq. (4) by the inverse matrix of Z_E, the external velocity matrix is obtained explicitly as

$$\{V_E(s)\} = [Z_E(s)]^{-1}\,\{F_E(s) - F_E^b(s)\}\,. \quad (7)$$

When the system is unrestrained at its exterior coordinates so that the externally applied forces F_E are zero, the velocity matrix is significant enough to warrant the special name "free velocity matrix" V_{EO}. Thus, the relationship between blocked forces and free velocities of the system can be written as

$$\{V_{EO}(s)\} = -[Z_E(s)]^{-1}\,\{F_E^b(s)\}\,. \quad (8)$$

Interconnection of Structures

Block diagrams representing two structures are shown in Fig. 1(a). The structures will be connected as shown by Fig. 1(b) and their combined behavior will be examined.

The individual performance of the structures prior to connection can be described by the set of external equations

$$[Z^{(1)}(s)]\,\{V^{(1)}(s)\} = \{F^{(1)}(s) - F^{b(1)}(s)\} \quad (9)$$

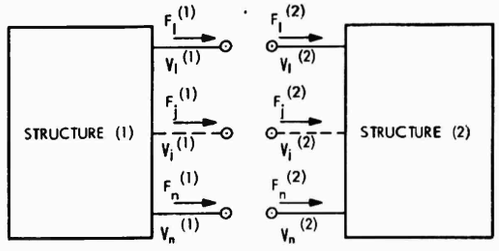

(a). Multi-dimensional structures before connection at exterior coordinates.

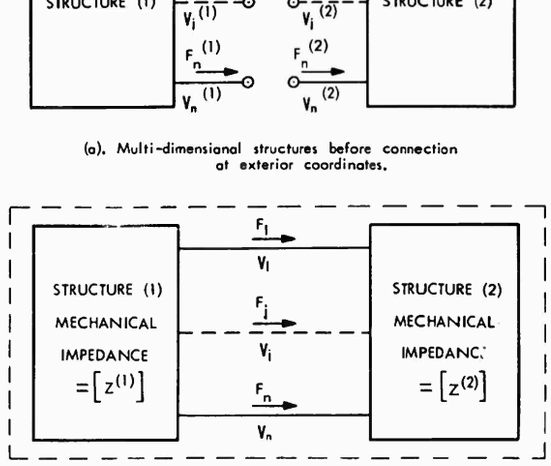

(b). Multi-dimensional composite structure

Fig. 1 - Block diagrams of composite structure and substructures

$$[Z^{(2)}(s)]\ \{V^{(2)}(s)\} = \{F^{(2)}(s) - F^{b(2)}(s)\}\ , \quad (10)$$

where the superscripts (1) and (2) designate a specific structure. The subscript E is dropped with the understanding that all quantities now refer to external equations.

When the structures are combined to form a complete system, Eqs. (9) and (10) must satisfy a force equilibrium condition

$$\{F(s)\} = \{F^{(1)}(s) + F^{(2)}(s)\}\ , \quad (11)$$

and a velocity compatibility condition

$$\{V(s)\} = \{V^{(1)}(s)\} = \{V^{(2)}(s)\}\ , \quad (12)$$

where the nonsuperscripted quantities refer to composite quantities at the interconnections. Implicitly these conditions define the nature of the mechanical connections made between the structures. The compatibility equations are written in composite form, and in order to impose them on the structures, the individual performance equations will have to be similarly described in terms of composite quantities. When summed, the "composite structural equation"

$$[H(s)]\ \{V(s)\} = \{R(s)\}\ , \quad (13)$$

where

$$[H(s)] \equiv [Z^{(1)}(s) + Z^{(2)}(s)] \quad (14)$$

and

$$\{R(s)\} \equiv \left\{ - \sum_{i=1}^{2} F^{b(i)}(s) + F(s) \right\}\ , \quad (15)$$

is obtained which is the equation of equilibrium in terms of the interconnection velocities for the complete structure.

Thus, in the calculation of the interconnection velocities, the complete structure has been regarded as an assembly of the substructures subjected to the external loading R of Eq. (15). The summation here implies addition of the corresponding interconnection reactions for interconnections blocked (blocked forces), while F is the loading matrix for externally applied forces on these interconnections. The negative sign with $F^{b(i)}$ is used to change the reactions into externally applied forces.

The matrix H is defined by Eq. (14) and is called the "composite structural matrix" of the system. Moreover, Eq. (13) may be solved for the natural frequencies by removing the forcing matrix R and setting the determinant of H to zero.

THEORIES OF APPLICATION

Analysis

The general equations of the preceding section show how the effects of mechanical impedance variations on mechanical structures can be determined. Although these determinations are usually quite involved, it is necessary that some applications (calculations or measurements) of this type be made on actual systems before their dynamic environments are firmly specified.

As an example, consider a one-dimensional structure which is otherwise separated into two component structures at some terminal. For this case then, the matrices in the foregoing "external equation" reduce simply to single elements. A general representation of such a system is depicted in Fig. 2 where for convenience its component structures are identified by the vehicle V_a and the spacecraft P_b. It is assumed that the vehicle is active because of the force f(t), and that the spacecraft is passive. In connection with this example, there

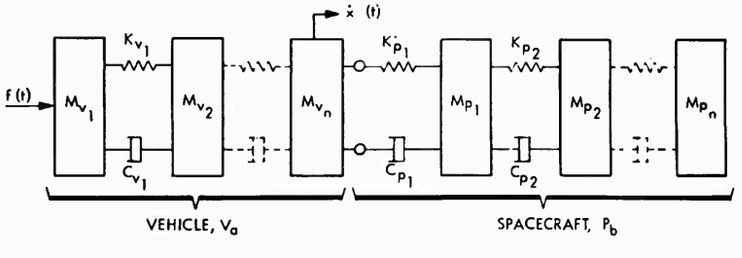

Fig. 2 - Lumped parameter representation of one-dimensional vehicle-spacecraft system

are generally three kinds of dynamics problems of interest:

1. Steady-state vibration
2. Transient motion
3. Random vibration

With this in mind, two major problems will be posed: (1) how does one analyze and define the dynamic environment at the input to the spacecraft, and (2) having defined the environment, how does one attempt to simulate the environment in the testing laboratory?

Steady-State Vibration – In accordance with the composite equation for one-dimensional structures, the steady-state response (or the transient response) at the joining terminal of the vehicle and the spacecraft, in which the force excitation is $f(t)$, is given by

$$V^{(V_{ab})}(s) = F^{b(V_a)}(s) \Big/ H_1(s), \qquad (16)$$

where

$$H_1(s) \equiv Z^{(V_a)}(s) + Z^{(P_b)}(s). \qquad (17)$$

$F^{b(V_a)}$ represents the transform of $f(t)$ measured at the connecting terminal when that terminal is blocked so that no motion occurs; $Z^{(V_a)}$ and $Z^{(P_b)}$ are the transform mechanical impedance of the vehicle and spacecraft looking back from the terminal respectively.

It will turn out to be convenient to express Eq. (16) also in terms of the free velocities:

$$V^{(V_{ab})}(s) = V_o^{(V_a)}(s)\, H_2(s), \qquad (18)$$

where

$$H_2(s) \equiv 1 + Z^{(P_b)}(s) \Big/ Z^{(V_a)}(s). \qquad (19)$$

For all practical considerations, the functions H_1 and H_2 represent a kind of frequency response since they can be shown to be dependent only on frequency.

In cases whereby either the vehicle or the spacecraft is replaced by some other structure, new interconnection response characteristics can be obtained. For example, consider the velocity response corresponding to a new spacecraft P_r on the same vehicle. From the composite equation for the old and new structure, the new interconnection response can be given in terms of the old interconnection response as

$$V^{(V_{ar})}(s) = \left(H_1(s)/H_3(s)\right) V^{(V_{ab})}(s), \qquad (20)$$

where

$$H_1(s) \equiv Z^{(V_a)}(s) + Z^{(P_b)}(s) \qquad (21)$$

$$H_3(s) \equiv Z^{(V_a)}(s) + Z^{(P_r)}(s), \qquad (22)$$

and $Z^{(P_r)}$ is the mechanical impedance of the new spacecraft.

Another case which might be of interest is the case of a spacecraft designed to ride on a launch vehicle, but it is to be vibration tested on a machine of mechanical impedance $Z^{(S_m)}$. To provide a realistic test, the impedance of the launch vehicle should be simulated by the test machine. Consequently the interconnection responses for the spacecraft with the launch vehicle and the spacecraft with the test machine are given respectively by

$$V^{(V_{ab})}(s) = V_o^{(V_a)}(s) \Big/ H_2(s) \qquad (23)$$

$$V^{(S_{mb})}(s) = V_o^{(S_m)}(s) \Big/ H_4(s), \qquad (24)$$

where

$$H_2(s) \equiv 1 + Z^{(P_b)}(s) \Big/ Z^{(V_a)}(s), \qquad (25)$$

and

$$H_4(s) \equiv 1 + Z^{(P_b)}(s) \Big/ Z^{(S_m)}(s). \qquad (26)$$

For condition of simulation, Eqs. (23) and (24) must be equated, and this requires that

$$V_o^{(S_m)}(s) = \left(H_4(s)/H_2(s)\right) V_o^{(V_a)}(s), \qquad (27)$$

must be satisfied. With these values for the free velocities of the test machine, the dynamic characteristics of the vehicle-spacecraft system can be simulated in the machine-spacecraft system.

Transient Motions – In the case of transient motions,[1] mechanical impedance can be defined as

[1] T. von Karman and M. A. Biot, Mathematical Methods in Engineering (McGraw-Hill Book Co., Inc., New York, N.Y., 1940), pp. 365-409.

$$Z(i\omega) = G_F(i\omega)/G_v(i\omega), \quad (28)$$

where G_F is the Fourier spectrum of the transient force $f(t)$ and G_v is the Fourier spectrum of the transient response $v(t)$. It follows that the equations for transient motions which correspond to the foregoing cases of the steady-state equations are:

from Eq. (16),

$$G_v^{(V_{ab})}(i\omega) = G_{F^b}^{(V_a)}(i\omega) \Big/ H_1(i\omega); \quad (29)$$

from Eq. (18),

$$G_v^{(V_{ab})}(i\omega) = G_{v_o}^{(V_a)}(i\omega) \Big/ H_2(i\omega); \quad (30)$$

from Eq. (20),

$$G_v^{(V_{ar})}(i\omega) = \left(H_1(i\omega)/H_3(i\omega)\right) G_v^{(V_{ab})}(i\omega); \quad (31)$$

and from Eq. (27),

$$G_{v_o}^{(S_m)}(i\omega) = \left(H_4(i\omega)/H_2(i\omega)\right) G_{v_o}^{(V_a)}(i\omega), \quad (32)$$

where

$$H(i\omega) = H(s)\big|_{s=i\omega}.$$

Since $v(t)$ and its Fourier spectrum $G_v(i\omega)$ constitute a transform pair, the time dependent $v(t)$ can be obtained from the general expression

$$v(t) = \int_{\omega=-\infty}^{\infty} G_v(i\omega)\, e^{i\omega t}\, d\omega. \quad (33)$$

Random Vibrations – In the case of random vibration[2] (in this case the excitations are stationary ergodic types of random processes with Gaussian probability distributions) mechanical impedance can be defined by

$$|Z(i\omega)| = \left(S_F(\omega)/S_v(\omega)\right)^{1/2}, \quad (34)$$

where S_F is the spectral density of the random force; S_v is the spectral density of the random response; and $|Z(i\omega)|$ is the absolute value of the complex impedance. It follows then that the equations for random vibrations corresponding to those of the steady-state cases can be obtained:

from Eq. (16),

$$S_v^{(V_{ab})}(\omega) = S_{F^b}^{(V_a)}(\omega) \Big/ |H_1(i\omega)|^2; \quad (35)$$

from Eq. (18),

$$S_v^{(V_{ab})}(\omega) = S_{v_o}^{(V_a)}(\omega) \Big/ |H_2(i\omega)|^2; \quad (36)$$

from Eq. (20),

$$S_v^{(V_{ar})}(\omega) = |H_1(i\omega)/H_3(i\omega)|^2\, S_v^{(V_{ab})}(\omega); \quad (37)$$

and from Eq. (27),

$$S_{v_o}^{(S_m)}(\omega) = |H_4(i\omega)/H_2(i\omega)|^2\, S_{v_o}^{(V_a)}(\omega). \quad (38)$$

The mean square values of these quantities may be obtained from the general expression

$$v\ (\text{mean square}) = \frac{1}{2\pi}\int_0^{\infty} S_v(\omega)\, d\omega. \quad (39)$$

Simulation and Control

After the dynamic environment is analyzed and defined, the next obvious step is to attempt to simulate it in the testing environment. In the following sections, some methods of applications that can be employed to achieve some degree of simulation are summarized.

Development of Specifications – The development of realistic shock and vibration specifications has been hindered largely by the fact that the true environmental conditions have not been known until the structure actually has undergone service environments. Consequently, attempts to consider new environments often result in merely modifying existing specifications into new specifications to be used for testing prior to subjecting the structure to service. Unless specifications are formulated on a sound basis, they can be much in error. It is evident from the foregoing developments that mechanical impedance (or some other similar property) must be considered.

Reshaping of Frequency Responses of Test-Machines – This method concerns the reshaping of frequency response characteristics of test-machines so that appropriate mechanical impedance compensations are introduced. This results in dynamic characteristics at the table of the machine that are simulations of the vehicles' terminal characteristics. In some

[2] S. H. Crandall, Random Vibration (John Wiley and Sons, Inc., New York, N.Y., 1958), pp. 77-90.

instances, the reshaping can be made by various spectrum-shaping techniques which employ present-day machine system equalization methods.

Let us suppose that the unmodified frequency response of a test-machine system is defined by

$$B(i\omega) = V_o^{(S_m)}(i\omega) \Big/ I(i\omega), \qquad (40)$$

where V_o is the free velocity of the machine and I is the armature current required. For simulation, the free velocities of the machine, as given by Eq. (27), can be expressed by the form

$$V_o'^{(S_m)}(i\omega) = K(i\omega)\, V_o^{(S_m)}(i\omega) \qquad (41)$$

and the new armature current now required by

$$I'(i\omega) = C(i\omega)\, I(i\omega), \qquad (42)$$

where K and C represent the necessary corrections. When Eqs. (41) and (42) are substituted in Eq. (40), we obtain

$$V_o'^{(S_m)}(i\omega) \Big/ I'(i\omega) = \left(K(i\omega)/C(i\omega)\right) B(i\omega), \qquad (43)$$

which shows that the simulated frequency response is the product of a correction function and the original frequency response $B(i\omega)$. The correction function may be introduced by mechanical or electrical means, or by both. Mechanically, it involves fixture designs; and electrically, it requires spectrum-shaping techniques.

Electronic Computer Applications – This method concerns the application of electronic computers as problem simulators. If a mechanical system is defined by appropriate mechanical impedances, the computer can simulate the reactions of the components of the system. Therefore when true dynamic inputs are employed, the computer outputs will yield realistic dynamic responses of the system.

CONCLUSION

The study, and possibly the control, of pertinent structural dynamic characteristics of linear structures is theoretically feasible, by use of mechanical impedance concepts. The usefulness of these concepts can be of three kinds: (1) As a means of expressing dynamic characteristics of component structures in a manner that concisely tells the experienced engineer what he needs to know about the structures; (2) as a description of integral parts of structures, since it can be used together with a comparable description of the dynamic inputs to specify the response at any desired terminal; and (3) if dynamic responses are known for a particular integrated structure, the modified responses when integral parts of the structure are altered can be determined provided impedance information for the new and old integrates structures are known. Moreover, to prove the suitability and efficiency of any new type of structural design or to improve existing designs, some amount of structural impedance consideration in design and qualification procedures is highly necessary.

The objective of this paper was not to investigate in detail the many existing problems in employing the concepts of mechanical impedance to dynamic environmental simulation, but rather to provide some guidelines based purely on theory whereby some aspects of simulation can be achieved. The proper extent of the practical applications of the developments covered in the foregoing theory can be determined by suitable experiments.

ACKNOWLEDGMENT

The author is greatly indebted to Mr. T. G. Butler of the Goddard Space Flight Center and to Dr. R. O. Belsheim of the U. S. Naval Research Laboratory, for their most helpful suggestions during the preparation of the manuscript.

DISCUSSION

Dr. Mains (General Electric): I have one comment and one question. The comment is that in the figure where you showed on the left a block representing the testing machine and on the right a block representing the space vehicle, you had an equation which said that you needed to get effectively the right impedance in the testing machine in order to have the simulation be proper. This depends on where you are controlling the motion. If you control at the interface,

you need only control motion. You don't care what the impedance is behind that point. However, if you control somewhere farther back in the system, then, you do need to have the right transfer impedance between that point and the interface. I think this is correct. My question is — how do you handle damping? Where do you get the C matrix in your solution?

Mr. On: I think the matrix equation of motion that I have written explains in itself the underlying assumptions which I have made in writing that expression. Now, of course, there are several difficulties in measuring C or even K. That the coefficients can be determined reasonably well is another assumption that I have made.

Dr. Mains: Do you have some good scheme for getting those coefficients?

Mr. On: Considering the nonlinearity of structures that has been discussed in a paper earlier in this Symposium, it seems that this would be a problem.

* * *

MECHANICAL IMPEDANCE MEASUREMENTS IN FOUNDATION STUDIES*

R. A. Darby
U.S. Navy Marine Engineering Laboratory

The application of mechanical impedance techniques to the analysis of the shipboard machinery noise control problem is discussed. It is shown that unless simple relatively symmetrical structures are involved, the experimental analysis becomes involved and it is difficult with present day techniques to measure specific impedance or mobility parameters. A measured impedance or mobility element is frequently affected by off-diagonal or mixed mobility elements, transducer cross-sensitivities, and mobility magnitudes of the vibration exciter as well as the magnitude of the mobility element desired. The need to evaluate more completely accelerometers and force gages and to develop new force generators is stressed. A magnetic force generator and gage combination which applies no (or nominal) constraints to the structure is described.

INTRODUCTION

Mechanical impedance techniques may be used advantageously in vibration analysis where several discrete structures are connected together to form the ultimate system. The experimental analysis of the waterborne sound radiation resulting from the vibration of resiliently mounted submarine machinery is the problem treated in this paper. Wright and Hagg,[1,2] provide the analytical approach to be utilized in treating the machine, the resilient isolation mounts, the machinery foundation, and the hull of the vessel as the discrete elements of the system to be analyzed, Fig. 1(a). It is shown that the sound radiation can be predicted if one can measure the velocity spectra of the machine at the input to the isolation mount, the transfer impedance of the isolation mount, the transfer mobility of the foundation, the drive point mobility of the hull, and the proper radiation transfer factors that characterize the hull without the presence of the machinery installation under consideration.

In the ideal situation, there would be only one structural path which possesses full symmetry about an axis normal to the hull and the only vibratory motion of the machine would be in the direction along the axis of symmetry. This system, pictured in Fig. 1(b), is approximately the situation reported in previous MEL reports.[3,4] If full symmetry does not exist, or if more than one direction of input velocity is to be considered, then the complexity of the analytical problem increases greatly, and it will be shown that current experimental impedance techniques become marginal or inadequate to analyze the system rigorously.

IMPEDANCE MEASUREMENTS IN THE LABORATORY

In dealing with realistic elements of machinery installations, one measures what is readily measurable and hopes to obtain significant correlation. For example; the blocked unidirectional transfer impedances of an isolation mount and a flexible exhaust joint have been

*This paper was not presented at the Symposium.

[1] D. V. Wright and A. C. Hagg, "Practical Calculation and Control of Vibration Transmission Through Resilient Mounts and Basic Foundation Structures," Westinghouse Research Lab Report 405FD208-R2 (Dec. 1959).

[2] D. V. Wright, et al., "Vibration Transmission and Impedance of Basic Foundation Structures," Westinghouse Research Lab Report 62-917-515-R1 (Oct. 1962).

[3] R. A. Darby and E. V. Stanley, "Impedance Studies of Tubular Columns as Basic Machine Foundation Elements," USNEES Report 820287B (July 1962).

[4] R. C. Hirsch, "Impedance Studies of an Asymmetrical Angle-Iron Column as a Basic Machine Foundation Element," MEL Report 82 287D (Aug. 1963).

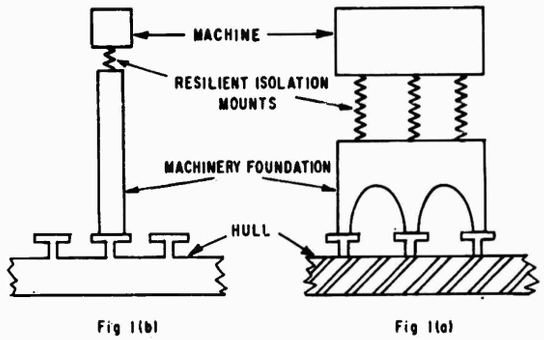

Fig. 1 - Elements of the structural system for machinery installation studies

measured[5,6] with results that have been applied to practical prediction problems.[7,8] The measurement is made by blocking one side of the device through a force gage to a large seismic mass and applying a measured unidirectional velocity input to the free end of the isolation device.

Though these devices are symmtrical about an axis (see Fig. 2), a three by three matrix of impedance parameters is necessary to define the device rigorously:

$$\begin{vmatrix} F_{bz} \\ F_{br} \\ F_{b\theta} \end{vmatrix} = \begin{vmatrix} \left(\frac{F_{bz}}{V_{az}}\right) & \left(\frac{F_{bz}}{V_{ar}}\right) & \left(\frac{F_{bz}}{V_{a\theta}}\right) \\ \left(\frac{F_{br}}{V_{az}}\right) & \left(\frac{F_{br}}{V_{ar}}\right) & \left(\frac{F_{br}}{V_{a\theta}}\right) \\ \left(\frac{F_{b\theta}}{V_{az}}\right) & \left(\frac{F_{b\theta}}{V_{ar}}\right) & \left(\frac{F_{b\theta}}{V_{a\theta}}\right) \end{vmatrix} \times \begin{vmatrix} V_{az} \\ V_{ar} \\ V_{a\theta} \end{vmatrix} \qquad (1)$$

The parameter which is simplest to measure is (F_{bz}/V_{az}) and is shown in Fig. 3 for the two isolation devices measured. Even this one measurement allows a quantitative evaluation of the flexible coupling compared to the 6E2000 isolation mounts used in the system and should serve as a guide to designers in deciding whether to concentrate effort on elaborate compound mount installations versus developing better flexible couplings to prevent them from "shorting" the isolated installation.

If the measurement is to represent the (F_{bz}/V_{az}) parameter independent of the other matrix elements, it can be seen that the velocity input must be unidirectional $(V_{ar} = V_{a\theta} = 0)$ and that the force gage must have low sensitivity to forces in the "r" and "θ" directions if the specimen to be measured has finite off-diagonal impedance elements. If one has sufficient confidence in knowing the transverse and rotational

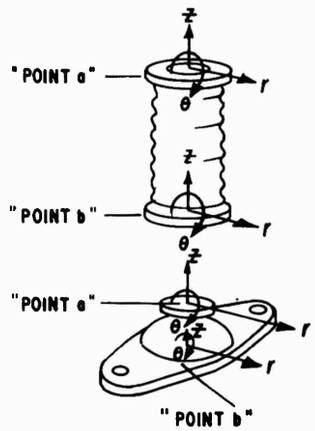

Fig. 2 - Geometries of flexible exhaust coupling and resilient isolation mount

[5] F. J. Cingel, "Mechanical Impedance Characteristics of Naval Type 7E450 Resilient Mounts," USNEES Report 82 288E (Nov. 1962).

[6] H. L. Rekate and J. I. Schwartz, "Behavior Study of a Curtis Wright Flexible Snorkel Exhaust Joint for Submarine Application," MEL Report 72 108 (Nov. 1963).

[7] R. Darby, "The Quantitative Evaluation of Vibration Isolation Devices for Mounted Naval Machinery Installations," MEL Report 82 287E (Aug. 1963).

[8] R. A. Darby, et al., "Noise Assessment of Proposed Main Propulsion Machinery Installations for a New Design A.S.W. Surface Ship," MEL Report 67 107 (Aug. 1963).

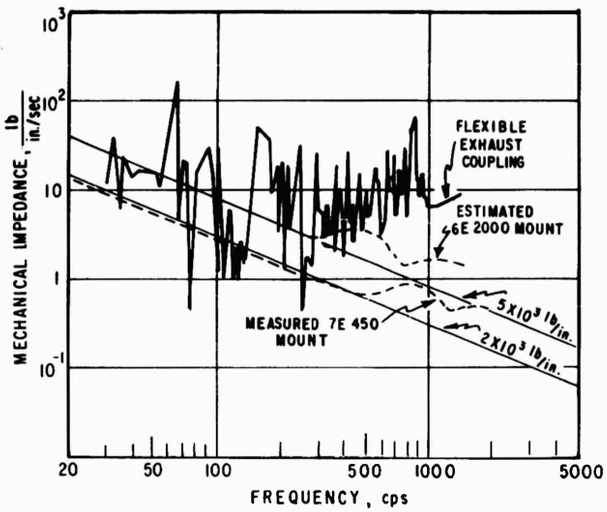

Fig. 3 - Magnitudes of transfer impedance for flexible exhaust coupling and two resilient isolation mounts

sensitivities of an accelerometer over the frequency range of interest, the velocity input can be controlled by monitoring the motions in the unwanted directions and correcting by adjustments on the vibration exciter drive.

An attempt to evaluate force-gage sensitivity to transverse and rotational forces has been carried out using the setup in Fig. 4 where the force gage is made an element of a short, stiff cantilever beam secured to a large seismic mass. A unidirectional force is applied via a wire drive or the magnetic exciter to be described later, and the shear force and moment at some reference point on the gage (usually approximating the crystal center) is noted. By changing the relative location of the force gage in the beam, one can observe the change in the output signal due to a change of moment while shear is constant. This type of evaluation leaves much to be desired, but serves to compare different force gages and to gain some insight into the cross-sensitivities of the force gage.

Obviously, the actual vibration of a machine does not honor our arbitrary coordinate system and output forces generated by velocity inputs V_{ar} and $V_{a\theta}$ may be of equal or greater

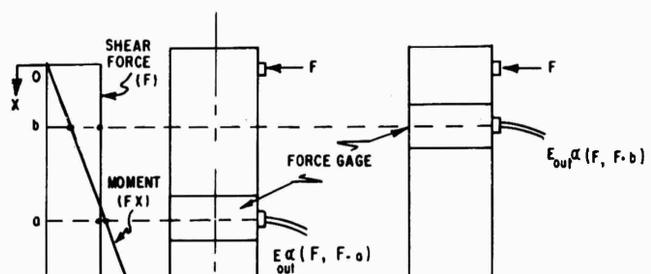

Fig. 4 - Method to evaluate force gage sensitivity to shear and moment

importance in contributing to the final radiation in the sea. Likewise, the off-diagonal parameters (for the mount and exhaust coupling, symmetry suggests only $(F_{br}/F_{a\theta})$), may be of importance. Some of the measurement techniques and instrumentation needed to obtain these parameters, particularly those involving rotation are being developed presently at MEL and DTMB.

IMPEDANCE AND MOBILITY MEASUREMENTS IN THE FIELD

In the analysis of the foundation as an element in the transmission path, a transfer mobility measurement across the foundation element is necessary. Also, a driving point mobility describing the hull at the point where the foundation is attached, is needed. Both of the measurements must be made at the location of the machinery installation, and they cannot be made under the controlled conditions obtainable in the laboratory. These measurements dictate controlling and measuring the force applied to the structure, as it is not desirable to locate force gages at the point where the foundation attaches to the hull. The transfer mobility measurement is therefore made by measuring the velocity at the attachment point and the force input at the location where the isolation device is attached.

In both cases, the desired mobility is defined by the matrix relation

$$V_{\ell j} = \left(\frac{V_{\ell j}}{F_{ki}}\right) F_{ki} ,$$

where ℓ and k are the point locations where the measurement is taken ($\ell = k$ for a driving point mobility, $\ell \neq k$ for a transfer mobility), and i and j are the direction indices with a maximum of six (three translational and three rotational). In the experiments outlined in Refs. 3 and 4, the physical picture is shown in Fig. 5, and assuming sufficient symmetry exists in a fore and aft (y) direction, the problem can be considered plane, and

$$\begin{vmatrix} V_{\ell x} \\ V_{\ell z} \\ V_{\ell \theta} \end{vmatrix} = \begin{vmatrix} \left(\frac{V_{\ell x}}{F_{kx}}\right)\left(\frac{V_{\ell x}}{F_{kz}}\right)\left(\frac{V_{\ell x}}{F_{k\theta}}\right) \\ \left(\frac{V_{\ell z}}{F_{kx}}\right)\left(\frac{V_{\ell z}}{F_{kz}}\right)\left(\frac{V_{\ell z}}{F_{k\theta}}\right) \\ \left(\frac{V_{\ell \theta}}{F_{kx}}\right)\left(\frac{V_{\ell \theta}}{F_{kz}}\right)\left(\frac{V_{\ell \theta}}{F_{k\theta}}\right) \end{vmatrix} \times \begin{vmatrix} F_{kx} \\ F_{kz} \\ F_{k\theta} \end{vmatrix} , \qquad (3)$$

where $\ell = b$, $k = a$ for the transfer mobility desired, and $\ell = k = b$ for the driving point mobility desired.

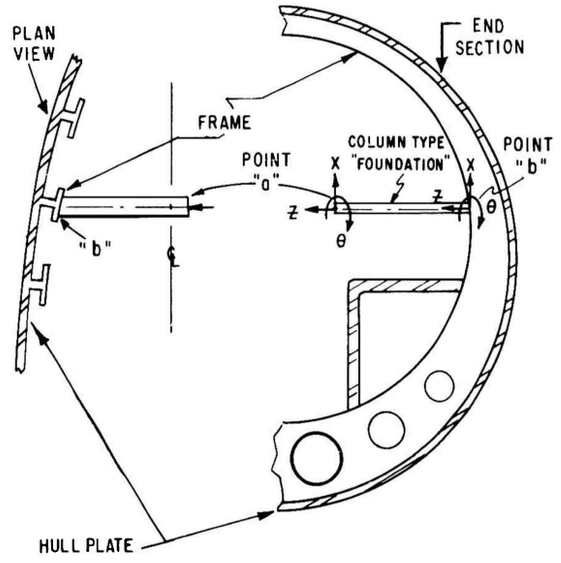

Fig. 5 - Details of column foundation test location in SS 427

Of interest in this experiment was the analysis of the column under excitation of compression waves in the axial (z) direction only. Assuming full symmetry of the hull about the attachment point, the problem theoretically degenerated to a two port system and the transfer impedance

$$Z_T = \frac{1}{(V_{bz}/F_{az})} = \left(\frac{F_{az}}{V_{bz}}\right)$$

was measured as was the driving point impedance

$$Z_H = \frac{1}{(V_{bz}/F_{bz})} = \left(\frac{F_{bz}}{V_{bz}}\right).$$

The magnitudes of these quantities are shown in Fig. 6. These measurements coupled with waterborne sound pressure measurements were adequate to show that present day experimental techniques were adequate to verify the theory of reference (a) for a simple system. Even in this experiment, however, meaningful data were finally obtainable only after many comparative measurements with different combinations of impedance heads and vibration exciters. Because of past experimental experience in this measurement location and the fact that the analytical problem served as a guide, data exhibiting the effects of strain sensitivity in accelerometers, impedance head contact area effects, transverse and rotational accelerometer sensitivity, electronic failures, and so forth, were known to be erroneous and discarded.

Problems of these types are resolvable by utilizing good transducer specifications and well disciplined experimental techniques.[9] The major problem area that needs better definition, if more complicated structural systems are to be analyzed, is associated with the control and measurement of the input force.

PROBLEMS IN MEASURING MOBILITY

This problem is best pointed out by observing various measurements of driving point mobility (V_{az}/F_{az}) taken in the free end of the column in Fig. 5. The driving point mobility in the "z" direction is obviously much less than the driving point mobilities in the transverse directions at the free end of the column. The system is also characterized by a moderate degree of asymmetry existing in the hull construction about the column attachment point so the off-diagonal or mixed driving point mobilities may be of some significance. With plane motion assumed for the sake of discussion, Eqs. (3) hold if $\ell = k = a$; so for point "a",

[9] F. Schloss, "Recent Advances in the Measurement of Structural Impedance," S.A.E. Reprint 426B.

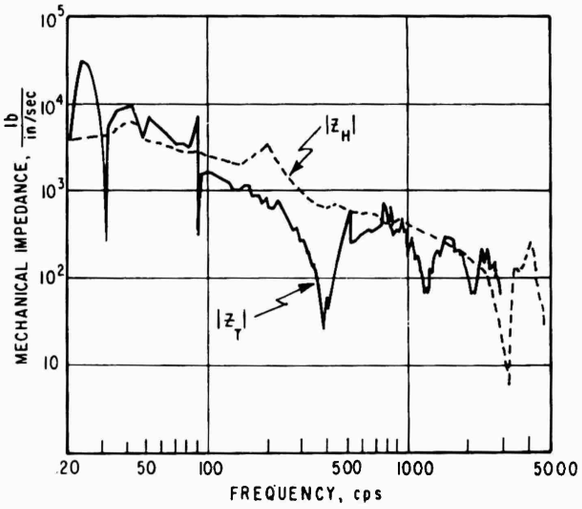

Fig. 6 - Measured hull driving point impedance magnitude $|Z_H|$ and column transfer impedance magnitude $|Z_T|$

$$\begin{vmatrix} V_x \\ V_z \\ V_\theta \end{vmatrix} = \begin{vmatrix} Y_{xx} & Y_{xz} & Y_{x\theta} \\ Y_{zx} & Y_{zz} & Y_{z\theta} \\ Y_{\theta x} & Y_{\theta z} & Y_{\theta\theta} \end{vmatrix} \times \begin{vmatrix} F_x \\ F_z \\ F_\theta \end{vmatrix} , \qquad (4)$$

where

$$Y_{ij} = \frac{V_i}{F_j} .$$

Figure 7 depicts three experimentally measured values of Y_{zz} using the same impedance head but with different vibration exciters and exciter attachment means as defined in the figure. The resonances I, II, and III, are definitely associated with the column characteristics in the "x" direction, i.e., as flexural modes predictable by considering the column as a clamped-free beam. The resonances IV, V, and VI are associated with compressional wave motion in "z" direction and are predictable by considering the column as a transmission line terminated into Z_{bz}.

If the vibration exciter is generating a truly unidirection force over the spectrum, i.e., $F_x = F_\theta = 0$, then

$$V_x = Y_{xz}F_z, \quad V_z = Y_{zz}F_z ,$$

and

$$V_\theta = Y_{\theta z}F_z . \qquad (5)$$

If the motion transducer has negligible cross-sensitivities, then

$$\left(\frac{V_z}{F_z}\right)' \approx Y_{zz} , \qquad (6)$$

where the prime indicates the experimentally measured value.

If the motion transducer has appreciable cross-sensitivities, i.e., where $c_{ij} = S_i/S_j$ is the ratio of the pickup sensitivity due to motion in the i^{th} direction over the pickup sensitivity due to motion in the j^{th} direction, then

$$\left(\frac{V_z}{F_z}\right)' = \frac{V_z + \Gamma_1\left[(c_{xz}, Y_{xz}F_z), (c_{\theta z}, Y_{\theta z}F_z)\right]}{F_z} . \qquad (7)$$

Though Γ_1 is probably a rather complicated relationship, experiment has shown that amplitude linearity does hold, so

$$\left(\frac{V_z}{F_z}\right)' = Y_{zz} + \Gamma_1\left[(c_{xz}, Y_{xz}), (c_{\theta z}, Y_{\theta z})\right] . \qquad (8)$$

There is a possibility that one of the curves in Fig. 7 is represented by either (6) or (7) and an evaluation of c_{xz} and $c_{\theta z}$ over the frequency range of interest is necessary.

The major problem, however, is in the fact that different sets of data were obtained even

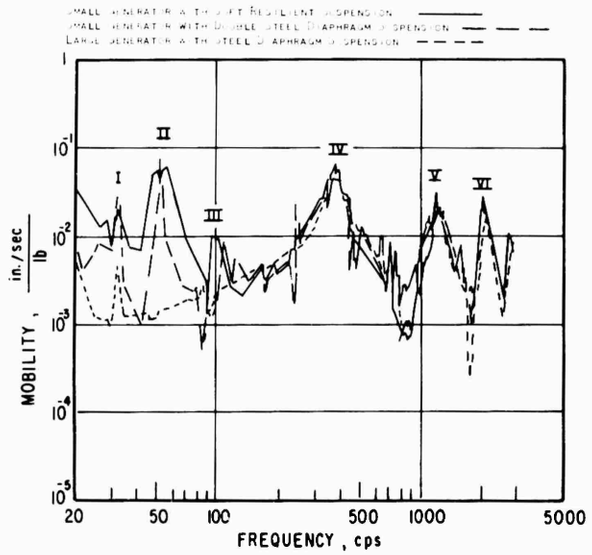

Fig. 7 - Measured driving point mobilities of simple column-hull system

though the transducer parameters were the same. Thus, the different vibration exciter arrangements must be responsible for applying different finite values of F_x and F_θ via constraints imposed on the structure by the driver at the attachment point. Figure 8(a) depicts a possible motion of the system that would exist under ideal conditions to measure the true driving point mobility. The schematic on the right shows the multi-port system representing point "a" with the ports associated with the x and θ directions "free" (devoid of constraints). Equations (4) or (6) are applicable in this case. The other limit is shown in Fig. 8(b) where the hull is seeing approximately the same displacement as in Fig. 7(a), but the very small transverse and rotational mobilities of the driver (represented in the schematic by "e") constrain the motion of the structure at point "a" to motion in the z direction only and cause forces F_x and F_θ to exist. In this case, $(V_z/F_z)'$ is a very complicated function involving all of the parameters in Eq. (2) as well as new parameters expressing the cross sensitivity of the force gage. In between these two extreme conditions is the situation where the mobilities of the force generator have a magnitude such that they also enter into $(V_z/F_z)'$ so that in Fig. 8(b), the "e" becomes another multi-port system that needs evaluation. Unfortunately, the data in Fig. 7, particularly at low frequencies, probably fall into this category.

Thus, it is apparent that if one desires to describe the necessary mobility parameters accurately and completely for the analysis of a real system of even moderate complexity, a great amount of transducer and force generator evaluation and development is needed. If impedance techniques are used, however, only to sample the degree of liveliness (i.e., "resonance hunting"), present day techniques are adequate and very useful. Likewise if a system analysis problem has sufficient symmetry to treat the analysis by unidirectional considerations, then the experimental technique can be sufficiently controlled to obtain meaningful data.

INSTRUMENT DEVELOPMENT

Continued effort to evaluate existing force and motion transducers with respect to cross-sensitivities as well as other anomalous phenomena will be very beneficial. Developments at MEL and DTMB are now underway to make impedance head and exciter systems that will

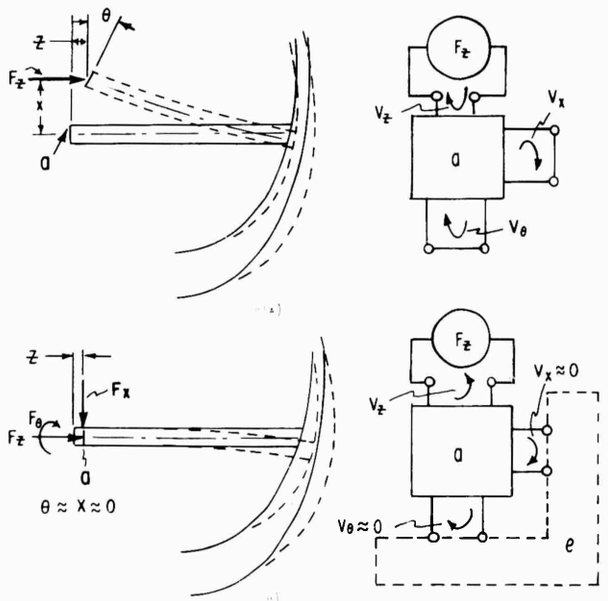

Fig. 8 - Physical and schematic representations of simple column-hull system behavior using different force generators

offer fewer (and hopefully negligible) undesirable constraints to the structure.

One approach under development at MEL is a force generator and gage that offers no or negligible mechanical constraints to the structure and also allows the force to be measured by means of accelerometers which are more highly developed and more fully evaluated than piezoelectric force gages. Figure 9 schematically depicts the device which consists of (a) an AC-magnetic-drive element biased with a permanent magnetic field in order to create a dynamic force between the head and the structure of the same characteristics as the applied dynamic electrical input, (b) a resilient suspension system, (c) a pneumatic spacer allowing optimization of the air gap between the magnetic head and the structure, and (d) monitoring accelerometers which allow calculation of the applied force by taking the product of the total mass (or inertia) times the acceleration. To date, the unit has been used to measure only unidirectional forces and the accelerometers oriented in the transverse directions were for monitoring purposes only. However, the number of accelerometers could be increased so that complete description of the acceleration of the mass in three dimensional space could be obtained and thus all the force components applied to the structures would be known.

In summary it can be said that the successful application of the impedance approach to the analysis of complicated structural systems depends on the evaluation and development of transducers and force generators to an extent that has not been accomplished (or in many cases, required) to date.

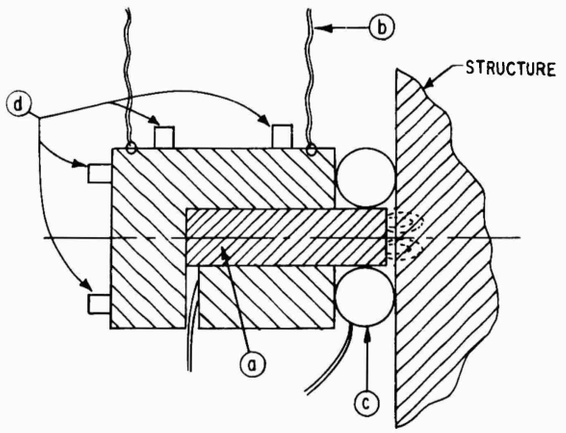

Fig. 9 - Force generator and gage

* * *

Section 2
PYROTECHNIC SHOCK

MECHANICAL SHOCK FROM FRANGIBLE JOINTS

V. R. Paul
Lockheed Missiles and Space Co.

This paper describes the work being done on the frangible joint shock problem at LMSC and gives the results obtained to date. The shocks produced from frangible joints during stage separation are of extremely high amplitude (100 to 3000 g) at high frequencies (600 to 6000 cps).

Frangible joints, which employ an explosive cord to cut or fracture a structural shell, are used in many of the satellite spacecraft and missile programs for such purposes as staging, shroud separation, and payload separation. Diagrams showing the placement of typical separation joints are shown in Fig. 1.

The designs which will be described in this paper are typical of those used at LMSC; similar devices are used by other aerospace companies. Two basic types of joints are now in use at LMSC. The earliest type developed employs a mild detonating fuse (MDF) to fracture a notched magnesium shell by explosive pressure. Figure 2 shows the joint configuration and the sequence of events during breaking. The MDF consists of a high explosive such as RDX or HMX which is formed into a cord and enclosed in a casing of lead. The lead casing serves to confine and channel the detonation so that it proceeds along the cord. The lead also serves as a protective cover and contributes to the transfer of energy between the explosive and the shell to be broken. The MDF is held in place against the shell by a backup ring. As detonation proceeds along the joint the lead is forced at high velocity against the shell and backup ring. A shock wave is produced in both the shell and backup ring and it is possible that a reflection or series of reflections of this shock causes failure at the center notch. It seems more likely that failure at the center notch does not occur until the shell is bent outward from the continuing action of the explosive pressure and a high tensile stress is built up. The separated strips continue to bend outward until they finally break at the extreme notches and fly off. The sudden release of load at rupture in these three places is probably a significant source of mechanical shock. During the time that the shell is being broken the backup ring is being forced inward to strike the overlap ring and transmit another shock. As the shell strips break free, the pressure bleeds off, but an impulse having both longitudinal and

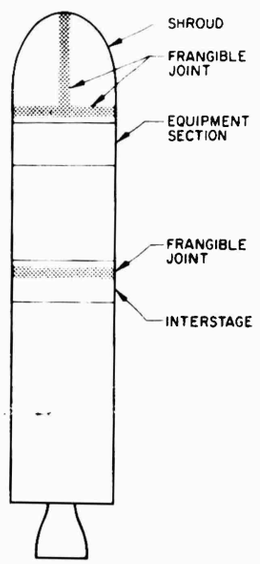

Fig. 1 - Typical placement of frangible joints

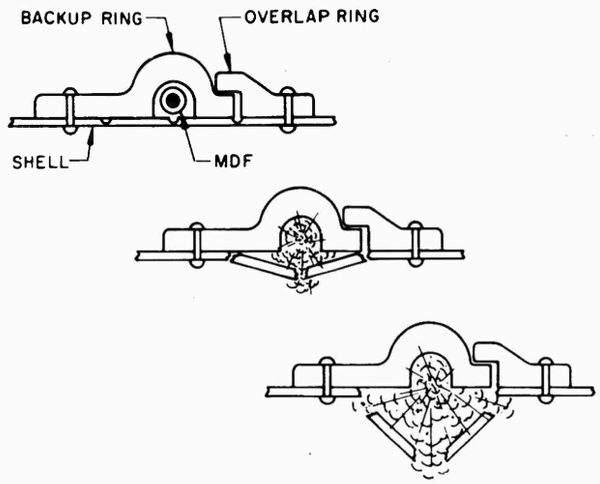

Fig. 2 - MDF joint

radial components is delivered to the structure by this decaying pressure.

The second basic joint design makes use of a flexible linear shaped charge (FLSC) in which the explosive and the lead casing are formed into a chevron cross section. Figure 3 shows the joint configuration and illustrates the manner in which cutting is believed to occur. The description which follows is a modification of that presented in Ref. 1 for conical charges. Figure 3(a) shows the lower half of the casing being forced into a converging stream of lead by the explosive pressure of the charge. By the time the process is completed at each cross section the stream is traveling at a speed of approximately 10,000 fps — a stagnation pressure of the order of 8,000,000 psi. Because the shear stress capability of the shell material is small compared to this pressure the shell directly underneath the impinging jet behaves like a liquid and a narrow gap is forced through the shell. Again a shock wave is produced in the shell and, to a lesser extent in the backup ring, by lead impact. When the shell is cut through the two halves are curled outward by the momentum they have acquired from the lead and by the continuing action of the explosive pressure. Strips do not fly off in this design and a higher total longitudinal impulse is delivered to the remaining structure by pressure acting on the curled edges of the shell. The rate of detonation varies somewhat with density[2] and is approximately 25,000 fps for both types of cord. The detonation pressure is approximately 5,000,000 psi. The size of both types of explosive cord is given in grains which refers to the weight of explosive per foot of length. Sizes ranging from 7 to 12 grains are presently in use at LMSC to break shells from 0.080 to 0.125 inch thick.

Frangible joints are used in preference to other separation systems such as explosive bolts and pin-pullers, because the structural geometry is simple and continuous, resulting in a lightweight, high-strength joint. Another advantage is that higher reliability can be obtained because a single initiation progresses completely around the shell. There is no need for each one of several charges to be ignited successfully. Added reliability can easily be obtained by adding extra initiators so that if any one functions the whole train is set off.

Our concern is more for the possible effects on equipment rather than for the integrity of primary structure because of the many successful separations in which structure has survived without damage. The possibility of damage to structure cannot be dismissed completely, especially if very brittle shell materials

[1] E. M. Pugh, R. J. Eichelberger, and Norman Rostoker, "Theory of Jet Formation by Charges With Lined Conical Cavities," J. Appl. Phys., Vol. 23 (1952), pp. 531-537.

[2] G. E. Duvall, "Some Properties and Applications of Shock Waves," Proceedings of the Technical Conference on the Response of Metals to High-Velocity Deformation, Estes Park, Colorado (1960).

with stress concentrations are used in close proximity to an explosive joint.

The first applications of frangible joints did not present a mechanical shock problem because no sensitive equipment, which was required to operate after separation, was located in the vicinity of the joint. In more recent designs potentially serious problems have developed. The first of these occurred during ground testing of missile subsystem. A relay located a few inches away from one of the separation joints was tripped during separation, causing a subsystem failure. The problem was complicated in this case by a large pre-tension across the joint. The shock displacements resulting from the sudden release of this pre-tension were believed to have contributed at least as much to the failure as the shock produced by the MDF explosive. A solid state switching device mounted on shock isolators was substituted for the relay and no further failures were encountered. Other failures from frangible joint separation have been suspected on more recent programs, but all of these have been traced to other causes. As of this writing, several successful flight tests and a ground test with operating equipment have been performed on missiles, which utilize an MDF joint. No harmful effects were observed due to separation on any of these tests. Three of the spacecraft programs at LMSC have had successful flight and ground tests of similar joints.

Acceleration measurements that have been made on structure and at equipment attach points in the general vicinity of frangible joints show extremely high acceleration levels ranging from 100 to 3000 g, at high frequencies from 600 to 6000 cps. In many cases these frequencies have been identified as local resonances. Shock measurements made on successive tests show a wide scatter of levels. Figure 4 shows a typical acceleration time history measured near an exploding joint. Much of the present concern that exists at Lockheed and at customer organizations stems from the fact that many of these acceleration levels are far higher than those produced by other environments or by environmental tests.

The severity of shock environments cannot be compared on the basis of acceleration levels only, and although these very high frequency shocks are much less damaging than lower frequency shocks of comparable amplitude, the fact remains that we have not, as yet, demonstrated that our equipment designs can consistently survive such shocks.

The nature of the shock produces some difficulties in measurement. Several of the measurements that have been attempted, to date, have been lost due to instrument malfunction. Some have been due simply to the wrong selection of range but many losses are caused by a "zero shift" phenomenon in which the data

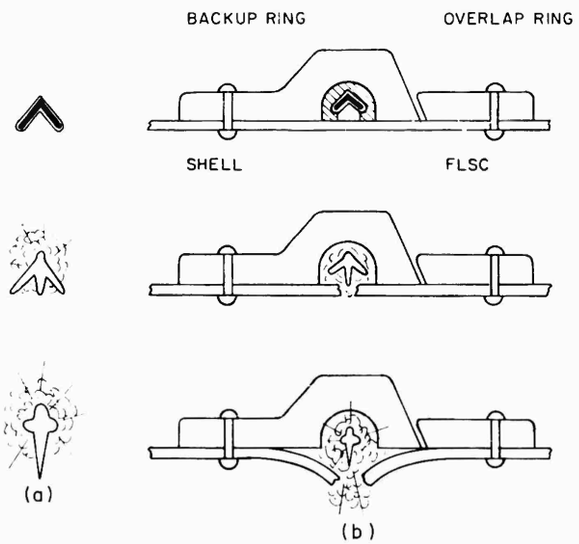

Fig. 3 - (a) Jet formation sequence, and (b) FLSC joint

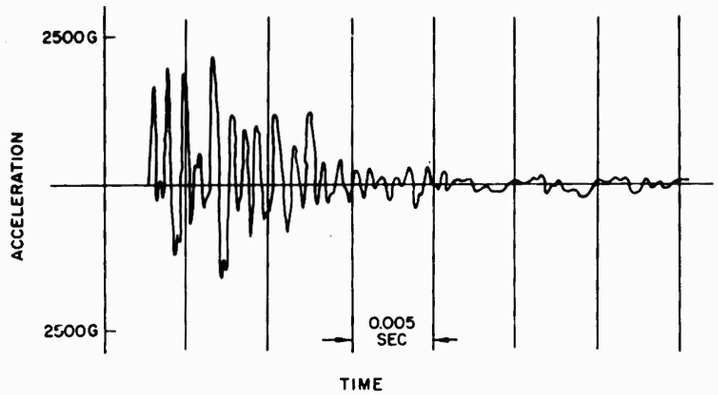

Fig. 4 - Typical acceleration record

is obscured by a sudden change in the zero acceleration line that decays exponentially in about 100 milliseconds. Recently developed piezoelectric pickups have eliminated this problem, or at least reduced it to negligible proportions. Other data have been lost due to electrical interference from the explosive cord initiators.

More serious than the problems mentioned above are those associated with making a meaningful interpretation of the data for the purposes of equipment design and equipment testing.

At the high frequencies shown by our accelerometer measurements, the dynamic response characteristics of the equipment and the equipment support structure involve normal modes of vibration that are much too complex to be computed. Measurements of dynamic response properties at high frequencies show that many of these modes are only important over a very local region of the missile involving a pound or two of structure and that structures which are made to the same drawings show large differences; these properties account for the wide variation of response on different parts of the structure and for much of the scatter of response from test to test. When we have obtained an acceleration measurement of a given point, say one corner of an equipment package, we have detailed knowledge of that point only. Other points, even the other three corners of the same package, are only similar in nature.

The traditional techniques for selecting equipment test procedures would result in only crude approximations of the actual environment. Standard practice consists of obtaining an estimate of the shock spectrum of the "design environment" based on statistical treatment of data taken in service of a similar environment. A shock machine is selected which has an output shock spectrum sufficient to envelope the "design environment." Most shock machines produce acceleration pulses which have a relatively large net velocity change as opposed to the roughly symmetrical acceleration transients, with negligible velocity change, produced by separation joint shocks. Figure 5 shows the effect of these properties on the shock spectra. The result of using a single pulse to simulate frangible joint shock would be some compromise between over-test of the low frequency modes of the equipment and under-test of the high frequency modes. This difficulty may be overcome by making a shock machine which produces no net velocity change, but there are other difficulties which may be even more serious and are much more difficult to evaluate.

The importance of simulating output impedance during shock and vibration testing has been discussed at some length in the literature.[3] The impedance problem is particularly serious in this case because of the very high frequencies associated with such shocks. A closely related problem is associated with the interdependence of motions at the different support points of a given equipment. Test machines are designed, as far as possible, with rigid tables to impose the same controlled environment at all input points; the separation shock environment differs greatly from point to point. It is believed that this difference would result in an overtest by some large, unknown factor.

[3] R. E. Blake, "Applications of Mechanical Impedance Information," Shock and Vibration Bulletin No. 30, Office of the Secretary of Defence (June 1962).

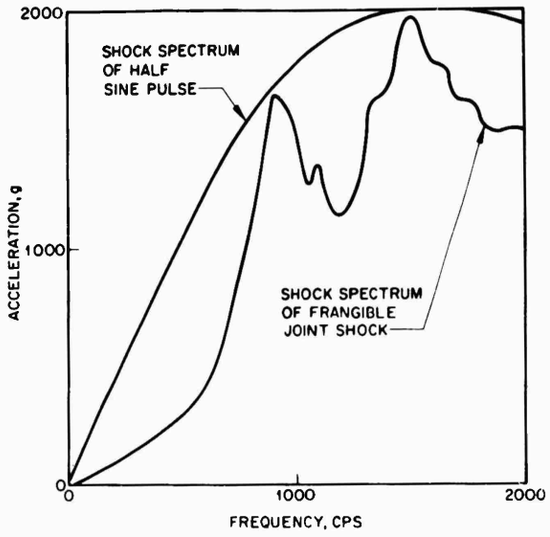

Fig. 5 - Shock spectra comparison

Because of the difficulties discussed above, the only reasonable equipment qualification test that we are able to run at this time is a realistic test of the equipment in the actual vehicle structure, subjected to the explosion of a frangible joint. The joint would be modified to produce a shock that is increased over the typical service environment by a controlled factor. This method should be very satisfactory for programs which are in the advanced stages of development but it does not answer the need for laboratory testing of equipment during the early stages of a program.

Several of the program organizations at LMSC have conducted experimental programs to determine how shock levels are influenced by changes in joint design.

In order to screen several suggested ideas without the cost of full structural testing, flat-plate samples have been used. A two-foot square test panel has become standard for this sample testing. Figure 6 shows a typical panel with accelerometer blocks mounted in the centers of each half; on future tests strain gage data and Fastax motion pictures will also be taken. The purpose of this panel testing is not so much to obtain specific data on the magnitude of strains or accelerations, but to gain a rough quantitative comparison between design concepts so that candidates can be selected for further full scale testing.

The joint characteristics which appeared most likely to influence the magnitude of shock were:

1. The kind of explosive charge used, FLSC vs MDF.

2. The size of charge used.

3. The thickness of shell being cut or broken.

4. The design of the backup ring.

5. The material of the shell being cut.

A preliminary series of tests on flat-plate specimens indicated that FLSC and MDF produced about the same shock in the configurations tested; that the size of the charge made no significant difference in the magnitude of the shock; and that even the backup ring did not greatly influence the shock, since a piece of FLSC simply taped in place on the sheet produced about the same acceleration levels as FLSC used in the standard backup ring. The thickness of the shell being cut appeared to be the only significant parameter.

To verify these results on a more realistic structure and to obtain data on other design changes, a series of tests were performed on the test setup shown in Fig. 7. A 1-foot segment

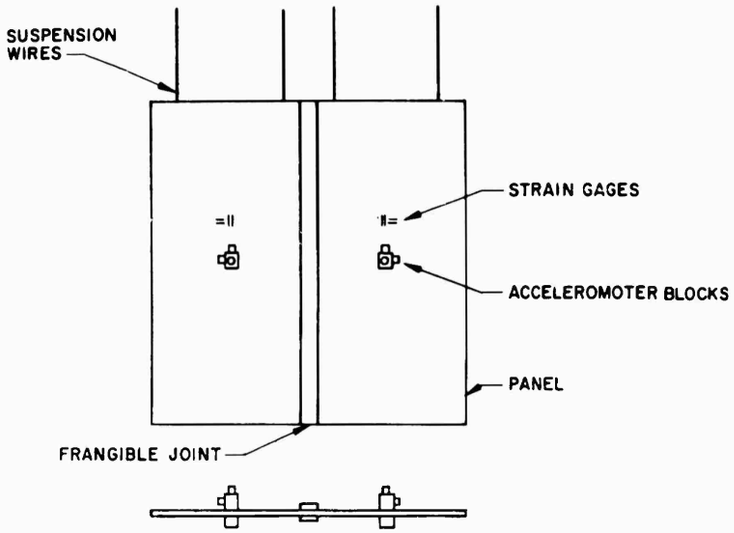

Fig. 6 - Flat-plate test specimen

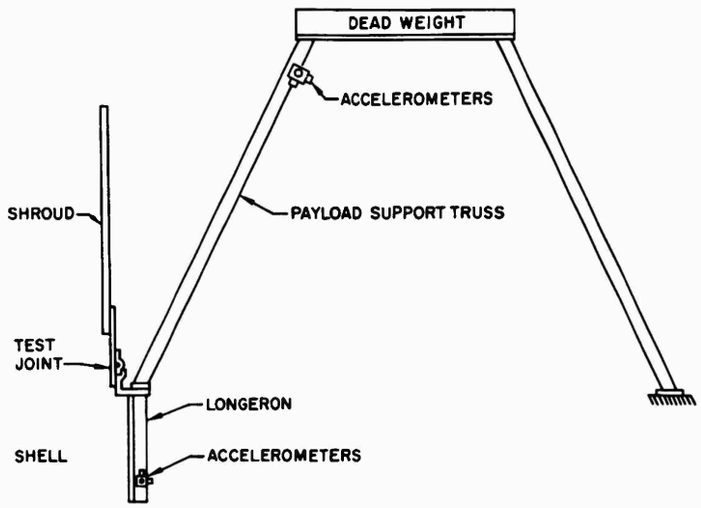

Fig. 7 - Shell segment test setup

of the shroud and satellite cylindrical sections, together with the assembly joint were connected to one leg of an eight-legged payload support truss. The other seven legs were supported, and the top of the truss carried a dead weight load. In addition to confirming the results of the previous tests, it was discovered that a reduction in acceleration of about 20 percent could be made by removing the backup ring overlap.

Three series of tests are now in progress. The first is designed to determine the overtest joint design for use on the qualification tests discussed above. A preliminary series of flat-plate tests is being made in which the breaking thickness and mass of the cut section are changed in various combinations. Promising designs will be selected for tests of full cylinder specimens. A series of repeated tests will

be made of the final design to obtain statistical data on the scatter of acceleration levels. The final choice of overtest factor will be based on these data.

The second program is designed to test specific ideas for reducing the shock produced during separation. These ideas are not intended as final practical joint designs but rather as promising design concepts. If they prove successful they could be modified to suit the needs of a specific vehicle. Specific design concepts which will be tested in the near future on flat plate specimens are shown in Fig. 8. All of these make use of symmetry to obtain local cancellation of part of the forces which act on the remaining structure during separation. The first three use mild detonating fuses to separate the cover plates. The method of obtaining stress concentration to aid in breaking is varied among the three. The third also incorporates two plates which fly off to carry part of the applied impulse away. The fourth design employs a flattened stainless steel tube, with an enclosed explosive charge, to separate the plates. The tube suddenly returns to a round shape but does not rupture when the charge is exploded. The next (detail f) uses two flexible linear shaped charges to cut the sheet. The charges are inclined to determine whether or not the longitudinal impulse, and thus the resulting shock, can be reduced in one direction.

The last detail of Fig. 8 shows a flexible linear shaped charge firing through the sheet into a reflector strip. The reflector strip is bonded weakly in place so that it can fly off after the first reflection. After this first group of tests has been run the results will be evaluated and other designs tried. Again, promising designs will be evaluated on tests of full cylinder specimens.

A third category of tests is designed to increase our understanding of the separation process and to help us judge the relative magnitude of the various forces acting on the structure during separation. Three tests are planned in this category. The first consists of a standard MDF joint in which the shell is pre-cut at the notches. The pre-cut shell strips are held in place by thin wooden strips at the top and

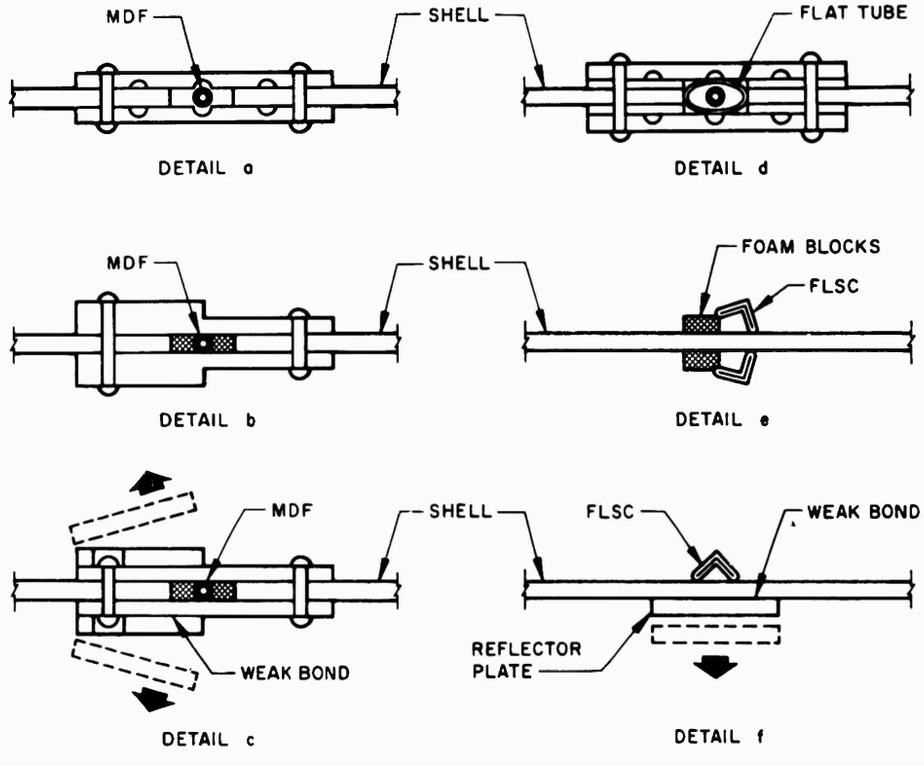

Fig. 8 - Proposed low shock joint design

bottom of the test panel. In a second test the strips are removed completely and the charge is fired in a bare backup ring. These two tests would determine the effects of gas pressure and backup ring contact without the influence of the forces generated in breaking the shell. A third test is a comparison between the shocks produced by an FLSC charge cutting a plate and then an identical charge firing through a narrow gap in a pre-cut plate.

At the conclusion of the test programs presently in progress we expect to be able to perform realistic and meaningful system qualification tests of equipment for programs that are advanced to the stage where realistic structure is available for use as a test stand; and to have evolved design concepts which, when applied to separation joints on future vehicles, will result in greatly reduced shock levels. But there is a great deal of experimental and analytical work that needs to be done before we can predict, even reasonably well, the shock environment that will occur on a future vehicle; design equipment and equipment support structure to withstand this environment; or build a shock machine that simulates the environment with acceptable realism.

DISCUSSION

Mr. Stewart (Douglas Aircraft): Was your opinion that a simple pulse shape simulated these shocks based on some experience? Did you actually perform tests using half-millisecond duration half-sine shocks on relays at 1000 g? Somehow, I don't have much feel for whether a half-millisecond shock is serious or not.

Mr. Paul: No, it wasn't based on actual experience because Lockheed doesn't have a shock machine available which will produce that kind of half-millisecond shock. The importance of doing this is probably not great for fairly small components which do not have low frequency resonances. Some people were seriously suggesting doing this for something such as an entire spacecraft. The stresses that would result from that kind of a velocity change are fantastic.

Mr. Stewart: You mentioned, when you were talking about the various design modifications, that you were attempting to see the effects of each on the shock level, and that skin thickness made a considerable effect. What was the effect?

Mr. Paul: The effect was approximately linear. A doubling of the skin thickness produced a doubling of the shock level. I say approximately because there's a good bit of scatter on repeated tests.

Mr. Stewart: Similarly, when you ran different materials, were these materials of the same thickness or the same strength?

Mr. Paul: They were of the same thickness.

Dr. Mains (General Electric): What is your concept of the mechanism by which the shock is transmitted into the surrounding structure once this explosive goes off?

Mr. Paul: I think there are several possible mechanisms. I believe the most important one is the residual gas pressure acting on the backup rings before it has a chance to bleed off. Another possibility, at least on the MBF joints, is the sudden release of load as the shell breaks. The very high frequency direct shock of the lead impact may be another mechanism, but I think it's too high in frequency to give us concern. It was too high to fall within the range of the instruments that we are using.

Dr. Mains: So the primary shock would be in the direction normal to the plane of cutting?

Mr. Paul: The primary shock, yes — the largest component. But there was an exception to that. In the diagram that showed the flexible linear shaped charge joint, you notice the edges were curled down. This exposes a fairly large longitudinal area to the gases and we noticed in our Fastax pictures that there was a considerable longitudinal impulse imparted to the two plate halves during this separation.

Mr. Bowman (Jet Propulsion Lab): What type of frequency response did your instrumentation have for looking at this information?

Mr. Paul: Up to 10,000 cps. This was our cutoff.

Mr. Bowman: I see. We have seen other explosives which produce frequencies in excess of 6 kc and even up to 10 or 11 kc. With regard to a previous question on relay problems, we have been doing some shock testing with half-millisecond pulses in the order of 200 to 400 g,

and yes, there is failure as a result of the terminal peak sawtooth pulse that we have been using.

Mr. Paul: Whereas they would not have failed under a transient of this sort?

Mr. Bowman: We haven't seen relay failure in the electronics. However, the level was considerably reduced because of their remoteness from the explosive.

Mr. Forkois (NRL): Did I understand you to say that the effect of this shock was transmitted to the entire body of the missile, or is it attenuated and disappears before it gets too far?

Mr. Paul: Well, it's a question of how you define too far. We were very much surprised at how far it did go. Our measurements extend to about 1 missile diameter from the joints and there was still appreciable shock, somewhat attenuated, but still significant at that point.

Mr. Bodner (Brown University): It seems that from your panel test where accelerometers were located in the middle of the panel, you'd be measuring the reflected waves from the edges. In that test, the reflections of the stress pulses back and forth would result in a much longer shock history than would be the case in a structure where the pulse would just travel down the structure. If this is the case, then, it seems from your first diagram that the pulse length with many oscillations would be much longer than one would expect from a single charge.

Mr. Paul: If I understand your question, the diagram in which I showed a typical acceleration trace was not taken from the flat panel test. It was taken from a test of a full cylindrical structure. We do see transient responses of many oscillations, both on the full cylindrical shell and on the flat panel. Your observation that the flat panel would ring for a long time is true, but, in both cases it's a transient of many cycles, not a single pulse.

Mr. Callahan (McDonnell Aircraft Corp): On the first slide you showed a separation of a shroud through the center, clamshell type. In any of the flights did you have measurements on the payload resulting from that type of separation?

Mr. Paul: Both the circumferential and the longitudinal joints are exploded simultaneously so that we would not be able to distinguish which of these two joints actually produces the shock, or to sort out how much came from each. During ground separation tests, where our best data come from, we were getting something of the order of 600 g on the forward part of the payload, or the part of the payload on top of the truss. It's different at different points but this is a rough average of the kind of data we were getting at equipment support points.

Mr. Sanders (North American Aviation): I have two quick questions. One, have you conducted any tests in which the shaped charge did not impinge on your test body to see whether you still have a shock environment? Number two, what type of reduction have you achieved with your tests thus far?

Mr. Paul: The answer to your first question is that we have not conducted such a test. It would be a fairly complicated joint to design and we were going to try to make a comparison between a flexible linear shaped charge cutting a panel, and a similar charge of the same size firing through a pre-cut gap to see if there is any significant difference between these two.

Mr. Sanders: My main question was, if you did not actually cut material, how much of the effect may be acoustic coupling or some other mode of coupling rather than the mechanics of cutting the material itself.

Mr. Paul: This is what we hope to discover. We would have the blast wave acting on the shell, but would get no cutting action whatsoever. There would be a gap through which the lead stream could flow without touching. So far we have not done this because none of the tests that were outlined on the eighth flight have been run yet. The best reduction we have been able to obtain so far is by reducing the shell locally as much as possible. This would depend on how much overstrength it had to begin with, in some cases this is a factor of 2 or so.

* * *

SHOCK ENVIRONMENTS GENERATED BY PYROTECHNIC DEVICES

H. J. Roberge and J. Rybacki
General Electric Company

A testing program to study shocks generated by pyrotechnic separation devices is described and typical shock response data is presented. Inadequacies of existing instrumentation, simulation, and analysis techniques are discussed. Remedial measures that were employed to negate the shock effects are described.

INTRODUCTION

Various pyrotechnic separation devices have been employed on several General Electric space vehicles. Prominent among these devices are shaped charges, either taped to the structure or encapsulated within a metal ring, which sever the structure when ignited, and clamp-type devices which are activated by explosive bolts. Instrumentation to monitor the shock response resulting from detonation of these devices was installed during tests performed to verify compliance of the system with rigid-body separation specifications. It was felt prior to these ground tests that extremely high acceleration levels occurring at high frequencies would be recorded in the proximity of the separation device and that a relatively short distance away, the levels would be insignificant due to large attenuations through the structure. However, very high accelerations (over 1000 g in some cases) were measured at significant distances from the separation plane. Since the levels measured were sufficiently severe to cause concern as to the capability of the electrical equipment to withstand the environment, additional ground test programs were undertaken to evaluate the effect on the electrical equipment.

This paper presents a brief summary of the information obtained from these tests programs. The problems encountered in measuring the shock resulting from separation are discussed along with the failure modes that were experienced as well as the remedial measurements that were employed. Typical data measurements are also presented.

TESTING PROGRAM

Initially, tests were conducted on partial sections (complete as to diameter, but not length) in order to demonstrate structural adequacy and equipment functioning in the area of the separation plane and to check out instrumentation techniques. The partial sections, weight ballasted to simulate actual weight and inertia, were suspended horizontally from long cables so that no static load was applied across the separation plane. The booster portion of the section was rigidly attached to a fixture. Considerable testing of this nature was conducted prior to attempting full scale tests.

The full scale tests conducted on prime operational vehicles differed from the section tests in that the prime vehicles were suspended nose down. The booster was simulated as much as was thought practicable and after separation the vehicle was caught in a net. Additional prime vehicle tests were conducted under near vacuum conditions. Extensive data measurements were made on all these tests.

Component shock tests were also performed to determine component behavior and to evaluate shock attenuation design changes.

INSTRUMENTATION

Recording System

Serious problems were encountered in trying to measure strain and acceleration data during these separation tests. Amplifier

saturation, accelerometer zero shift, strain gage power variations, and low recording system frequency response were encountered.

The acceleration measuring system, which was the most satisfactory, consisted of Endevco Model 2225 accelerometers matched directly into tape recorders by Columbia Research Lab cathode followers. Cathode followers were selected because of their ability to accept high-input-signal voltages. The tape recorders were run at 60 ips in the FM mode which resulted in a 10 to 10,000 cps frequency response. The recording system was checked prior to each test to maximum level with a square wave generator using the voltage insertion technique.

The strain measuring system consisted of independently powered potentiometer circuits which were matched into the tape recorder using CEC Model 112C linear amplifiers. The tape was run in the FM mode at 60 ips which resulted in a 0 to 10,000 cps frequency response.

It was also possible to use the AM mode which afforded a 100- to 30,000-cps frequency response on the strain data and a 100- to 100,000-cps response on the acceleration data, but this very high frequency response was found to be unnecessary since the recordings that were made showed the upper frequency to be approximately 10,000 cps; also, it was particularly important to record the acceleration data on FM because the zero frequency response allowed recording of the accelerometer zero shift.

Acceleration Transducers

Zero shifts in the response data were very much in evidence during the early tests. This phenomenon[1] was characterized by a sharp increase in displacement of the reference voltage followed by a slow decay to the original voltage level (see Fig. 1). The presence of this shift

[1] R. R. Bouche, "Survey Report on Quasi-Constant Voltage Outputs from Piezoelectric Acceleration Pickups Subjected to High Shock Accelerations," Endevco Corporation (Aug. 1962).

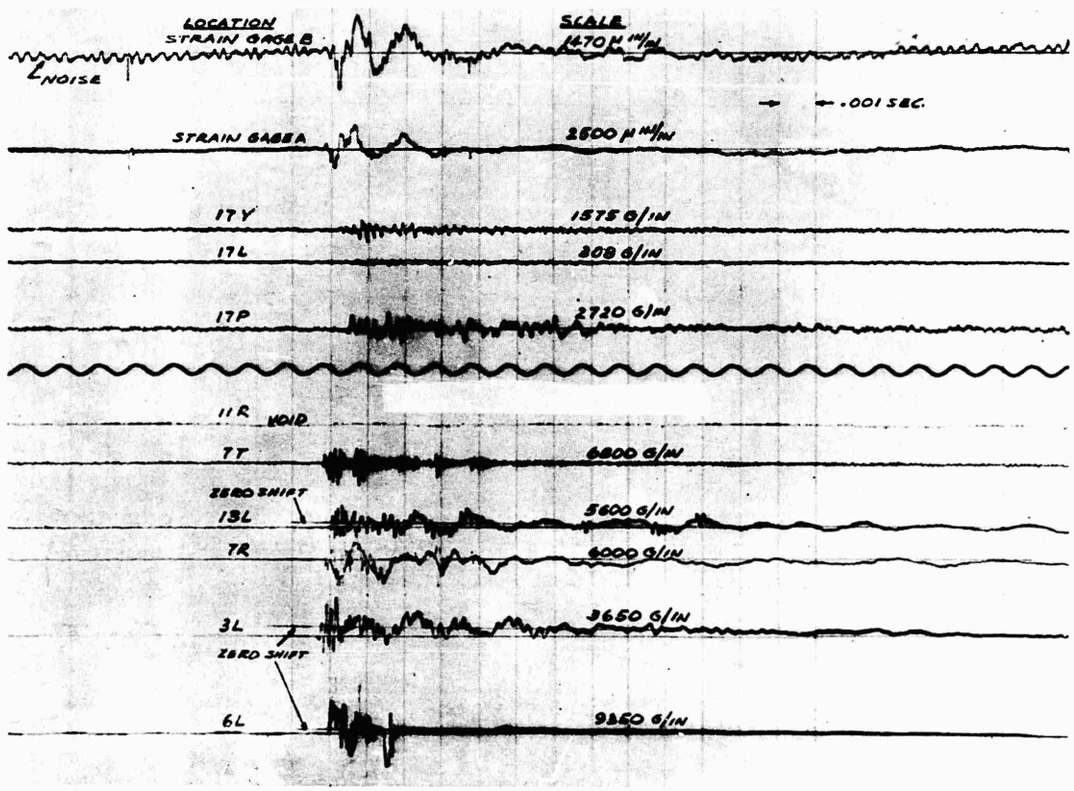

Fig. 1 - Records illustrating zero shift

cast doubt on the validity of the dynamic data which was superimposed on the displaced reference line since the acceleration readings were dependent upon the readers' interpretation. Eventually, Endevco Model 2225 shock accelerometers were used, since these accelerometers displayed lower incidence of zero shift than other accelerometers. Calibration of the accelerometers up to the anticipated high amplitudes and frequencies was accomplished at the factory by use of the method and equipment discussed in Ref. 2.

Data Playback

Two data playback schemes were employed. In one scheme, data were played back into a Miller electron beam oscillograph which had a 70-kc frequency response. The paper speed used was 400 ips. The second scheme utilized conventional oscillographs but the tape playback speed was reduced by a factor of four to obtain the required frequency response.

Relay Chatter Indicator

A silicon controlled rectifier (SCR) circuit was designed for individual relays to record relay chatter and switching. A relay malfunction was indicated by the lighting of a light bulb which remained lit after the malfunction. With these circuits, it was possible to monitor chatter durations of either 10 or 100 microseconds.

SHOCK RESPONSE DATA

Shock response data were obtained for the vehicle separation event for two types of vehicles which employed circumferential shaped charges. Shaped charges that were either taped to the structure or were encapsulated in metal rings were both investigated with no appreciable difference in shock severity being noted. This same conclusion was reached when the powder charge was reduced 50 percent from 15 to 7.5 grains/ft. Shock responses were obtained under ambient conditions and in near vacuum for which it was noted that, in general, the vacuum responses were higher in magnitude and were cleaner in appearance. The validity of data obtained under ambient conditions was always subject to question since the extent of the measured response due to acoustic excitation of the structure could not be accounted for. Shock responses were also obtained for a vehicle employing a Marmon type clamp and explosive bolts. Final data from these latter tests are not presented because of their unavailability at this time; however, preliminary test results are discussed. Typical response data that were obtained are shown in Figs. 1-3. Initial and maximum acceleration amplitudes and associated half-cycles are presented in Table 1.

Vehicle Test — Shaped Charge Separation

Figure 2 contains the responses of several accelerometers located on the structure plus the recorded signal sensed by a microphone inside a prime vehicle. These data were measured on a re-entry vehicle which had ablation material along its entire length which provided a high degree of structural damping as evidenced during vibration tests. In addition the vehicle had a soft phenolic spacer ring in the transition section between the separation plane and the re-entry vehicle. Significant attenuation of the shock transient was provided by this damping and by the impedance mismatch of the plastic ring, but high structural responses were still measured.

Note the following significant points in Fig. 2:

1. Notice the fairly uniform frequency and time-to-peak exhibited on all traces.

2. There appears to be no difference in response intensity in either the radial or longitudinal directions.

3. Extremely high acceleration levels occurring for short durations were recorded on channels 1R, 2L, 2R, and 3R which are located on primary (very stiff) structure within a foot of the separation plane. (R and L indicate radial and longitudinal directions.)

4. Notice the very high levels and short durations on channels 6R and 9L which are located on primary (very stiff) structure some 5 feet from the separation plane.

5. Note the high level and short duration on channel 7L. This component is mounted on a partial bulkhead and has a fairly low mounting frequency (70 to 100 cps).

6. The Statham accelerometer (located 5 feet from the separation plane — last trace)

[2] R. R. Bouche, "The Absolute Calibration of Pickups on a Drop-Ball Shock Machine of the Ballistic Type," Endevco Corporation (Apr. 1962).

TABLE 1

Location	Distance from Separation Plane (in.)	First Pulse		Other Pulse	
		Level (g peak)	Duration (μsec)	Level (g peak)	Duration (μsec)
Data from Fig. 2					
1T	11	855	100	1070	250
9L	95	181	450	217	500
7L	60	256	560	370	750
6R	24	115	150	138	500
2R	11	543	200	1267	500
2L	11	1218	150	870	500
1R	11	360	200	512	500
Statham Microphone	95 Center Sep. Plane	125 185 db SPL or 8-psi peak	750	212	750
Data from Fig. 3					
1	8	2430	91	1458	360
2	39	1284	109	1200	250
3	109	126	390	203	625
4	10	211	198	500	23
5	10	142	198	214	486
6	22	560	456	675	395
7	22	174	440	276	548

responded at its natural frequency (750 cps) at a very high level. This is indicative of the response which could be expected for a component mounted at this location having the same frequency and damping as the accelerometer.

7. The microphone (second trace from the top) located at the center of the separation plane indicated approximately 185 db.

Figure 3 contains the responses at three points along a stringer, the responses at the bases of two typical black boxes, and the responses of accelerometers located alongside the relays. A sketch showing this instrumentation layout is presented in Fig. 4. During the test from which this data was obtained, the chatter indicator that was used recorded chatter of three of five relays on the forward box and of one relay on the aft box. Indication of unlatching of one of the relays from the normally open position was also observed for a relay in the forward box. Note the following items of significance in Fig. 3.

1. Significant attenuation of the shock transient was provided by the structure. The peak response of accelerometer #1 located 8 inches from the separation plane was 2430 g. Approximately 30 inches away at accelerometer #2 the peak recorded g level was only 1280 g, while accelerometer #3 approximately 100 inches away indicated a level of 200 g. It is apparent from the traces that the high frequency portion of the shock transient is appreciably attenuated. The amount of attenuation of the low frequency content is not as obvious and it appears to be of a much lesser degree.

2. The marked difference in the chatter behavior of the relays in the two identical boxes was attributed to the difference in attenuation characteristics of the two mounting arrangements. (The aft box was on a softer mount.) Note that the peak response of the stringer near the attachment point of the aft box bracketry was 2400 g while the input into the box had a peak value of only 300 g. Note that for the forward box the peak stringer response is approximately 1500 g while the input into the box exceeded 600 g. The responses of the tops of the two boxes to these different inputs are similar in shape; however, the response of the forward relay box is slightly higher — 276 g-peak response for the forward box as opposed to 214-g peak response for the aft box.

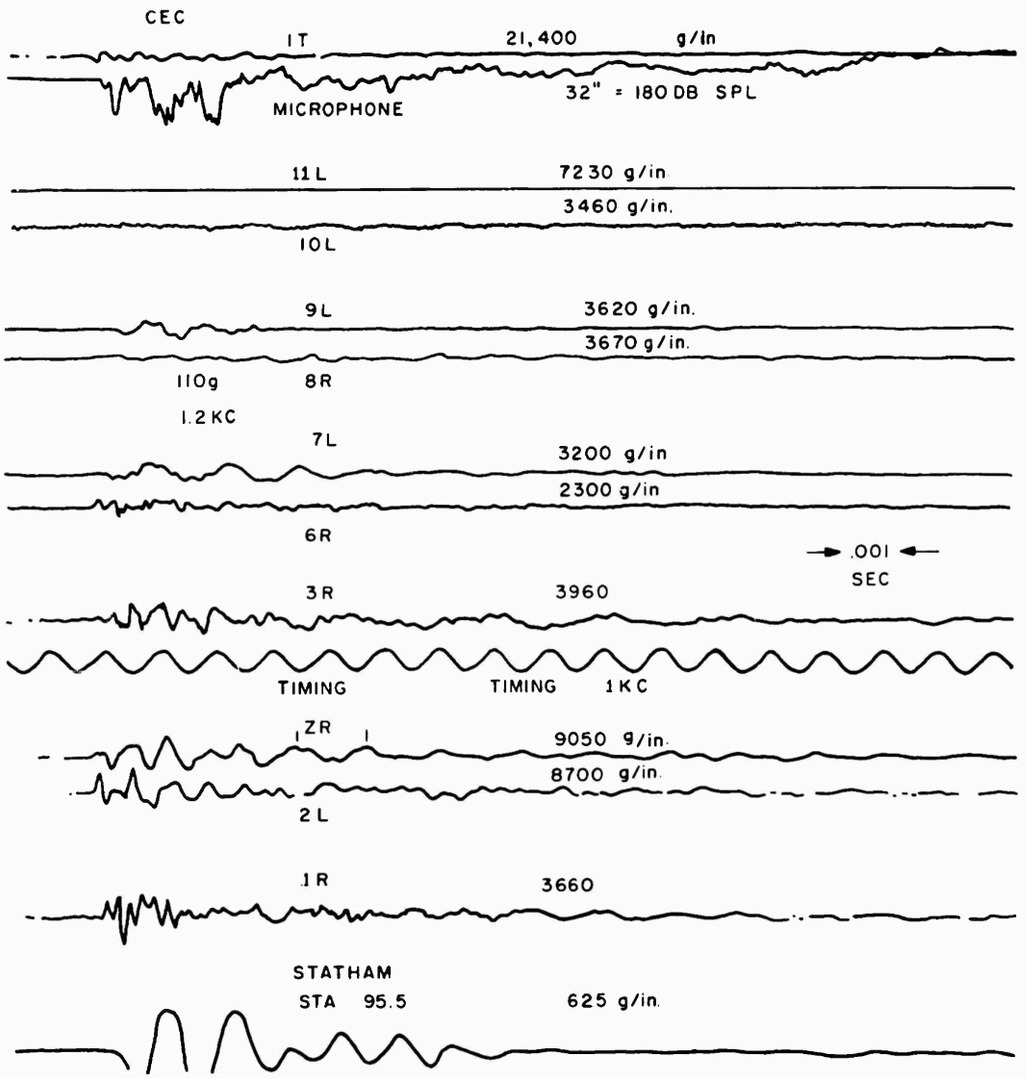

Fig. 2 - Accelerometer and microphone responses

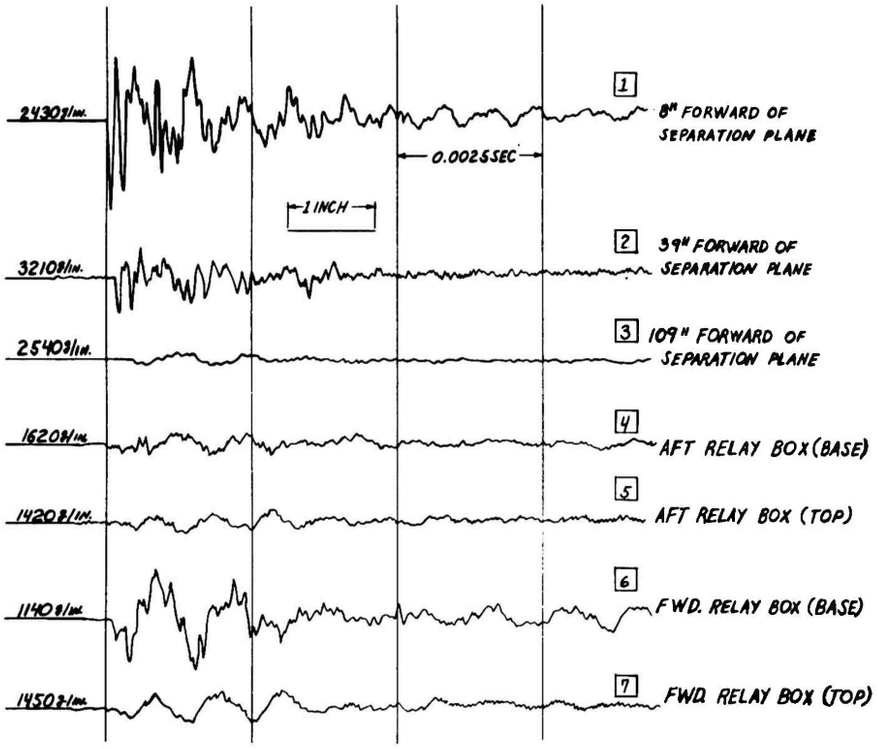

Fig. 3 - Responses along stringer

Vehicle Tests — Clamp Release

Separation tests employing a clamp device with explosive bolts were performed using an instrumentation layout identical to that used in one of the shaped charge separation tests (Fig. 4). No relay malfunctions were detected during these tests, but acceleration levels were still fairly high; 500 g was indicated by accelerometer #1. This level, though high, was attenuated sufficiently by the structure so that levels in proximity of the relays were less than 50 g. The mechanism of the shock resulting from the clamp release differs from the previous shock mechanism since part of the shock arises from the quick release of the structure from the compressed position existing after the clamp band is installed and tightened.

FAILURE MODES

R. F. switch failures and magnetic tape recorder failures attributable to the separation shock have occurred during flight on some vehicles. The ground test programs have shown that the separation shock may induce chatter and switching in relays. It was also shown in ground tests that the shock will cause flaking off of thermal coatings on the vehicle shell. Other malfunctions which are possible, but which were not experienced, are failure of brittle components such as glass resistors and diodes. In the case of taped shaped charges, care must be taken to insure that mechanical devices in the vicinity of the separation plane are not damaged or jammed by the flying shrapnel and that the thermal properties of adjacent surroundings are not altered since a thermally conductive lead deposit covers everything in the proximity of the separation plane. These latter effects are of course not experienced by encapsulated shaped charges.

SIMULATION OF SHOCK IN THE LABORATORY

Component shock tests were undertaken to eliminate the cost and complexity of continued full scale vehicle testing. Acceleration "half-cycles" were selected from the time histories of the responses measured at the mounting points of components during full scale vehicle

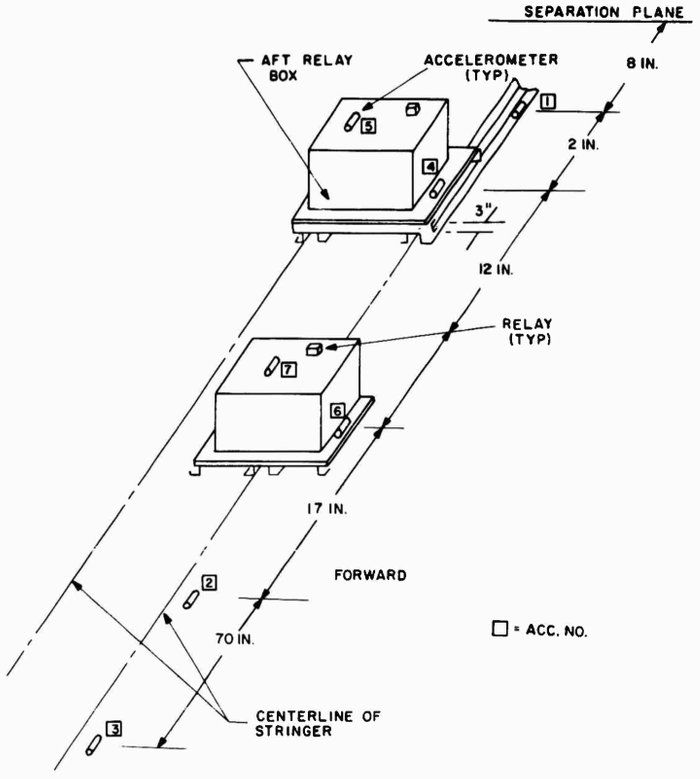

Fig. 4 - Instrumentation layout

tests and were used as "ball park" inputs for the laboratory shock tests. The testing was nondestructive, since the only failures consisted of relay chatter or switching, or both, and therefore allowed repetitive testing at a variety of half-cycle periods and amplitudes.

The test apparatus consisted of a drop test machine, a fixture containing the component and necessary accelerometers and recording equipment. A test was conducted by releasing the anvil of the drop test machine which then fell straight down onto the top of the test fixture. The amplitude and period of the input were controlled by varying the drop height and by varying the thickness of heavy paper that was used to cover the contact area. The apparatus and procedure were successful to the extent that the first half-cycle of the applied shock matched the desired input. The decay of the transient from this point in time did not resemble the time histories experienced in the vehicle very closely, but this situation was acceptable since there was no attempt made to duplicate the entire time histories. If anything, the laboratory transient regarding the number of peaks and the magnitude of the peaks was thought to be less severe than the shock transient experienced by the components in the vehicle.

The component tests resulted in relay malfunctions at shock levels consistently lower than those measured for these items during the prime vehicle tests. This can only be attributed to the improper simulation of the component mounting characteristics and the associated shock input. Shock spectra analysis of the shock transients experienced by the component in the vehicle and during the individual component tests would have been of great assistance in determining the area of overtest; however, these were not obtained. An attempt to improve the laboratory simulation of the shock in the components was not made since it was felt this approach would be nearly as complex and costly as prime vehicle tests for the number of components under consideration.

Despite the drawbacks of the component shock tests, they provided very useful information to evaluate proposed mechanical and electrical redesigns. This was borne out when it was shown by test that the relays were less susceptible to malfunction if power was maintained in the electrical circuits. These tests have provided confidence in the final redesigns since it was shown that they were conservative. (Relay malfunctions occurred at lower shock levels than those measured in prime vehicles.)

ANALYSIS TECHNIQUES

Analytical predictions of structural responses to separation shocks have been attempted with limited success to date. The familiar problem of designating the dynamic characteristics of the structure (mass, stiffness, and structural damping) is accentuated in analytically treating the present shock loading due to the extremely high frequency characteristics of the excitation and structural response. The problem is compounded since a definite description of the forcing function involved is not available. Further complications arise from the predicament that the responses that are sought are those for very small electrical parts (e.g., relays and diodes) which are themselves contained in small black boxes. This means that to do a proper prediction and evaluation, the dynamic properties of the individual components must be ascertained and included in the structural model. Even after the responses of a relay are predicted, the relay must then be subjected to this environment to determine whether or not it will malfunction.

The above discussion presents a discouraging picture. Some encouragement has been offered, however, as a result of one analysis which was moderately successful. The acceleration amplitudes resulting from this analysis were very close to measured amplitudes within the vehicle although the force required to cause this axial response was very high.

At the present time, the following approach is being followed: On upcoming tests, greater emphasis will be placed on attempting to determine a description of the forcing function. The analysis will concentrate on predicting the response of the entire component and the effect on the relays, and so forth, within the component will be determined by imposing this environment in the laboratory. Drawbacks in trying to simulate this shock in the laboratory exist, as pointed out elsewhere in this paper, but, it is felt that the benefits derived from performing controlled tests will give valuable information for evaluating and ferreting out potential malfunctions.

REMEDIAL MEASURES

Two types of design modifications were utilized. These were used on different types of vehicles and were not employed simultaneously. The first type of redesign came about as a result of the component shock tests and consisted of shock mounting the critical components and maintaining power on the relays in these components. Lord BTR mounts were used and were selected so that the natural frequency of each mounted item was approximately 70 cps. Levels of 75 to 125 g at frequencies from 300 to 800 cps were still measured on these equipments. The second type of redesign consisted of replacing the shaped-charge-separation device with a clamp-type device employing explosive bolts to release the clamp. This redesign provided the most certainty regarding alleviation of the shock, but it resulted in an increased vehicle weight. No modifications were made regarding flaking off of the protective coating as the separation event occurred at a time when the coating was expendable.

Other protective measures showing great promise were proposed but were not investigated in great detail. Among these were:

1. Design a structural joint between the separation plane and the remaining structure and incorporate a design having inherent attenuation capability and include a large impedance mismatch.

Shock tests on long segments[3,4] have shown that appreciable attenuation can be expected across some types of structural joints. Attenuations as high as 30 to 60 percent may be expected across matched angle joints, whereas riveted butt joints provide literally no attenuation. It is also shown that the attenuation across the joint may be greatly enhanced if large impedance mismatches are incorporated in the joint design. Impedance mismatch may

[3] "Propagation of Elastic Waves Through Structural Connections," Cornell University, Department of Engineering Mechanics and Engineering Materials, Progress Report #1 (Jan. 15, 1954).

[4] "Propagations in Solid Media," Cornell University, Department of Engineering Mechanics and Engineering Materials, Final Report (June 1, 1953).

be brought about if materials having large difference in acoustic impedance are installed. For example, a spacer composed of thin layers of dissimilar material could be used to separate the two halves of the joint.

2. Design the electrical circuits so that all the relays are reset immediately following the separation event. This type of "fix" would be ineffective for those cases where unscheduled uncorrectable events could occur before the reset event. Other methods would have to be devised to protect these circuits.

CONCLUSIONS

It has been demonstrated by ground and flight tests that (1) there are no deleterious effects on the structure as a result of utilizing pyrotechnic separation devices, and (2) electrical malfunctions may be caused by shaped-charge-separation devices. Relay switching and chatter have been the only electrical malfunctions detected conclusively, and as a result, it has become necessary to scrutinize electrical systems to ensure that these malfunctions do not ruin a flight. No method other than test has been found to predict the occurrence of these relay malfunctions.

* * *

Section 3
TRANSPORTATION ENVIRONMENT

TRACK-VEHICLE MISSILE SYSTEM DYNAMIC ENVIRONMENT DATA ACQUISITION AND APPLICATION

R. Eustace
Martin Company
Orlando, Florida

This paper reports on the development of a flexible system level track-vehicle engineering development road test program which can be conducted at any convenient location and is capable of reproducing with reasonable accuracy all but the endurance courses at Aberdeen.

In addition, typical data are presented for the Pershing missile on an XM474E2 track vehicle when subjected to these course conditions. A method of presentation of these data is shown which can provide, in a condensed format, an insight into the system response characteristics. The application of these data toward verification of the static and dynamic criteria is reviewed.

INTRODUCTION

In recent years, a clear trend has been toward increased mobility in the field army. The requirement for a weapon system to operate with considerable flexibility under tactical conditions often makes mobility a significant weapon system design parameter. The term mobility has many definitions. As used herein, mobility is restricted to the rough ground performance of a vehicle system over firm inelastic cross-country terrain.

In order to design a weapon system properly, with sufficient ruggedness for cross-country operation, a clear definition of cross-country is, of course, required. Unfortunately, a satisfactory definition of cross-country does not currently exist. Until such definition is made, it is the usual practice to provide a weapon system which can withstand the punishing Aberdeen Proving Ground test conditions at speeds indicated in the vehicle system utilization goals, without restrictions if possible.

At present, there are three recognized classes of vehicle-system mobility tests. These are (1) smooth road surfaces, (2) selected Aberdeen Proving Ground (APG) Munson courses appropriate for a given type of vehicle, and (3) cross-country courses designed for endurance road testing. Currently, all military vehicles are exposed to these APG course conditions.

Prior to formal road testing of a vehicle or system at APG, compatibility road testing of equipment on the carrier vehicle is desirable to verify the system design criteria early in the design phase, establish human tolerance limitations, and to locate critical speeds and course conditions which require special attention in subsequent design. Formal APG tests are normally conducted in the latter stages of a program at a point when revisions in criteria seldom can be tolerated.

DISCUSSION

Design Criteria

The two principal dynamic environmental conditions of interest in establishing and verifying design criteria are:

1. Low frequency quasi-static loading due to rigid-body response of the vehicle.

2. Higher frequency dynamic response due to tracklaying.

Preliminary criteria are established to cover these conditions based on experience, judgement, and review of related programs. As soon as is practical in the development program, the entire system should be subjected to the design environment to confirm or improve upon the established criteria.

Test Courses

The APG Munson courses are engineering development courses and are intended to evaluate, under reasonably controlled conditions, the response of a vehicle to specific inputs. At present, two Munson courses are commonly used to evaluate the system response of track vehicles. These include the 6-inch washboard course and a spaced ramp course (Fig. 1). The 6-inch washboard course consists of a permanent concrete sinewave course. The ramp course consists of 6-foot long ramps, 6 inches in height, spaced as needed for a given test.

Both course conditions can be simulated with satisfactory results at little cost using ramps of a slightly revised design (Fig. 2). A reduction in the length of the APG ramps from 6 to 5 feet allows these ramps to also reproduce the washboard course (Fig. 3).

Spacing of these ramps varies for various types of vehicles. The spacing of the ramps for a particular program is based on utilization objectives, the recommendations of APG, an intuitive judgement of course conditions critical for a given vehicle, the results of an analog computer simulation of the vehicle traversing ramps on various spacings at representative road speeds, or a combination of the above methods.

To be successful, an analog computer simulation of the vehicle must be able to account for nonlinear vehicle springs, lifting of vehicle wheels off of the course surface, bottoming of the suspension system, and the constraints offered by the track in limiting the motion of the roadwheels.

Analog Computer Simulation

A novel method for simulation of these conditions has recently been devised and it seems to offer promise as a means of controlling these parameters. This method is based on varying the spring rate as a function of the roadwheel spring length.

In a typical case, equations of motion are generated for a two-degree-of-freedom system (vertical translation and pitch about the center-of-gravity) as shown in Fig. 4.

Load-deflection curves are plotted for the vehicle roadwheels with the points at which bottoming will occur, the static deflected

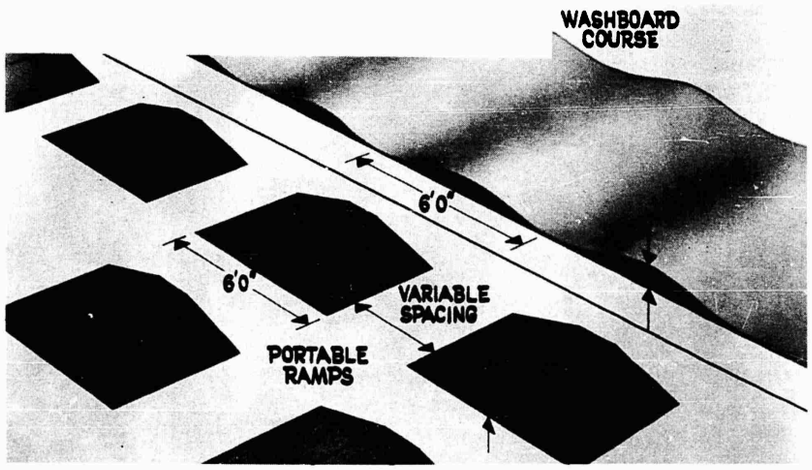

Fig. 1 - Aberdeen Proving Ground Munson track-vehicle system courses

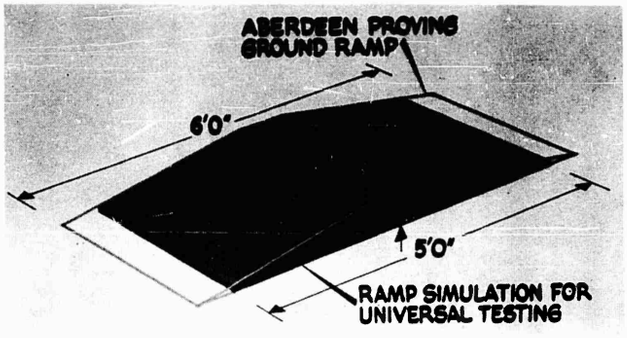

Fig. 2 - A comparison of the Aberdeen ramp with its simulation

positions of the springs, and the average minimum spring forces carefully noted. The minimum spring force for a given roadwheel assumes that the spring cannot be fully extended due to constraint offered by the track. Nonlinear springs are then generated from these curves as shown in Fig. 5. The analog problem is set up using the static deflected position of each spring as the initial condition. Subsequent spring rates are selected by the computer as a function of the length of each spring. A severe nose-down pitching condition, for example, shortens the spring until bottoming occurs. At this time a significantly higher spring rate is introduced. Conversely, a nose-up pitching condition lengthens the spring until the minimum spring force is attained. At that point, the spring rate is reduced to zero, corresponding to removal of that spring from the system. The resulting slight increase in the weight of the suspended mass and the corresponding increase in pitching moment of inertia are usually negligible and normally can be neglected.

The final requirement of the simulation considers the generation of the ramp forcing functions. The significant requirements of this generation are the need to provide a separate "course" for each roadwheel with a time-delay introduced between simulations to account for the position of the wheels on the vehicle and the forward velocity of the vehicle (Fig. 6).

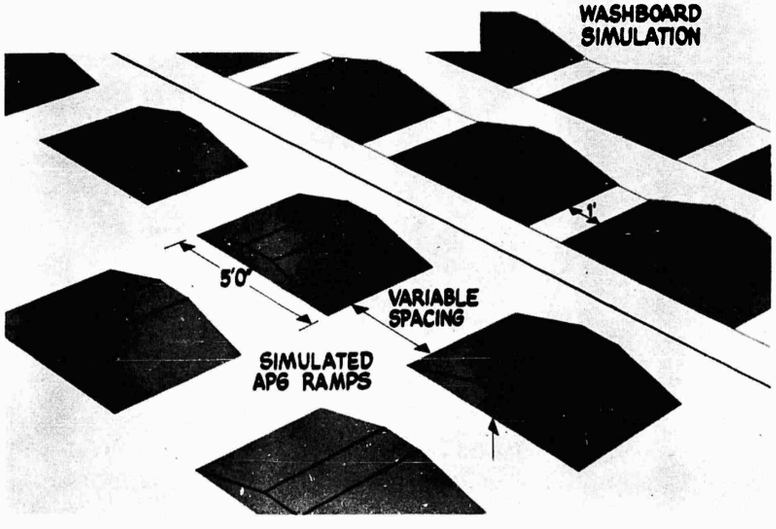

Fig. 3 - Simulation of Munson track-vehicle system courses

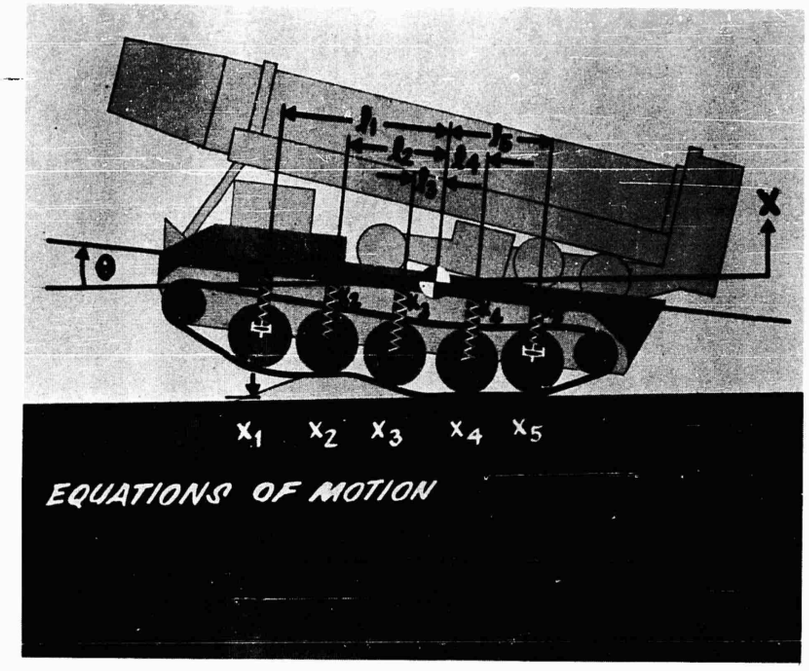

Fig. 4 - Equations of motion for a two-degree-of-freedom system simulation

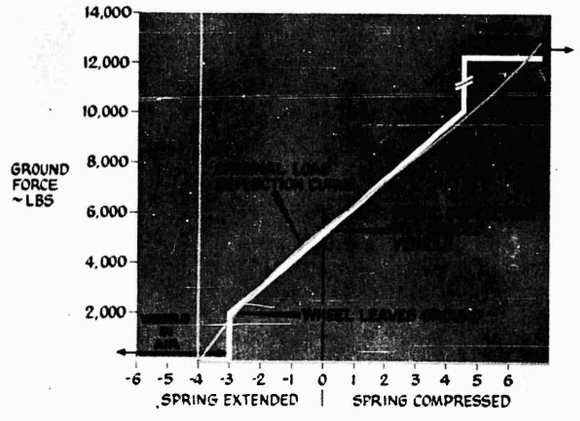

Fig. 5 - Nonlinear vehicle suspension system spring simulation

Provisions for changes in spacing of the ramps and changes in vehicle velocities are required in the simulation.

Vehicle Tests

The selection of ramp spacings for use in both preliminary tests and at Aberdeen Proving Ground is then completed, based on the aforementioned methods.

vehicle motion in service (Fig. 7). The smooth road course was selected to generate steady-state vibratory response of the system induced by tracklaying. Speeds were selected in 2-mph increments for all courses to cover the anticipated speed ranges of the vehicle. Instrumentation was carefully selected and located to produce data of greatest value in verification of criteria. Statham unbonded strain gauges were used in these tests in order to obtain flat frequency responses from dc to about 150 cps.

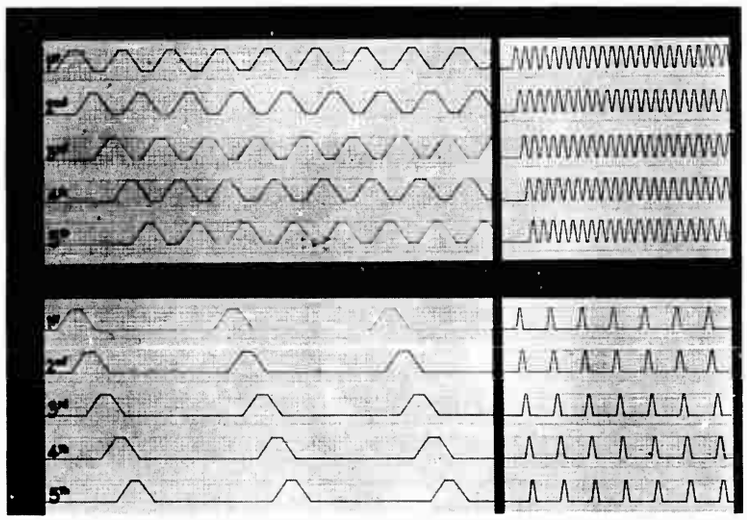

Fig. 6 - Analog representations of washboard (A) and spaced ramp (B) course conditions

In the Pershing weapon system, three ramp courses were selected in addition to a smooth road course. The former were obtained by spacing the ramps as follows:

1. To reproduce the APG concrete washboard course — 6-foot centers.

2. To obtain vertical translation and pitch of the vehicle — 111-inch centers (distance between front and rear roadwheel centerlines of the XM474-E2 vehicle).

3. To induce vehicle roll — 14-foot staggered.

These courses were selected to subject the Pershing system to the anticipated severity of

Data Processing and Utilization

Track vehicles provide a dynamic response environment which lends itself to an organized graphic presentation. Two significant classes of data are obtained, i.e. (1) steady-state excitation of the system at a frequency proportional to forward speed due to tracklaying, and (2) rigid-body response due to traversing irregular terrain. Excitation of the vehicle by engine and transmission vibration was negligible.

The method of data presentation takes advantage of this orderliness and is shown in Figs. 8 and 9. Data is grouped by pairs of accelerometers (Fig. 10) selected to assist in comparison and evaluation of the data and to improve readability of the large quantities of

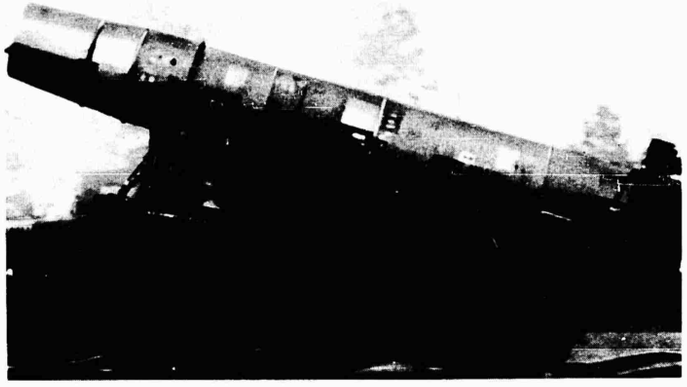

Fig. 7a - Vehicle traversing 111-inch spaced ramp course

data presented. The data is grouped and plotted in three bands as follows:

1. Rigid-body response of the system.

2. Tracklaying response (proportional to roadspeed).

3. Response at other frequencies (included for completeness although no significant forcing function exists in these ranges and the measured g-levels are low).

The acceleration measurements at the front of the vehicle due to tracklaying were consistent in amplitude for all courses as indicated by comparison of the tracklaying response of Figs. 8 and 9. These levels are independent of the traversed courses since the excitation at these frequencies is a function of the tracklaying process alone. The attenuation of these vehicle levels from (A) to (B) and then to (C) in the figures clearly shows how the vehicle response is transmitted through the structure. The low frequency response due to rigid-body motion is, of course, different for each course condition and is indicative of the response of the system in cross-country operation.

The resulting plotted data is then compared with design criteria in the following manner.

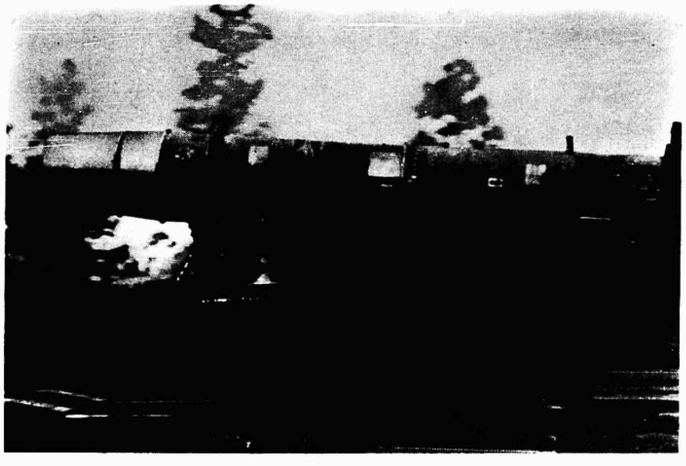

Fig. 7b - Vehicle traversing 111-inch spaced ramp course

Fig. 7c - Vehicle traversing 111-inch spaced ramp course

The low frequency data is compared with the static design criteria since, at these frequencies, the acceleration levels are seen by the structure as static loads. The response of the system to tracklaying is then compared with the dynamic design criteria. Adjustments in the respective criteria can then be objectively made, as necessary, to reflect the mobility philosophy of the system as compared with the observed response of the vehicle in traversing these courses prior to testing at Aberdeen Proving Ground.

DISCUSSION

Dr. Licari (North American Aviation): I noticed you have accelerometer B placed directly over accelerometer A. Were there any other accelerometers placed along the length of the missile?

Mr. Eustace: Yes. I mentioned in the discussion that we used two only for the purpose of this presentation. We used 15 to 17 accelerometers. They were placed on the forward end of the tracked vehicle, on the aft end over the erector-launcher (which is the missile supporting element), and at the forward, center, and aft sections of the missile proper. For this paper we included only the two which would present the data in the form in which it could be seen and understood clearly, but we did have data elsewhere in the structure. I intended to point out if I didn't do so, that we paired all of our data. As you noticed here, I compared positions A and B. Elsewhere in the system, in the report, I compare all of the other positions of the system in pairs also, in such fashion as to assist in making the presentation, and in making the point about the rigid body motion, either translational or rotational. Does that answer your question?

Dr. Licari: Yes. One other question. The system you have here was supposed to simulate some proving ground. Has anything been done to include an elastic foundation?

Mr. Eustace: Are you referring now to the terrain elasticity?

Dr. Licari: Yes.

Mr. Eustace: In our weapons system, in the work that we have done at the Martin Company, we have not considered this. As a point of explanation, our weapons system uses a vehicle supplied as government furnished equipment, and it was our intent in design to neglect the terrain mobility, assuming that the manufacturer of that equipment would have taken this into consideration.

Dr. Devreotes (USA Electronics R&D Lab., Ft. Monmouth): We have used simulated courses

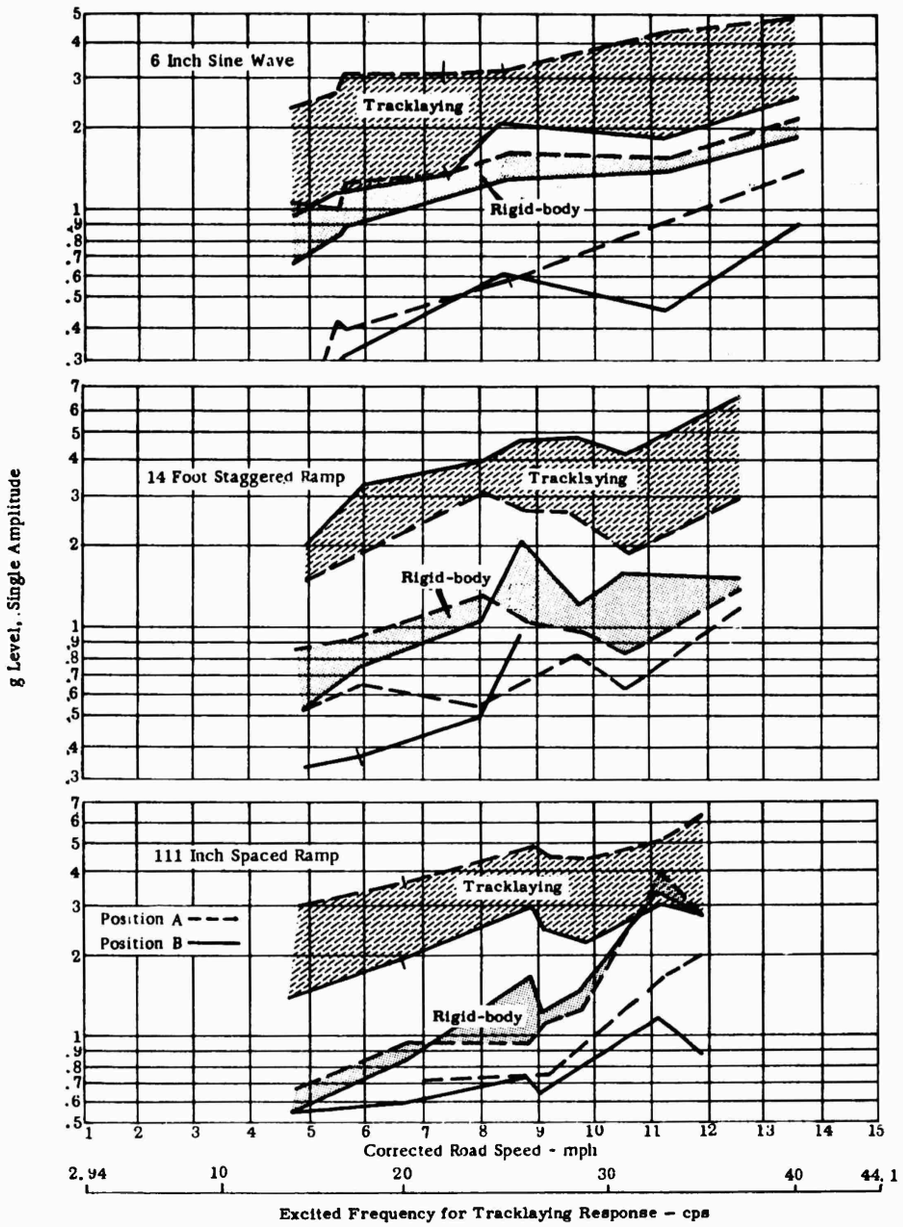

Fig. 8 - Comparison of g-levels at forward end of vehicle (A) and top of missile launcher (B). Data at frequencies other than those identified are indicated in background.

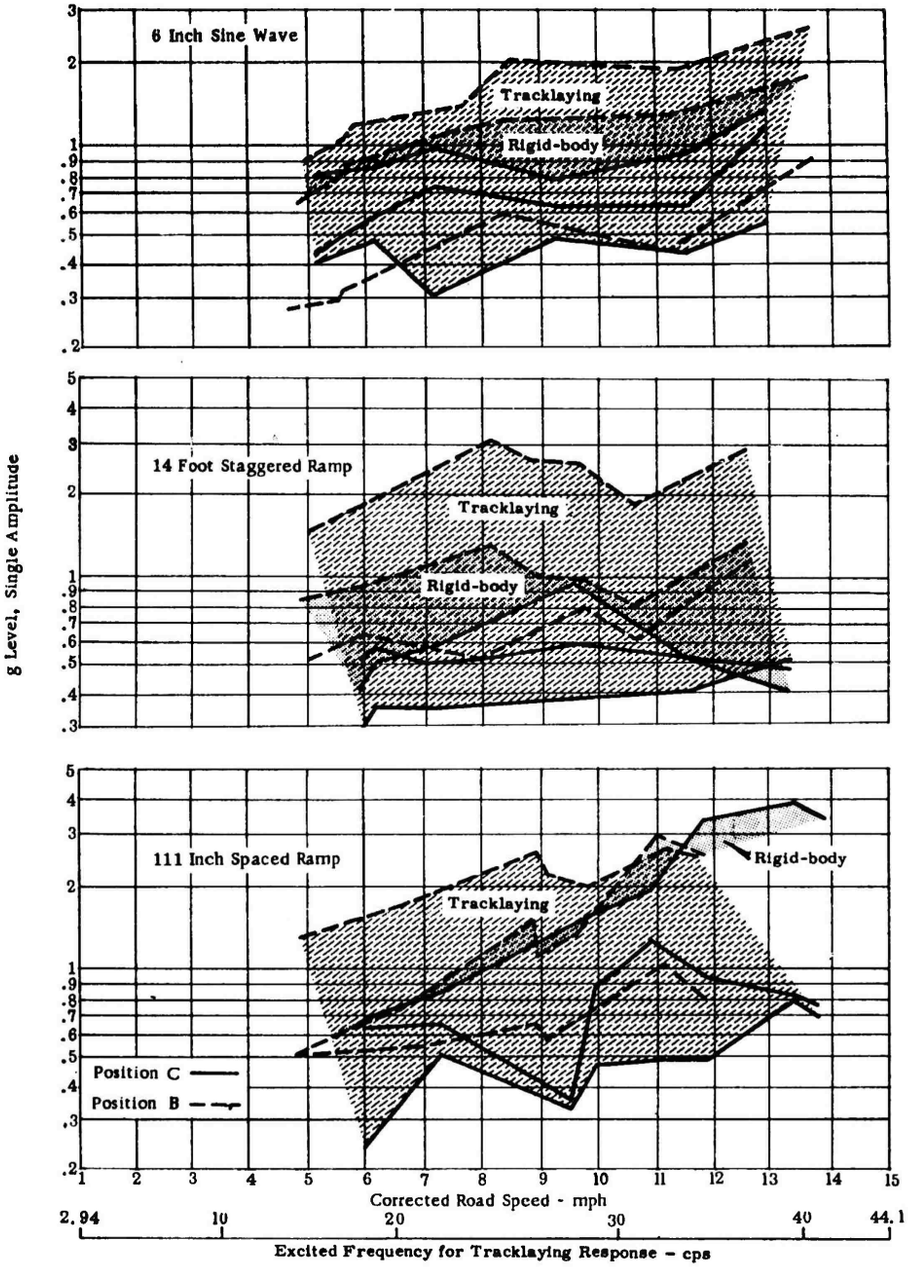

Fig. 9 - Comparison of g-levels at top of missile launcher (B) and top of missile (C). Data at frequencies other than those identified are indicated in background.

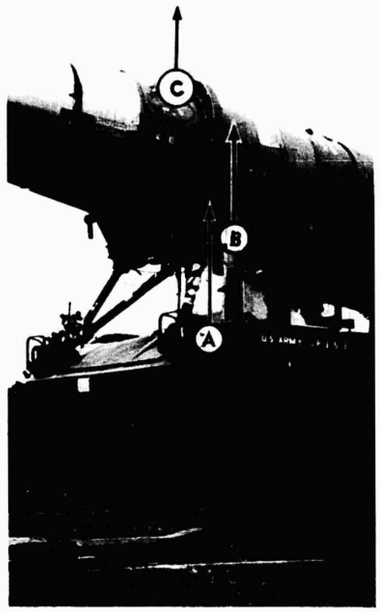

Fig. 10 - Accelerometer locations referred to in text

in several installations over the country, and it has worked out excellently for development purposes. It helps in the early stages. You are to be commended for doing such an excellent job. Most of the companies which work with the Laboratory do not do this until the final stages.

Mr. Eustace: I appreciate your comment. One point I might make, and there is a representative from Aberdeen here, who was associated with the program, our weapons system went to Aberdeen and had a most successful test program. We were going for three or four months there under all types of endurance tests and the like. We were complimented very highly on the ability of our weapons system to sustain these course conditions the first time with very little difficulty. Only a couple of relays and a few similar items caused any trouble. There was very little structural damage; so this again points out that a few minutes spent early in the design will prevent many, many problems later on.

Mr. Gorton (Pratt & Whitney Aircraft): The question is a little bit off the subject of road hazards of the kind you describe, but what happens when the tank driver who is used to crashing through underbrush and such, pokes the quarter million dollar nose of this thing into a 2-inch tree branch?

Mr. Eustace: We had one experience like that, fortunately we had a dummy system. All we succeeded in doing was denting the vehicle a little bit; but, of course, something like this is a serious problem. We have designed the weapons system for what we would call reasonable operating conditions. If we should run into a tree, or a 3-foot stone in the road, or if we should introduce other unusual conditions that would introduce shock levels, we might hard-bottom our suspension system. This, by the way, is hard to do. These conditions could be introduced in the system. To be practical, however, in our system, we took two considerations into mind. First, as you noticed, the driver is sitting directly underneath that missile. He doesn't know that if we hard-bottom that system the forward support won't fail. Well, we know it won't, but he doesn't. We found in our experience with these people that they are extremely concerned about this very, very heavy object sitting directly over their heads, and rightly so. We have found, also, that the vehicle which was supplied to us for use in this system is an excellent vehicle in every sense of the word. It's a modification of the 113 vehicle built by FMC of San Jose, California, and we found it almost impossible to bottom the system, even at Aberdeen. We were able to do it only once, and in that instance we had a most unusual set of circumstances develop, so in that sense, bottoming the suspension system is rather difficult.

Mr. Gorton: In regard to the overhead hazard, is there any reason the whole package couldn't have been turned around and its vulnerable nose put in the rear?

Mr. Eustace: Well, that's one I hadn't thought of. I would say there are first, many logistic reasons why the system was set up the way it was. Also, the vehicle was never originally designed for the weight that we put on it. Therefore, we are operating with a suspension system in a little bit more deflected position than normally encountered, and really, the front end of the system is by far the best place from the standpoint of the shock and vibration environment.

* * *

A SURVEY OF VIBRATION ENVIRONMENT IN VEHICLES TRAVELING OVER PAVED ROADS

J. E. Rice
Goodyear Aerospace Corporation

A problem which has plagued engineers responsible for providing adequate protection for items being shipped is the lack of measured values of accelerations to be experienced in trucks and trailers traveling over first class paved highways. The information which has been made available in the past has been for vehicles traversing Munson road courses and is hardly representative of what is usually experienced. Also most of the measurements presented in the past have failed to differentiate between the occasional shock due to bottoming the oleo struts and the steady state condition due to vibration. The consequence of using such information is serious overdesign of packages, which can be quite costly. The purpose of this paper is to present a number of measurements which are felt to be representative so that a feel may be had for the over-the-road vibration environment. There is always a certain amount of danger associated with drawing firm conclusions from a limited amount of data; however, it is felt that this data provides useful information.

The acceleration traces reveal that the dynamic response is a complex signal which may be composed of random and/or quasi-discrete frequencies associated with transient (shock) phenomena. Amplitude, on the other hand, is usually a randomly varying phenomena. In general the amplitude distribution is not Gaussian. A great deal of the data presented are from Aberdeen Proving Ground and the data are presented as three values which are: (1) rms, (2) the amplitudes which were exceeded 1 percent of the time, and (3) the peak amplitude. Provisions were taken to separate shock response from steady-state. It is felt that this method of presentation is certainly a step forward from the practice of only listing peak values without due regard to identifying distribution.

The fact that the dynamic response is random is to be expected since measurements of highway profiles taken by Purdue University and others have revealed the random nature of the amplitudes of the highway surface.

The information presented in this paper was obtained from a survey of 21 tests which furnished measured acceleration values. All of the data presented for trucks is from tests performed at Aberdeen Proving Ground under the direction of Messers R. Johnson and H. Cline. The trucks varied in gross weights from 7500 to 52,000 pounds. The types of vehicles ranged from two driving axles to eight driving axles.

The data for fifth wheel trailer and missile carriers, in general, is not from Aberdeen Proving Ground and, for the most part, consists of only maximum values with no differentiation between shock and vibration. Also the location of the pickups varied.

Measurements which are representative of the survey are displayed in Tables 1 and 2. Table 1 is for trucks of various gross weights and numbers of driving axles. Most of the recorded values are from accelerometers located at the vehicle c.g. It is interesting to note the fact that except for the extremely heavy vehicle (52,000 lb) that the r.m.s. accelerations are about equal for trucks that vary in gross weight from 7500 to 25,500 pounds. The same is true for the values exceeded 1 percent of the time.

Table 2 displays only maximum values of accelerations. It is the intent of Aberdeen Proving Ground to conduct tests on fifth wheel type trailers if possible. The currently available measurements are inadequate to draw firm conclusions; however, it is felt that, in general, the levels in the trailers will exceed the values displayed for trucks particularly in the area near the fifth wheel coupling device.

TABLE 1
Trucks Driving Over First Class Paved Roads

Measurements	Description of Vehicle				
	2-1/2 Ton 6x6 Cargo Truck	3/4 Ton 4x4 Cargo Truck	10 Ton 6x6 Cargo Truck	5 Ton 6x6 Cargo Truck (Acc. on Loaded Skid)	2-1/2 Ton 8x8 Cargo Truck
Gross weight of vehicle (lb)	17,500	7,500	52,000	25,500	13,750
Velocity of vehicle (mph)	50	48	42	50	45
Accelerometer position	c.g.	c.g.	c.g.	On loaded skid	c.g.
Maximum Accelerations					
Vertical	0.80	0.73	0.43	0.79	0.91
Lateral	0.33	0.20	0.15	0.75	0.17
Longitudinal	0.25	0.21	---	0.31	0.17
Accelerations Exceeded 1% of Time					
Vertical	0.50	0.49	0.26	0.48	0.56
Lateral	0.20	0.12	0.09	0.54	0.11
Longitudinal	0.14	0.12	---	0.22	0.12
r.m.s. Accelerations					
Vertical	0.20	0.20	0.10	0.19	0.22
Lateral	0.08	0.04	0.04	0.22	0.04
Longitudinal	0.05	0.05	---	0.09	0.05

TABLE 2
Tractor-Trailers Driving Over First Class Paved Roads

Measurements	Description of Vehicle					
	Missile Transporter	5th-Wheel Trailer for Syncom Antenna	2-Wheel 6-Ton Semi-Trailer 5th-Wheel	2-Wheel 6-Ton Semi-Trailer 5th-Wheel	16-Wheel Trailer (with Tow Bar)	Missile Motor Transporter (Accelerometer on Motor)
Gross weight of vehicle (lb)	38,182	53,000	33,820	33,400	40,000	Unknown
Velocity of vehicle (mph)	25	20	30	35	35	40
Maximum Accelerations						
Vertical	1.47	0.80	0.50	0.30	1.2	1.35
Lateral	0.42	0.10	0.10	0.10	0.5	0.35
Longitudinal	---	---				

To summarize, the values in Table 1 provide three ranges of acceleration for trucks. For extremely valuable cargoes, one might design for maximum values but for cargoes that can sustain an occasional loss, the 1 percent values are adequate.

The values in Table 2 are all maximums, but they at least provide some feel for the range of accelerations to be expected.

All values listed are for first class roads.

DISCUSSION

Mr. Judd (MB Electronics): As a maker of equipment, I was interested in what kind of velocities and displacements you encountered.

Mr. Rice: When you say velocities, you're talking about sinusoidal or vibrational velocities aren't you, rather than the forward velocities?

Mr. Judd: Yes, and the frequency range in general.

Mr. Rice: This data are expressed in terms of power spectral density, and almost all of the power is located below 200 cycles per second. This is due to the filtering effect of the sprung and unsprung weights. Very little of the power is above 20 cycles per second.

Mr. Collopy (AVCO Corporation): Would the levels measured on a trailer be about half as much in the lateral direction as in the vertical direction?

Mr. Rice: In general, they can be much greater. A pot hole can induce rolling of the vehicle and it, therefore, depends upon how tall your fixed object is. When I say the lateral vibration is half, this is measured on the truck cab. If you have a very tall object, of course, it will increase. If anyone wants to look at the data I have with me I can show this to you.

Mr. Collopy: I was referring to the truck cab, that is on the floor of the truck?

Mr. Rice: I don't think you can make a positive statement on this because it depends upon the rear weight of the truck. I have discovered that some trucks have a viscous coupling. It is longitudinal to lateral coupling and more pronounced in a trailer. Occasionally you will get a trailer that will whip on you just as a house trailer. This is unusual, but it is possible.

* * *

SHOCK AND VIBRATION DATA OBTAINED FROM TRUCK AND RAIL SHIPMENT

J. W. Lahood
Raytheon Company
Bedford, Massachusetts

Shock and vibration data are presented for truck and rail shipment. Emphasis is placed on presenting the data in a form useful to both designers and test engineers. Future plans are described.

INTRODUCTION

The intent of this paper is to present shock and vibration data, obtained from transportation (truck and rail) testing, in a style that is useful for both design and test engineers. In addition, the data is tabulated and defined as well as possible wherever it is feasible. Past experience, while researching shock and vibration data related to various transportation modes, has indicated that documented data in this general area is vague, incomplete, and often undefined.

The information contained in this paper should be of significant value from a practical standpoint to all engineers who are currently concerned with such data. Also, with a view toward the future, the writer sincerely anticipates that this paper will be supplemented with shock and vibration data obtained from other modes of transportation, namely aircraft, ship, helicopter, carrier pigeon, and the like. In addition, a contribution of data from other sources will greatly enhance the objective of this paper. A desirable end result will be a compilation of all pertinent field-test data related to all forms of shipment that can be presented in a universal document.

SHIPMENT BY TRUCK

The following types of trucks were used for rough-road testing:

1. U-shaped flat-bed, pulled by a 6-wheel conventional cab with testing component mounted on an M-390 U.S. Army Trailer.

2. M-36 Army Truck (10-wheel) (Fig. 1).

Regardless of which truck was used, the specimen was tied down by means of steel cables or chains.

Since it is very difficult to obtain correlation on different test components, the reported levels are restricted to truck inputs induced from rough road testing. Only general statements will be made with respect to component levels. Table 1 delineates the results obtained from two truck input strain-gage-type accelerometers on a flat-bed trailer.

The tabulated levels are maximum values (measured at the peak of 1 cycle). The nature of the waveforms were quasi-sinusoidal and the vibratory signals induced by the shock input lasted from 5 to 10 cycles (depending on type of input) before decaying to negligible amplitudes. In general, the maximum levels obtained on the component were 3 g; however, increased truck speeds induced higher shock levels.

After determining the predominant fundamental frequency transmitted from the trailer to the component to be in the range of 2-5 cps, it was decided to construct a washboard to excite this frequency range utilizing predetermined truck speeds. The washboard was constructed with 11 2x4's, spaced 2.75 feet apart, for a total length of 27.5 feet. The results are tabulated in Table 2.

In general, the 5-mph truck speed, which excited system resonance, produced the highest vibratory g-levels as indicated by the accelerometers mounted on the component. The majority of g-levels ranged between $\pm$ 1.0 and $\pm$ 1.5 g. Higher excited frequencies produced lower g levels on the component.

Fig. 1 - Shelter shown mounted to flat-bed of M-36 Army Truck

TABLE 1
U-Shaped Flat-Bed Data

Station	Location	Direction	Truck Speed (mph)	Road Condition	Predominant Fund. Freq. (cps)	± Peak Shock (g)
1	Center of flat bed	Vertical	7	Ditches & potholes	2-5	1[a]
2	On wood near M-390 tire	Vertical	7	"	"	1
1			12	"	"	No signal
2			12	"	"	2
1			18	"	"	No signal
2			18	"	"	2.5
1			25	"	"	2.1
2			25	"	"	1.7

[a]This data was obtained on a stretch of hard-packed-sand road, approximately 120 yards long, with a random distribution of ditches and potholes.

TABLE 2
Washboard

Station	Location	Direction	Truck Speed (mph)	Road Condition	Predominant Excited Freq. (cps)	Vibration ± Peak (g)
1	Center of flat bed	Vertical	5	Washboard	4	2.80
2	On wood near M-390 tire	"	5	"	4	2.80
1	"	"	15	"	5-7	1.5
2	"	"	15	"	5-7	0.8
1	"	"	20	"	10-11	2.6
2	"	"	20	"	10-11	1.2
3[a]	Extreme rear of flat bed	"	5	"	4	4.5

[a]This location is generally removed from the normal shipping surface.

TABLE 3
M-36 Army Truck Data

Station	Location[a]	Direction	Truck Speed (mph)	Condition	Predominant Fund, Freq. (cps)	± (g)
1	Specimen floor, 2-3 ft left of c.g.	Vertical	25	Hard-packed sand-and-gravel road	1.5 - 3.5	0.3
2	Specimen floor, 2-3 ft right of c.g.	"	25	"	"	0.5
3	Specimen floor, c.g.	"	25	"	"	0.5
4	Truck bed, back end	"	25	"	"	0.6
1		"	13	9-in. pothole	2.0 - 4.0	1.0
2		"	13	"	"	1.0
3		"	13	"	"	0.5
4		"	13	"	"	1.2
1		"	14	Cobblestone hill	4.0 - 5.0	0.65
2		"	14	"	"	0.4
3		"	14	"	"	0.4
4		"	14	"	"	0.7
1		"	36	8-in. x 8-in. x 4-ft wooden block under each wheel	2.0 - 7.0	1.0
2		"	36	"	"	1.0
3		"	36	"	"	1.0
4		"	36	"	"	1.4
1		"	35	Railroad track	2.0 - 4.0	1.4
2		"	35	"	"	0.9
3		"	35	"	"	1.1
4		"	35	"	"	0.8
1		"	40	"	"	1.1
2		"	40	"	"	0.9
3		"	40	"	"	1.0
4		"	40	"	"	0.7

[a]The accelerometers remained in the same station location during each change in speed and condition.

Table 3 depicts the testing results obtained from adverse road conditions utilizing an M-36 Army truck to transport an Army spare parts shelter.

The levels reported in Table 3 are an average of two cycles of vibration. The M-36 Army Truck exhibited excellent shock and vibration isolation capability, and the obtained signals were quickly damped to zero amplitude (2-4 cycle duration).

The maximum level obtained on the component was ± 1.5 g.

SHIPMENT BY RAIL

Cross-Country

Figures 2 and 3 are representative of shock and vibration data encountered from Andover, Massachusetts, to El Paso, Texas. The length of the trains varied from 60 to 120 cars, however, the instrumented car was at the end of the train in each case. The data presented represent maximum levels that occurred during humping, starts and stops, slack run-outs, steady runs, and steady runs over rough track.

Of the conditions just mentioned, humping and slack run-outs were the most severe. Humping and starts and stops produced similar shock inputs to the flatcar. Humping occurred only during the changeover from one railroad to another, and, in most instances, only a few couplings were made during each changeover. Starts and stops were infrequent during this trip, since most trains were of the express type and averaged only three or four stops per 10-16 hours of travel. Slack run-outs provided the most frequent shock occurrence. The severity of the shock depended upon the speed and length of the train, generally being more severe on the longer trains at a moderate speed than on the shorter trains at a higher speed.

The steady runs were the most important contributor to vibratory acceleration and the severity depended upon the roughness of the tracks.

Samples of cross-country levels for humping and slack run-outs are shown in Figs. 4 and 5 (observe only the nature of the flatcar signals, vertical, lateral, and longitudinal). Figure 6 shows the components mounted on the flatcar, and the instrumented caboose car prepared for cross-country travel.

Humping (Lawrence Freight Yards)

Figures 7-9 are representative of maximum shock and vibration levels obtained from rail humping. Impact velocities were determined from stopwatch timing of two torpedo explosions. The mass ratio between the impacting freight car and the instrumented flat-bed car was approximately 2.5:1. In all cases, the accelerometer was rigidly mounted on the instrumented car, close to the point of impact.

The nature of the shock waveform varied anywhere from a square wave, a triangular pulse, to a half sine. This was dependent upon the characteristics of the coupling structure. The nature of the recordings were such that accurate pulse durations were difficult to extrapolate; however, the amplitudes were fairly repeatable and easily read. Pulse durations ranged from 10-100 milliseconds.

Figure 10 is included to display the variation in longitudinal shock from rail humping at any one velocity range. Figures 11, 12 and 13 show the impacting coal car, the instrumented car, and the input accelerometer mounted on the coupling of the impacted flatcar.

COMMENTS BY J. A. KELL, C&O RAILWAY COMPANY

I think Mr. Lahood has performed an excellent task with the presentation of these data. There are, however, several points which if added would, I believe, increase the value of the paper.

The car used in the impact tests at Lawrence was a 70-ton flatcar, 53' 6" over end sills, and equipped with trucks having a maximum (free to solid) spring travel of 1-5/8" (AAR 1936 springs) and probably included a snubber of doubtful effectiveness. The draft gear was probably a standard type with 2-1/4" travel. At least that's what the car started out with. If you had tried to find a worse car, you could only have looked for one with stuck (inoperative) draft gears. I presume the car used for the road tests was similar. Today, all cars are built with more than twice the spring travel in the trucks. There are cars available now with draft equipment allowing travels up to 30". In other words, this test was run with equipment at the poorer end of the scale. We need similar data presented by disinterested people, such as The Raytheon Company, but on a few more cars.

I would like to see a description of the instrumentation used, included in the paper. A description of the weight of load and distribution on the car would also be of interest. In some tests made by us, efforts were made to place the accelerometers as near to the body bolster

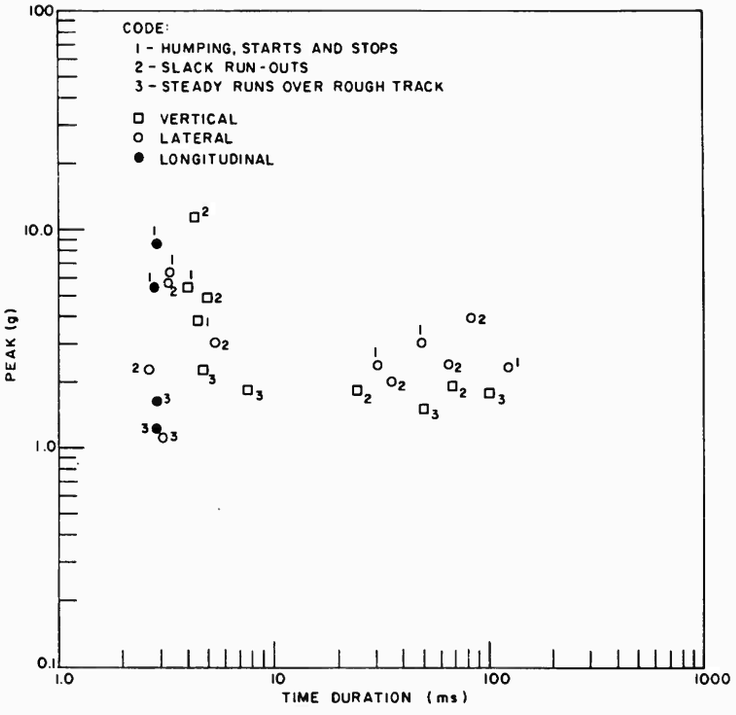

Fig. 2 - Maximum shock levels encountered in cross-country transport by rail (Andover, Mass. to El Paso, Tex.)

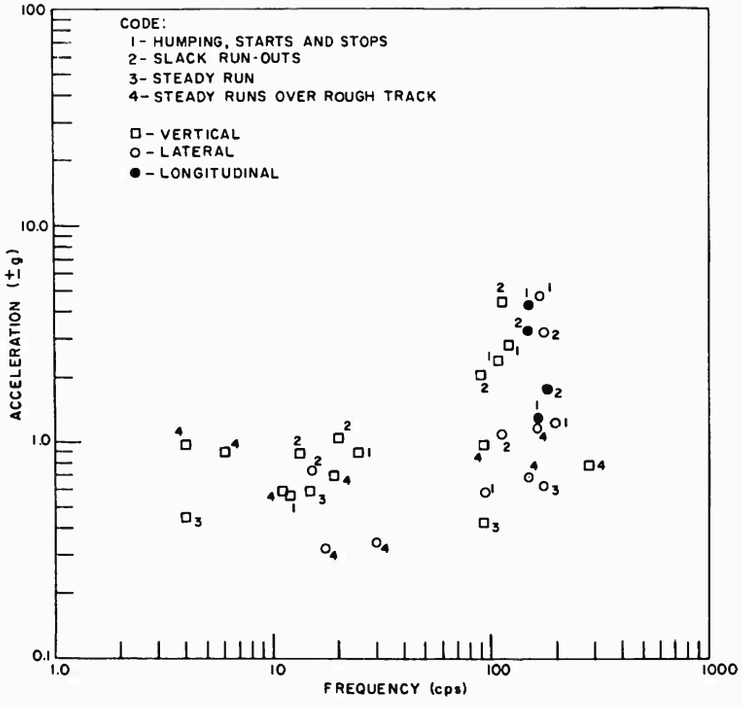

Fig. 3 - Maximum vibration levels encountered in cross-country transport by rail (Andover, Mass. to El Paso, Tex.)

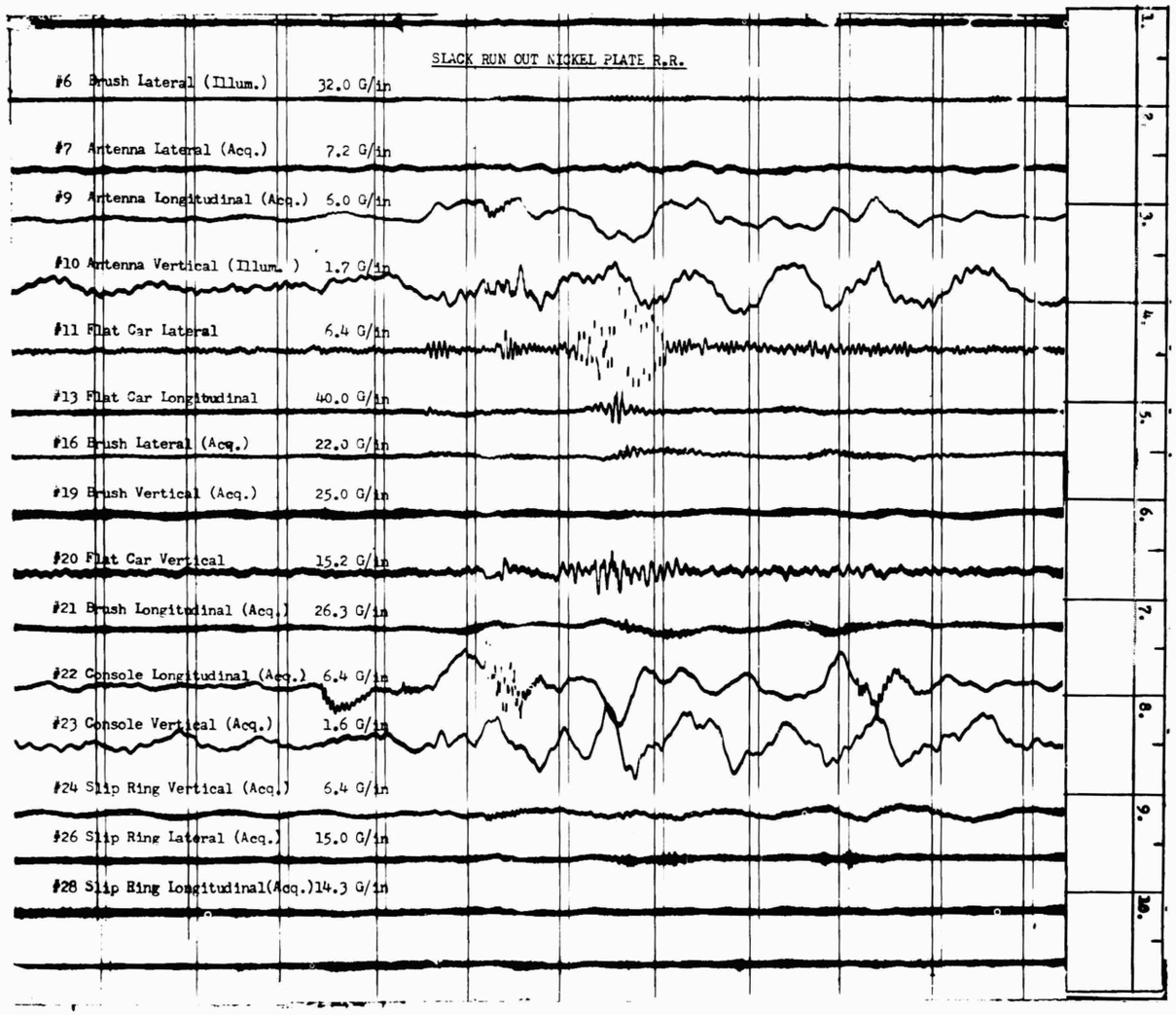

Fig. 4 - Slack run-out nickel plate R.R.

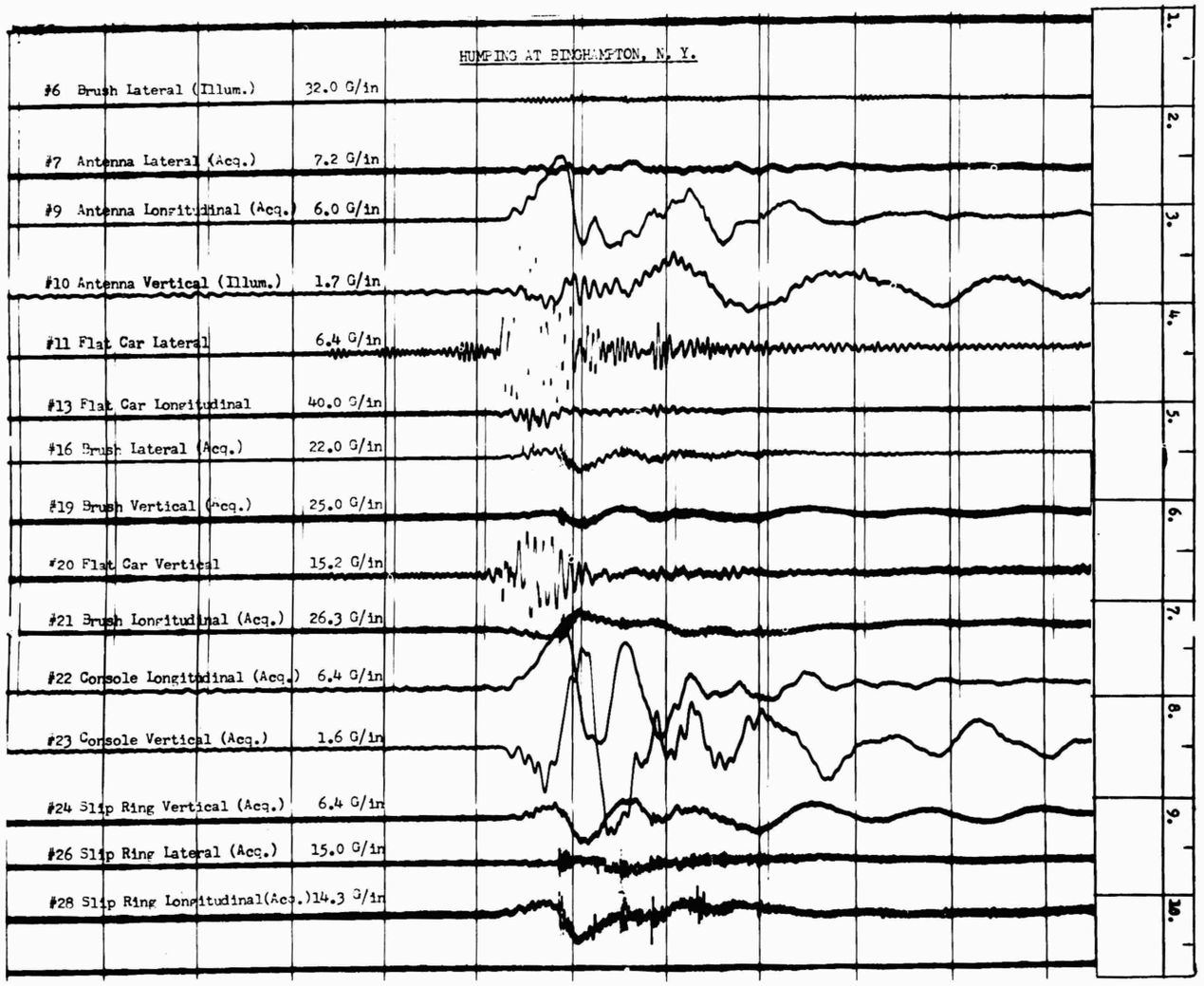

Fig. 5 - Humping at Binghampton, N. Y.

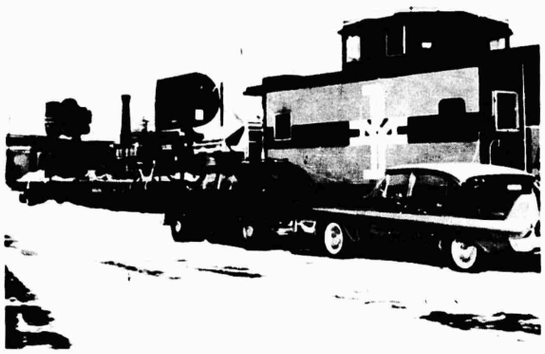

Fig. 6 - Testing components mounted on flatcar and connected to instrumented caboose car

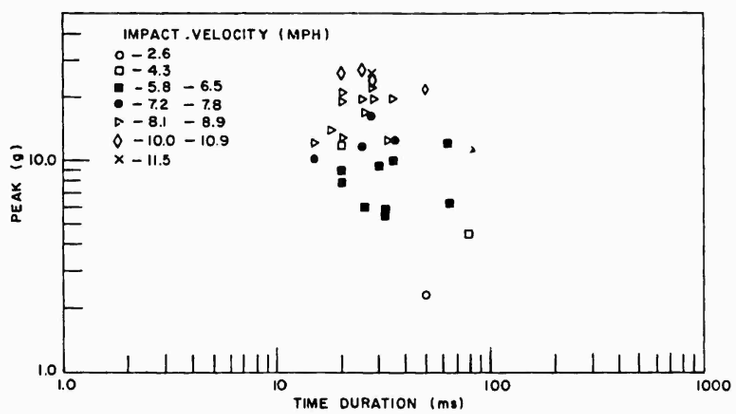

Fig. 7 - Humping at Lawrence Freight Yards, Lawrence, Mass., railroad flatcar, longitudinal shock

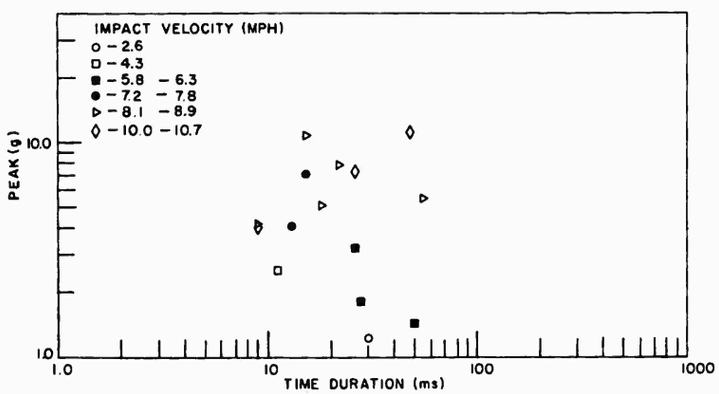

Fig. 8 - Humping at Lawrence Freight Yards, Lawrence, Mass., railroad flatcar, vertical shock

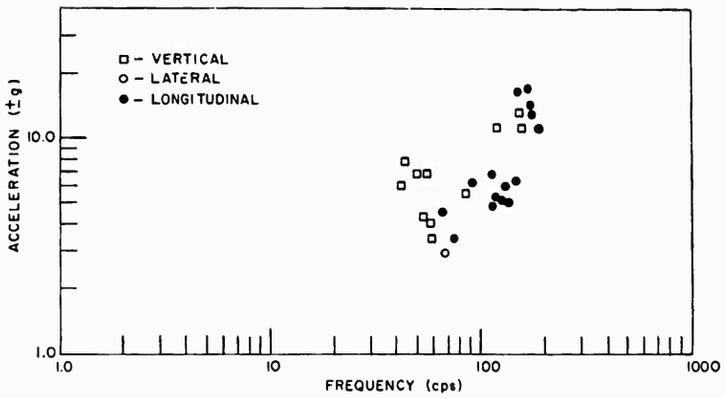

Fig. 9 - Maximum vibration induced by rail humping at Lawrence Freight Yards, Lawrence, Mass., railroad flatcar

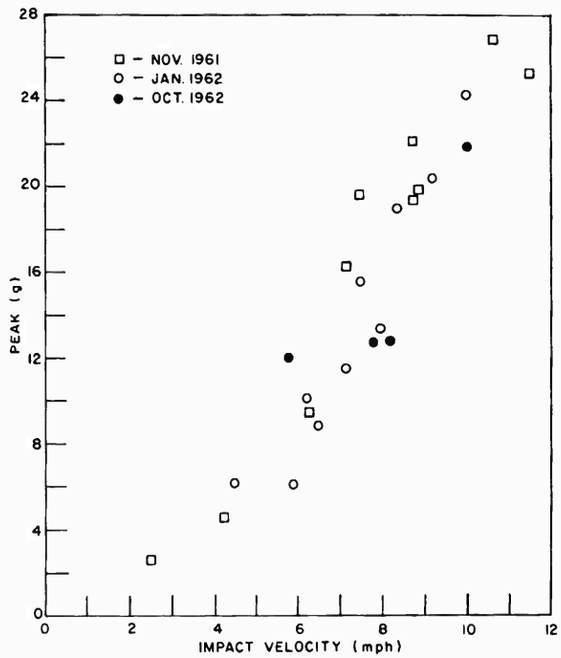

Fig. 10 - Variation of longitudinal shock with impact velocity, time duration varied from 10 - 100 ms

Fig. 11 - Diesel engine connected to coal car

Fig. 12 - Overall view of shelter on flat-bed train car strategically positioned in front of boxcar on which instrumentation is located

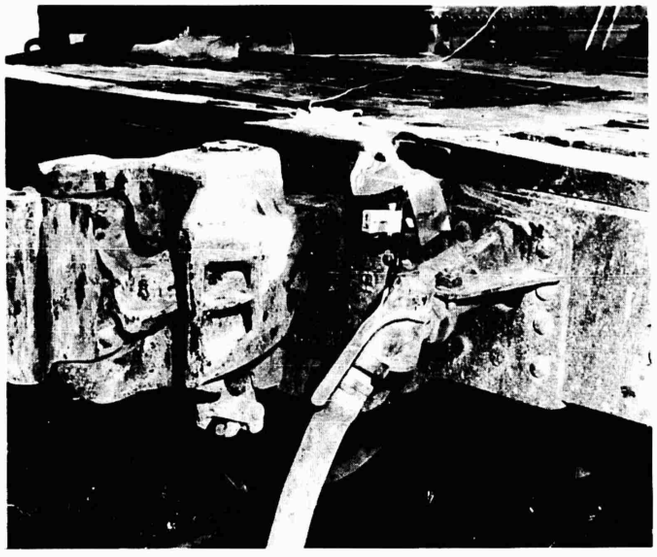

Fig. 13 - Train car input accelerometer

as possible since this is the only point that can be repeated from car to car. Other parts of the car reflected car construction as well as truck and draft gear action, and although they are interesting from a packaging viewpoint, if truck and draft gear action are improved, probably the body member vibrations will be reduced.

Longitudinal shocks in trains are the result of road contour, engineering effectiveness and type of draft gear as well as train speed and length. They also depend a good deal on the location in the train. On some tests run by us, they varied from 2 g maximum at the rear to nearly zero near the locomotive. With a stuck draft gear the shocks were as high as 6 g. However, the instrumentation on this test was a Statham Accelerometer recorded by a Type A Heiland Galvanometer and the record is attenuated starting at 5 cps. These tests were made with diesel engines as the motive power. When steam engines are the motive power, there is a pulsating longitudinal vibration on the cars near the head end. We have no time duration information on these shocks and records were made on one car only. These values agree closely with those found by Mr. Lahood.

Longitudinal force developed in any particular car when it is switched or humped depend on the type of draft gear. We assembled some data from various sources on forces measured by a dynamometer coupler. Some of these devices have the same force at 9 mph as standard gears have at 4. There are even more exotic devices available for fragile lading that have travels up to 30" as against the 2-1/4" for standard draft gear.

Presented this year, at the AAR Annual Business Meeting of the Mechanical Division, was a report on the "Field Survey of Impact Speeds." This is presented in two forms, as a bar graph, and as a cumulative total. Standard draft gears go solid at about 4.5 mph and 65 percent of all impacts in hump yard and flat yard switching operations are above this speed. The acceleration depends on the type of draft gear used. See Figs. 14 and 15.

The vertical force on cars when switched or humped depends on the type of draft gear and the type of snubbing employed on the trucks. On the road, vertical force depends on speed, track condition, spring travel and snubbing. A large amount of data on this subject was presented at the 15th and 16th Shock and Vibration Symposia.

The lateral forces measured by Mr. Lahood seem to be somewhat higher than ours and looking at the record, I wonder where they were measured and with what instrumentation. Also, none of the usual 2-3 cps lateral seems to have shown up in this test. This is of such low amplitude, about .2 g maximum, that we did not report on it and perhaps the same is true here.

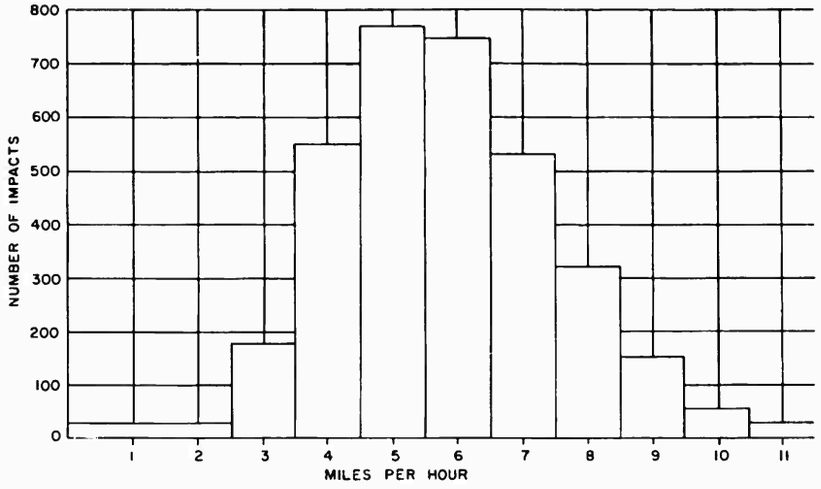

Fig. 14 - Field survey of impact speeds
(total number of impacts - 3369)

A final word of caution, as we improve our equipment we develop new problems and our new larger capacity cars are no exception. While they ride well with capacity loads, they are not much heavier than present day boxcars. As a result, they are mostly over snubbed at light loads and will give a very hard ride. Efforts are being made to correct this condition, but a simple answer has not yet been found. The present answer is to load a car to at least 50 percent or better of its rated capacity. This is true for any modern car with adequately snubbed trucks.

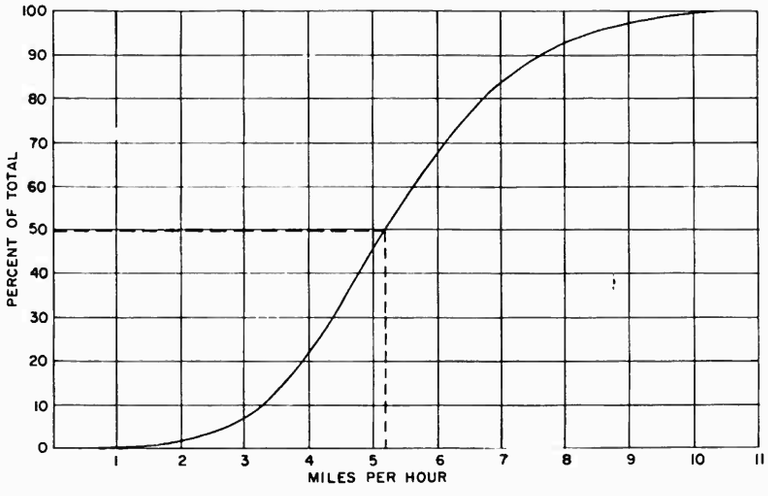

Fig. 15 - Field survey of impact speeds (cumulative impacts)

* * *

THE DYNAMIC ENVIRONMENT OF THE S-IV STAGE DURING TRANSPORTATION

R. W. Trudell and K. E. Elliott
Saturn-Acoustics and Structural Dynamics
Missiles and Space Systems Division
Douglas Aircraft Co., Inc.

With the advent of large and expensive space boosters, the need has arisen to assure that the reliability of these vehicles is not jeopardized in the course of transportation and handling. Measurement of the shock and vibration environment experienced by each vehicle in the course of shipment from the factory to the launch pad is imperative to determine if the vehicle has been subjected to loads in excess of the design criteria. A series of tests have been run by Douglas Aircraft Company to define the environment experienced by the Saturn S-IV stage during various modes of transportation.

This paper presents a detailed discussion of shock and vibration measurements obtained on the S-IV stage during transport on (1) a soft tire land transporter, (2) a hard tire land transporter, (3) a seagoing freighter, (4) a seagoing barge, and (5) a modified B-377 aircraft (Pregnant Guppy). The primary emphasis is on the aircraft mode of transportation. The vibration levels measured on vehicle components and structure are compared with levels measured during individual component qualification tests, and with design criteria. Levels measured on the various carriers listed above are also discussed.

Test limitations, instrumentation, and data processing techniques are outlined. The acceptability of shock and vibration environments produced by each of the transportation modes listed above is established for the S-IV stage.

INTRODUCTION

With the advent of large and expensive space vehicles, the need has arisen to assure that the reliability of these vehicles is not jeopardized in the course of transportation and handling. The Douglas Aircraft Company monitors the transportation shock and vibration environment on each S-IV vehicle shipped, to assure that design specifications have not been exceeded.

When an S-IV is completed on the assembly line, it is sent from the factory in Santa Monica, Calif. to the Douglas Aircraft Company, Sacramento Test Facility for static firing. After it has been static fired, it is shipped from Sacramento to the Atlantic Missile Range at Cape Canaveral.

There are two ways in which an S-IV may be transported to these destinations; by surface land and water routes, and by air via the Pregnant Guppy (See Fig. 1). Because of the large diameter of the S-IV, it cannot be shipped by rail.

When the S-IV stage is transported by surface routes, it moves from the Santa Monica plant to the Los Angeles Harbor on a transporter. At the harbor, it is transferred to a barge which transports the stage and transporter to San Francisco Bay and from there to Cortland, Calif. via the Sacramento River. At Cortland, the stage and transporter are offloaded and the remaining 45 miles to the Sacramento Test Facility are traveled by road. After static firing tests have been completed, the transportation process is reversed as far as San

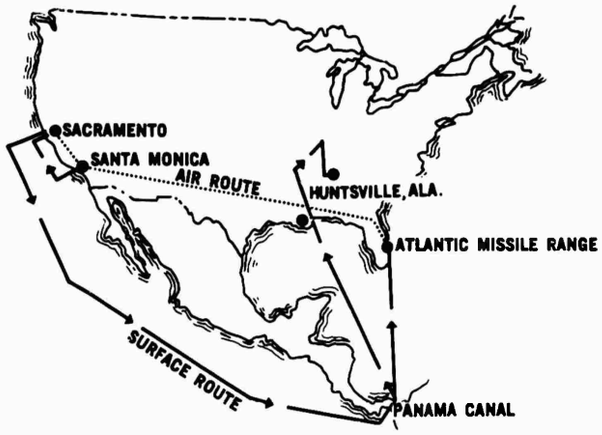

Fig. 1 - S-IV stage transportation routes

Francisco Bay. Here the stage and transporter are transferred to a freighter for a two week ocean voyage to Cape Canaveral via the Panama Canal.

When the S-IV is transported by air using the Pregnant Guppy aircraft, the stage is transported to Los Angeles International Airport from the Santa Monica factory. After the stage is loaded on board, the Guppy flies to Mather Air Force Base in Sacramento. From there it is only a short road trip of 5 miles to the test stand. After test firing, the stage is flown from Mather to the air strip at Cape Canaveral.

All phases of movement were instrumented to record the shock and vibration environment encountered during each mode of transportation. This paper describes and defines the various shock and vibration environments encountered by the S-IV stage during its transportation. Instrumentation and data analysis methods are described in the appendix.

SURFACE TRANSPORTATION

The Dynamic Environment of the S-IV Stage Transporter

The S-IV Stage Transporter is a device designed to convey the stage over land routes from the factory to a seaport and from a seaport to the test stand and launch-pad, Fig. 2. It has the additional capability of changing the vehicle orientation with respect to the ground,

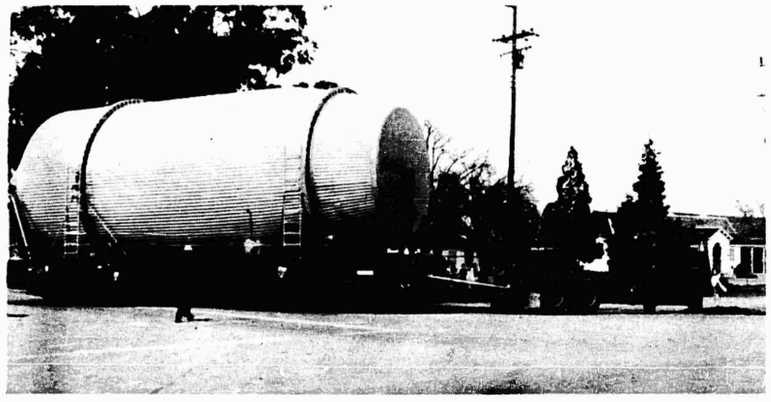

Fig. 2 - S-IV stage on DACO transporter

both by "rolling" the vehicle which is cradled in two rings, and by providing a base to erect the vehicle to a vertical position.

As a means of conveyance for the S-IV, this transporter represents an uncommon approach to the problem of isolating the S-IV vehicle from road shocks. This transporter employs only very large balloon tires at 14-15 psig air pressure for isolation of the transporter bed from the road. No leaf or coil springs are used. The large volume of the tires combined with the low pressure make them a rather soft spring. In fact, the transporter tends to oscillate at only 1.6 cps in the vertical direction.

The damping ratio R/R_c is around 0.05. Therefore, the transmissibility of the system at frequencies above 2 cps is practically zero. Further, the "footprint" of these tires is several square feet, so they literally fill in small holes and flow over sharp bumps. This, coupled with a speed limit of 10 mph, make the probability of a short-base-time, high amplitude shock virtually nil during road transport.

Figures 3 and 4 illustrate statistical distributions of the vibration levels recorded during a number of road trips with an S-IV vehicle on the transporter. The data were recorded with an oscillograph and all the data occurred notably at one frequency — 1.6 cps. The maximum level ever recorded during transport of a stage was 0.6 g. The primary disadvantage of this type of suspension is the high transmissibility at resonance. But a frequency of 1.6 cps means large amplitudes of oscillation for low values of acceleration (e.g., 0.5 g = 3.7 in. peak to peak). Therefore, should road conditions induce bouncing, it is visibly apparent that vibration amplitudes are becoming large and the tow truck can slow down long before these amplitudes become troublesome. Instrumentation is operated and maintained during each trip to keep a constant check on the levels encountered.

The Dynamic Environment of the S-IV Barge

The S-IV Barge, Fig. 5, is used to transport the S-IV stage transporter from Los Angeles Harbor to Cortland — a point near the Douglas Aircraft Company's Test Facility at Sacramento, California.

The barge is operated by the Pacific Towboat Co., and is an oceangoing type. It is towed from place to place at the end of a 1000-foot cable. Its draft is approximately 3 feet and it has a shelter built on the deck to house the S-IV and transporter.

Normal Pacific Ocean weather produces only long period gentle swells. The accelerations induced by these swells are presented in Fig. 6. The periods of these accelerations range from 4-12 seconds per cycle. No other vibration levels were recorded during these conditions.

During one shipment, however, strong winds off Pt. Dume, California, produced an 8- to 10-foot chop. The shallow draft of the barge proved quite disadvantageous as it began to "spank."

The "spanking" induced responses in the barge and transporter at around 9 cps. A

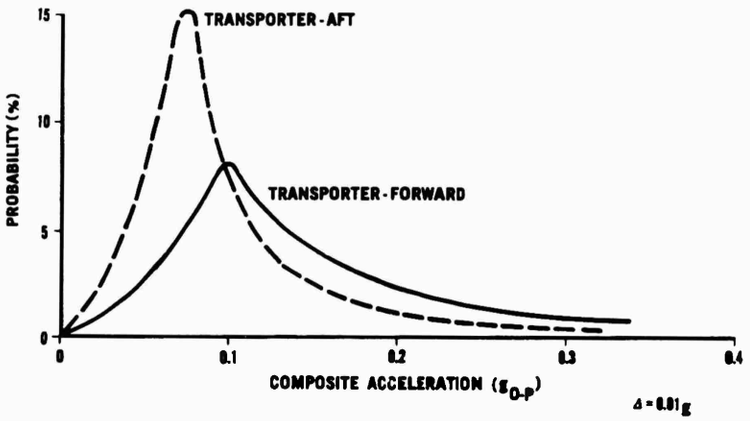

Fig. 3 - DAC transporter vibration levels, vertical direction

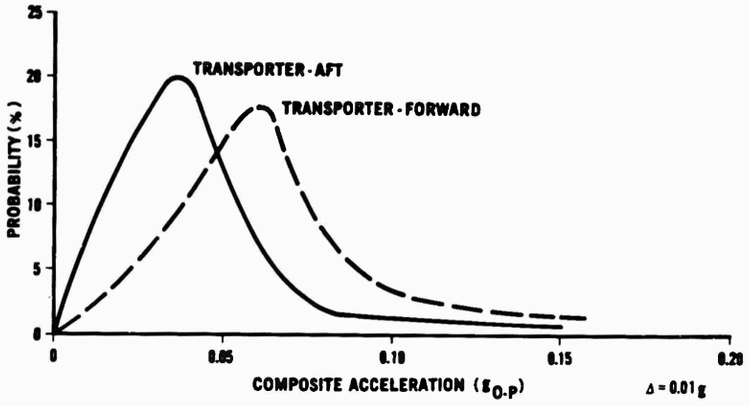

Fig. 4 - DAC transporter vibration levels, lateral direction

distribution of the levels recorded is given in Figs. 7 and 8. The levels recorded approached 0.7 to 0.8 g at times. Figure 9 illustrates the distribution of durations of these transients in seconds. The times indicated are times required for the transient to decay to 1/2 of the initial value.

The value of a transportation vibration monitoring system is here illustrated in that it assured Douglas that the stage was not weakened structurally by these transients.

Dynamic Environment of the S-IV Stage on a Freighter

The S-IV stage is shipped to AMR via the Panama Canal on a freighter of the Victory type, Fig. 10. Victory ships are almost 500 feet long. They displace more than 10,000 tons of water and draw about 28 feet. They are powered by an 8500 shp compound turbine which turns a single 22-1/2-foot diameter, four blade propeller at 75-85 rpm. Normal cruise for this ship is 17 knots.

There are two possible sources of vibration on a ship; rough weather and/or propeller and machinery. The vibration levels due to propeller and machinery were practically zero. Rough weather in the Gulf of Tehuantepec off the south-west coast of Mexico was responsible for the maximum recorded levels. A summary of these levels is given in Fig. 11. The periods of these accelerations ranged from 4 to 10 seconds per cycle. These levels do not constitute

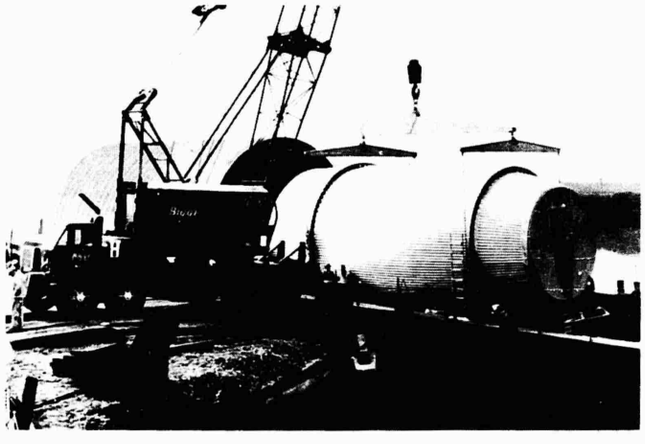

Fig. 5 - S-IV stage and transporter on barge

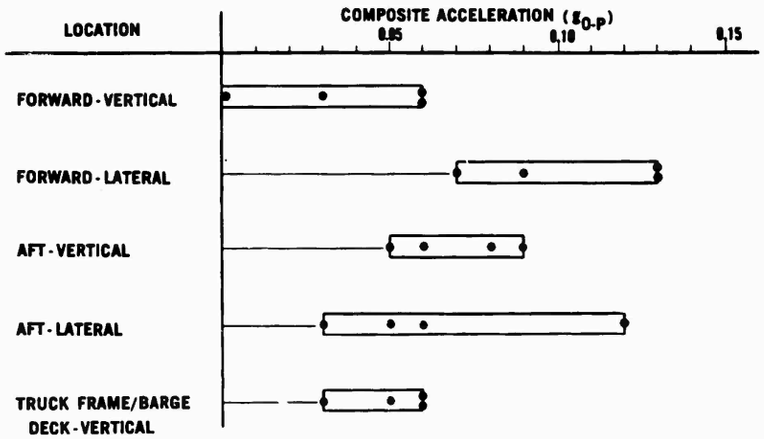

Fig. 6 - Maximum acceleration levels, S-IV transporter on barge - gentle swells

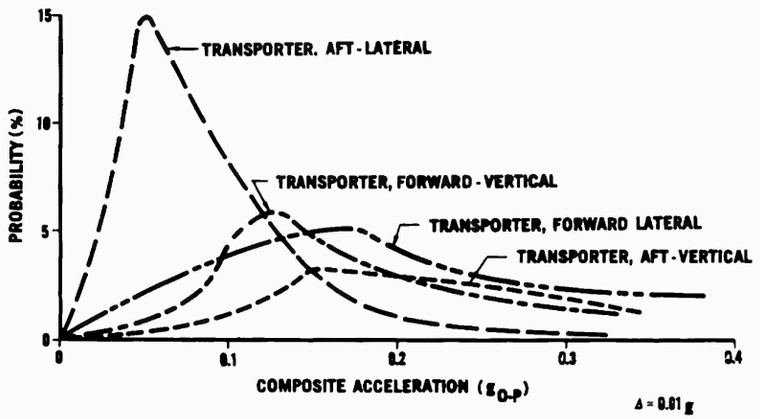

Fig. 7 - Transient vibration levels, S-IV transporter on barge - heavy seas

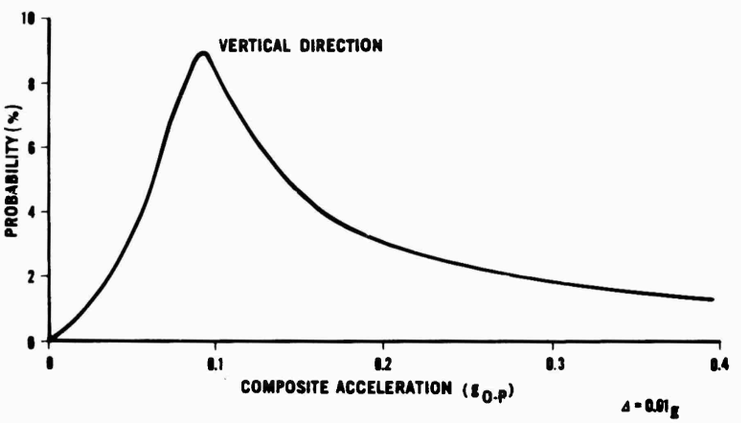

Fig. 8 - Transient vibration levels, S-IV barge deck - heavy seas

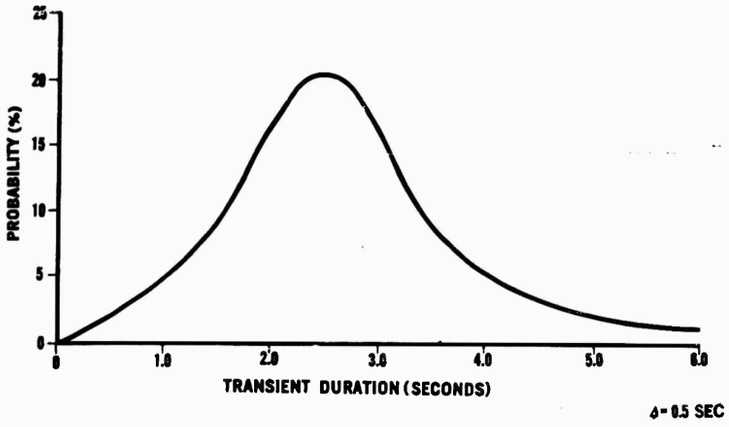

Fig. 9 - Duration of transients, S-IV transporter on barge - heavy seas

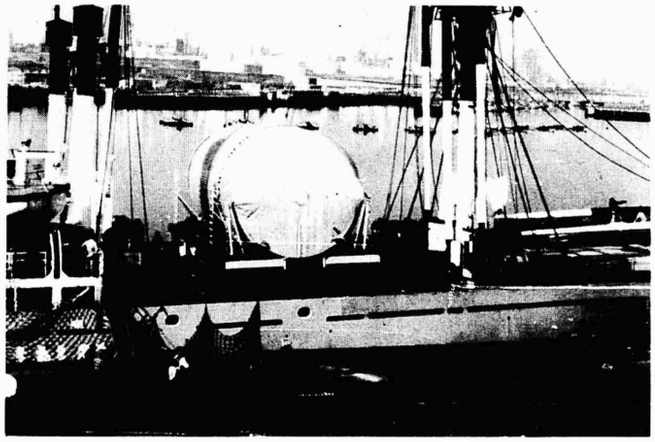

Fig. 10 - S-IV stage and transporter on freighter

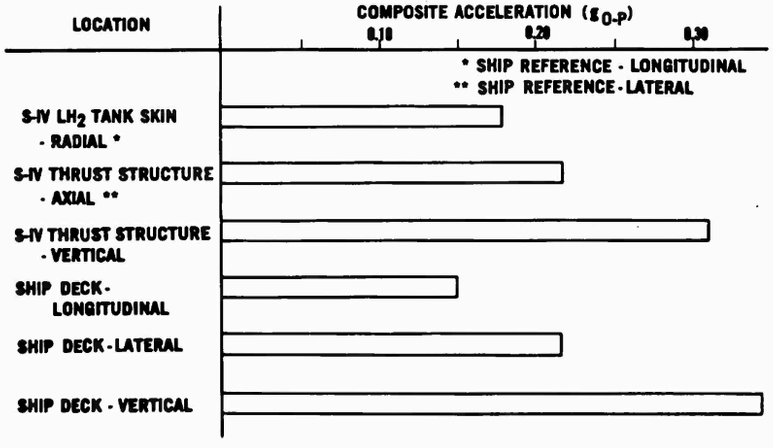

Fig. 11 - Maximum acceleration levels, S-IV stage on freighter

a problem for the S-IV, as they are well below the maximum allowable load factors for the stage.

Data were taken in the form of samples every few hours. Instrumentation is maintained and operated during every shipment of an S-IV via ship to keep a constant monitor on the levels encountered.

AIR TRANSPORTATION

The reality of air transportation for large space vehicles was brought about by the successful flight testing of an aircraft called the "Pregnant Guppy." Basically the Pregnant Guppy is a Boeing 377 Stratocruiser which has been lengthened by some 200 inches and enlarged to over 240 inches in diameter. Figure 12 shows the Pregnant Guppy in flight with an S-IV aboard.

Adopting the Pregnant Guppy as a mode for S-IV stage transportation posed some special problems, both dynamic and mechanical. The mechanical problem was brought about by the need for a transporter with a lifting platform to raise the S-IV to the Pregnant Guppy cargo deck for loading. Since the Douglas transporter lacked this capability, MSFC provided Douglas with a device aptly named the "Cargo Lift Trailer." This device, shown with an S-IV stage in Fig. 13, has the capability of raising the S-IV for loading (illustrated in Fig. 14) as well as transporting it to and from airports. The dynamic problem was posed by (1) the possible effects of exposing an S-IV stage to appreciable vibration for a long period of time in the Pregnant Guppy, and (2) the unknown dynamic characteristics of the CLT.

The Dynamic Environment of the Cargo Lift Trailer

When the CLT arrived at Douglas, its dynamic characteristics were completely unknown. Douglas, therefore, undertook road testing of the CLT to determine the vibration environment produced by this vehicle.

The CLT is a four-wheel, transporter-lift platform with a conventional multi-leaf spring suspension. No dashpots are used. The tires are inflated to 90 psig and are the conventional truck type. The damping ratio, though not determined by drop testing, appears to be higher than that of the Douglas transporter. One would surmise that a fairly decent damping ratio existed since the leaf spring stack is nearly as high as it is long, and inter-leaf friction would be high. Figure 15 illustrates the levels recorded over each wheel during the road tests. The characteristic frequency of the CLT is 1.8 cps.

The S-IV stage is supported on the CLT by means of two rings which rest on a movable pallet. One ring is around the forward end of the vehicle and the other is around the aft end. These rings are attached to the pallet by means of four tubular supports called adapters. The adapters house "oil springs" which act to cushion sharp shocks. They are true shock mounts since the resonance of the vehicle-oil spring system is higher than that of the transporter-leaf spring system. The effect of the oil springs

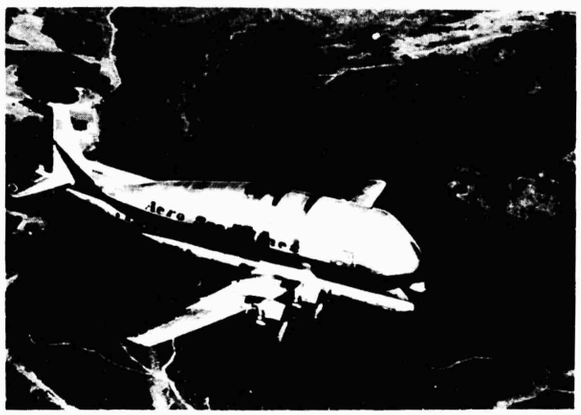

Fig. 12 - The Pregnant Guppy

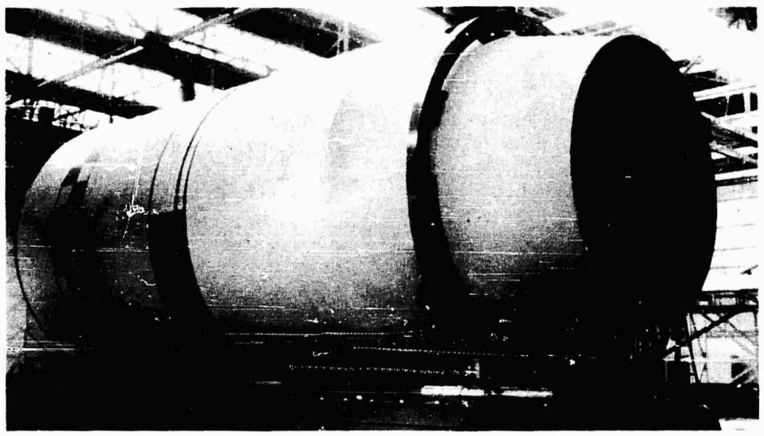

Fig. 13 - S-IV stage on MSFC cargo lift trailer

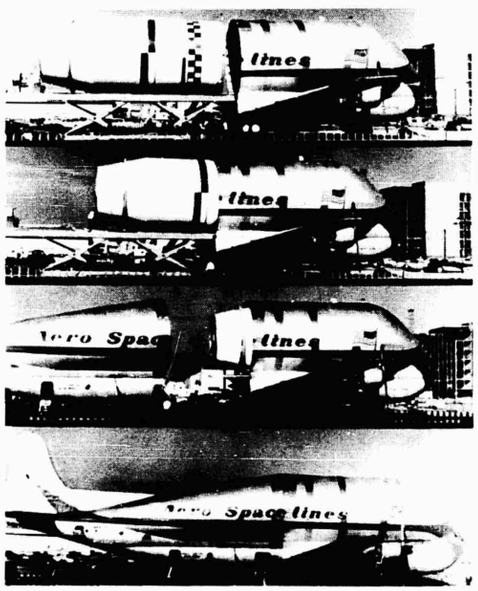

Fig. 14 - Pregnant Guppy loading sequence

is shown in Fig. 16 which compares the rigid body response of the S-IV with the CLT input.

The levels produced by the CLT can be directly compared with the levels produced by the Douglas Transporter since the frequencies involved are in the same range. Since the data was taken over equivalent routes, we are, in effect, comparing a conventional suspension (CLT) with a non-conventional one (Douglas transporter). The comparison is graphically made in Fig. 17 and it can be seen that the Douglas transporter levels average 20-30 percent less for equivalent probabilities in the region of the statistical mode.

This data was acquired using the same type of recording system that was used on the Douglas transporter. Instrumentation is operated during each road trip using the CLT to transport the S-IV stage.

Dynamic Environment of the Pregnant Guppy Aircraft

Once the stage is loaded aboard the Pregnant Guppy (Fig. 14) our concern turns to the vibration environment of this airplane. This environment is more likely to cause a failure than any of the previous environments discussed in this paper. The probability of high levels combined with long durations made an extensive vibration measurement program mandatory.

In the aircraft, measurements were made forward and aft, where the vehicle is supported by the aircraft. These "input points" are at Pregnant Guppy stations 268 and 670 + 22. Statistical distributions of the composite levels measured on the aircraft during takeoff, climb, and cruise are given in Figs. 18 and 19. Fundamental frequencies during each of these conditions are 67, 60, and 51 cps, respectively.

A vibration spectrum from a sample of data recorded at station 268 during takeoff is given in Fig. 20. The spectrum shape is comparable for climb and cruise although the levels

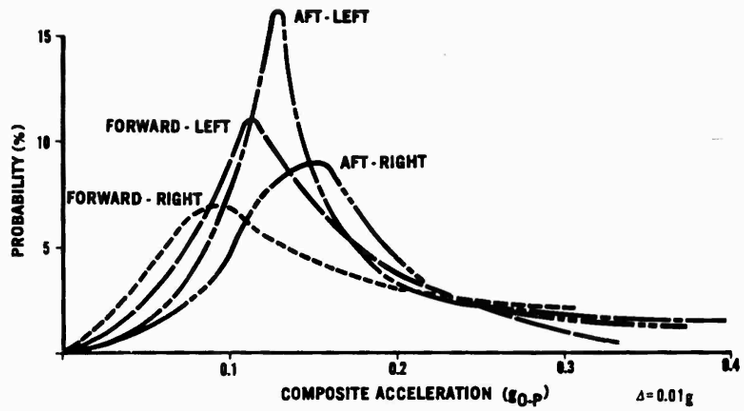

Fig. 15 - Cargo lift trailer vibration levels, vertical direction

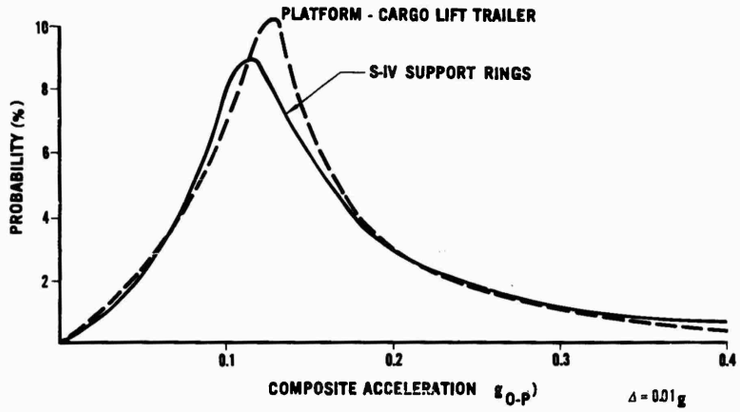

Fig. 16 - Comparison of vibration levels, cargo lift trailer input vs S-IV stage response

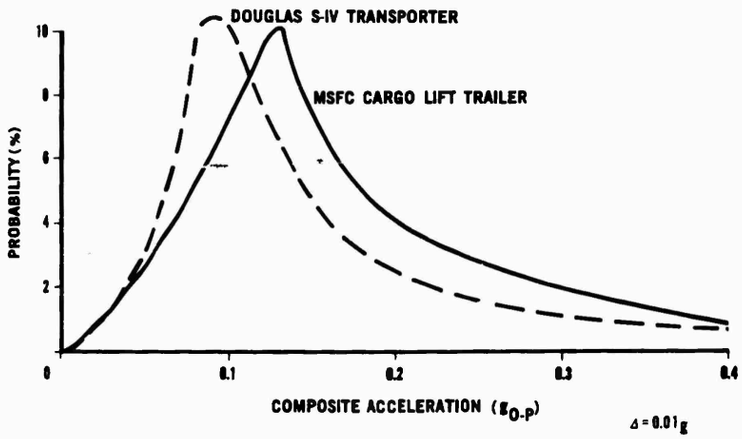

Fig. 17 - Comparison of vibration levels, DAC S-IV transporter vs MSFC cargo lift trailer, vertical direction

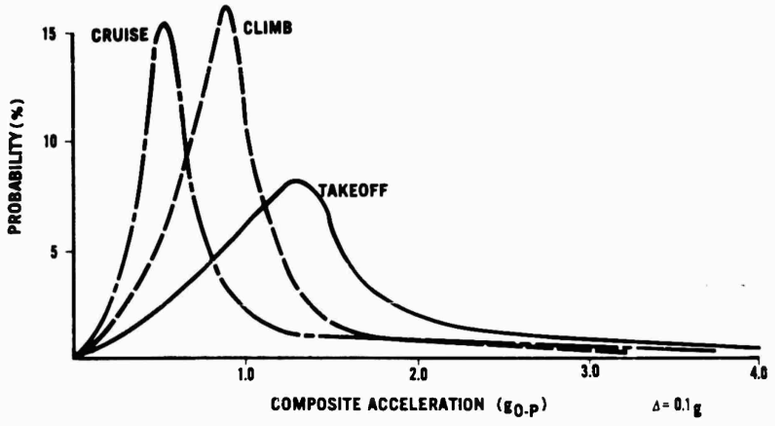

Fig. 18 - Aircraft vibration levels, Pregnant Guppy Station 268, vertical direction

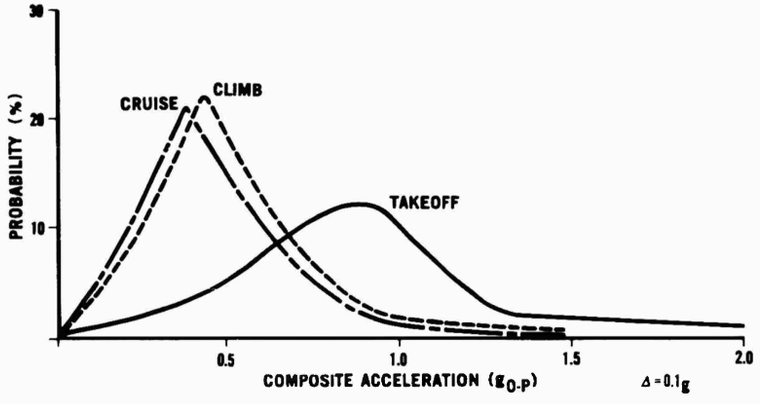

Fig. 19 - Aircraft vibration levels, Pregnant Guppy Station 670 + 22, vertical direction

Fig. 20 - Aircraft vibration spectrum, Pregnant Guppy Station 268, vertical direction

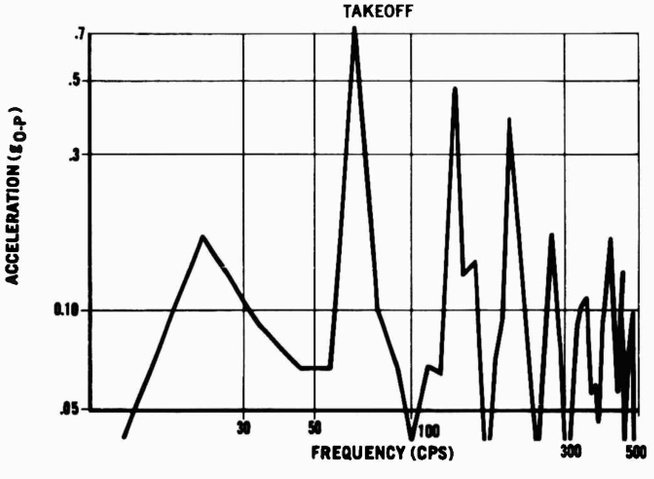

differ. At station 670+22 the spectrum shape is also similar for each flight condition.

Vibration levels encountered during landing are not illustrated, as they are extremely low unless prop reversal is used. Flights of the Guppy, with a simulated S-IV aboard, indicate that prop reversal produces severe vibration levels. During air shipment of S-IV stages, prop reversal has been avoided.

Figure 21 illustrates some of the accelerometer locations used to monitor S-IV vehicle responses to the Guppy environment. In the forward end of the vehicle, mounted on the forward interstage structure, there is a rack with telemetry electronics on it. Two accelerometers were placed at the base of the rack — one in the radial direction and one in the tangential direction (vehicle reference). Figures 22 and 23 show the composite vibration inputs to this rack in each direction listed above. Figure 24 shows the spectrum shape for takeoff taken from a sample of data in the radial direction. It exhibits some, but not all, of the harmonics recorded at station 268. Note that the level at 350 cps is higher than the corresponding level at station 268. This amplification is not a problem, however, as the input is low to begin with. The spectrum shape for the tangential direction, Fig. 24, is comparable to the radial direction.

The LH_2 tank skin is instrumented with one accelerometer in the radial direction to determine the nature of the "ring" modes and to monitor the vibration input to a set of helium spheres within the tank. The composite levels are shown in Fig. 25. These comprise the highest levels recorded on the vehicle. A spectrum plot, Fig. 26, reveals that the levels at specific frequencies are not as serious as the composite might lead one to believe. Figure 26 is a spectrum for takeoff vibration, but climb and cruise spectra are of comparable shape. It is thought that the vibration levels in the tank skin are acoustically, as well as mechanically, induced since the frequency spectrum of the response is broadband, Fig. 26. The sound pressure level in the space between the Guppy fuselage and the tank skin is 125-135 db SPL (re. 2×10^{-4} dyn/cm^2).

Levels recorded inside the vehicle thrust structure in the vicinity of electronic components were very low. The composite levels are shown in Fig. 27 for the sequencer — one of the black boxes in the thrust structure. The levels are too low to plot spectra but the primary energy exists at the fundamental frequency that is characteristic of each flight condition, i.e., 67, 60, and 51 cps.

Figure 28 compares the Pregnant Guppy flight vibration levels recorded on the telemetry rack with the qualification test levels for the telemetry rack. The maximum duration possible at the aircarry level shown, is 800 minutes. This is 100 times longer than the dwell times at any 1 frequency during qualification test. In spite of the long duration, the aircarry level is low enough to produce negligible fatigue damage.

Figure 29 compares the input levels to the helium spheres with the qualification test levels

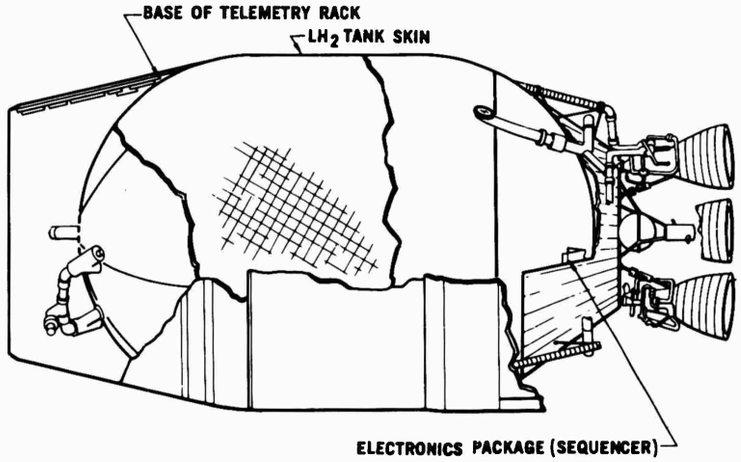

Fig. 21 - S-IV accelerometer locations, Pregnant Guppy aircarry

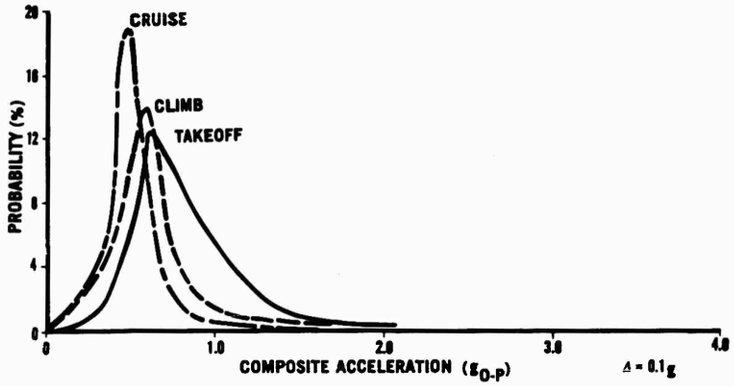

Fig. 22 - Aircraft vibration levels, forward telemetry rack, radial direction

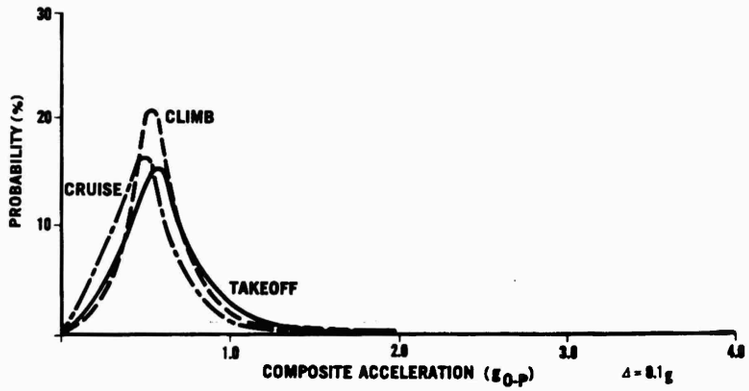

Fig. 23 - S-IV aircarry vibration levels, forward telemetry rack, tangential direction

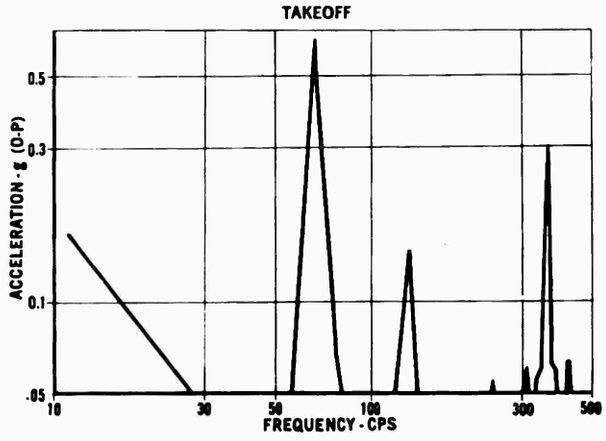

Fig. 24 - S-IV aircarry vibration spectrum, forward telemetry rack, radial direction

Section 4
DESIGN TECHNIQUES

DAMPING CHARACTERISTICS OF ISOLATORS WHEN USED IN OTHER THAN CG MOUNTED CONFIGURATIONS*

F. H. Collopy and R. H. Coco
AVCO Corporation
Wilmington, Massachusetts

INTRODUCTION

At present, there is a tendency for packaging engineers responsible for the isolation of large systems to use a center-of-gravity isolator configuration. This is a relatively simple system to design. At some time it might be necessary, however, to utilize a non-c.g. mounted system as would be dictated by (a) a handling requirement, (b) accessibility considerations, (c) undesirable structural elements to support the isolators, and/or (d) space requirements. Although there is available some information on the vibration characteristics[1-3] of non-c.g. mounted isolation systems, it deals mostly with non-resonant conditions. Damping is neglected and the available information explains what frequency ratios not to operate near. It is contended, that what is lacking in the state-of-the-art is a good knowledge of the vibration behavior at the resonant frequencies.

There even is an apparent lack of this knowledge among the mount manufacturers themselves. Although analyses of this type of system have been performed by them, little or no comparative testing has been conducted. The engineer designing equipment to present vibration specifications which call out for vibration inputs from 1 to 300 cps for GSE requirements has to design within this frequency range and thus should be able to determine the characteristics of the system at its resonant frequencies.

PROBLEM

Figure 1 illustrates the system under consideration. K_s and K_c represent the shear and compression-spring rates of a single isolator. Equation (1) contains the undamped equations of motion needed to describe the system when subjected to lateral vibration:

$$\begin{aligned} M\ddot{X} + 4K_s(X - X_o) - 4aK_s\theta &= 0 \\ J\ddot{\theta} - 4aK_s(X - X_o) + 4\left[K_c b^2 + K_s a^2\right]\theta &= 0. \end{aligned} \tag{1}$$

In matrix notation, the above equations appear as

$$\begin{bmatrix} M & 0 \\ 0 & J \end{bmatrix}\begin{bmatrix} \ddot{X} \\ \ddot{\theta} \end{bmatrix} + \begin{bmatrix} 4K_s & -4_aK_s \\ -4_aK_s & 4\left[K_c b^2 + K_s a^2\right] \end{bmatrix}\begin{bmatrix} X \\ \theta \end{bmatrix} = \begin{bmatrix} 4K_s \\ -4aK_s \end{bmatrix}[X_o],$$

or more simply as

$$[M][\ddot{q}] + [K][q] = [F], \tag{2}$$

where [M], [K], and [F] represents the mass, spring, and force matrices, respectively, and [q] is a generalized displacement matrix. If damping is included, Eq. (2) becomes:

*This paper was not presented at the Symposium.

[1] C. M. Harris and C. E. Crede, Editors, Shock and Vibration Handbook (McGraw-Hill Book Co., Inc., New York, 1961).

[2] J. N. McDuff and J. R. Curreri, Vibration Control (McGraw-Hill Book Co., Inc., New York, 1958).

[3] C. E. Crede, Vibration and Shock Isolation (John Wiley & Sons, Inc., New York, 1951).

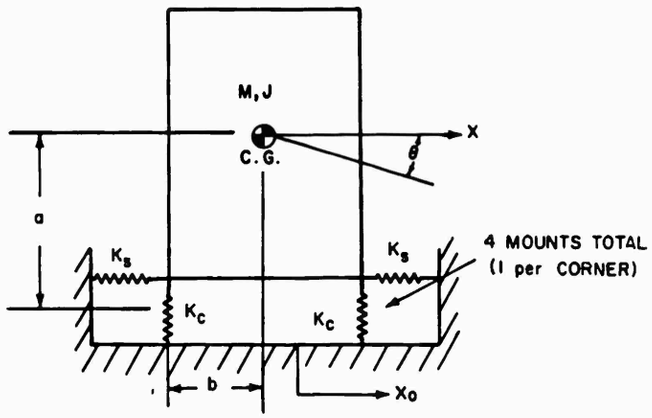

Fig. 1 - Dynamic model

$$[M][\ddot{q}] + [C][\dot{q}] + [K][q] = [F] , \qquad (3)$$

and [C] , the damping matrix, represents an array of elements, such that

$$[C] = \begin{bmatrix} C_{11} & C_{12} \\ C_{21} & C_{22} \end{bmatrix} .$$

In order to analyze system behavior at resonance, it is imperative to be able to determine [C] properly and accurately.

PURPOSE

The purposes for which this paper was written are:

1. To indicate the scarcity of information now available.

2. To illustrate the wide range of results that can be obtained using different assumptions.

3. And mainly, to arouse interest among designers, engineers, isolator manufacturers and research companies so that testing programs may be conducted, correlation with analysis may be made, and subsequent results may be published.

The brief testing program utilized for supporting this paper, although supplying these authors with some valuable information, is by no means the conclusive evidence needed to nurture the absolute formulation to the solution of this problem. Other supporting tests are planned in the future, and it is hoped they will provide more much-needed information.

ASSUMPTIONS

For the particular system discussed in this paper, the following basic assumptions are made:

1. The system is linear.

2. The system supported by the isolators is rigid.

3. The spring rate of the isolators is the same in tension as in compression.

4. The isolators are below the rigid body and are symmetrically located about the vertical axis through the center of gravity.

TEST MODEL

A test was proposed and a model was constructed that had the following properties:

M = 0.217 lb-sec^2/in.,

J = 59.0 lb-in.-sec^2,

a = 19.5 inches, and

b = 7.0 inches.

Since the shock mount vendor only lists a plus-or-minus range of values of spring rates in shear of any particular isolator and an

approximate expected ratio between the compression and shear values, it was mandatory for the authors to determine accurately these values for this particular application. These values were obtained by coordinating results of a shock test, a resonant search on the entire system, individually testing a single isolator, and the vendor's information. From this, it was determined that the applicable spring values to be used in this analysis are K_s = 550 lb/in., and K_c = 3300 lb/in. Using the values listed above, the mass and spring matrices are

$$[M] = \begin{bmatrix} 0.217 & 0 \\ 0 & 59.0 \end{bmatrix},$$

and

$$[K] = \begin{bmatrix} 2200 & -42900 \\ -42900 & 1.485 \times 10^6 \end{bmatrix}.$$

The isolator vendor indicated a percent of critical damping (ζ) of 10 (percent), both in shear and in the tension-compression direction. Presented below are three different methods employed to obtain a damping matrix.

METHOD 1

For the first attempt to obtain a suitable damping matrix, a method was employed as described in chapter 3 of Ref. 1, and is described in the appendix of this paper. The method basically consists of calculating the ij^{th} damping element as a function of the ij^{th} stiffness element in the K matrix and the total mass. When calculated in this manner, the [C] matrix is

$$[C] = \begin{bmatrix} 4.37 & -85.1 \\ -85.1 & 2185. \end{bmatrix}, \quad \text{method 1.}$$

An analysis was performed using this matrix and the results for motion at the center of gravity of the system are compared to the test results, in Fig. 2.

METHOD 2

Another approach which would have seemed reasonable was to assume that each mount had an inherent damping value, which was a function of stiffness, c/c_{cr}, and the percentage of mass it had to support. This approach is described in the appendix, and it is illustrated that this [C] matrix is identical with that obtained by method 1. A close look at the two methods indicates they should be equal, since

$$2\zeta\sqrt{4KM} = 4\left[2\zeta\sqrt{K\frac{M}{4}}\right],$$

$$[\text{method 1}] = [\text{method 2}].$$

The only difference lies in the fact that the second method appears to be more logical.

METHOD 3

A third method (shown in the appendix) was proposed in which modal analysis techniques were used. It was assumed that the percent of critical damping in each of the normal modes

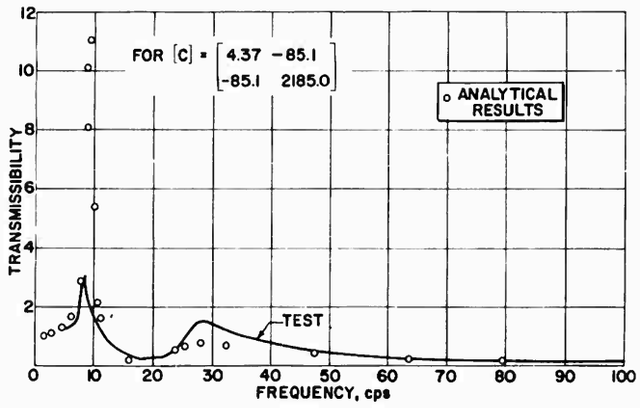

Fig. 2 - Test and analytical correlation (Method 1)

of motion, lower rocking mode and upper rocking mode, was the same (10 percent) as quoted by the manufacturer for the shear direction or tension-compression direction. The [C] matrix determined by method 3 is

$$\begin{bmatrix} 3.8 & -36.2 \\ -36.2 & 1780.0 \end{bmatrix}, \quad \text{method 3.}$$

An analysis was performed using this matrix and the results for motion at the center of gravity are compared to the test results (Fig. 3).

TEST AND ANALYSIS CORRELATION

It is apparent from Fig. 2 that the analytical results using method 1 do not compare favorably with the test results; but that the results of Fig. 3 using method 3 do compare well. To determine the actual damping matrix inherent in the system, method 3 was used whereby the amount of damping per mode was determined by measuring the quality factor,[1] Q, in each mode, from the test results, and utilizing the tools of a modal analysis to obtain a [C] matrix as demonstrated in the appendix (method 3). Figure 4 illustrates the meaning of the quality factor, Q, at a resonant frequency. This can be applied in a multi-degree-of-freedom system, with fairly good accuracy if the resonant peaks are not too close to each other. As shown in the appendix, the [C] matrix determined from the test results is:

$$[C] = \begin{bmatrix} 4.33 & -37.5 \\ -37.5 & 1944.0 \end{bmatrix} \quad \text{Test Values.}$$

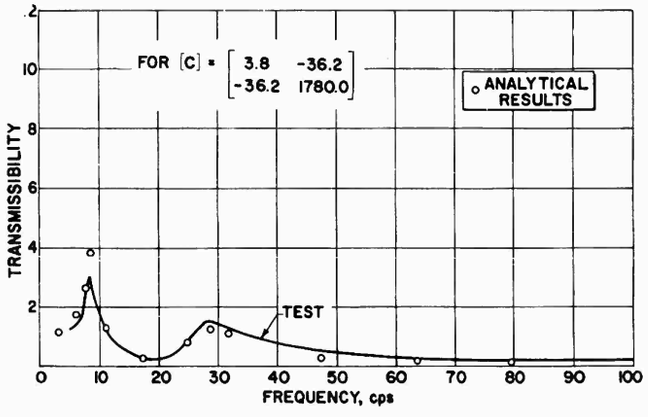

Fig. 3 - Test and analytical correlation (Method 3)

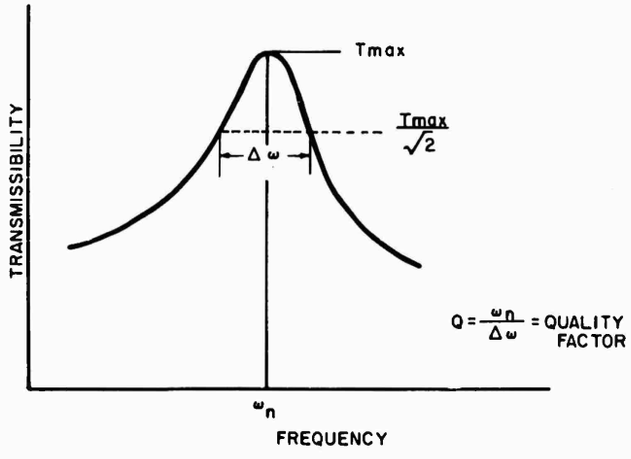

Fig. 4 - Quality factor, Q, determination

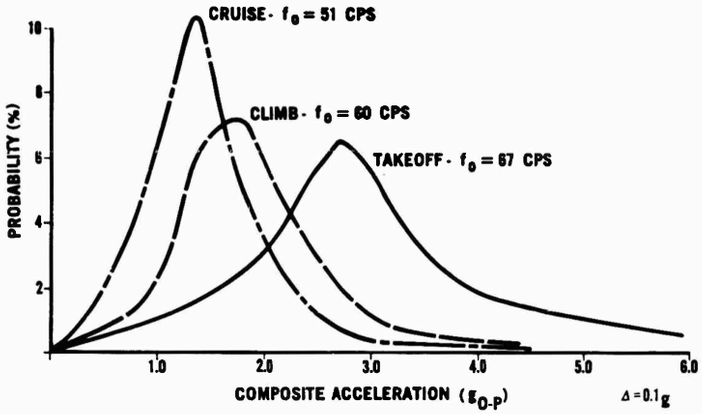

Fig. 25 - S-IV aircarry vibration levels, LH_2 tank skin, radial direction

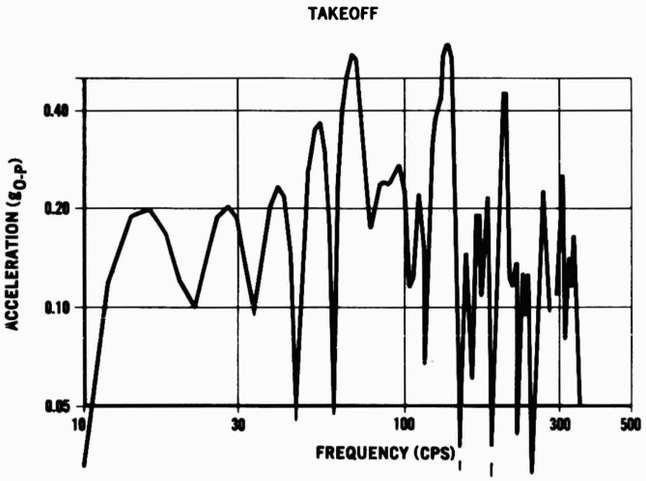

Fig. 26 - S-IV aircarry vibration spectrum, LH_2 tank skin, radial direction

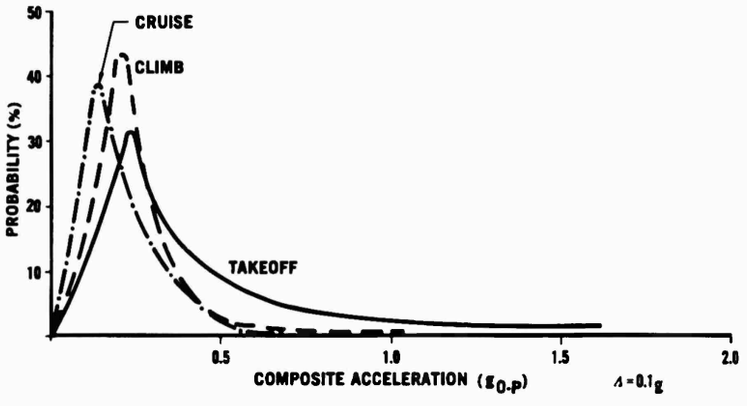

Fig. 27 - S-IV aircarry vibration levels, sequencer, axial direction

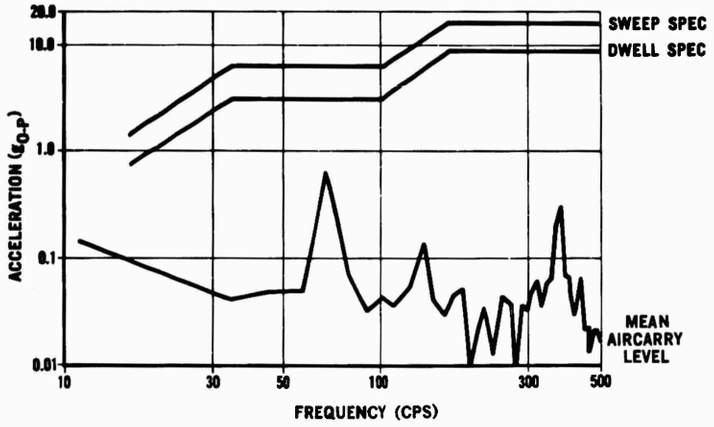

Fig. 28 - Comparison of S-IV aircarry levels with qualification test levels, forward telemetry rack

for the helium spheres. Once again the aircarry spectrum is well below the dwell spec. The "maximum aircarry level" plot, shown in the graph, is based on the highest recorded composite level. This maximum level will occur for only a few seconds on rare occasions. Therefore, it presents no cause for concern.

Based on this and other data, the normal vibration environment produced by the Pregnant Guppy does not produce a hazard for the stage. But because of the possibility of the occurrence of extreme vibration levels, given the right combination of circumstances, instrumentation monitors the environment during each S-IV airshipment.

SUMMARY

In this paper we have reviewed the vibration environments which the S-IV stage encounters during transportation. Based on the facts presented in this paper, it appears that the vibration environment encountered during the surface transportation of S-IV stages consists primarily of frequencies below 10 cps. Further, it appears that the normal vibration environment does not endanger the integrity of the stage. During air transportation, vibration levels have been recorded at frequencies from below 2 to above 600 cps. The levels over this range are well below design specifications.

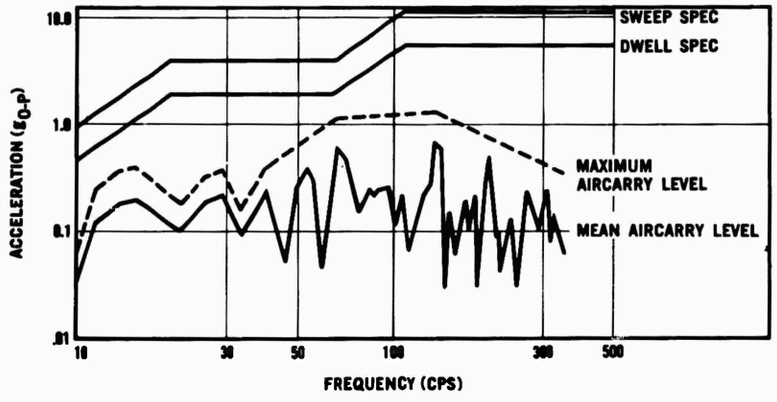

Fig. 29 - Comparison of S-IV aircarry levels with qualification test levels, LH_2 tank, cold helium spheres

Instrumentation will be maintained, however, during each future S-IV shipment to assure that unexpected occurrences have not produced levels that will exceed S-IV stage specifications

APPENDIX

Instrumentation and Data Analysis

INSTRUMENTATION FOR SURFACE TRANSPORTATION

The instrumentation utilized in this phase of transportation was carried with the vehicle on the transporter. It consisted of strain gage type accelerometers directly driving the galvanometers in an oscillograph. During road transportation the oscillograph was run continuously and during other phases data was taken in intermittent samples. The overall frequency response of the system was 0 to 50 cps. The oscillograph paper speed was sufficient to resolve beyond 50 cps.

INSTRUMENTATION FOR PREGNANT GUPPY FLIGHTS

This instrumentation was carried with the vehicle on the Pregnant Guppy pallet. This system used piezoelectric accelerometers at various locations on the vehicle and aircraft. Their signals were fed to amplifiers which drove the galvanometers in an oscillograph. The oscillograph is run continuously during takeoffs and landings, and intermittently during climb and cruise.

The overall frequency response of this system is from 5 to 500 cps. Paper speeds, sufficient to resolve 500 cps, were used in short bursts because of the high paper consumption involved. During the greater part of each data sample the oscillograph is run at 1/10 of the high speed rate.

FREQUENCY SPECTRUM PLOTS

The frequency spectra, plotted in this paper, were obtained by Fourier analysis. A sample of data were optically enlarged 10-20X. They were then digitized by hand at the rate of 1000 samples per second of data. This data was punched onto cards and fed to a computer programmed for Fourier analysis of digital tapes.

* * *

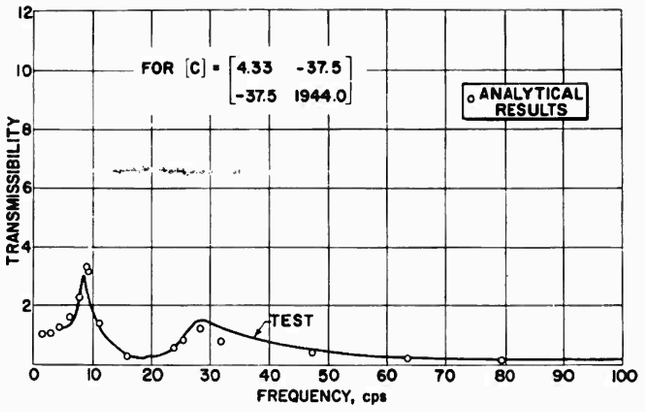

Fig. 5 - Test and analytical correlation (Test values)

An analysis was performed using the matrix and these results are also compared with the test results (Fig. 5). It is really seen that the analytical values compare favorably with the test results.

In comparing the derived [C] matrices of methods 1, 2, and 3 and the above [C] matrix derived from the test results, it is interesting to note that the C_{11} and C_{22} terms are approximately the same, and the C_{12} and C_{21} terms vary appreciably. This suggests that these terms strongly influence the analysis, and that they must be selected carefully.

CONCLUSIONS

The authors realize that the testing data used in support of this paper are rather sparse; however, it should serve as a beginning point for future work in this area. Certain conclusions can be made as a result of the work performed:

1. Depending on how one obtains the damping matrix, a wide range of results can occur. For example, in this paper the results of method 1 give values of four times the test values at the low frequency and only one-half the test values at the high frequency.

2. Single-mount data should be obtained as accurately as possible. This can be accomplished by an acceptance test.

3. Based on the test results presented in this paper, a reasonable approach would be to utilize a modal analysis. An assumption would be made that the amount of damping expected in each of the normal modes of vibration is equal to the percent of critical damping in the pure shear direction or in the tension-compression direction as quoted by the isolator vendor. The procedure would then be either to use a modal analysis to calculate the response directly or to use a matrix algebraic technique as shown by method 3 in the appendix to determine the [C] matrix from the modal damping matrix $[\overline{C}]$.

4. More work has to be done on this subject, especially in the testing area, in order to better understand the damping properties of non-c.g.-mounted configurations; primarily, so that analyses can be performed which will predict with some degree of accuracy the expected vibratory motions in such a system.

The authors intend that this paper serve as an invitation for more people to take an interest in this particular problem and welcome any information, suggestions, comments, or criticisms which will enable advancement on this type of system.

APPENDIX

METHOD 1

This method is as proposed in chapter 3 of Ref. 1, and is applied to the system as demonstrated:

$$C_{11} = 2\zeta\sqrt{K_{11}M} = 2\zeta\sqrt{4K_sM}$$

$$= 2(0.10)\sqrt{2200(0.217)} = 4.37$$

$$C_{21} = C_{12} = -aC_{11} = -85.1$$

$$C_{22} = \left[2\zeta\sqrt{4K_cM}\right]b^2 + \left[2\zeta\sqrt{4K_sM}\right]a^2 = 2185.$$

METHOD 2

This method considers the spring rate of the individual mount in each direction separately, and the portion of the mass which it supports (in this problem, M/4):

$$C_s\ (\text{Shear}) = 2\zeta\sqrt{K_s\frac{M}{4}}$$

$$= 2(0.10)\sqrt{550\ \frac{0.217}{4}} = 1.09$$

$$C_c\ (\text{Comp.}) = 2\zeta\sqrt{K_c\frac{M}{4}}$$

$$= 2(0.10)\sqrt{3300\ \frac{0.217}{4}} = 2.68$$

$$C_{11} = 4C_s = 4.36$$

$$C_{12} = C_{21} = -4aC_s = -85.1$$

$$C_{22} = 4\left[C_cb^2 + C_sa^2\right] = 4\left[2.68(7)^2 + 1.09(19.5)^2\right] = 2185.$$

METHOD 3

If in Eq. (3) we introduce the relation $[q] = [\phi]\,[Z]$, where $[\phi]$ is a matrix of mode shapes and $[Z]$ is a set of modal coordinates, then (3) becomes (dropping bracket notation)

$$M\phi\ddot{Z} + C\phi\dot{Z} + K\phi Z = F. \qquad (4)$$

Premultiplying Eq. (4) by ϕ^T and normalizing such that $\phi^TM\phi = I$, we obtain

$$I\ddot{Z} + \bar{C}\dot{Z} + \omega_n^2 Z = \phi^TF.$$

The modal mass matrix is unity and $\bar{C}$, the modal damping matrix, is:

$$\bar{C} = \begin{bmatrix} \frac{\omega_{n_1}}{Q_1} & 0 \\ 0 & \frac{\omega_{n_2}}{Q_2} \end{bmatrix}$$

Since $\bar{C} = \phi^TC\phi$, then it follows

$$C = \phi^{T^{-1}}\,\bar{C}\phi^{-1}. \qquad (5)$$

Using $Q_1 = 5.0$ and $Q_2 = 5.0$ (10 percent equivalent viscous damping per mode) and utilizing Eq. (5) the [C] matrix is obtained as

$$[C] = \begin{bmatrix} 3.8 & -36.2 \\ -36.2 & 1780.0 \end{bmatrix}.$$

C MATRIX OBTAINED FROM TEST

The quality factors measured from the test data are $Q_1 = 4.2$ and $Q_2 = 4.6$ using Eq. (5), the [C] matrix is obtained as:

$$[C] = \begin{bmatrix} 4.33 & -37.5 \\ -37.5 & 1944.0 \end{bmatrix}.$$

* * *

THE EFFECTS OF A SPRING CLEARANCE NONLINEARITY ON THE RESPONSE OF A SIMPLE SYSTEM*

J. P. Young
Goddard Space Flight Center
Greenbelt, Maryland

INTRODUCTION

There appears to be very little published data on the response characteristics of systems containing "freeplay" which provides aid or guidelines to the designer of such systems. References 1-5 contain information of varying nature on the effect of "freeplay" in mechanical systems. It seems paradoxical that so little coordinated effort has been put forth to generate design information for systems with clearance in view of the fact that clearance in systems is a common occurrence. Clearance occurs mostly as an unwanted by-product of imperfect manufacturing methods. Occasionally, "freeplay" is utilized deliberately to produce desired system performance characteristics.

This paper is based on the investigation of the response, to a sinusoidal input, of a simple nonlinear system consisting of a single undamped mass and a spring with clearance as shown in Fig. 1. In addition to the obvious distinguishing features of this system, three other features that contribute to the "classification" of the results of this investigation are (1) the spring load is zero under zero external loading conditions, (2) transients produced by initial conditions different from zero are damped out, and (3) initial conditions that may be imposed are not sufficient to produce a shift in the character of the steady-state response (e.g., subharmonic responses are not generated). The stipulation of zero spring load in item (1) above was prompted by the physical situation of the near vertical launch of a rail guided rocket. The results can also be extended to include the moving foundation case shown in Fig. 2.

SUMMARY

This investigation was performed analytically through the use of the Ritz Averaging Method[1,6] and by simulation on an analog

*This paper was not presented at the Symposium.

[1] K. Klotter, "Nonlinear Vibration Problems Treated by the Averaging Method of W. Ritz," Stanford Univ., Tech. Rept. No. 17, Parts I and II, Contract N6ONR-251-II (June 1951).

[2] T. Y. Wu, "Sled-Track Interactions and a Rapid Method For Track - Alignment Measurements, Part II - Shoe Clearance Effects in a Gravitational Field," AER, Inc. Technical Report No. 114(114-8-1) (June 30, 1958).

[3] G. E. Padgett and E. L. Kessler, "Use of Free-Play as a Vibration Isolator," Shock, Vibration and Associated Environments Bulletin No. 27, Part I (June 1959).

[4] C. S. O'Hearne, "Studies Applicable to the Evaluation of the Effect of Fastening Looseness on Equipment Response to Foundation Oscillations," Institute of Environmental Sciences Annual Meeting (April 1961).

[5] H. F. Bauer, "Methods in Nonlinear Vibration Theory," Aeroballistics Internal Note #40-62, Marshall Space Flight Center (Nov. 1962).

[6] "Shock and Vibration Handbook," Vol. 1, Chapter 4 (McGraw-Hill Book Co., Inc., New York, 1961).

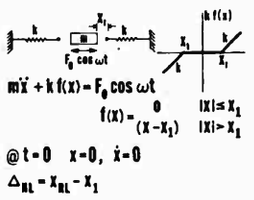

Fig. 1 - Forced mass case

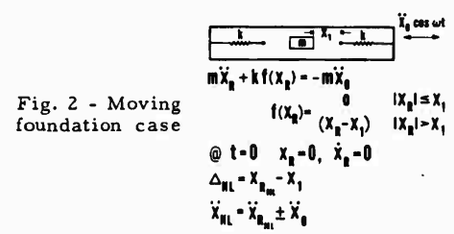

Fig. 2 - Moving foundation case

computer. Reference 1 has compared the results of the Ritz Averaging Method, for this system, with exact results based on the use of the linear differential equations which apply to the individual segments and shows very good agreement outside the superharmonic response region. Both the mass displacement and the mass acceleration frequency response functions were determined in this investigation, with considerable effort devoted to defining the superharmonic response characteristics of this simple system. The superharmonic response is shown to radically modify the system response in the low frequency ratio range. Based on these displacement and acceleration frequency response functions, the remaining part of the investigation was devoted to comparing the maximum spring load and the maximum mass acceleration with corresponding response parameters for a linear system produced by eliminating the clearance. This comparison is presented as a ratio of nonlinear to linear response vs frequency ratio for both the forced mass and the moving foundation cases.

RESULTS

The use of the Ritz Averaging Method, to determine analytically the frequency response curves, was chosen because of its simplicity of application. The derivation of the frequency response equation was performed as follows:

$$m\ddot{x} + k f(x) = F \cos \omega t$$

$$f(x) = \begin{cases} 0 & |x| \le x_1 \\ (x - x_1) & |x| > x_1 \end{cases}$$

From Ref. 6, assuming $x = x_{NL} \cos \sigma$,

$$\left(\frac{\omega}{\omega_0}\right)^2 = \frac{1}{\pi x_{NL}} \int_0^{2\pi} f(x_{NL} \cos\sigma) \cos\sigma \, d\sigma \mp \frac{F_0}{m\omega_0^2 x_{NL}} .$$

$$\int_0^{2\pi} f(x_{NL} \cos \sigma) \cos \sigma \, d\sigma$$

$$= \int_{-\sigma_1}^{\sigma_1} (x_{NL} \cos \sigma - x_1) \cos \sigma \, d\sigma + \int_{\pi-\sigma_1}^{\pi+\sigma_1} (x_{NL} \cos \sigma - x_1) \cos \sigma \, d\sigma$$

$$= \left[x_{NL} (2\sigma_1 + \sin 2\sigma_1) - 4x_1 \sin \sigma_1\right]$$

$$\sigma_1 = \cos^{-1}\left(\frac{x_{NL}}{x_1}\right)^{-1}$$

$$\left(\frac{\omega}{\omega_0}\right)^2 = \frac{2\sigma_1 + \sin 2\sigma_1}{\pi} - \frac{4}{\pi\left(\frac{x_{NL}}{x_1}\right)} \sin \sigma_1 \mp \frac{F_0}{m\omega_0^2 x_{NL}} .$$

From above, it is seen that only a single term approximation is used, and therefore solutions containing higher harmonics will not be predicted.

To perform a check on the single term Ritz Averaging Method solution outside the region of higher harmonic solutions and to investigate the superharmonic response region, the system was programmed on a PACE TR-10 analog computer. Two biased diodes were used to generate the "dead spot" type restoring force. To obtain the steady-state solution for this undamped case, damping was introduced into the system to dampen the starting transients and then the damping was slowly removed.

The displacement frequency response characteristics, as determined by this investigation, are shown in Fig. 3. The family of lines, a function of the magnitude of the forcing function, were generated from the approximate frequency response equation derived above. The curves approach, asympotically, a vertical line passing through the frequency ratio of 1. The data points, obtained from the analog computer results, show good agreement with the calculated values above the frequency range where superharmonic responses are present. Also shown are the harmonic "backbone" curves of the 2d and 3rd order. These curves were generated simply by taking 1/2 and 1/3 sub-multiples of the frequency of the free vibration response curve. The free vibration response curve is the "0" input level curve. It is in the region of the backbone curves that one would expect superharmonic response effects. This is illustrated in Fig. 4 where the region in the neighborhood of the backbone curves is expanded. The peaks on the right correspond to 2d superharmonic response region, and the peaks to the left are in the 3rd superharmonic response region. The three isolated points on the extreme left are 5th (input levels "2" and "4") and 7th (input level "1") superharmonic responses. It should be clearly understood that the response curves which are presented are based on the peak values which are the sum of the fundamental and higher harmonics. To be noted, is the fact that the superharmonic response curves, as drawn, pass continuously through the 2d order peak, but a discontinuity

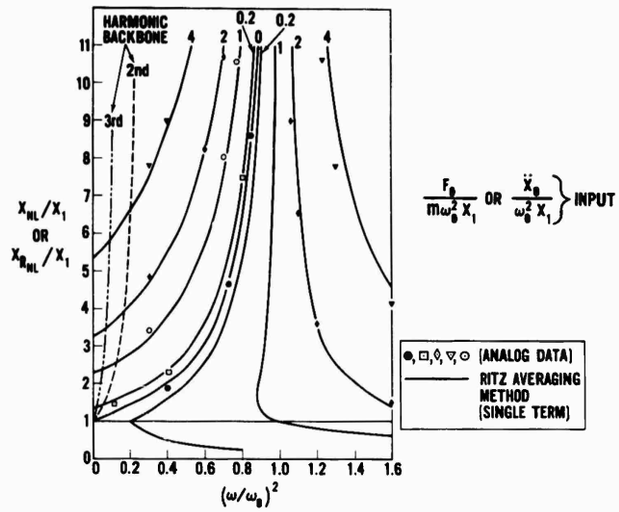

Fig. 3 - Displacement frequency response

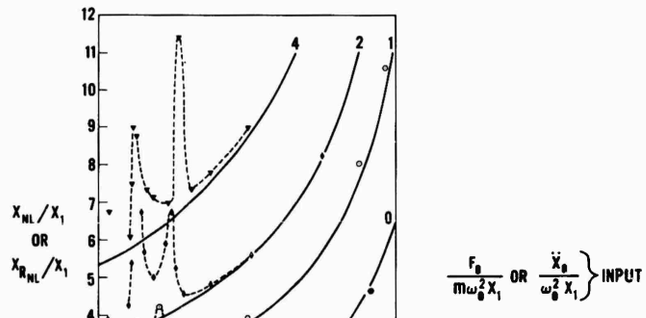

Fig. 4 - Displacement frequency response (superharmonic resonance region)

exists at the 3rd order response region. This manner of drawing the superharmonic response curves reflects the character of the generated waveforms. The 2d superharmonic peak waveform showed a "clean" 2d harmonic distortion with the "peaking out" obtained by sweeping slowing through the frequency region. In the region of the 3rd superharmonic response, the situation was somewhat different. As the 3rd order region was approached from the left, the system went into an "out of phase" 3rd order harmonic distortion easily enough, but extensive searching across the pertinent frequency range was unable to produce an "in phase" 3rd order harmonic distortion. In the region of the discontinuity, efforts were unsuccessful to produce a response without the presence of appreciable transients. This phenomenon of nonlinear systems, known as superharmonic response, can be pictured as a "forced

resonant" vibration which is generated when the frequency of the forcing function is near 1/n of the frequency of the free-vibration response curve. This "forced resonant" vibration is superimposed on the fundamental response.

Turning attention from displacement response to acceleration response, Fig. 5 illustrates the acceleration frequency response for this system. The lines were generated from the displacement response curves, shown in Fig. 3, simply by taking a balance of forces on the mass at the point of maximum displacement. The results of performing this force balance are as follows:

$$\left.\begin{aligned} \frac{\ddot{x}_{NL}}{\omega_0^2 x_1} &= \left(\frac{x_{NL}}{x_1} - 1\right) \mp \frac{F_0}{m\omega_0^2 x_1} \\ \frac{\ddot{x}_{R_{NL}}}{\omega_0^2 x_1} &= \left(\frac{x_{R_{NL}}}{x_1} - 1\right) \mp \frac{\ddot{x}_0}{\omega_0^2 x_1} \end{aligned}\right\} \quad x_{NL} \text{ or } x_{R_{NL}} > x_1$$

$$\left.\begin{aligned} \frac{\ddot{x}_{NL}}{\omega_0^2 x_1} &= \frac{F_0}{m\omega_0^2 x_1} \\ \frac{\ddot{x}_{R_{NL}}}{\omega_0^2 x_1} &= \frac{\ddot{x}_0}{\omega_0^2 x_1} \end{aligned}\right\} \quad x_{NL} \text{ or } x_{R_{NL}} < x_1 .$$

The analog data points again show good agreement with calculated values.

Looking again in more detail at the superharmonic response region, Figs. 6 and 7 illustrate the peaking effect for the acceleration response. As would be expected, the acceleration at or near the superharmonic response peaks is made up predominately of the higher harmonic. As a result, due largely to the frequency squaring effect, the percentage increase in acceleration response, is appreciably greater than the corresponding increase in the displacement response.

The ultimate objective of this investigation is to make an evaluation of the effect of "free play" or clearance on the response of this simple system. This nonlinear clearance effect can be evaluated on the basis of the amount of spring deflection produced and also on the magnitude of the mass acceleration.

First, the spring deflection for the nonlinear case will be compared to the corresponding spring deflection for a linear case generated by eliminating the clearance. The spring deflection comparison, which is of the same form for both types of excitation, can be made as follows:

$$\frac{\Delta_{NL}}{\Delta_L} = \frac{x_{NL} - x_1}{\left(\frac{F_0}{m\omega_0^2}\right)(MF)_L} = \left(\frac{F_0}{m\omega_0^2 x_1}\right)^{-1} (MF)_L^{-1} \left(\frac{x_{NL}}{x_1} - 1\right) ,$$

or

$$\frac{\Delta_{NL}}{\Delta_L} = \left(\frac{\ddot{x}_0}{\omega_0^2 x_1}\right)^{-1} (MF)_L^{-1} \left(\frac{x_{R_{NL}}}{x_1} - 1\right) ,$$

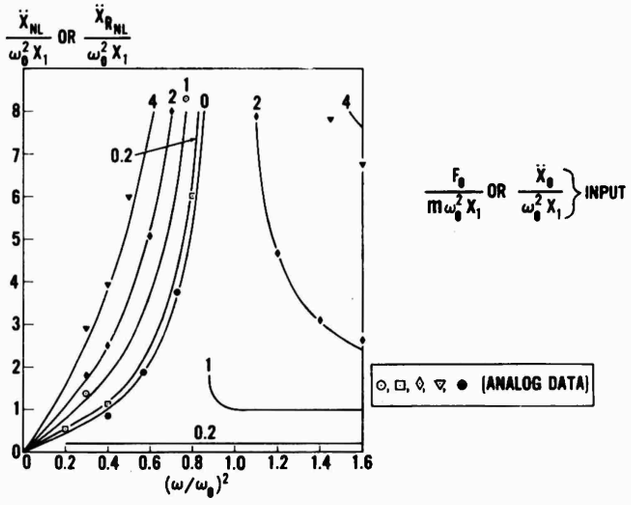

Fig. 5 - Acceleration frequency response

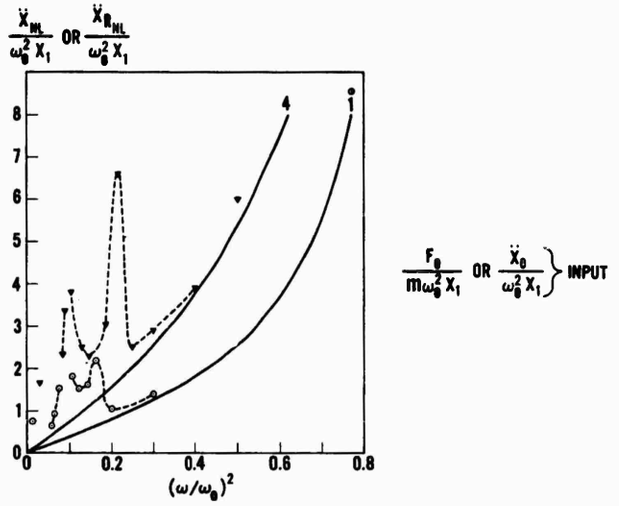

Fig. 6 - Acceleration frequency response (superharmonic resonance region)

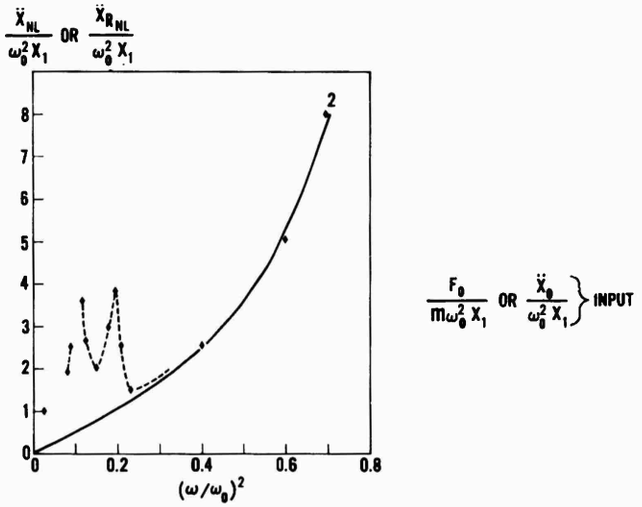

Fig. 7 - Acceleration frequency response (superharmonic resonance region)

where Δ = spring deflection,

$$\omega_0^2 = \frac{k}{m}, \text{ and}$$

$$(MF)_L = \frac{1}{1 - \left(\frac{\omega}{\omega_0}\right)^2}.$$

From the above derived expression and the displacement frequency response curves in Figs. 3 and 4, the ratio of nonlinear to linear response was determined as illustrated in Fig. 8. The effect of superharmonic response is shown for input levels of "1" and "4." The most obvious conclusions to be made from Fig. 8 are (1) the nonlinear effect amplifies the response for frequency ratios <1, but attenuates the response for frequency ratios >1; (2) the superharmonic response magnifies the detrimental effect of the nonlinearity in the low frequency range; (3) for a constant input, increasing the amount of clearance is detrimental for $(\omega/\omega_0)^2 < 1$, but beneficial for $(\omega/\omega_0)^2 > 1$; and (4) when $(\omega/\omega_0)^2 = 1$, the conclusions are not so clear cut since there is a discontinuity in the curves. At input levels of "1" or less, the discontinuity is particularly significant in that the spring deflection ratio goes from some value greater than 1 to zero. At which of the two values the system will actually operate, depends on the initial energy the system possesses or in other terms on the initial conditions. Physically, what is happening, of course, at the lower response of the low input levels is that the mass is not coming into contact with the spring.

Looking now at the mass acceleration comparison, the ratio of nonlinear to linear response will be of different forms for the two types of excitation. The resulting expressions are as follows:

Forced Mass Case

$$\frac{\ddot{x}_{NL}}{\ddot{x}_L} = \frac{(x_{NL} - x_1)\,\omega_0^2 \mp \frac{F_0}{m}}{\omega^2 \left(\frac{F_0}{m\omega_0^2}\right)(MF)_L} = \frac{\left(\frac{x_{NL}}{x_1} - 1\right) \mp \frac{F_0}{m\omega_0^2 x_1}}{\left(\frac{\omega}{\omega_0}\right)^2 \left(\frac{F_0}{m\omega_0^2 x_1}\right)(MF)_L}.$$

Moving Foundation Case

$$\frac{\ddot{x}_{NL}}{\ddot{x}_L} = \frac{\ddot{x}_{R_{NL}} \pm \ddot{x}_0}{\ddot{x}_0 (MF)_L} = \frac{\left(x_{R_{NL}} - x_1\right)\omega_0^2}{\ddot{x}_0 (MF)_L}$$

$$= \left(\frac{\ddot{x}_0}{\omega_0^2 x_1}\right)^{-1} (MF)_L^{-1} \left(\frac{x_{R_{NL}}}{x_1} - 1\right).$$

Based on the above expressions and the system frequency response functions, the ratio of nonlinear to linear mass acceleration response was determined as illustrated in Figs. 9 and 10. For the forced mass case, Fig. 9, the effect of superharmonic response is shown only for the input level of "4." The lower input levels would show even more extreme peaking in the superharmonic response region. This peaking effect is

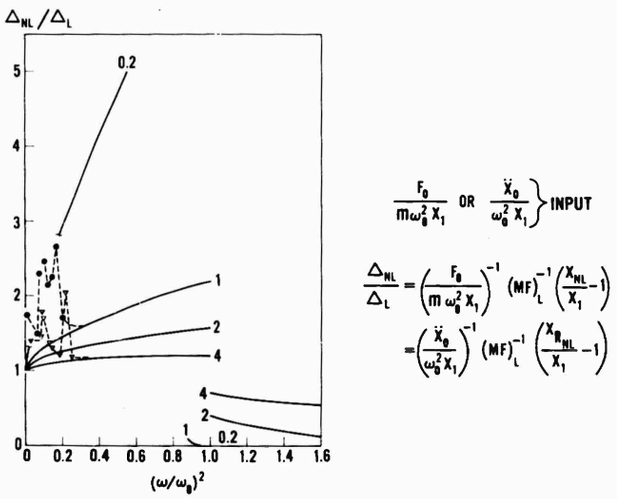

Fig. 8 - Spring displacement ratio (nonlinear/linear)

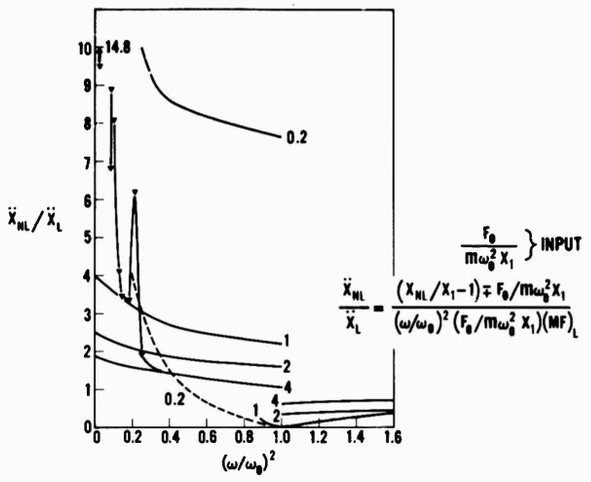

Fig. 9 - Mass acceleration ratio (nonlinear/linear)

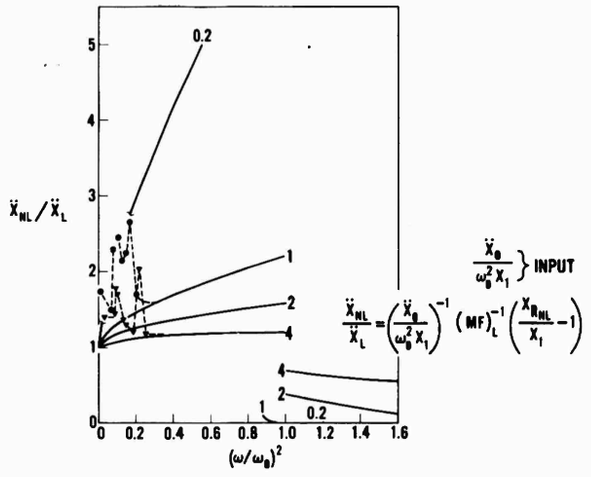

Fig. 10 - Mass acceleration ratio (nonlinear/linear) moving foundation

magnified for the forced mass case since, for the linear case, the mass acceleration is rapidly approaching zero in this low frequency ratio range. The mass acceleration ratio for the moving foundation case, Fig. 10, is exactly of the same form as for the spring displacement ratio (Fig. 8). The same general conclusions that were made for the spring displacement ratio curves (Fig. 8) can also be made for the mass acceleration ratio curves (Figs. 9 and 10).

CONCLUSIONS

Two general conclusions that can be made are (1) the overall effect of the clearance nonlinearity is to amplify the response for $(\omega/\omega_0)^2 < 1$ and attenuate the response for $(\omega/\omega_0)^2 > 1$, and (2) the superharmonic response characteristic of this simple system has a significant influence in magnifying the adverse effect of the clearance nonlinearity in the low frequency ratio range.

The comparison of nonlinear to linear response, as presented in Figs. 8-10, should be of value to a designer faced with a vibration problem involving clearance. It has been illustrated quantitatively, for the simple model investigated here, how the presence of "freeplay" can significantly modify the system response characteristics, and it is hoped that qualitative observations of these results can be applied to more complicated systems.

ACKNOWLEDGMENT

I would like to acknowledge Mr. Ray Hartenstein of Goddard Space Flight Center for his invaluable contribution to this investigation in programming the problem on the analog computer and in operating the computer.

* * *

DETERMINATION OF THE RATE DEPENDENCE OF THE YIELD STRESS FROM IMPULSE TESTING OF BEAMS*

S. R. Bodner
Brown University
Providence, R. I.

and

J. S. Humphreys
Avco, RAD Division
Wilmington, Mass.

A method for obtaining analytical expressions that approximately represent the strain rate dependence of the yield stress of structural materials is described. The procedure depends upon subjecting cantilever beam specimens to impulsive loading, and obtaining the strain rate law by fitting the predictions of a rate dependent rigid plastic theory to the test results. In the present paper this is carried out for a magnesium alloy, AZ-31B(0). The resulting strain rate law could be used in other studies on blast damage prediction.

INTRODUCTION

An important material property parameter in problems of determining the final deformations of structures due to blast loading is the strain rate dependence of the yield stress. The significance of this property in damage prediction has, however, not been adequately evaluated. Investigations on beams,[1-3] have shown that not only is the rate dependence of the yield stress an essential factor in determining the final deformation, but that, in general, it must be incorporated into the basic theory and cannot be applied as a final correction factor. The inclusion of rate dependence in the analysis of complex structures is a difficult task, and numerical procedures have been proposed.[4] There are some indications from tests on plates,[5] that the strain rate sensitivity may have relatively small influence on complex structures that have many mechanisms of energy absorption. The evaluation of this observation still depends on substantial theoretical and experimental work.

Analytical studies in this field depend upon knowledge of the strain rate dependence of the yield stress of the structural materials. This information appears to be readily available for only a limited number of materials (e.g., mild steel, pure aluminum, and pure copper,[6,7]

*This paper was not presented at the Symposium.

[1] S. R. Bodner and P. S. Symonds, "Experimental and Theoretical Investigation of the Plastic Deformations of Cantilever Beams Subjected to Impulsive Loading," J. Appl. Mech., 29:719-728 (1962).

[2] T. C. T. Ting and P. S. Symonds, "Impact of a Cantilever Beam with Strain Rate Sensitivity," Proc. Fourth U.S. National Congress of Applied Mechanics, ASME, 1153-1165.

[3] S. R. Bodner and W. G. Speirs, "Dynamic Plasticity Experiments on Aluminum Cantilever Beams at Elevated Temperatures," Journal of the Mechanics and Physics of Solids, 11:65-77 (1963).

[4] E. A. Witmer, H. A. Balmer, J. W. Leech, and T. H. H. Pian, "Large Dynamic Deformations of Beams, Rings, Plates, and Shells," AIAA Journal, 1:1848-1857 (1963).

[5] J. W. Lisanby, J. E. Rasmussen, and H. M. Schauer, "Comparison of Dynamic Yield Effects on Steels," Report No. 10-57, Underwater Explosions Research Div., Norfolk Naval Shipyard, Portsmouth, Va. (June 1957).

[6] A. Nadai and M. J. Manjoine, "High Speed Tension Tests at Elevated Temperatures, Parts II and III," J. Appl. Mech., 8:A77-A91 (1942).

[7] M. J. Manjoine, "Influence of Rate of Strain and Temperature on Yield Stresses of Mild Steel," J. Appl. Mech., 11:211-218 (1944).

aluminum alloy 2024-0[8]) although other results appear occasionally in technical reports. Obtaining new data for other materials from strain rate tension tests generally involves relatively sophisticated equipment and instrumentation. It appears, however, that this information can be obtained directly from the relatively simple blast testing of cantilever beam specimens. This technique would seem to be especially useful for composite or heterogeneous structural elements. Beam bending tests would also give an average of the strain rate sensitivity in both tension and compression. Since the structural deformations in blast damage problems are generally due to bending, beam tests are also likely to correspond more closely to the prototype conditions.

The previous investigations on cantilever beams[1-3] have shown that when the strain rate dependence of the yield stress is incorporated into a dynamic rigid plastic theory, the predictions are in good agreement with controlled experiments that satisfy the required mechanical conditions (e.g., large energy inputs). These theoretical predictions depend upon prior knowledge of the strain rate law. The good agreement that has been obtained suggests the use of such experiments for the inverse procedure, that is, the determination of the rate law from the test results.

The present paper is concerned with describing a test program and a computational procedure for determining the strain rate dependence of the yield stress of a magnesium alloy, AZ-31B(0). A previous study[3] has shown that the predicted final deformation is not sensitive to the exact analytical form of the law used to describe the rate dependence. To attempt the reverse procedure would therefore require that a relatively large number of tests be performed. In addition, the complexity of the governing equations requires that a trial and error procedure be used to obtain a strain rate law that leads to reasonable agreement with the experiments.

In the present case, a strain rate law is obtained from 11 tests on the basis that the overall average of the ratios of predicted to measured deformation angles is set equal to unity. The mean absolute deviation of the ratios from the overall average was 7 percent (the maximum deviation was 16 percent), which is only slightly greater than the estimated accuracy of the experimental results themselves (about 5 percent). In principle, the strain rate law obtained could be used in other analyses for the prediction of the plastic deformation of structures due to blast loading.

[8]D. S. Fields, Jr., and W. A. Backofen, "Temperature and Rate Dependence of Strain Hardening in the Aluminum Alloy 2024-0," Trans. Am. Soc. Metals, 51:946-960 (1959).

EXPERIMENTAL ARRANGEMENT

All of the cantilever beams used in this series of tests were machined from the same piece of 1/4-inch magnesium AZ-31B(0) sheet stock, and a static stress-strain curve was obtained from a piece of this sheet using a Tinius-Olsen testing machine. The yield stress was determined to be 21,600 psi using the conventional definition of this value as the stress level at which the strain is offset by 0.2 percent from the linear part of the curve. The stress strain curve exhibited a long flat plastic yield region before any appreciable strain hardening set in.

A heavy ballistic pendulum setup, shown in Fig. 1, was used to determine the impulse input to the beams. The pendulum swing for these tests was never more than 1 inch (zero to peak), so that with a 12-foot radius arm the linear pendulum equation can be expected to give a very close approximation to the motion of the recording pen on the flat table surface. The beams were mounted on this ballistic pendulum and covered with a layer of foam rubber and a layer of sheet explosive (Dupont EL-506D), as shown in Fig. 2. The sheet explosive was 15-mil thick (the minimum that can be reliably detonated) for each test. The foam rubber (1/4-inch thick) was provided both to prevent spalling and to even out the load from the explosive strip, which in many cases was narrower than the beam. The length L was varied from 2.5 inches to 4 inches. The final shape of the beam was almost straight over most of its length with a region of large curvature near the base, Fig. 2. The deformation parameter was taken to be the angular rotation of the straight portion of the beam, θ_f. Measurements were made of the final deformation angle θ_f and of the pendulum swing. The latter gives a measure of the initial pendulum velocity and hence the applied impulse by invoking conservation of momentum.

Two assumptions are inherent in the successful use of this technique, and both have been confirmed in previous similar beam tests by means of high-speed (Fastax) photography. The first is that the loading time is short compared to the beam motion so that the load can be treated as a pure impulse. The detonation speed of the sheet explosive is about 22,000 fps, and the entire loading takes place in well

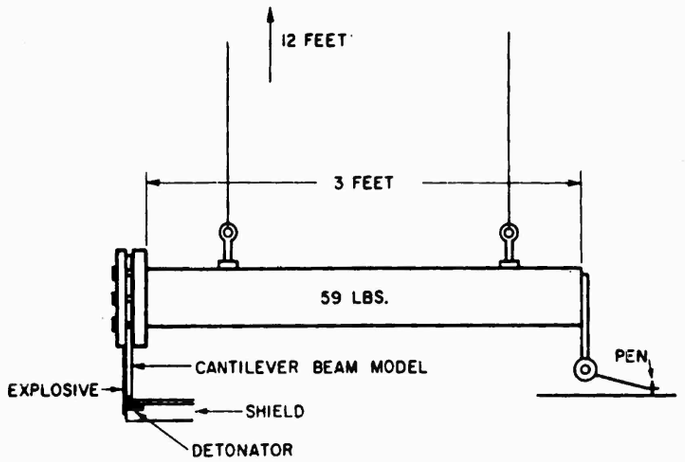

Fig. 1 - Ballistic pendulum arrangement

under 50 μsec, whereas the beam motion occupies several milliseconds. On the other hand, this beam motion time is very short compared to the pendulum swing time (1/4 period = 1.11 sec). The second assumption, namely, that all plastic beam deformation has ceased and all momentum has been transferred to the pendulum before the pendulum has reached its maximum displacement, is thus a reasonable one, and the initial pendulum impulse can be equated to the initial beam impulse. The experimental data are summarized in Table 1.

The column headed (θ_f) (Theoretical) in Table 1 refers to the theoretical solution for the final deformation angle based on a rate independent rigid plastic material idealization. This solution was obtained in Ref. 9 and is discussed in Ref. 1. For the present test conditions it is

[9] T. J. Mentel, "The Plastic Deformation due to Impact of a Cantilever Beam with an Attached Tip Mass," J. Appl. Mech., 25:515-524 (1958).

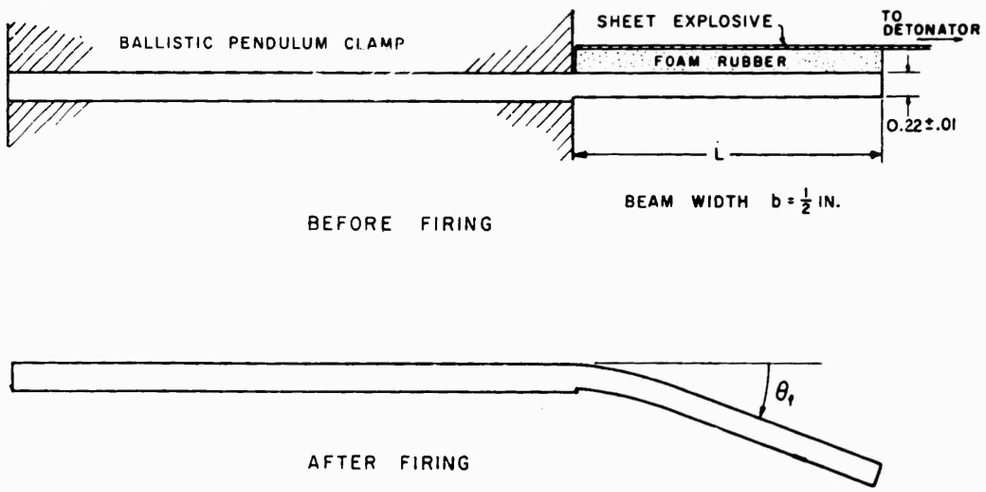

Fig. 2 - Beam geometry

TABLE 1
Test Results for Magnesium Beams

Test No.	Beam Length L (in.)	Width of Explosive Strip (in.)	Pendulum Motion (in.)	Total Impulse (lb sec)	Impulse per Unit Area (lb sec/in.^{2})	θ_f Measured (Experiment) (degrees)	θ_f Theoretical (Rate Independent) (degrees)	$\frac{(\theta_f)\ \text{Theor.}}{(\theta_f)\ \text{Exper.}}$	Energy Ratio R
1	3.25	1/2	0.665	0.1440	0.0887	38.0	55.5	1.46	13.1
2	3.25	1/4	0.35	0.0758	0.0466	12.0	15.3	1.28	3.6
3	3.25	3/8	0.51	0.1104	0.0680	20.0	32.6	1.63	7.7
4	2.50	1/4	0.27	0.0585	0.0468	7.5	11.9	1.59	3.7
5	2.50	1/2	0.48	0.1040	0.0832	23.2	37.5	1.62	11.6
6	2.50	1/4	0.29	0.0628	0.0502	7.5	13.6	1.81	4.2
7	2.50	1/4	0.27	0.0585	0.0468	8.0	11.9	1.49	3.7
8	2.50	3/8	0.38	0.0822	0.0658	16.5	23.4	1.42	7.2
9	2.50	3/8	0.40	0.0866	0.0693	16.3	26.0	1.60	7.8
10	4.00	1/4	0.46	0.0996	0.0498	13.5	21.5	1.59	4.0
11	3.25	1/4	0.385	0.0833	0.0513	11.4	18.5	1.62	4.3
								Avg. = 1.55	

Pendulum Weight: 59 lb

Pendulum Period: 4.43 sec

σ_o = 21,600 lb/sq in.

ρ = 0.064 lb/cu in.

$$\theta_f = \frac{3I_A^2 L}{2\sigma_o h^3 \rho}, \qquad (1)$$

where I_A is the applied impulse per unit area, L is the beam length, σ_o is the (static) yield stress, h is the beam thickness, and ρ is the mass density.

The column headed R in Table 1 is the ratio of the applied energy input to the maximum elastic energy storable in the beam.

$$R = \frac{(I_T^2/2m)}{(M_o^2 L/2EJ)} \qquad (2)$$

where I_T is the total impulse, m is the total beam mass, M_o is the (static) plastic limit moment, E is the elastic modulus, and J is the moment of inertia of the cross section. The final deformation could be expected to be independent of elastic effects if this ratio were sufficiently large. This would tend to justify the assumption in the analysis of rigid behavior prior to yielding. The previous work on cantilever beams[1] has shown that this assumption is a reasonable one for cantilever beams if R is greater than about 4.

NUMERICAL PROCEDURE

The analysis of a strain rate dependent rigid plastic cantilever beam subjected to a sudden velocity change was presented by Ting and Symonds.[2] The case of a beam subjected to a uniform impulse along its length, which was the present experimental condition, is obviously the same since the impulse imparts a uniform velocity instantaneously to the beam. The expression describing the strain rate dependence of the yield stress used in the analysis was

$$\dot{\varepsilon} = D\left(\frac{\sigma_y}{\sigma_o} - 1\right)^p, \qquad (3)$$

where $\dot{\varepsilon}$ is the strain rate, σ_y is the dynamic yield stress, σ_o is the static yield stress, and D and p are constants that depend on the material. This expression, (3), is relatively simple to incorporate into a dynamic rigid plastic analysis. It also seems to have sufficient generality to be able to fit most available experimental data by proper choices of D and p.[1]

The analysis of Ref. 2 does not lead to a simple solution for the deformation angle θ_f, and a numerical solution of the governing equations is necessary. This has been programmed for the Brown University, IBM 7070 computer which was used for the numerical computations.

The previous investigations on beams had been concerned with comparing theoretical predictions, obtained by using values of D and p fitted to available experimental strain rate data, with the results of controlled tests. In the present investigation, the rate dependent analysis and the beam test results are used to determine the material constants D and p. The complexity of the equations, however, does not permit a direct solution of those constants when the test conditions, geometry, and final deformation angles are given. Instead, values for the material constants must be assumed and the analytical results are compared to those of the experiments. The desired values of D and p are those for which the theoretical results would best fit all of the experimental data.

The specific procedure was to assume a value for p and to calculate the theoretical deformation angles of the specimens for different values of D. Guided by the previous work, values of p from 3 to 10 were considered. The ratio of the theoretical to experimental deformation angles was obtained for each specimen for the different D's. For each value of D the average of these ratios for all the specimens was computed, and after a few trials it was possible to find the value of D that would make this average equal to unity. This was facilitated by plotting the D's against the average of the angle ratios and noticing that a straight line was obtained on a semi-log plot in the vicinity of the average equal to unity. This process was repeated for the different values of p.

The combination of p and D that was considered to best fit the test results was that which led to the minimum mean absolute deviation of the ratios from the overall average (unity). A more proper criterion would be the pair of values for which the root mean square deviation from the overall average would be minimum. However, the deviations themselves were generally small and the slight difference that might result did not appear to justify the additional computation.

The results of the computations are shown in Table 2. The combination p = 6, D = 6200 sec^{-1} resulted in the minimum value for the mean absolute deviation, so was taken to be the best representation for the strain rate law. The last line in Table 2 indicates the result obtained when a simple numerical factor is applied to the static yield stress in the rate

independent analysis in order to make the average of the angle ratios for all the specimens equal to unity.

TABLE 2
Computation of Constants in Strain Rate Law for Agreement in the Average of Theoretical and Experimental Results

$$\left[\dot{\epsilon} = D\left(\frac{\sigma_y}{\sigma_o} - 1\right)^p\right]$$

p	D (sec^{-1})	Mean Absolute Deviation from Average (%)	Maximum Deviation from Average (%)
3	860	7.95	16.3
4	1,700	7.43	16.4
6[a]	6,200	6.95	16.7
8	20,000	6.96	16.7
10	65,000	7.00	17.2
Correction Factor of 1.55 on Results of Rate Independent Theory		10.40	25.9

[a]Considered to be best fit.

The theoretical deformation angles for the strain rate law

$$\dot{\epsilon} = 6200\left(\frac{\sigma_y}{\sigma_o} - 1\right)^6 \ (sec^{-1}) \qquad (4)$$

are given in Table 3. This equation is plotted in Fig. 3 along with the expressions that have been previously used in Ref. 1 for mild steel and aluminum alloy. Although the strain rates vary spacewise over the specimen and vary during the deformation history, a rough average of the strain rate at which most of the plastic deformation occurred in these tests would be about 170 sec^{-1}. Equation (4) is considered to be a reasonable representation for the material behavior in the strain rate range 1 sec^{-1} to 500 sec^{-1}.

DISCUSSION

The result obtained is considered to be a reasonable representation for the strain rate dependence of the yield stress of the material in the range indicated. A larger number of tests would probably have lowered the mean deviation to the accuracy of the experimental measurements which was considered to be about 5 percent.

The relatively low mean deviation of 10.4 percent that could be obtained by a simple

TABLE 3
Results of Strain Rate Dependent Analysis

$$\left[\dot{\epsilon} = 6200\left(\frac{\sigma_y}{\sigma_o} - 1\right)^6 (sec^{-1})\right]$$

Test No.	θ_f Theoretical (Rate Dependent) (degrees)	$\frac{(\theta_f)\ \text{Theor.}}{(\theta_f)\ \text{Exper.}}$	Deviation from Average (%)
1	35.22	0.927	-7.3
2	10.15	0.846	-15.4
3	21.06	1.053	+5.3
4	7.63	1.017	+1.7
5	23.27	1.003	+0.3
6	8.76	1.167	+16.7
7	7.63	0.954	-4.6
8	14.76	0.895	-10.5
9	16.33	1.002	+0.2
10	14.51	1.075	+7.5
11	12.19	1.070	+7.0
		Avg. = 1.0007	Mean Absolute Deviation = 6.95

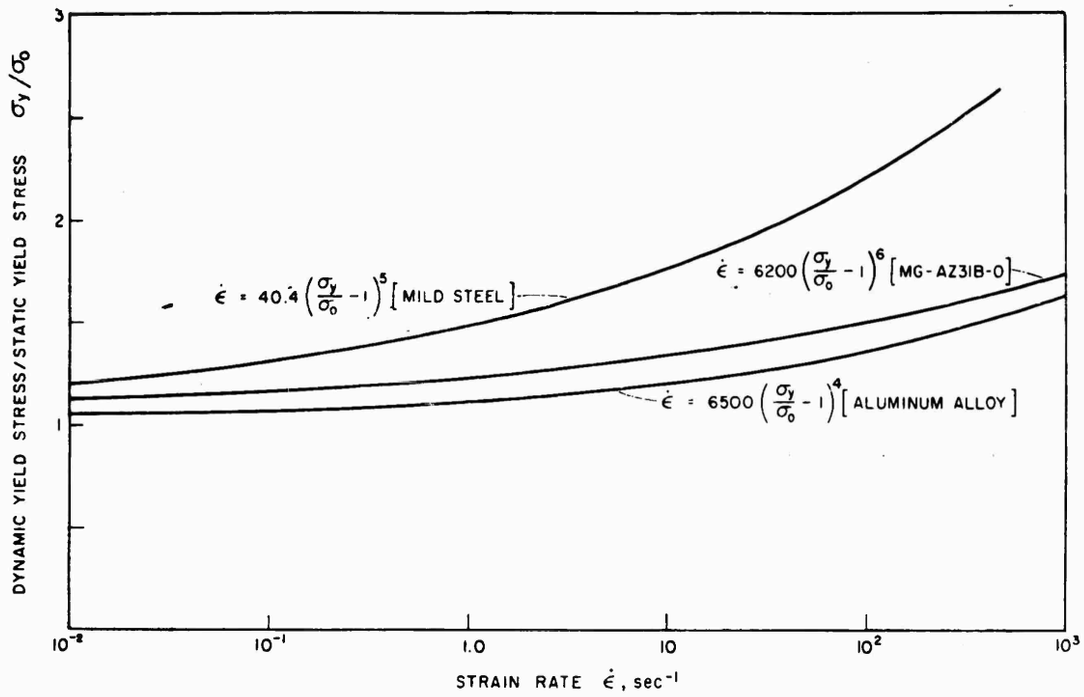

Fig. 3 - Effect of rate of straining on yield stress

correction factor on the rate independent theoretical results is somewhat misleading and is due to a weakness in the test program. This appears to be due to the specimens not exhibiting a very wide range of strain rates in the tests. Although the strain rates in the impulsively loaded cantilever beam vary both spacewise and timewise, most of the significant plastic strains occur at an almost uniform rate near the base of the beam. Added to this is the fact that the material under investigation was relatively insensitive to strain rate (e.g., compared to mild steel). A wider range of specimen geometries and applied impulses would have tended to overcome this weakness in the test program.

An alternative arrangement, a cantilever beam with a tip mass subjected to a tip impulse, experiences a somewhat greater strain rate variation than a uniformly impacted beam and may have been better for the present purposes. The rate dependent analysis for this loading condition also leads to a relatively simple solution for the final deformation angle which does not require the use of a computer.[1,3] The experimental setup, however, is slightly more complicated. In any event, the same general procedure outlined in this paper would serve for the determination of the strain rate law.

* * *

REDUCTION OF VIBRATION FROM ROTOR UNBALANCE BY USE OF A FORCE-CANCELING SYSTEM (AN ACTIVE VIBRATION ABSORBER)*

C. S. Duckwald and T. P. Goodman
Advanced Technology Laboratories
General Electric Company
Schenectady 5, New York

The force due to unbalance in rotors is an important source of water borne noise in marine propulsion equipment. In an effort to minimize the transmission of this noise to the hull of the ship, the General Electric Company, under contract with the U.S. Dept. of the Navy, Bureau of Ships (Contracts NObs78932 and NObs86829) has undertaken the development of a force-canceling system, in which weights rotating in synchronism with the rotor generate unbalanced forces equal and opposite to those of the main rotor.

Provision for this force canceling system is desirable even though marine propulsion and auxiliary power sets are carefully balanced prior to shipboard installation, since in balancing this equipment a compromise is necessary to minimize the vibration levels over the entire operating range of the equipment. In addition, the unbalanced forces observed on shipboard may be greater than those measured prior to installation. The increased forces can be caused by shipboard mounting and loading conditions not simulated in a land test or by changes in balance with time due to wear, accumulation of dirt, and similar causes. The force-canceling system provides a means for continuously canceling the unbalanced forces transmitted to the hull. In addition, this system will provide a means for accumulating information that can be used to make a permanent balance correction when the power equipment is shut down.

Each system of force-canceling weights was mounted as close to the bearing as possible. A representative system is shown schematically in Fig. 1 where four rotating weights are mounted directly on a bearing pedestal and are arranged symmetrically with respect to the shaft of the main rotor. In the system used in the General Electric Company tests, the force-canceling weights were driven by 400-cycle synchro receivers from a synchro transmitter driven at the main rotor speed and in synchronism with it. The phase angles of the eccentric masses in the force-canceling units, relative to an arbitrary reference vector in the main rotor, were controlled by synchro differential transformers to give both amplitude and phase control of the net inertia force of the four rotating masses.

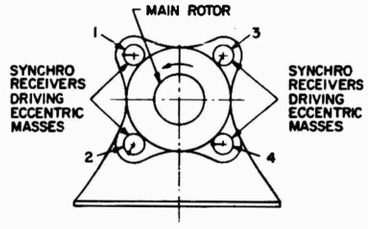

Fig. 1 - Schematic of force-canceling bearing pedestal

The well-known principle of using two equal rotating masses to get both magnitude and phase correction is shown schematically in Fig. 2. Shifting the force vectors represented by the two masses closer together or further apart increases or decreases, respectively, the net magnitude of the inertia force. Shifting these force vectors in unison yields a net phase shift with respect to the main rotor. The four masses are arranged symmetrically as shown in Fig. 1 with eccentric masses 2 and 3 in the same

*This paper was not presented at the Symposium.

phase; this eliminates any net couple about the bearing axis of the main rotor.

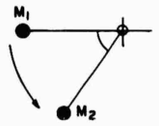

Fig. 2 - Use of two fixed masses for magnitude and phase correction

Each of the force-canceling weights represent an unbalance of 2.5 inch-ounces. The body of each force-canceling weight is essentially a steel disc (see Fig. 3) in which axial holes were drilled to give the net unbalance. These holes were then covered by two thin aluminum cover plates so that each force-canceling weight was externally smooth on all faces thereby minimizing the effect of windage losses.

The electrical arrangement of the synchros for each bearing pedestal is shown schematically in Fig. 4. A synchro transmitter rotating at main rotor shaft speed drives the four synchro receivers through two synchro differential transformers. The differential transformers are mounted in a control console, Fig. 4, with two knobs; one for the amplitude control, and one for the phase control of the net rotating force-canceling vector. The amplitude control knob, in the control console, is connected to gears that turn the stators of the two differential transformers in opposite directions, while the force control knob is connected to gears that turn the rotors of the differential transformers in unison. This mechanizes the scheme shown in Fig. 2 for the two fixed masses to obtain magnitude and phase correction.

The results of numerous laboratory tests using force-canceling systems indicate that, when properly installed, these units result in phenomenal reduction in vibration amplitudes due to rotor unbalance. Also, if there is twice per rev. component of force generated by the rotor, an additional system of force-canceling weights operating at twice per rev. could effectively cancel this force.

The test results discussed in the balance of this paper were obtained by mounting two force-canceling systems on a three-bearing turbine-generator auxiliary set. These tests were run in the test area of the Small Steam Turbine Department, General Electric Company, Fitchburg, Massachusetts. Figure 5 shows an overall view of the test area. This photograph shows the generator end of the turbine-generator set and the vibration instrumentation used. One set of force-canceling weights was mounted on

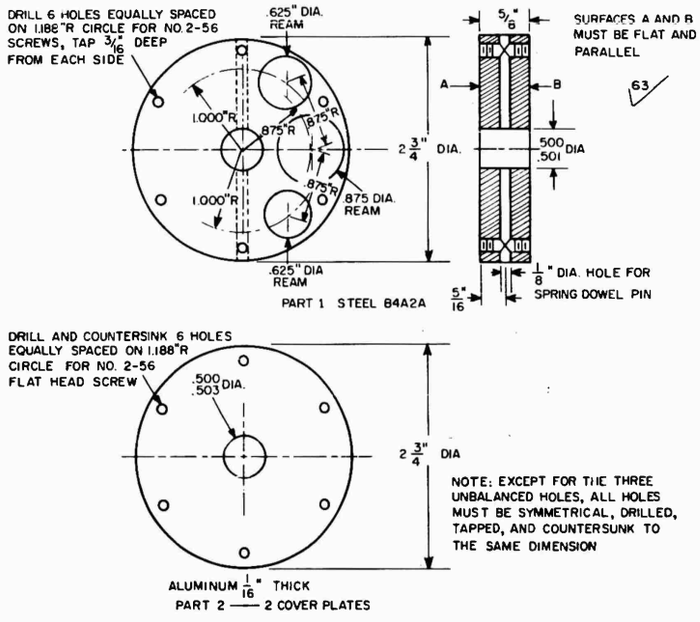

Fig. 3 - Counterweight for unbalance test machine

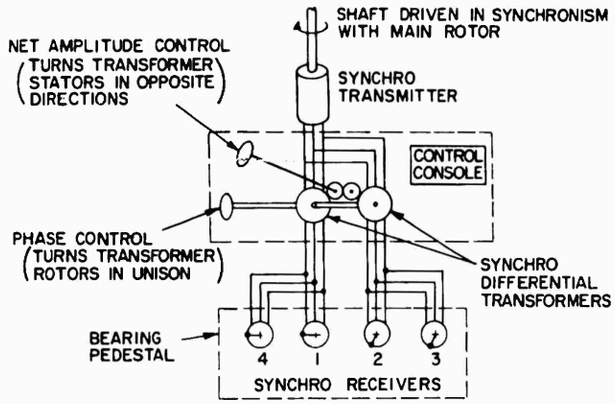

Fig. 4 - Schematic of electrical connections

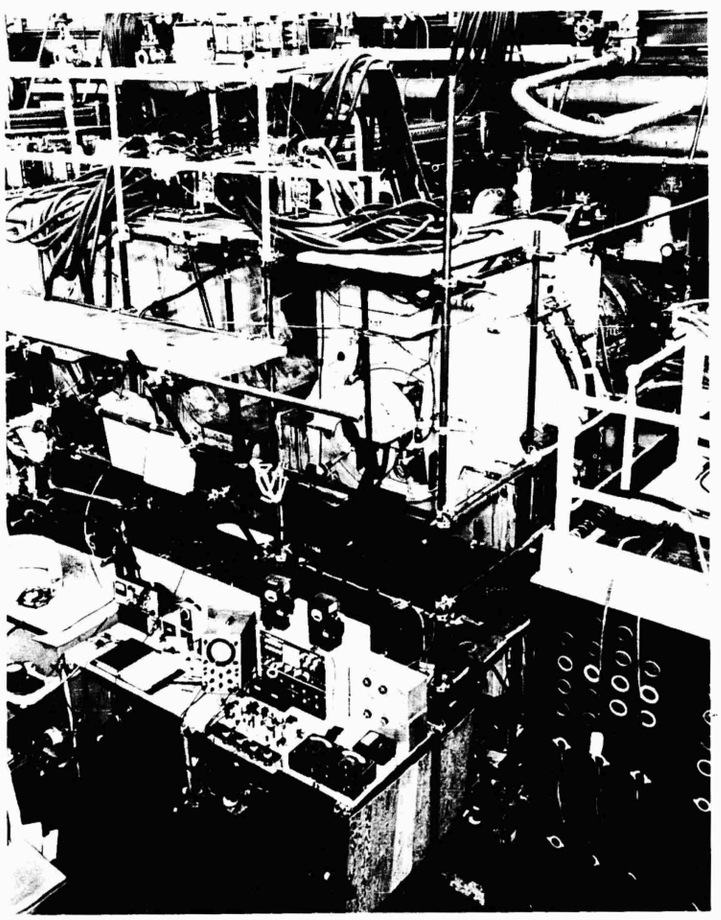

Fig. 5 - Overall view turbine-generator set on test stand

the generator end bearing as shown in Fig. 6 and the other set on the middle bearing pedestal between the turbine and generator as shown in Fig. 7.

The driving power for the force-canceling weight system is obtained from a Universal motor driving two selsyn transmitters shown in Fig. 8. On the same shaft with the Universal motor is a small synchronous motor driven from the generator of the turbine-generator set. This synchronous motor was used to establish and maintain the phase relation between the synchro-transmitters and the main turbine-generator rotor.

With the force-canceling weights rotating in synchronism with the generator rotor, the relative phase angles between the individual weights was adjusted by rotating the controls on the control console shown to the right in Fig. A-4 of the appendix. This adjustment was made by the operator until a vibration signal was minimized. Vibration signals were obtained from accelerometers located on the sub-base. In most cases the vertical vibration motion of the port side of the base above the vibration isolation motion of the port side of the base above the vibration isolation mounts was minimized. The instrumentation used to make these adjustments is discussed in the appendix. The numbering system used and the location of all pick-ups is shown in the sketch of Fig. 9.

Results obtained using the force-canceling system are shown in bar graph form in Fig. 10. In all cases the force-canceling weights were adjusted to give a minimum of vibration at points 7 and 10 (vertical motion of the base directly above the vibration isolation mounts on the port side). This figure shows the results obtained from three conditions of unbalance. From this graph it is apparent that the effectiveness of the force-canceling system depends

Fig. 6 - Close-up view of generator bearing counterweights

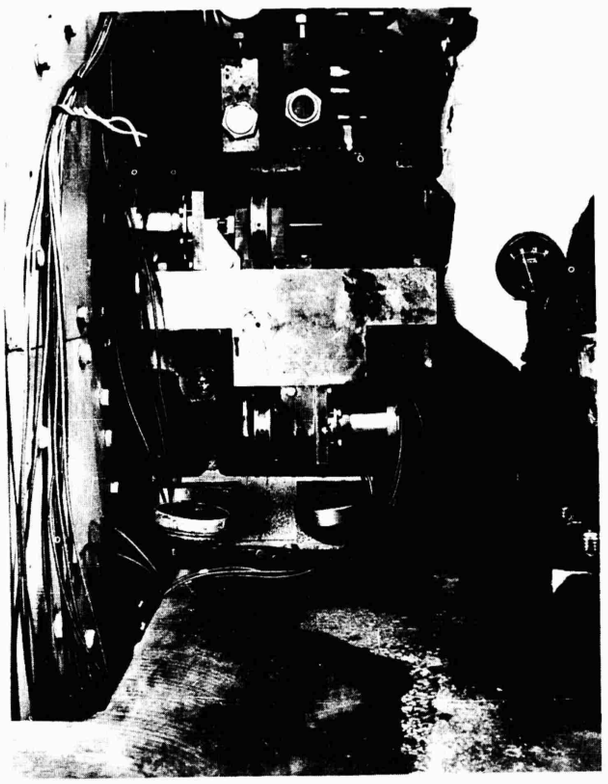

Fig. 7 - Close-up view of center bearing counterweights

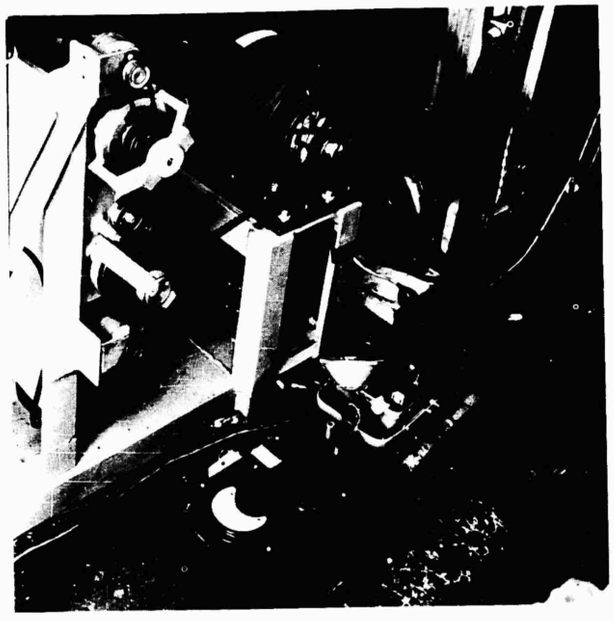

Fig. 8 - Drive system for selsyn transmitters

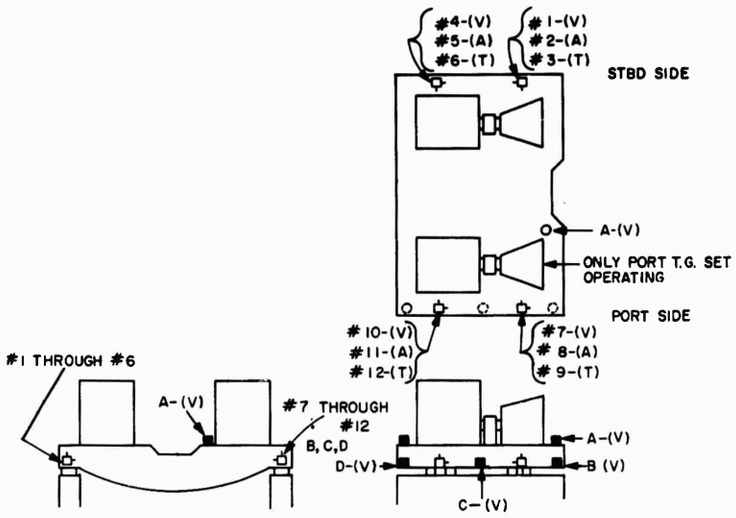

Fig. 9 - Passive and active vibration absorber evaluation tests; location and identification of vibration pickups

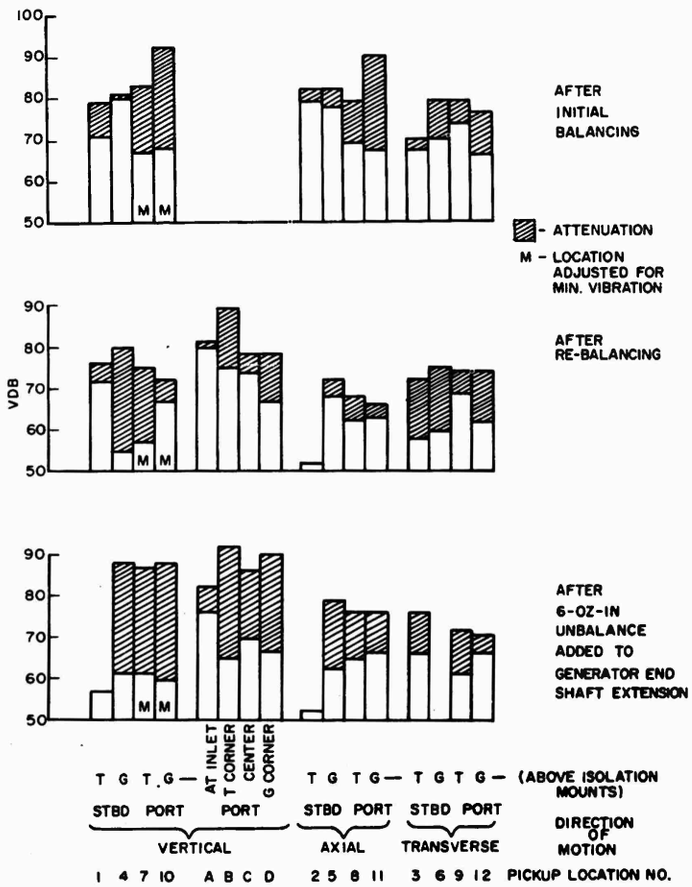

Fig. 10 - Force canceling system tests, once per revolution, four force canceling weights at each bearing (total of 8 weights)

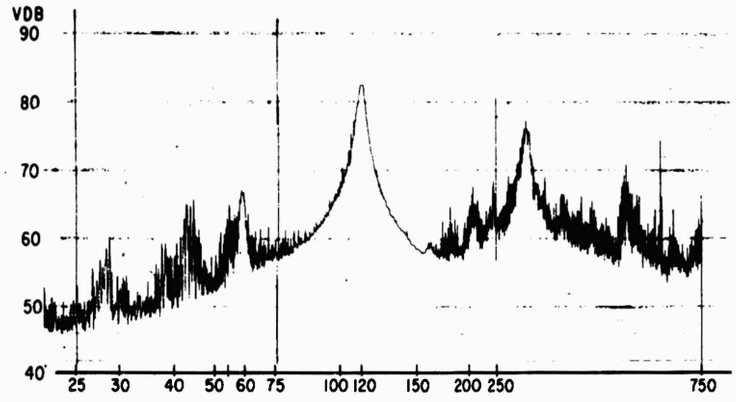

(a) Frequency spectrum of vibration motion at point 7

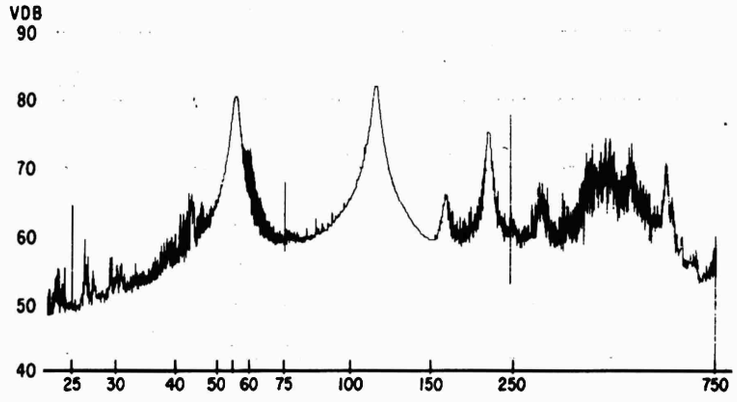

(b) Frequency spectrum of vibration motion at point 10

Fig. 11 - Force canceling system tests once per revolution force canceling weights at each bearing

upon the unbalanced weight distribution within the turbine-generator set. Under ideal conditions a vibration amplitude reduction of at least 25 vdb was realized at points 7 and 10. The bar graph also shows that the vibration amplitudes were reduced at almost every other point on the base where readings were taken.

For the same operating conditions used to obtain the data for the third bar graph series in Fig. 10, frequency spectrums were taken of the vibration motions at points 7 and 10. These spectrums are shown in Figs. 11a and 11b. These two spectrums show almost no response at 55 rps which was the running speed of the set during all force-canceling tests. The 60-cycle peak in both curves is primarily due to electrical pick-up in the instrumentation. It was because of this 60-cps electrical interference that the tests were tun at 55 rps allowing the two effects to be separated.

The bar graphs in Fig. 12 show the results obtained when two force-canceling weights are used at each bearing in place of four. With the two weights there was insufficient force available to completely balance the motion at both points 7 and 10. These graphs, however, still show that a sizable reduction in vibration amplitudes throughout the set can be obtained using just a 2-weight system.

A summary of the results obtained in this series of tests is as follows:

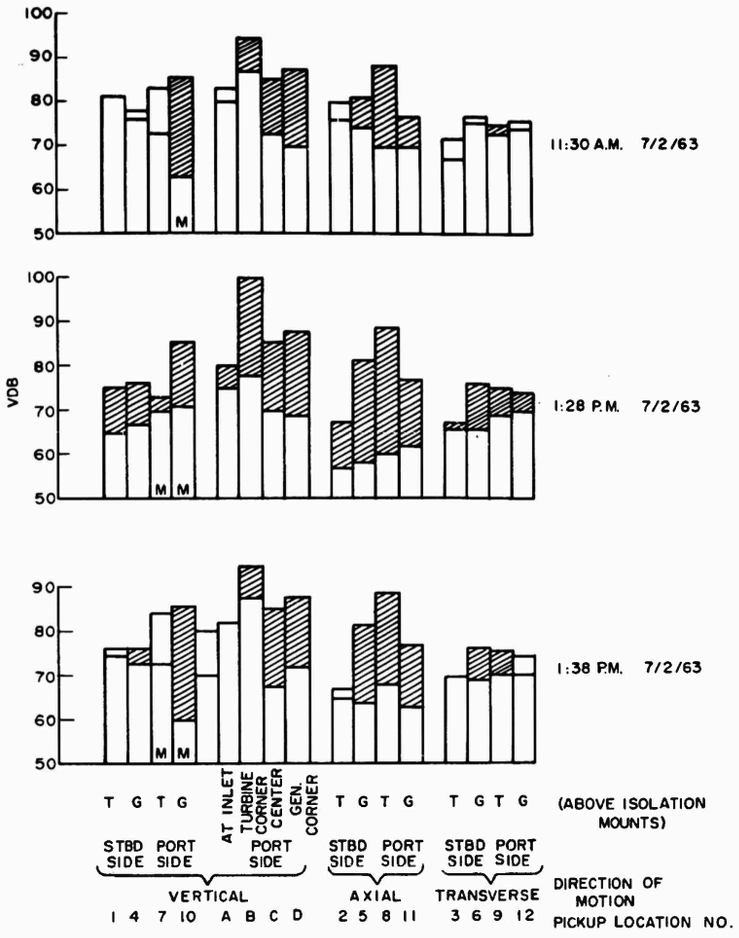

Fig. 12 - Force canceling system tests once per revolution, two force canceling weights at each bearing (total of 4 weights)

1. It is possible to obtain very sizable, over 25 vdb, reductions in vibration amplitudes using force-canceling weights.

2. This test showed the effectiveness of force-canceling systems mounted on two of the three bearings on the turbine-generator set. Under these conditions it became apparent that the effectiveness of the force-canceling system depended upon the unbalance conditions within the set. Much better results could have been obtained if all three bearings of this set had been equipped with force-canceling systems.

3. The tests seemed to indicate that the force-canceling systems, to be most effective, should be located as close as possible to the source of the vibration force to be cancelled.

APPENDIX

Instrumentation

VIBRATION AMPLITUDE READINGS

Vibration pickups were mounted in three directions at four points on the base and one pickup was used as a roving pickup to measure the vertical motions at four other points on the base. Pickup locations and numbers are shown by the sketch in Fig. 9.

The electronic instrumentation used in conjunction with the vibration pickups is indicated by the block diagram in Fig. A-1 and is shown in the photograph, Fig. A-2. In general, the signal from the pickups is amplified, integrated, filtered for either 1/rev. or 2/rev. indications and read out on a level recorder directly in velocity decibels (vdb) ref. (rms) 1×10^{-6} cm/sec.

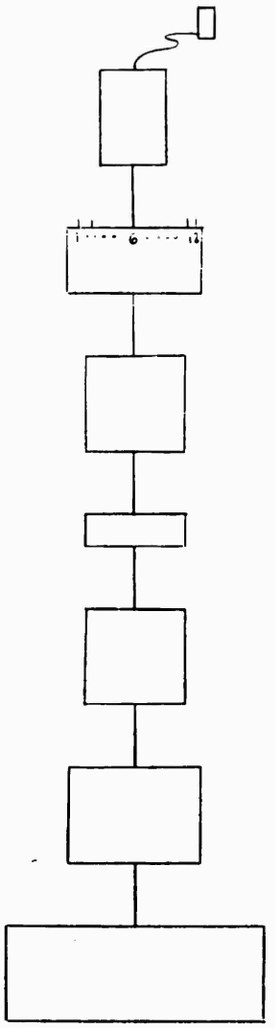

Vibration Pickup
MASSA M-198A

Pre-Amplifier MASSA M-114B
Power Supply MASSA M-116D

Switch (Special)

Voltage Amplifier
Ballantine Mod 220B

Integrator (Special)

Voltage Amplifier
H.H. Scott Type 140B

Vibration Analyzer
General Radio Type 762-B

Level Recorder
Bruel-Kjaer Type 2305

Fig. A-1 - Vibration instrumentation block diagram

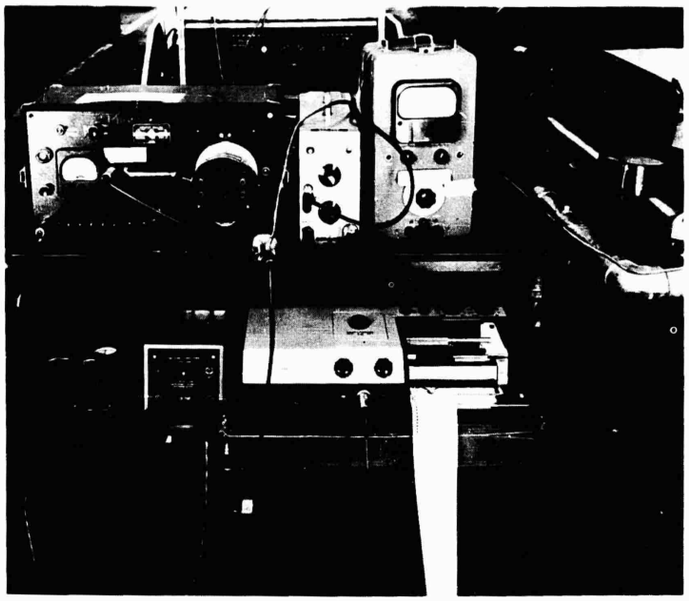

Fig. A-2 - Instrumentation for vibration analysis and survey

FORCE CANCELING SYSTEM INSTRUMENTATION

This instrumentation is used in conjunction with the adjustment of the amplitude and phase controls in the force canceling system. The instrumentation provides a vector display of the vibration velocity of the base in which both the amplitude phase variations are shown continuously. With this display the operator has a two-dimensional picture of the effects of his adjustments of the control console knobs. By watching the motion of the spot, the operator, with a minimum of changes in control positions, can bring the vibration amplitude to almost zero.

The block diagram in Fig. A-3 indicates the system used to yield the vector display. The photograph, Fig. A-4 shows this equipment and also the control console for the force canceling system.

The two channel multiplier-computer acts as a very effective "self-tuning" filter which automatically takes into account all changes in rotor speed. This self-tuning or tracking filter takes advantage of the filtering action of a wattmeter type of multiplying circuit. In general, the system used operates as follows: the reference signal is the sine wave output from a special two-phase tachometer that is driven in synchronism with the generator rotor. The signal from the vibration pickup is multiplied by the two signals from the two-phase sine wave generator giving two dc voltages whose amplitudes are proportional to that component of the vibration amplitude that is in phase with each of the two phases of the sine wave generator. The multiplier outputs are passed through low pass filters to remove the ac voltages, and the resulting dc voltages are used as the x and y inputs, respectively, of a cathode ray oscilloscope giving a spot on the scope face. By noting the coordinates of the position of this spot, both the amplitude and phase of the rotor once/rev. (or twice/rev.) unbalanced component can be observed.

For these tests, the amplifier, multipliers, and low pass filters were assembled from analog computer components. For later work, this equipment could be packaged in a compact unit. There is also similar instrumentation, using wattmeters for multiplication and low pass filtering, which is commercially available; however, the electronic equipment has the advantage that the time constant of the low pass filters can be varied at will by the operator to achieve an optimum compromise between effectiveness of filtering and the speed of response.

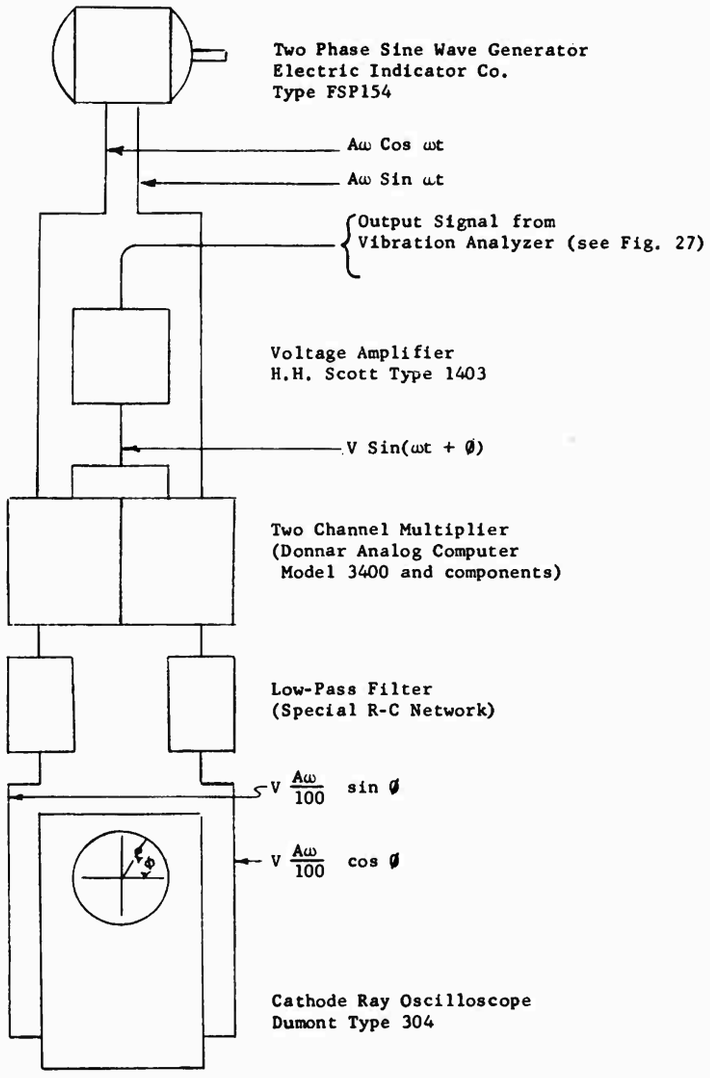

Fig. A-3 - Force canceling system instrumentation

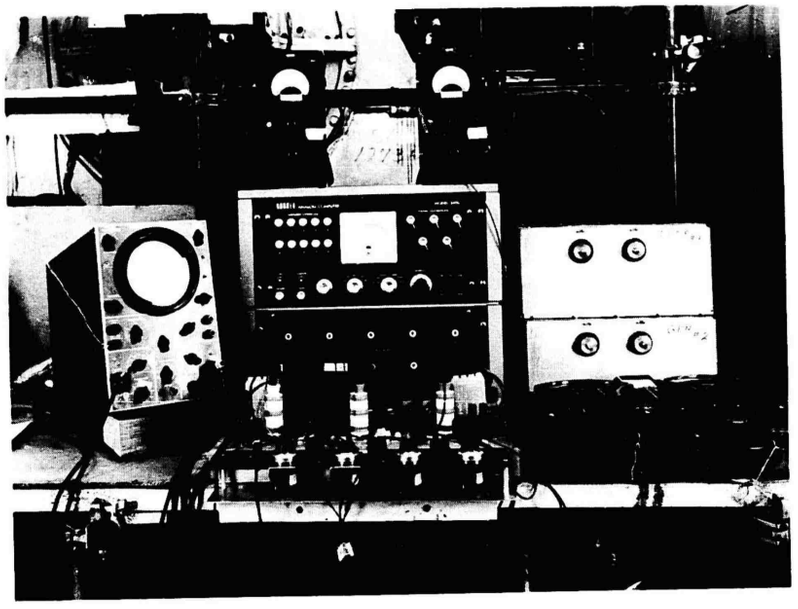

Fig. A-4 - Force canceling instrumentation for adjusting amplitude and phase controls

* * *

DYNAMIC MATHEMATICAL MODEL FOR EVALUATING AIRBORNE EXTERIOR LAMPS*

David Ehrenpreis
Consulting Engineers, Inc.
New York, N.Y.

and

John DeJong
Naval Air Station
Patuxent River, Maryland

SUMMARY

This paper presents the new mathematical model simulating the dynamic properties and characteristics of typical airborne exterior lamps. This model includes as parameters single coil filament, double coil filament, filament supports, preload, partial fixity, distribution of masses, distribution of inertias, Young's modulus of tungsten at elevated temperature and forcing function. The environment includes random vibrations, population of random shocks, periodic vibrations, and single pulse complex form transients. The paper determines natural frequencies, mode shapes, bending moments, shears, torsional shears, reactions, stresses, margins of safety, buckling, allowable strengths, deflections, and rotations. The model is designed for use by manufacturers and users of electrical equipment for optimum strength, stiffness, and reliability in the dynamic environment.

The equations determining the distribution of masses and inertias of two different types of airborne exterior lamps are presented. Algebraic equations are included to determine natural frequencies of a spectrum of airborne lamps and other electrical equipments. The methods used to determine the dynamic properties and characteristics of these lamps may also be used to determine natural frequencies and responses of other lamps and electrical equipments.

A generalized system of equations using the Myklestad notation is presented. This method requires the use of a high-speed digital computer to perform the repetitive, cumbersome, numerical calculations. Mathematical regimes are established to determine mode shapes, natural frequencies, responses, and margins of safety.

The paper should aid the designer of airborne exterior lamps and other electrical equipments in the preliminary and final sizing of all structural and mechanical members. The designer can select through more rigorous calculations materials and cross-section properties to resist the dynamic environmental loads without permanent deformation or failure.

INTRODUCTION TO THE PROBLEM

Today, in the United States, it is requisite to analyze and design airborne exterior lamps to withstand an increasingly severe dynamic environment. This environment consists of periodic vibrations, complex-form hash-type vibrations, and the population of random shocks and transient pulses. It is the intent of this paper to present a rigorous, but nevertheless feasible and relatively simple mathematical model to simulate the distribution of stiffnesses and masses of aircraft lamps.

LIST OF SYMBOLS

a = Preload deflection of filament spring (in.)

d = Diameter of wire or coil (in.)

d_w = Diameter of wire (in.)

*This paper was not presented at the Symposium.

D_c = Filament coil diameter (in.)

E = Modulus of elasticity (psi)

F = Internal rotation

f_{n_I} = First mode natural frequency (cps)

f'_{n_I} = First mode natural frequency taking into account preload on filament (cps)

G = Shear modulus of rigidity (psi)

H = Internal deflection (in.)

i = Designated point number on filament

I = Area moment of inertia of filament portion ($in.^4$)

I_w = Filament wire area moment of inertia of filament portion ($in.^4$)

K = Coefficient

K = Internal shear (lb)

K = Spring constant filament wire (lb/in.)

K' = Internal resisting bending moment (in.-lb)

ℓ = Length of portion of filament (in.)

L = Length of portion of filament (in.)

M = Externally applied bending moment (in.-lb)

n = Number of coils of filament wire

n = Number of coils of filament wire per given dimension (in.)

P_{cr} = Critical stability load of filament wire (lb)

Q = Externally applied shear (lb)

Q = Transmissibility at resonance

S = Thrust in filament wire due to preload (lb)

w = Uniformly distributed 1-g weight (lb/in.)

W_i = Weight of element i (lb)

x = Distance from origin along length of structural beam of filament wire (in.)

y = Externally applied deflection (in.)

y = Deflection (in.)

α = Externally applied rotation

β_o = Flexural stiffness coiled portion of filament (lb-$in.^2$)

γ_o = Shear stiffness (lb)

δ = Deflection (in.)

ξ = Flexural stiffness double coiled portion of filament (lb-$in.^2$)

ρ = Density of wire or prong material (lb/cu. in.)

ω_n = Natural frequency (rad./sec)

MYKLESTAD'S METHOD GENERALIZED FOR LAMPS

A high-speed digital computer is often available to perform the cumbersome numerical calculations requisite to rigorously determine orders of magnitude of natural frequencies and mode shapes.

A variation of the well-known Myklestad method (1)[1] is recommended. The differential equations are implied in the recursion equations. The recursion equations relate the internal deflection, internal slope, internal shear, and internal bending moment from sub-station to sub-station along every sub-system of the dynamic mathematical regime.

By definition, a regime is all of the recursion equations, boundary equations, geometric constants, matrices, and solutions, which define the dynamic properties and characteristics of the airborne lamps in one of the three mutually perpendicular axes.

A sub-system is a continuous structural member of the airborne exterior lamps.

A sub-station is one of the internal or external points of the sub-system under investigation.

Internal bending moment is the moment at any internal sub-station of the sub-system as

[1] N. Myklestad, Fundamentals of Vibration Analysis (McGraw-Hill Book Co., Inc., New York, N.Y., 1956).

determined by the appropriate recursion equation, if the beam is cut at the sub-station and a free body diagram is taken.

Internal shear is similarly the shear at any internal sub-station of the sub-system determined by the recursion equation.

Internal slope is the rotation of the beam at any internal sub-station of the sub-system, determined by the appropriate recursion equation.

Internal deflection is the deflection at any internal sub-station of the sub-system.

External moment is the bending moment at the end boundary point sub-stations of the sub-system.

External shear is the shear at either of the two end boundary point sub-stations of the sub-system.

External slope is the beam rotation at either of the two end boundary point sub-stations of the sub-system.

External deflection is the deflection at either of the two end boundary point sub-stations of the sub-system.

Influence coefficient is the effect of one sub-station caused by unit dummy virtual load upon any sub-station.

The recursion equations, Eqs. (1)-(4) are derived in Ref. 1 (additional background is obtained from Refs. 2 and 3):

$$F_n = F_{n-1} - v_{F_{n-1}} K_{n-1} - v_{M_{n-1}} K'_{n-1}, \quad (1)$$

$$H_n = H_{n-1} - L_{n-1} F_n - d_{F_{n-1}} K_{n-1} - d_{M_{n-1}} K'_{n-1}, \quad (2)$$

$$K_n = \sum_{i=1}^{n} m_i \omega_n^2 H_i, \quad (3)$$

and

$$K'_n = \sum_{i=1}^{n-1} L_i K_i, \quad (4)$$

where

F_n = The internal slope at sub-station n,

F_{n-1} = Internal slope at sub-station n - 1,

$v_{F_{n-1}}$ = Slope influence coefficient at sub-station n - 1 due to unit shear (rad./lb),

K_{n-1} = Internal shear at sub-station n - 1 (lb),

$v_{M_{n-1}}$ = Slope influence coefficient at sub-station n - 1 due to unit moment (rad./in.-lb),

K'_{n-1} = Internal bending moment at sub-station n - 1 (in./lb),

H_n = Internal deflection at sub-station (in.),

H_{n-1} = Internal deflection at sub-station (in.),

L_{n-1} = Distance from sub-station n - 1 to sub-station n (in.),

$d_{F_{n-1}}$ = Deflection influence coefficient at sub-station n - 1 due to unit shear (in./lb),

$d_{M_{n-1}}$ = Deflection influence coefficient at sub-station n - 1 due to unit bending moment (in./lb),

K_n = Internal shear at sub-station n (lb),

m_i = Mass at sub-station i,

ω_{n_a} = Natural frequency of the lamp filament, mode "a" (rad./sec),

H_i = Internal deflection of mass i (in.),

K'_n = Internal bending moment at sub-station n (in./lb),

L_i = Length of sub-station i (in.), and

K_i = Internal shear at sub-station i (lb).

It is recommended that a table be set up to define the proposed new design filament geometry. The filament should be subdivided into approximately three appropriate sub-systems. Each sub-system is subdivided into 10 sub-stations. Each sub-system has its own geometry table. The table presents the mass, moment

[2] J. Rayleigh, The Theory of Sound (Dover Publications, Inc., New York, N.Y., 1894).

[3] A. E. H. Love, A Treatise on the Mathematical Theory of Elasticity (Dover Publications, Inc., New York, N.Y., 1927).

of inertia, and the geometric influence coefficients of each sub-station. Equations (5) through (8) define the geometric coefficients:

$$v_M = \frac{L^2}{EI} , \tag{5}$$

$$d_M = \frac{L^2}{2EI} , \tag{6}$$

$$v_F = \frac{L^2}{2EI} , \tag{7}$$

and

$$d_F = \frac{L^3}{3EI} , \tag{8}$$

where

v_M = Slope at sub-station n due to unit externally applied bending moment at sub-station n-1,

v_F = Slope at sub-station n due to unit externally applied shear at sub-station n-1,

d_M = Deflection at sub-station n due to unit externally applied bending moment at sub-station n-1, and

d_F = Deflection at sub-station n due to unit externally applied shear at sub-station n-1.

A value (usually unity) is initially assumed for ω_n, and substituted into the recursion equations. The recursion tables are completed for the preliminary assumed value of ω_{n_1}.

The boundary equations relate the dynamic sub-systems of the mathematical regime.

Figure 1 presents a beam, and its boundary conditions.

Sub-stations "a" and "b" denote the ends of the beam.

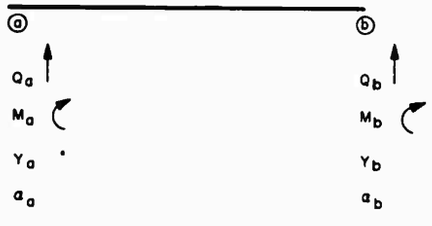

Fig. 1 - Beam

Equations (9) through (12) determine the boundary equations of the beam of Fig. 1 (partial fixity is included at each boundary end of the beam):

$$y_a = y_b H_a^{y_b} + \alpha_b H_a^{\alpha_b} + Q_b H_a^{Q_b} + M_b H_a^{M_b} , \tag{9}$$

$$\alpha_a = y_b F_a^{y_b} + \alpha_b F_a^{\alpha_b} + Q_b F_a^{Q_b} + M_b F_a^{M_b} , \tag{10}$$

$$-Q_a = y_b K_a^{y_b} + \alpha_b K_a^{\alpha_b} + Q_b K_a^{Q_b} + M_b K_a^{M_b} , \tag{11}$$

and

$$-M_a = y_b K_a'^{y_b} + \alpha_b K_a'^{\alpha_b} + Q_b K_a'^{Q_b} + M_b K_a'^{M_b} , \tag{12}$$

where

α_b = The unknown rotation at "b,"

$H_a^{\alpha_b}$ = The internal deflection contribution at point "a" due to unit rotation at "b,"

$\alpha_b H_a^{\alpha_b}$ = The true internal deflection at point "a" due to the true rotation at "b,"

Q_b = The true externally applied unknown shear at "b,"

$H_a^{Q_b}$ = The internal deflection at point "a" due to a unit shear at "b,"

$Q_b H_a^{Q_b}$ = The internal deflection at point "a" due to the true shear at "b,"

M_b = The external moment at "b,"

$H_a^{M_b}$ = The internal deflection at point "a" due to a unit moment at "b," and

$M_b H_a^{M_b}$ = The internal deflection at point "a" due to the true moment at "b."

Similarly, Eq. (10) defines the four internal contributions to the external rotation at "a." Equation (11) defines the four internal contributions to the external shear at "a." Equation (12) defines the four internal contributions to the external bending moment at "a."

The coefficients of the boundary equations are next plotted in matrix format. The equations are linear.

The values α, y, Q, and M appear as unknowns in the boundary equation matrix. The quantities F, H, K, and K' appear as non-zero coefficients of the matrix.

The non-zero coefficients of the boundary equation matrix are determined by recursion tables. Each sub-system has a basic data table defining its geometric properties. The subsequent tables for the sub-system generate the influence coefficients.

The influence coefficients are the rotation, deflection, shear, and moment at left-hand key boundary points due to a unit-applied external rotation, deflection, shear, or moment applied at right-hand boundary point.

The coefficients are plucked by the computer from the recursion tables and set into the boundary equation matrix of the regime.

The recursion tables are set up to determine the distribution of deflection, rotation, shear, and moment from sub-station to substation of a sub-system due to a unit-applied load.

The values of the recursion tables are polynomials in terms of ω_n since they are dependent upon the natural frequency.

All equations are linear. All equations are simple, homogeneous, algebraic equations.

Since the equations are homogeneous, they are to be solved in terms of one unknown. Therefore the equations format is such that there is always one more equation than necessary. The last equation becomes the error function equation[4] and holds true when the error function equals zero. An illustrative example of a regime mathematical model of a multi-degree of freedom system of electronics is presented in Ref. 4.

Assumed values for ω_n have been placed in the recursion tables. The coefficients for the matrix have been taken from the recursion tables of the lamp.

The dynamic matrix is solved for all unknowns for each of the mathematical regimes of the lamp.

The matrix is solved in two cycles and residues are determined and compared.

ω_n is the Eigenvalue and is present in the coefficients of the matrix.

A plot is made of assumed natural frequency, ω_n, versus error function. When the error function curve crosses the abscissa and changes sign, we have a true ω_n or Eigenvalue.

Orders of magnitude of natural frequencies and mode shapes of the lamp are thus determined.

If the compression or shear stress of the lamp filament exceeds the critical allowable buckling stress for stability,[5] the spring constants and influence coefficients are no longer linear. The equations may be linearized by determining the maximum deflection and the slope of the load-deflection curve at the maximum deflection of the lamp filament. This slope replaces the influence coefficient due to unit load on the lamp filament structure substation.

Quantitative tradeoffs[6] should now be generated relating stiffness, reliability, cost, and lamp performance to determine the optimum lamp design for maximum overall system worth.

The method presented above will enable the designer of airborne lamps to predict the stiffness and natural frequency of the lamp structure filament.

In the design of alternate filament schemes, the first mode natural frequency of each proposal should be analytically determined. A goal of minimum design analysis value for natural frequency of 700 cps is recommended.

The following method of rapid analysis of natural frequency is recommended where a high-speed, digital-type computer is not available.

Two different lamp configurations are presented as illustrative examples.

MATHEMATICAL MODEL TO DETERMINE FIRST MODE γ NATURAL FREQUENCY FOR AIRBORNE #1506 TYPE LAMP

The following is a step by step recommended procedure to determine rapidly the approximate relative stiffness and first mode

[4] D. Ehrenpreis, "Analysis and Theoretical Investigation of New Military Electronic Missile and Aircraft-Borne Equipment," IRE National Convention Record (1958).

[5] S. P. Timoshenko and J. Gere, Theory of Elastic Stability (McGraw-Hill Book Co., Inc., New York, N. Y., 1961).

[6] D. Ehrenpreis, "Analytical Dollar Tradeoffs for Development of Electronic Equipment," IRE Transactions (1961).

natural frequency of an airborne exterior lamp. The mathematical model is presented in Fig. 2. The lamp filament is supported by two filament supports.

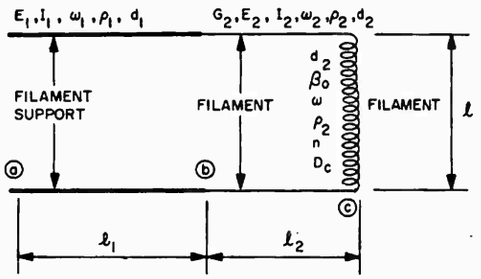

Fig. 2 - Mathematical model #1506 lamp

Step 1

Calculate the following requisite parameters:

1. β_o[7] = Flexural stiffness coiled portion[6] of filament (lb-in.^{2}),

$$\beta_o = \frac{2E_2 I_2 G_2}{\frac{n}{L}\pi\frac{(D_c)}{2}(2G_2 + E_2)} .$$

The nomenclature is defined earlier in the List of Symbols.

2. γ_o[7] = Shear stiffness[6] (lb),

$$\gamma_o = \frac{8L E_2 I_2}{\pi n (D_c)^3} .$$

3. w = Unit weight of filament per Fig. 2 (lb-in.),

$$w = \frac{n\pi D_c \frac{\pi}{4} d_2^2 \rho_2}{L} = \frac{\pi^2 n D_c d_2^2 \rho_2}{4L}$$

$$= \frac{w_2 n \pi D_c}{L} .$$

4. w_1 = Unit weight filament support per Fig. 2 (lb/in.),

$$w_1 = \frac{\pi d_1^2 \rho_1}{4} .$$

5. w_2 = Unit weight filament wire per Fig. 2 (lb/in.),

$$w_2 = \frac{\pi d_2^2 \rho_2}{4} .$$

6. I_1 = Moment of inertia filament support (in.^{4}),

$$I_1 = \frac{\pi d_1^4}{64} .$$

7. I_2 = Moment of inertia filament wire (in.^{4}),

$$I_2 = \frac{\pi d_2^4}{64} .$$

Step 2

Determine deflection, δ_c, of support of coiled portion of filament (point c, Fig. 2), by substitution into the following equation:

$$\delta_c = \frac{wL L_2^3}{6E_2 I_2} + \frac{w_2 L_2^4}{8E_2 I_2} + \frac{w_1 L_1^3 \left[0.75 L_1 + L_2\right]}{6E_1 I_1}$$

$$+ \frac{\left(\frac{wL L_2}{2} + \frac{w_2 L_2^2}{2}\right)\left(\frac{L_1^2}{2} + L_1 L_2\right)}{E_1 I_1}$$

$$+ \frac{\left(\frac{wL}{2} + w_2 L_2\right)\left(\frac{L_1^3}{3} + \frac{L_1^2 L_2}{2}\right)}{E_1 I_1} .$$

Use the coefficients previously calculated in Step 1. The equation defining δ_c is derived using the bending moment diagram presented in Fig. 3.

Step 3

Determine deflection, Y_{Σ_i}, at tenth points, i, of coiled portion of filament, Fig. 4, due to flexure, $Y_{bending}$, and shear, $Y_{shear} \cdot \beta_o$ and w have been determined in Step 1.

$$Y_{bending} = \frac{1}{24}\frac{w}{\beta_o}(x^4 - 2Lx^3 + L^3 x) ,$$

and

$$Y_{shear} = \frac{w}{2\gamma_o}(Lx - x^2) .$$

[7] A. M. Wahl, Mechanical Springs (McGraw-Hill Book Co., Inc., 1963), 2 Ed.

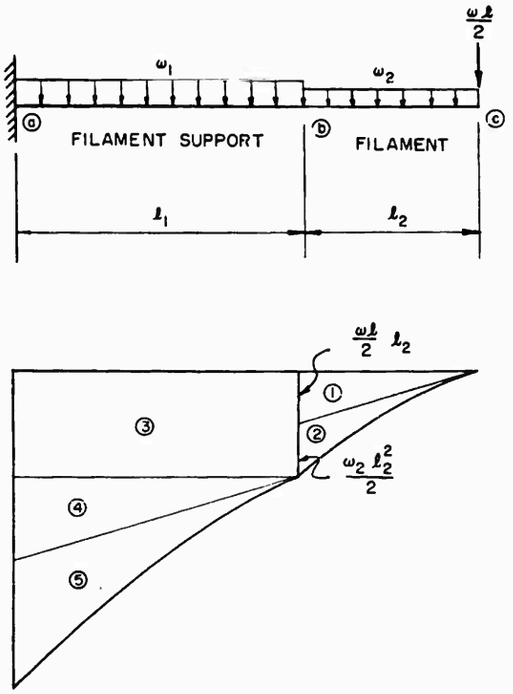

Fig. 3 - Bending moment diagram

Determine for each tenth point, i, Fig. 4, total deflection, $Y_{\Sigma_i} \cdot \delta_c$ has been determined in Step 2. γ_o has been determined in Step 1.

$$Y_{\Sigma_i} = Y_{bending} + Y_{shear} + \delta_c .$$

Determine the approximate natural frequency first mode (cps), f_{n_I}, neglecting preload on spring of Fig. 2.

$$f_{n_I} = \frac{1}{2\pi} \times \sqrt{\frac{g\left[\frac{K_1}{5} - \frac{K_2}{6} + K_o\right]}{L^4\left[\frac{31}{630}K_1^2 - \frac{17}{210}K_1K_2 + \frac{2}{5}K_oK_1 - \frac{1}{6}K_2^2 - \frac{1}{3}K_oK_2 + K_o^2\right]}},$$

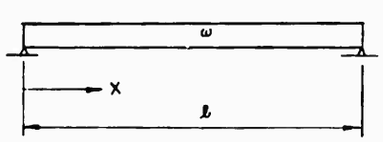

Fig. 4 - Model

where

$$K_o = \frac{\delta_c}{L^4},$$

$$K_1 = \frac{1}{24}\frac{w}{\beta_o},$$

and

$$K_2 = -\frac{w}{2\gamma_o L^2}.$$

Step 4

Determine approximate effect upon the first mode natural frequency, f_{n_1}, of preload on spring of Fig. 2.

a = Preload deflection of filament spring (in.),

K = Spring constant coil spring (lb/in.),

$$K = \frac{G_2 d_2^4}{8n D_c^3},$$

S = K · a = Thrust in spring due to preload (lb). Sign convention: compression loads positive,

P_{cr} = Stability compression column allowable of spring (lb).

$$P_{cr} = \frac{\pi^2 \beta_o}{L^2}, \quad \text{and}$$

$$f'_{n_1} = f_{n_1}\sqrt{1 - \frac{S}{P_{cr}}},$$

where f'_{n_1} = Natural frequency lamp filament (cps).

MATHEMATICAL MODEL TO DETERMINE FIRST MODE ~ NATURAL FREQUENCY FOR #1524 TYPE LAMP

Step 1

Determine the following parametric constants for the airborne lamp of Fig. 5. This lamp filament is double coiled.

1. $$\beta_o = \frac{2E I_w G}{n_o \pi[(d_c)/2](2G + E)},$$

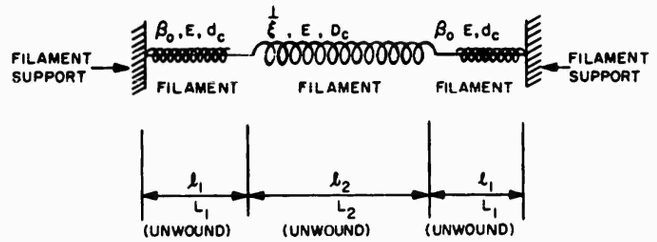

Fig. 5 - Mathematical model #1524 lamp

where

n_o = Number of small coils in 0.04 in. ÷ 0.04 in.

The other notation is defined earlier in the paper.

2. $I_w = \frac{\pi}{64} d_w^4$,

where

d_w = Diameter of wire.

The other notation is defined earlier in the paper.

3. $\frac{1}{\xi} = \frac{D_c \pi N}{2 \beta_o L_2} + \frac{32\, d_c D_c \pi N n_o}{E d_w^4 L_2}$.

4. $W = L_\Sigma \frac{\pi}{4} d_w^2 \rho$,

where L_Σ = Total unwound length of wire (in.), and
W = Total weight of wire (lb).

Step 2

Assuming negligible deflection of supports (Fig. 5) of coiled filament compared to actual deflection of filament, determine shear, δ_i'', flexure, δ_i', and total deflections, δ_{Σ_i}, at all tenth points of filament wire.

Determine end partial fixity conditions of filament by moment distribution.

Flexure deflections, δ_i', may be calculated by moment area method, or

$$\delta_i' = \sum_{i=1}^{10} \frac{M m \Delta S}{C_B} .$$

Determine shear deflection, δ_i'' (Fig. 5):

$$\delta_i'' = \sum_{i=1}^{10} \frac{V v_i \Delta S}{C_S} ,$$

where

C_B = β_o in region of small coil and ξ in region of large coil, and

C_S = γ_o in region of small coil and $K(\gamma_o)$ in region of large coil.

Determine the total deflection, δ_{Σ_i}:

$$\delta_{\Sigma_i} = \delta_i' + \delta_i'' .$$

Step 3

Determine f_{n_I}, the ~ first mode natural frequency (cps) neglecting preload by substitution into the following equation:

$$f_{n_I} = \frac{1}{2\pi} \sqrt{\frac{g \sum_{i=1}^{10} W_i \delta_i}{\sum_{i=1}^{10} W_i (\delta_i)^2}} .$$

Step 4

Determine correction to natural frequency, f_{n_I}, due to filament preload, S (usually tension).

Determine effect upon f_{n_I} of preload, S, on filament spring (Fig. 5):

S = Thrust in spring due to preload (lb). Sign convention: compression loads positive,

P_{cr} = Stability column allowable of spring (lb),

$$P_{cr} = \frac{\pi^2 \beta_o}{L^2} ,$$

and

$$f'_{n_I} = f_{n_I} \sqrt{1 - \frac{S}{P_{cr}}} ,$$

where f'_{n_I} = Lamp (Fig. 5) natural frequency (cps).

CONCLUSIONS

1. It is possible to predict close orders of magnitudes of natural frequencies and mode shapes of airborne exterior lamp filaments.

2. Future airborne lamps should be designed rigorously taking into account dynamic structural, as well as electrical, performance properties.

3. Where a high-speed digital computer is available, the Myklestad method generalized for lamps is recommended to determine stiffness, natural frequency, and mode shape.

4. Methods are presented to analyze rapidly orders of magnitude of two different configurations of exterior aircraft-borne lamps without use of a computer.

* * *

SOLID PROPELLANT DYNAMIC PROPERTIES AND THEIR EFFECT ON VIBRATION RESPONSE OF MODEL SOLID PROPELLANT STRUCTURES*†

G. J. Kostyrko
Aerojet-General Corporation

Three types of vibration tests have been improved and applied to the laboratory measurement of the dynamic mechanical properties of solid rocket propellants over the range 0.1 to 300 cps. These include a free-vibration reed test, a free-vibration torsion test, and a forced-vibration disc test. Computer techniques, based on linear viscoelastic theory, have been devised or improved to yield complex elastic moduli and loss tangents.

Both temperature and frequency influence the dynamic properties. The Williams-Landel-Ferry time-temperature superposition principle is applicable. The relationship between reduced resonant frequency and temperature is proposed as a fundamental and useful property of a material. This relationship, measured on laboratory specimens, appears to be applicable to the prediction of the effect of temperature changes on the dynamic response of missiles.

INTRODUCTION

The successful performance of a solid rocket motor depends in part on the capability of the system to withstand the stresses of handling, temperature cycling, and vibration environments. At present, it is impossible or impractical to determine these stresses in the missile itself. The stresses must be derived from mechanical properties measurements of laboratory samples and stress analysis calculations.

In this paper three simple dynamic laboratory tests are discussed, briefly including theory and practical application. Viscoelastic response of the solid propellants from a frequency of 0.1 to 300 cps can be obtained. This range provides viscoelastic response parameters adequate for structural analysis of a rocket motor subjected to vibrations.

VISCOELASTIC BEHAVIOR

Solid propellants are considered linear viscoelastic because their mechanical behavior is time-dependent (frequency-dependent to oscillating loading). When viscoelastic material is subjected to oscillating stresses (sine wave), the strain wave will be a sine wave with the same frequency, perhaps out of phase with the original stress wave.

In the tests discussed here, the specimen is subjected to either free or forced vibration, and the dynamic response of the specimen is ultimately expressed as complex modulus. The complex modulus is a vector quantity that is separable into a real and an imaginary component. The real component, E', is related to the portion of the strain wave that is in phase with the stress wave, and is sometimes called the storage modulus because it is a measure of the elastic or recoverable energy of the material. The imaginary component, E'', is related to the portion of the strain wave that is 90 degrees out of phase with the stress wave, and is a measure of the energy lost as dissipated heat.

The variation of the real and imaginary components with frequency is used in the prediction of vibration response of a solid propellant motor. Until recently, prediction of

*Supported in part by the Air Force under Contract AF 33(600)-36610.
†This paper was not presented at the Symposium.

propellant response was based on propellant mass alone, because viscoelastic properties were not available. There are now several methods for using the viscoelastic data in motor behavior prediction, including direct analog computer simulation.[1]

There is no single test, as yet, that covers the frequency range required. The three following tests together cover the necessary range. One of them yields tensile dynamic modulus, and the other two yield shear.

VIBRATING REED TEST

The vibrating reed test is a free vibration test in which a specimen, fixed at one end and free at the other, acts as a reed. The specimen vibrates at a resonant frequency determined by the specimen dimensions, weight, and mechanical properties. Measurements may be made at various resonant frequencies by changing the dimensions of the specimen. This test covers a frequency range of 2.0 to 30 cps.

A test is conducted by deflecting the free end of the specimen, allowing it to oscillate freely, and recording the oscillations. Full test procedure and equipment discussions are contained in Refs. 2 and 3.

The present analysis for complex modulus determination from the vibrating reed test was developed by R. D. Glauz[4] through the use of the generalized linear viscoelastic stress strain law. The equations he derived (derivation discussed in Refs. 2 and 4) are

$$E' = \frac{m\ell^4}{I\psi^4}(\omega^2 - \lambda^2)$$

and

$$E'' = \frac{m\ell^4}{I\psi^4}(2\omega\lambda),$$

where

E' and E'' = real and imaginary components of the complex modulus,

m = mass/unit length = lb-sec^2/in.^{2},

ℓ = length of reed (in.),

$I = cd^3/12$ = moment of inertia of cross section,

c = width (in.), and
d = thickness (in.),

ω = circular frequency (rad/sec = $2\pi f$),

λ = damping factor (1/sec), and

ψ = Eigen value = 1.8751 for unweighted reed.

TORSION PENDULUM TEST

The torsion pendulum test is another free vibration test, covering the frequency range 0.1 to 5 cps. The vibrating reed test was used to determine the complex Young's modulus, and the torsion pendulum test is used to determine the complex shear modulus.

One end of the specimen is attached to a fixed support and the other end is twisted and allowed to oscillate freely in a torsional mode. A discussion of the test and equipment may be found in Ref. 5. As the specimen twists and untwists at its resonant frequency (determined by the specimen dimensions, the moment of inertia of the disc attached to the free end of the specimen, and the specimen's mechanical properties), the vibration is recorded. The material of the specimen has an inherent damping effect, and the amplitude of vibration decreases with time. From the resonant frequency and the rate of amplitude decrease, the loss tangent and the components of shear modulus can be computed.

The deformation of the specimen with time leads to a second order partial differential equation of motion. Modulus is expressed in terms of linear, time-dependent, stress-strain operators in a fashion similar to that developed by Glauz for the vibrating reed. The final equations (see Ref. 5 for derivation) are

[1] T. E. Depkovich and L. Peterson, "Direct Analog Dynamic Analyses of Minuteman Second-State Motors," Aerojet-General Corporation TM 208 SRP (Jan. 31, 1963).

[2] G. J. Kostyrko, "Development and Use of a Free Vibrating Reed Test for Evaluation of Solid Propellant," Aerojet-General Corporation TM 228 SRP (Aug. 1963).

[3] ICRPG Solid Propellant Mechanical Behavior Manual, Section 4.6.2.4, Free Vibrating Reed Method (Sept. 1963).

[4] R. D. Glauz, "Transient Analysis of a Vibrating Reed," J. Polymer Sci., Part A, I, 1693-1700 (May 1963).

[5] G. J. Kostyrko, "Development and Use of a Torsion Pendulum Test for Evaluation of Solid Propellants," Aerojet-General Corporation TM 229 SRP (Aug. 1963).

$$G' = \frac{\gamma' \ell^2}{g\psi^2} (\omega^2 - \lambda^2)$$

and

$$G'' = \frac{\gamma' \ell^2 2\omega\lambda}{g\psi^2} ,$$

where

G' and G'' = real and imaginary components of complex shear modulus,

γ' = density (lb/in.^{3}),

ℓ = length of shaft,

ω = circular frequency (rad/sec),

λ = damping factor (1/sec),

g = gravity conversion factor: 386, and

ψ = Eigen value.

VIBRATING DISC TEST

The vibrating disc test is a forced vibration test, covering the frequency range of 50 to 300 cps. A specimen disc is mounted by its edges in a rigid support fixture on the driving table of an electromagnetic shaker, and accelerations are measured at the edge and center of the disc. Equipment and procedure for this test are given in Ref. 6.

The implicit functions from this test are obtained by computer and will not be discussed in this limited space. The rigorous discussion of the vibrating disc problem is to be found in Ref. 7.

DATA

The results of the vibrating reed test provide an example of the data obtained from these tests. The output from this test consists of an amplitude vs time trace, either as an oscilloscope photograph or oscillograph tracing. This record consists of sinusoidal vibration with exponential damping of the amplitude, and these are reduced to yield the natural frequency (f), and the exponential damping (λ). The measured quantities mass (m) and moment of inertia (I) depend on specimen dimensions. The Eigen value (ψ) of the system is a constant, dependent on the end loading and mode of vibration.

Complex modulus is obtained by the above means for the specimen at various frequencies and at various temperatures (Figs. 1 and 2). Since there is a significant change in complex modulus with change in temperature, an extension of range sufficient for a frequency vs modulus curve may be obtained by using the Williams-Landel-Ferry[8] shift equation in order to use low temperature data to predict behavior at higher frequencies, and vice-versa. This equation uses the glass transition temperature of the material and two general constants to compute a shift factor. The original equation is:

$$\log a_T = \frac{-8.86 (T - T_s)}{101.6 + (T - T_s)} ,$$

where

a_T = shift factor,

T = absolute temperature (°K) of tested specimen,

$T_s = T_g + 50°K$, and

T_g = glass transition temperature.

Thus, smooth curves can be drawn through the points for each specimen, extending the useful frequency range of the tests, singly or together for comparison purposes. The data of Figs. 1 and 2 are shown shifted in Fig. 3 so that such lines could be drawn.

The points obtained by the Williams-Landel-Ferry equation on the vibrating reed data are comparable to the data obtained under the other tests in their respective frequency ranges, Fig. 4.

CONCLUSIONS

Each solid propellant tested behaved as a linear viscoelastic material and has produced a

[6] G. J. Kostyrko, "Application of the Forced Vibrating Disc Method to the Evaluation of Minuteman Wing II, Second Stage Propellant," Aerojet-General Corporation TM 230 SRP (Aug. 1963).

[7] J. H. Baltrukonis, W. G. Gottenberg, and R. N. Schreiner, "The Dynamic Response of a Finite Rigid Mass Concentrically Carried by a Viscoelastic Disc," Report STL/TR-60-0000-19331.

[8] M. L. Williams, R. F. Landel, and J. D. Ferry, "The Temperature Dependence of Relaxation Mechanisms in Amorphous Polymers and Other Glass Forming Liquids," J. Am. Chem. Soc., 77, 3701-7 (1955).

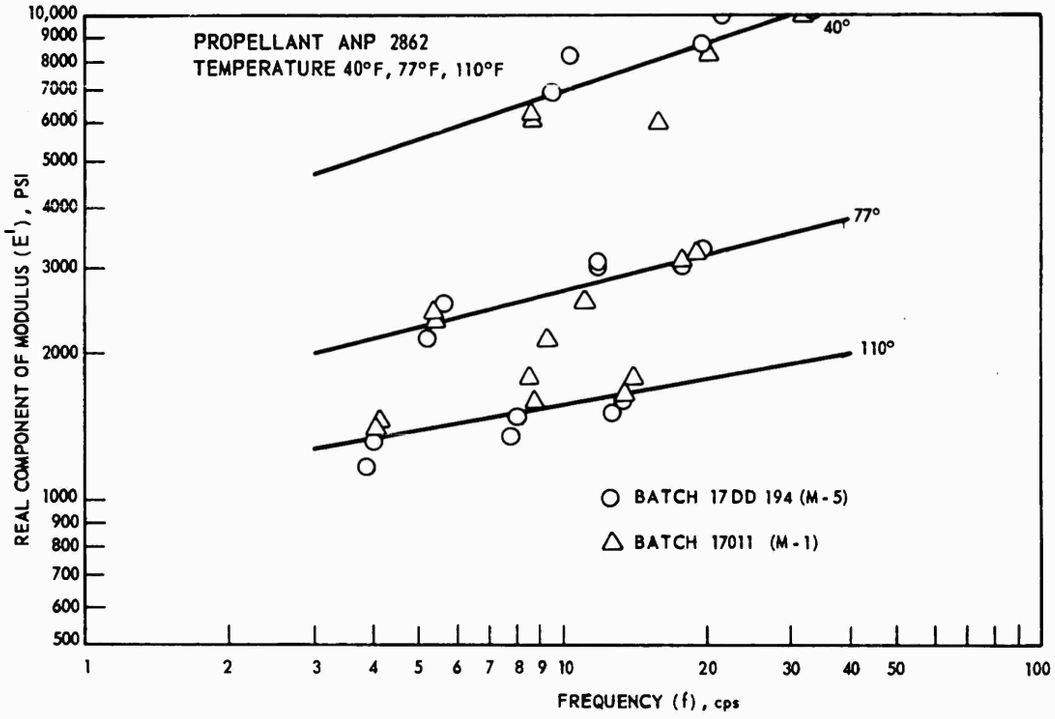

Fig. 1 - Vibrating reed test, real component of complex modulus E^1 vs frequency

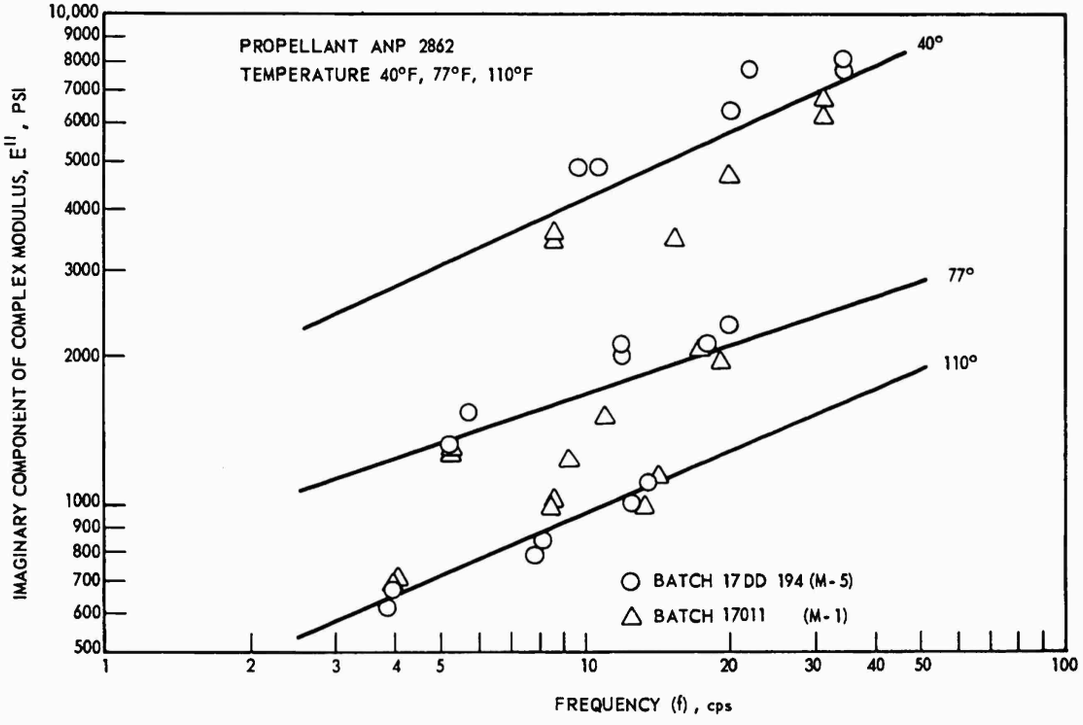

Fig. 2 - Vibrating reed test, imaginary component of complex modulus E^{11} vs frequency

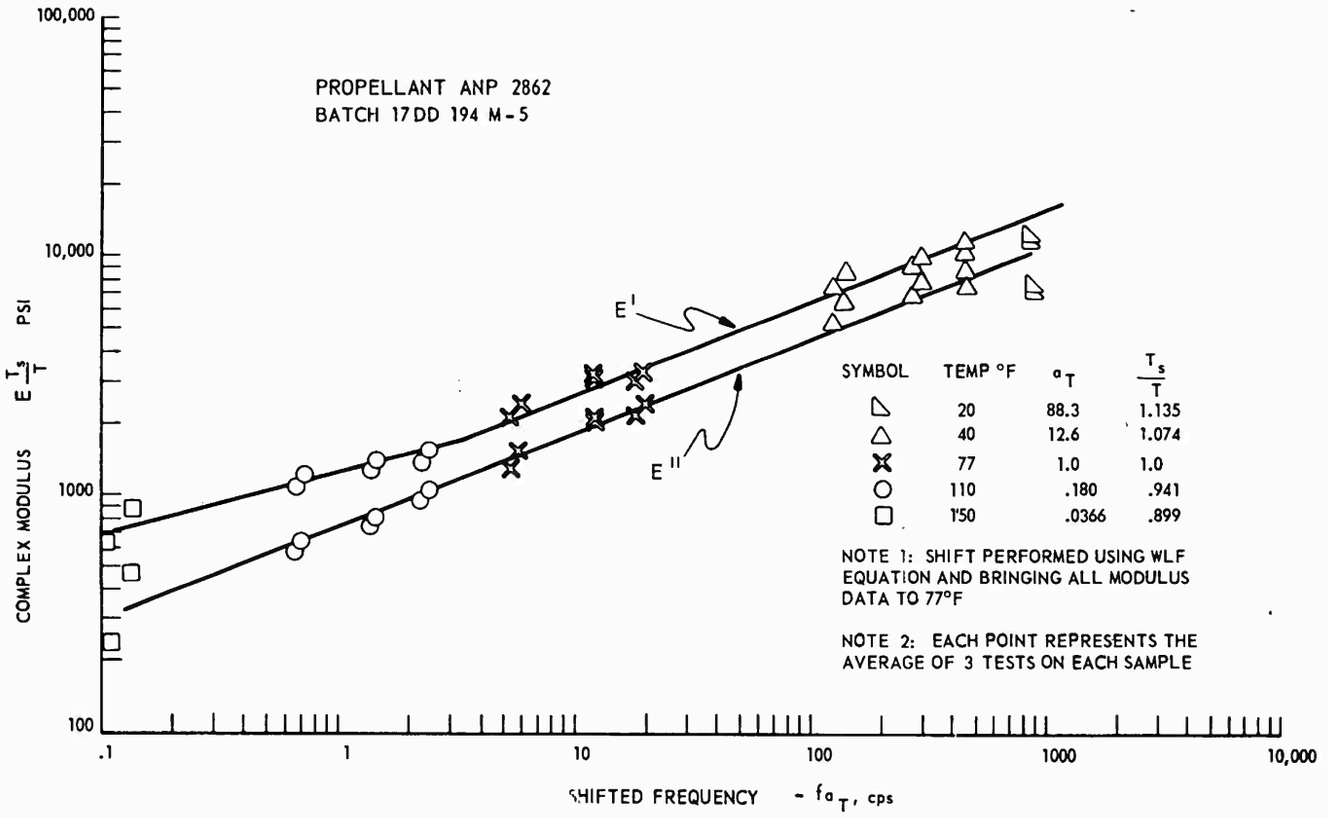

Fig. 3 - Vibrating reed test, corrected complex modulus $(E(T_s/T))$ real and imaginary components vs shifted frequency (fa_T)

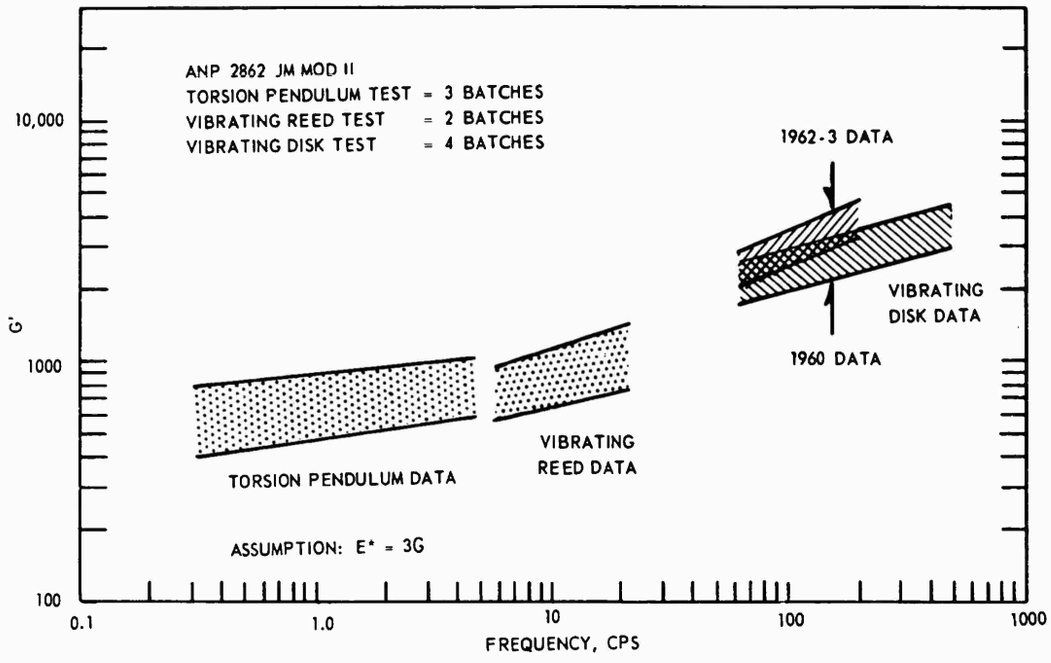

Fig. 4 - Real component of complex shear modulus vs frequency for three types of vibration tests

different and characteristic temperature vs resonant frequency curve, supported by all tests run on the material. Figure 5 shows such curves for several propellants. Indications are that these characteristic curves may be related to a fundamental dynamic property of viscoelastic materials.

These conclusions are supported by the results obtained recently by Tormey and Britton,[9] in which forced longitudinal vibration of solid propellant produced a decrease in resonant frequency as the test progresses.

In a subsequent tension-compression test on a model solid propellant structure performed at Aerojet-General Corporation, it was found that the resonant frequency did change with time of vibration, as indicated by Tormey and Britton; this decrease in the resonant frequency was due to an increase in propellant temperature caused by internal heat generation. The result of this test is shown in Fig. 6, which also includes the curve obtained from torsion pendulum tests at different temperatures, indicating the predictive value of the sample tests.

Practically, this concept seems to indicate that the resonant frequency of a missile structure incorporating solid propellant is not temperature independent, as has been previously supposed. Rather, the presence of propellant in the missile makes the resonant frequency of the system temperature dependent. Fortunately, this temperature shift of the resonant frequency can be predicted by tests on small samples of the propellant alone. This concept was tested on vibration of several small solid propellant motors.

[9] J. F. Tormey and S. C. Britton, "Effect of Cyclic Loading on Solid Propellant Grain Structures, AIAA Journal, 1, 8, 1763-1770 (1963).

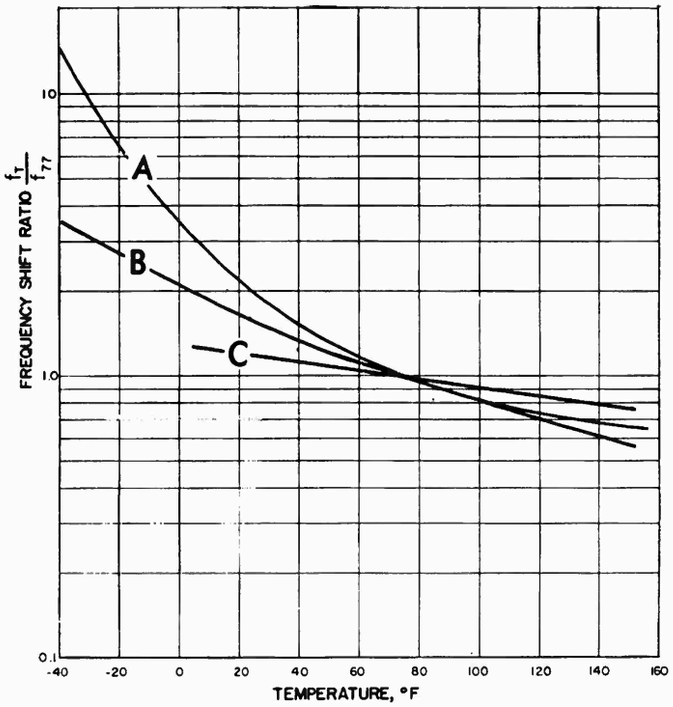

Fig. 5 - Shift in frequency due to change in temperature, A B C propellants

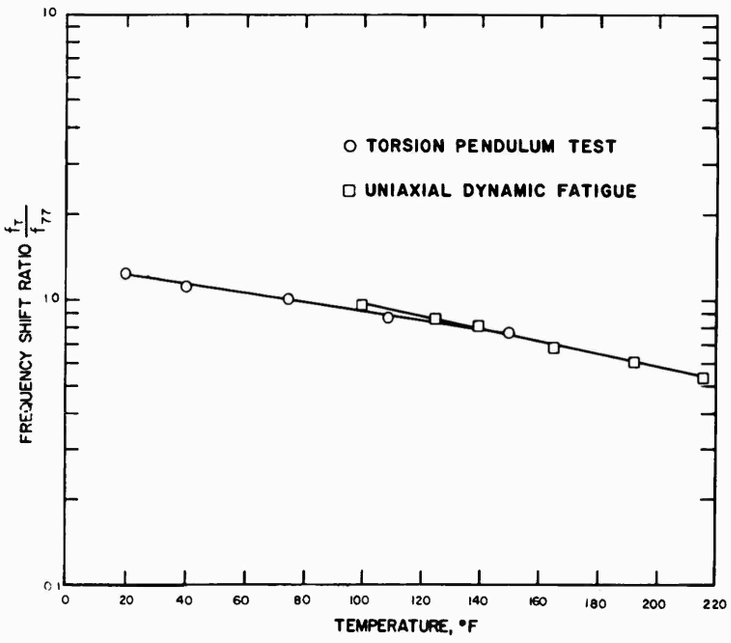

Fig. 6 - Shift in frequency due to change in temperature, polyurethane propellant

* * *

DESIGN CONSIDERATIONS OF LARGE SPACE VEHICLES DUE TO AXIAL OSCILLATIONS CAUSED BY ENGINE-STRUCTURAL COUPLING

D. McDonald
North Carolina State College
Raleigh, North Carolina

and

T. R. Calvert
Lockheed Missiles and Space Co.
Sunnyvale, California

A sustained longitudinal oscillation occasionally occurs in large space vehicles. The cause and mechanics of this oscillation are reviewed and experimental data, obtained from ground vibration tests of an elaborate dynamic model, are correlated with flight test data.

INTRODUCTION

The highly complicated missile systems in use and under development present a wide class of problems involving the dynamic interaction of liquid propellants, structure, and propulsion system. This paper describes one particular such problem which has been encountered, its effect on structural design, and the analysis and tests performed and proposed in determining appropriate design criteria.

The Thor-boosted Agena vehicle has a characteristic axial oscillation which has appeared on virtually all flights. It was first recorded on the flight instrumentation of the earlier model Agena A and, though the magnitude of the loads associated with the oscillation was small relative to the design values, an allowance was made in prescribing the loads for the larger Agena B. The general characteristics have been repeated from flight to flight, though the amplitude and frequency changed with the introduction of the Agena B. (Because most of the investigation was done after the first Agena B flights, the following description pertains to that model.) The oscillation first appears during the last 30 or 40 seconds of first stage boost, increases in amplitude to a maximum from 5 to 15 seconds before engine shutdown, and rapidly decays, usually to zero before booster engine shutdown. An envelope of the amplitude, plotted on the rigid body acceleration, is shown as a function of flight time in Fig. 1. The frequency varies with time in the same way as the calculated fundamental frequency of free axial vibration, but is slightly lower numerically.

Accelerometers mounted at various locations on the vehicle confirmed that the response was predominantly in the fundamental longitudinal mode. The maximum recorded vibration level in the payload area is 3.22 g (zero to peak), compared with a maximum rigid body acceleration of about 7 g. In the usual case, the maximum total acceleration in the forward section of the vehicle was that due to rigid body motion and occurred at booster engine shutdown. Occasionally, however, the maximum vibration occurred late enough in flight so that the augmented rigid body acceleration exceeded rigid body value at burnout. In addition to the accelerometers, pressure transducers installed in the propulsion system, both upstream and downstream of the propellant pumps, showed the oscillation at the same frequency as the accelerometers with a small phase difference between the two records. At high amplitudes, however, the pressure oscillation showed a characteristic nonlinear hard spring response, with sharp peaks and smooth valleys.

MECHANISM OF OSCILLATION

Certain features of the oscillation can be explained by analysis of the idealization shown in Fig. 2. The propulsion system is represented by the propellant, feed lines, pump, and engine. The structure is reduced to the engine

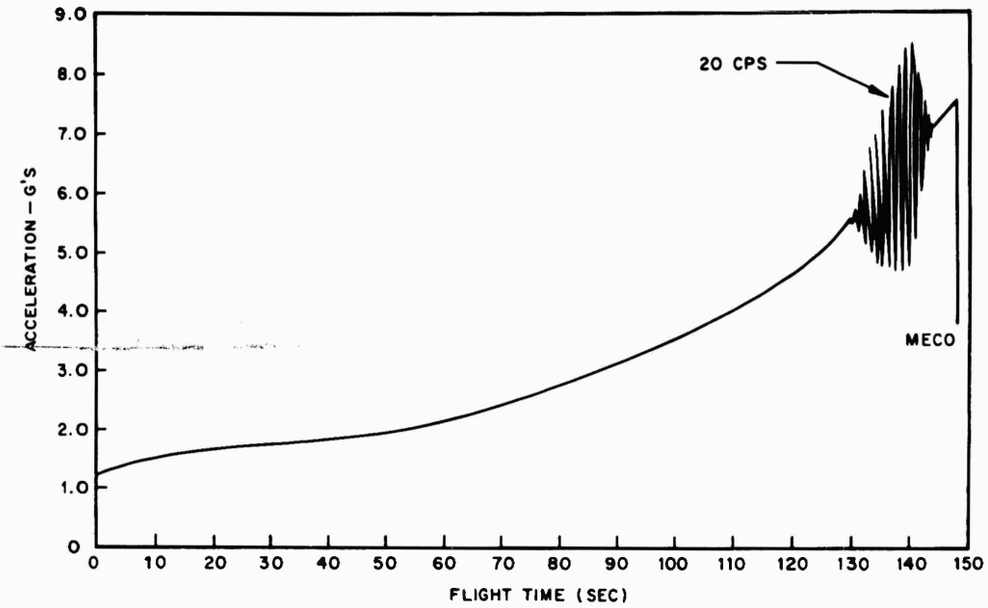

Fig. 1 - Longitudinal acceleration vs flight time

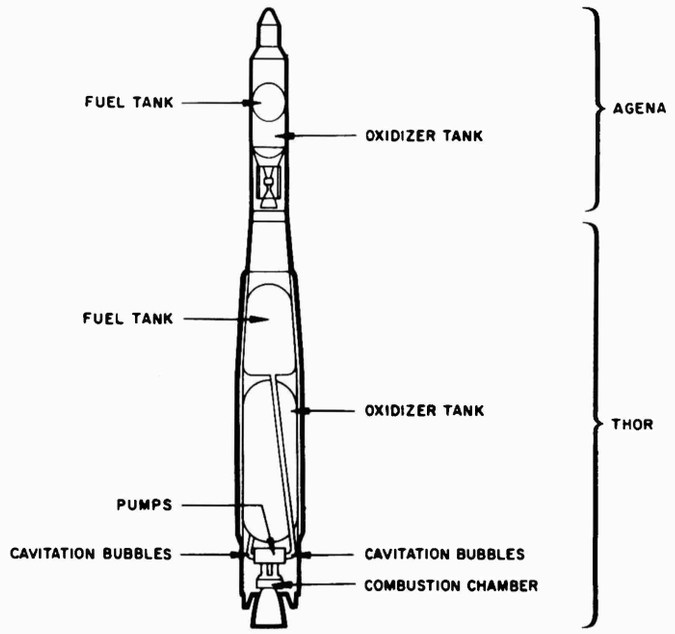

Fig. 2 - Missile configuration

thrust structure, oxidizer tank, and vehicle generalized mass. In addition, a capacitance, shown in the figure as an entrapped compressible bubble in the incompressible liquid is postulated to exist ahead of the oxidizer pump. In the normal case, that is without the bubble, structural and pressure oscillations caused by a variation in the engine thrust are dissipated by system damping. The expansion and contraction of the hypothesized bubble, however, tends to magnify the pressure perturbations, which are transmitted across the pump to the combustion chamber, and result in a larger thrust oscillation. This in turn is transmitted back into the structure and again to the liquid. Closely coupled capacitance and structural frequencies result in a resonance which in this simplified model is unstable unless unreasonably large values of damping are assumed in the system. Conversely, the system is stable when the frequencies are sufficiently separate.

The diagram in Fig. 3 summarizes the dynamic process outlined above. This is typical of several variances of this system, which have been studied. A more complete model includes both fuel and oxidizer sides of the propulsion system plus time varying parameters, such as structural frequency and generalized mass, propulsion system parameters, and the like. With a proper choice of parameters, the simplified version will reproduce certain important characteristics of the actual phenomenon, such as the frequency, the rate of increase of amplitude, the nonlinear shape of the pressure oscillations and the downward shift in the system frequency from the structural frequency. On the other hand, the rapid decay of the oscillation just before burnout, the time of beginning, and the amplitude to be expected are important characteristics which are not predicted by this formulation. In view of the apparent randomness of some of the variables, it seems likely that the latter two cannot be explained by a completely deterministic analysis.

Other vehicles have exhibited sustained longitudinal oscillations. In early flights of the Jupiter missile, pressure oscillations were recorded in the suction line of the liquid oxygen pump which interfered with the thrust control feedback circuit. No structural coupling was present, probably because of a wide separation between engine and structural frequencies. Here the trouble was pinpointed as resulting from the presence of cavitation bubbles ahead of the pump. This was verified by analysis and measurements made during a water tunnel pump test. A relatively minor pump modification inhibited cavitation, and fluctuations were reduced to an acceptable level. Since the Jupiter and Thor engines are similar, it was assumed that the same modification would eliminate the present problem. This did not prove to be the case and subsequent analysis showed the more complicated nature of the Thor oscillation.

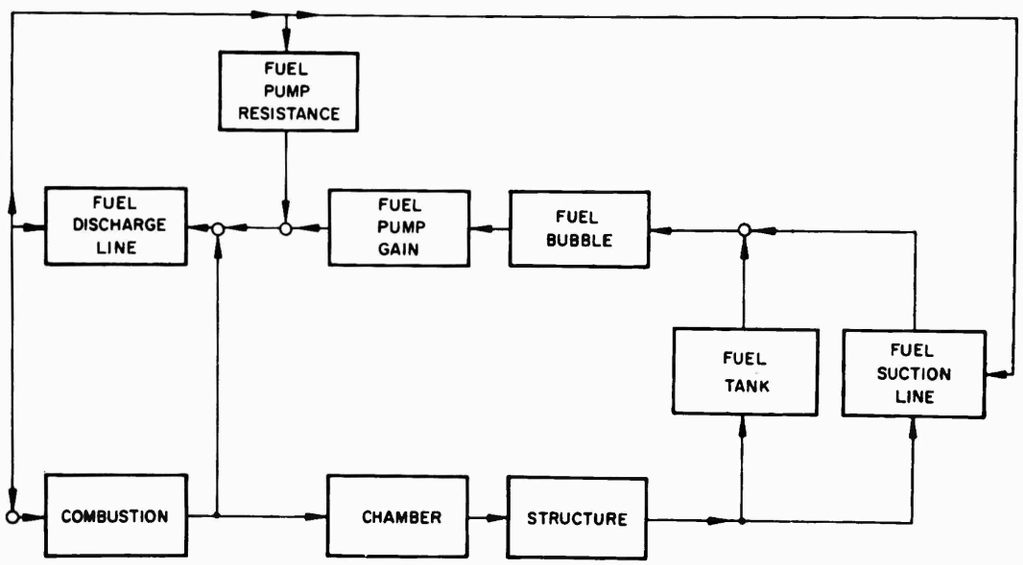

Fig. 3 - Model block diagram

In the Titan II vehicle, an oscillation with characteristics similar to the one described in the Thor-Agena, is under investigation. The same mathematical model has been used in this study, though there is no particular reason to believe that the same capacitive element is behind the trouble in both vehicles. In fact, a change in material of the propellant feed lines which altered significantly the level of the oscillation indicated that any number of capacitive elements are possible within the propulsion system.

AGENA DESIGN CONSIDERATIONS

The Agena vehicle has been used to place a large variety of payloads in orbit, many of which have frequencies in the range of the fundamental frequency of the Thor-Agena. During flight often lightly damped structures are then subjected to high amplitude support excitation at or near a resonance condition. Even in the case of lateral payload frequencies in this range, sufficient coupling due to misalignment and lack of symmetry exists to require a large increase in vibration-qualification levels. Studies of flight data have shown that the duration of amplitude levels greater than 90 percent of the maximum level is approximately 3 seconds and the duration of amplitudes greater than 75 percent of the maximum level is about 5 seconds. This indicates that the large vehicle vibration amplitudes are present for a sufficient time to allow the payload motion to reach its maximum value. Also, the variable nature of the dominant frequency, because of changing vehicle mass, causes the driving force to sweep through all frequencies in the critical range.

The critical section in the primary structure of the Agena is a short segment of cylinder aft of the oxidizer tank attachment point. Because the design of this section is governed by elastic buckling, an analysis, according to theory of Ref. 1, was made to determine any increase in allowable load possible because of the vibratory nature of the loading. In this Reference it is shown that a cylinder designed from static considerations can withstand an additional periodic load. (This in essence would permit an increase in the allowable without structural redesign.) Unfortunately, preliminary results show that the permissible increase in loading is negligible.

[1] J. C. Yao, "Dynamic Stability of Cylindrical Shells Under Static and Periodic Axial and Radial Loads," AIAA Journal, 1, 6 (June 1963).

THEORETICAL DYNAMIC TANK MODEL

Because of the nature of the problem, the distribution of loads in the vehicle is highly dependent on the continuously changing fundamental longitudinal mode. In load calculations the representation of the structure originally was by the usual mass-spring arrangement, with the fuel merely added to the appropriate structural mass point. The oxidizer was lumped into a point mass and a linear spring, the stiffness of which was determined from considerations of the motion of the center of gravity of the liquid due to bulging of the spherical part of the tank. Calculations with various values of the oxidizer spring showed that though there was only a minor change in the fundamental frequency with a change in the spring stiffness, the load in the structure due to the oscillation was more sensitive to the value selected. This result led to the following more detailed consideration of the fluid motion and its effect on the vibration modes of the vehicle.

In this representation of the Agena tank section, the tank structure is concentrated into discrete point masses as in the remainder of the structure. The walls are assumed to act on the liquid as an elastic membrane with zero radial inertia. The stiffness of the springs connecting the structural point masses are calculated from the equations of plane stress and therefore have a contribution from radial motion of the tank walls. The liquid is also divided into segments, with a peculiarity of the division being that the planes, normal to the longitudinal axis of the vehicle, which divide the liquid into segments are at the same vehicle station as the structural tank point masses. The liquid is assumed inviscid, incompressible, and the flow is axisymmetric and irrotational.

The equation of motion can be derived from equilibrium consideration of a liquid element. A simpler derivation, however, can be obtained by resorting to an energy formulation of the problem. The character of the deformation of each segment is assumed and the motion of the liquid within the segment is expressed in terms of coordinates selected for the segment. For example, a segment of the circularly cylindrical part of the tank is assumed to move in such a way that it remains a right circular cylinder. From this assumption the kinetic energy of a particle within the segment can be expressed as a function of the velocity of the top and bottom surfaces of the segment. The radial motion of the adjacent tank equals that of the liquid segment. Therefore, the strain energy of the tank can be calculated from the coordinates of the liquid and the longitudinal motion of the tank

wall coordinates. In this way, the total energy of the liquid and structure is obtained in terms of the motion of a set of liquid surfaces and concentrated mass points of the structure. Substitution of these energy expressions into Lagrange's equations yields a set of second order differential equations describing the dynamic motion of the liquid-tank combination.

A detailed derivation of the equations of motion for the Agena tank configuration, shown in Fig. 4, is not appropriate because of the particular character of the Agena tank configuration. The equation for the general cylindrical element is of wider interest and therefore follows. The motion of the two structural elements in Fig. 5 is designated u_{j-1} and u_j, and that of the liquid surfaces originally adjacent to these elements $\bar{u}_{j-1}$ and $\bar{u}_j$. The assumption of an incompressible liquid and the prescribed nature of the liquid motion result in the radial displacement $\bar{v}_j(r)$ of a liquid particle a distance r from the axis as

$$\bar{v}_j(r) = \frac{r}{2h_j}(\bar{u}_j - \bar{u}_{j-1}),$$

where h_j is the depth of the element, and a longitudinal displacement

$$\bar{u}_j(\xi) = \bar{u}_{j-1} + (\bar{u}_j - \bar{u}_{j-1})\frac{\xi}{h_j}.$$

The functional notation $\bar{v}_j(r)$, $\bar{u}_j(\xi)$ denotes displacements within the j-th element and ξ is the distance from the top of the element. The integral of

$$\rho\left\{\left[\dot{\bar{u}}_j(\xi)\right]^2 + \left[\dot{\bar{v}}(r)\right]^2\right\} dV$$

over the volume V of the element gives the kinetic energy $\bar{T}_j$ of the liquid as follows:

$$\bar{T}_j = \frac{1}{2}\bar{m}_j\left[\dot{\bar{u}}_j\dot{\bar{u}}_{j-1} + \left(\dot{\bar{u}}_{j-1} - \dot{\bar{u}}_j\right)^2\left(\frac{1}{3} + \frac{a^2}{8h_j^2}\right)\right],$$

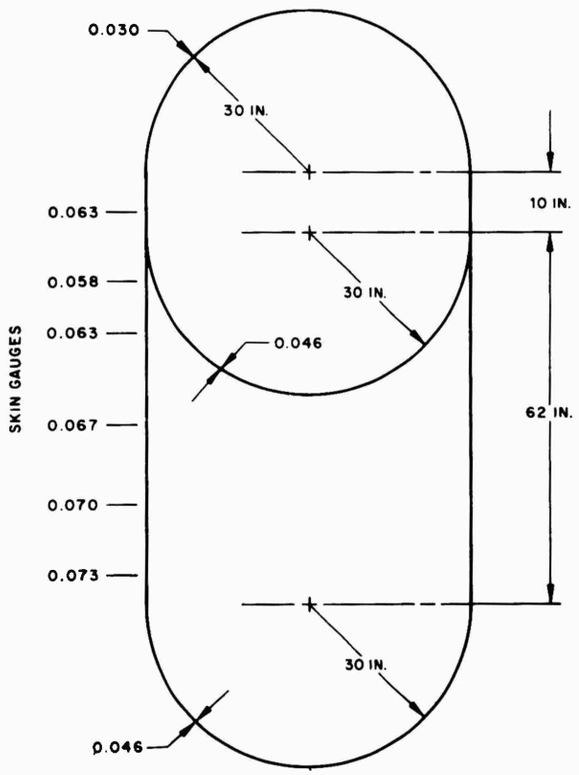

Fig. 4 - Tank geometry

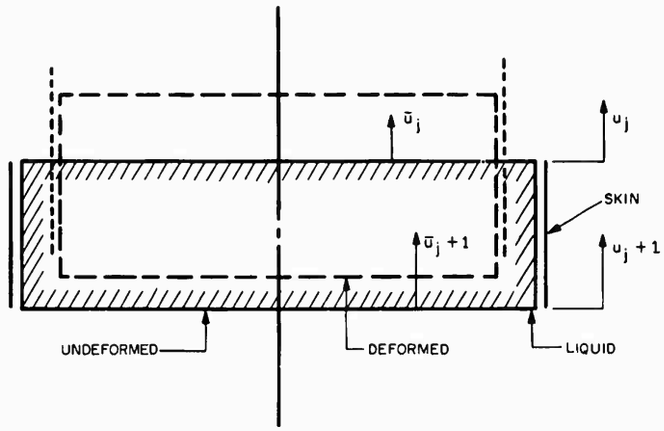

Fig. 5 - Liquid element

where $\bar{m}_j$ is the liquid mass in the j-th element, a is the tank radius, and ρ is the mass density. According to the membrane theory of shells,[2] the strain energy U_j is given by

$$U_j = \frac{1}{2} \frac{2\pi E t_j a}{(1-\nu^2)} \int \left(\epsilon_{xj}^2 + 2\nu \epsilon_{xj} \epsilon_{\phi j} + \epsilon_{\phi j}^2 \right) dx ,$$

where ϵ_{xj}, $\epsilon_{\phi j}$ are the axial and circumferential strain components, respectively, E is Young's modulus, t_j the thickness, and ν is Poisson's ratio. The strain displacement relations are

$$\epsilon_{xj} = \frac{1}{h_j} (u_{j-1} - u_j) ,$$

and

$$\epsilon_{\phi j} = \frac{v_j}{a} ,$$

where $v_j = \bar{v}_j(a)$.

The second of these equations expresses the compatibility of displacement between the liquid and the tank wall. Combination of these equations gives the desired expression for the strain energy as

$$U_j = \frac{1}{2} \frac{k_j}{(1-\nu^2)} \left[(u_{j-1} - u_j)^2 + \nu (u_{j-1} - u_j)(\bar{u}_j - \bar{u}_{j-1}) + \frac{1}{4} (\bar{u}_j - \bar{u}_{j-1})^2 \right] ,$$

in which

$$k_j = \frac{2\pi E a t_j}{h_j} .$$

Lagrange's equation for a conservative system can be written

$$\frac{d}{dt} \left(\frac{\partial T}{\partial \dot{q}_j} \right) + \frac{\partial U}{\partial q_j} = 0 ,$$

where q_j is the generalized coordinate, in this case the u_j and $\bar{u}_j$. Substitution into this equation of the energy expressions yields the following equation of motion of the element:

$$\left(\frac{1}{6} - \frac{1}{8} \frac{a^2}{h_j^2} \right) \bar{m}_j \ddot{\bar{u}}_{j-1} + \left[\left(\frac{1}{3} + \frac{1}{8} \frac{a^2}{h_j^2} \right) \bar{m}_j + \left(\frac{1}{3} + \frac{1}{8} \frac{a^2}{h_{j+1}^2} \right) \bar{m}_{j+1} \right] \ddot{\bar{u}}_j + \left(\frac{1}{6} - \frac{1}{8} \frac{a^2}{h_{j+1}^2} \right) \ddot{\bar{u}}_{j+1} - \frac{k_j}{4(1-\nu^2)} \bar{u}_{j-1} + \frac{(k_j + k_{j+1})}{4(1-\nu^2)} \bar{u}_j - \frac{k_{j+1}}{4(1-\nu^2)} \bar{u}_{j+1} = 0 .$$

A comparison was made between the frequencies calculated as outlined above for a uniform circular cylindrical tank with a flat bottom and free surface, the dimensions of which were nominally those of the Agena tank, and the known exact solution of this problem. The error

[2] W. Flugge, Stresses in Shells (Springer, Berlin, 1960).

in the first three frequencies was 3.9, 3.9, and 11.8 percent respectively, and increasing for the higher frequencies. Because of the wide separation between adjacent tank frequencies, it was concluded that the dynamic motion of the vehicle was affected essentially by the first two modes and that therefore this analysis should be adequate.

TESTS

The purpose of the structural analysis was to determine the vehicle load distribution during the oscillation. A check of the calculated load below the tank attach point can be obtained from pressures measured during flight. A considerable number of pressure measurements from the pump inlets are available and a load calculated using these data was found to be approximately 20-percent higher than that obtained from the analysis. Some uncertainties are associated with this load. The data are from measurements made at a low commutation rate; a correction has to be made for the motion of the bellows and standpipe between the pump and tank bottom; and a theoretical pressure distribution in the tank has to be used.

A comparison between loads obtained with the propellant included in the structure, the oxidizer represented by a branched one mass-spring system and the fuel included in the structure, and the above described model is shown in Fig. 6. A considerable variation in load is obtained depending on the tank model used, and the importance of the model is further emphasized if it is kept in mind that the elastic load is approximately 40 percent of the rigid body load. The discrepancy between the theoretical load and that obtained from the flight measurements can be resolved finally only by testing. Two test programs are planned or in progress:

1. Flight tests with continuous channel measurements of tank bottom pressures and accelerations at various stations; and

2. Ground vibration test of a liquid filled Agena tank.

From the data of the flight tests, in conjunction with the pressure distribution obtained from the ground test, the change in load at the tank attach points can be calculated. Also, the flight test will provide several points on the vehicle mode shape. These can be compared with the values predicted from the analytical model. The ground test will make possible a careful measurement of the tank modes and frequencies for a comparison with the model, and from these data adjustments can be made to the model. From this correlation it will be possible to calculate the oscillation loads on future vehicles.

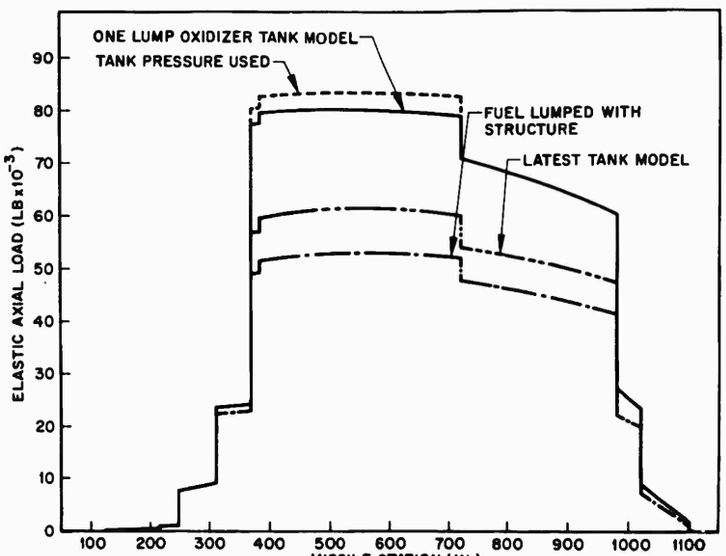

Fig. 6 - Elastic axial load distribution

The test arrangement and instrumentation of the tank vibration test are shown in Figs. 7 and 8. The tank, loaded with simulated propellant and pressurized to half flight pressure, is suspended by a relatively soft spring. Two shaker systems provide the excitation: one 15,000-pound electrodynamic shaker and four smaller 150-pound shakers attached, two at the top and two at the bottom. During the modal tests, the large shaker will be used for a sweep through the frequency range which will determine the important frequencies; the smaller shakers will be used for finer tuning of the modes. The usual lissajous technique will be used in which the current from the armature is connected to the x-axis of a dual channel oscilloscope and the velocity measured at the application of force is connected to the y-axis. During these tests, pressures, accelerations, and strains will be measured at sufficient points to establish the mode shape. The test will be run first with the propellant tanks full and then with the oxidizer tank off-loaded in order to be able to evaluate the importance of the interaction between the fuel tank bottom and the oxidizer.

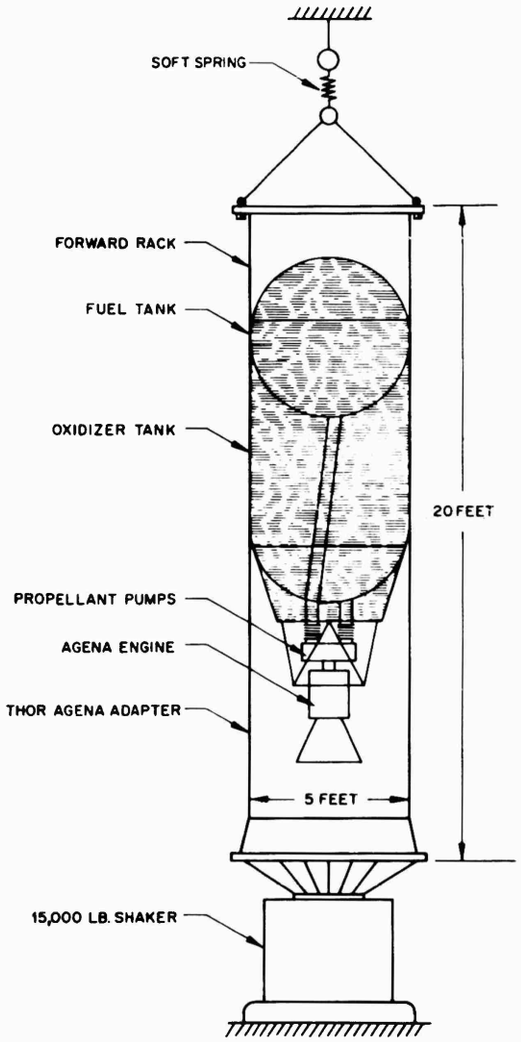

Fig. 7 - Vibration test setup

In addition to obtaining the natural frequencies, modeshapes, and pressure distribution, an attempt will be made to determine the impedance of the tank section and in this way get another check of the load. If the tank is considered as a "black box" whose transfer function is known and the remainder of the structure is known, the load can be determined for any part of the vehicle except the tank section.[3] The transfer function is determined by finding the impedance matrix E defined by

$$\begin{Bmatrix} F_1 \\ y_1 \end{Bmatrix} = \begin{bmatrix} a_{11} & a_{12} \\ a_{21} & a_{22} \end{bmatrix} \begin{Bmatrix} F_2 \\ y_2 \end{Bmatrix} = [E] \begin{Bmatrix} F_2 \\ y_2 \end{Bmatrix},$$

where

F_1 = Input force (oscillatory),

y_1 = Associated deflection,

F_2 = Force in the top of the vehicle (oscillatory), and

y_2 = Associated deflection.

The a_{ij} are all functions of frequency. As the frequencies of interest are far from the suspended vehicle frequency, F_2 can be regarded as zero in this frequency range, and a_{12} and a_{22} are easily determined from the above equation. To determine a_{11} and a_{22} with maximum accuracy, y_2 should be zero, that is the upper part of the vehicle should be fixed. This is of course impossible to attain and an investigation of the structure required to obtain a reasonably high frequency showed that this approach was not practical. An alternative is to apply the shaker force to the top of the vehicle, but this was also considered impractical. A fairly simple way of obtaining the remaining two

[3] C. T. Molloy, "Four-Pole Parameters in Vibration Analysis," Colloquium on Mechanical Impedance Methods, ASME, New York, 1958, edited by R. Pluukoff.

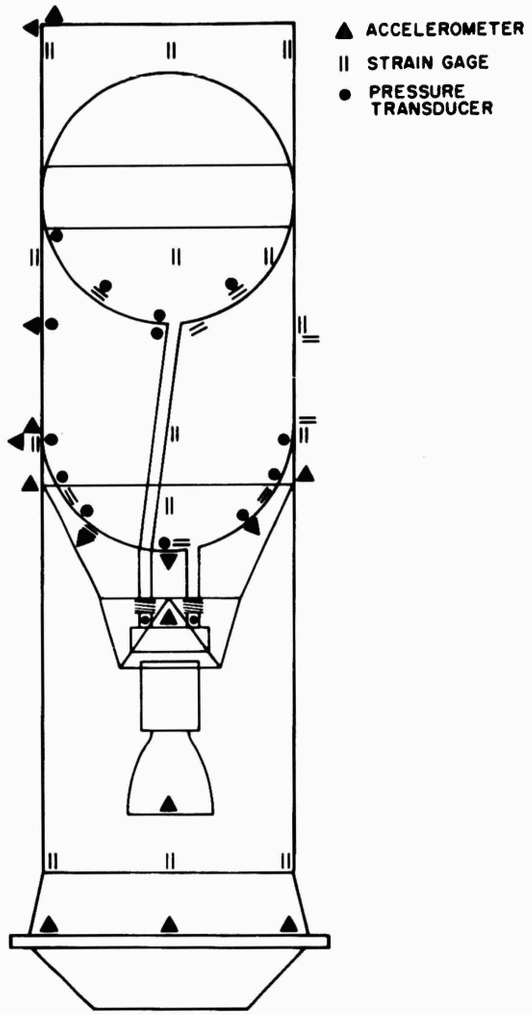

Fig. 8 - Instrumentation

coefficients is to add a heavy weight to the top of the vehicle. An analysis showed that a weight equal to half the weight of the vehicle would be adequate to give good accuracy and thus this approach was adopted.

TEST RESULTS

Continuous pressure data of the Agena oxidizer tank bottom has been obtained from one flight. This data point correlates quite well with the data extrapolated from the commutated pump inlet pressures. By plotting the pressure level versus oscillatory acceleration level during the buildup of the oscillation, it was also confirmed that the pressure varies linearly with acceleration.

The result of the modal test is not available at this time. However, in conjunction with qualifying an advanced tank which as far as dynamic representation is concerned is very similar to the old tank, very interesting results were obtained and this turned out to be an excellent "dry run" for the forthcoming test. The main differences between the two tests are that only the large 15,000-pound shaker was used, the

instrumentation was far less extensive, and the time available for this test very limited.

Some unexpected problems were encountered during this test. The 20-cps region was of special interest, but some extremely violent excitation of antisymmetric shell modes of the cylindrical portion of the tank occurred and disguised all of the data in this frequency band.

The frequency of the excited mode was twice that of the input, i.e., approximately 50 cps. For safety reasons the test was planned without pressurization but the appearance of the shell mode made it necessary to pressurize the tank in order to eliminate the oscillation, or at least shift it out of the range of immediate interest. As analysis is underway at LMSC to predict shell mode frequencies and mode shapes of pressurized liquid filled cylinders, the pressure was increased in steps to obtain the effect of pressure on frequency and amplitude. Figure 9 shows that a pressurization of 15 psi almost completely eliminated the high frequency response and increased the driving frequency at maximum response from 23 to 31 cps.

In the region between 40 and 52 cps considerable excitation of shell modes was also observed which made it difficult to search this region for structural frequencies. These vibrations appeared to be unaffected by changes in pressure.

Analysis of the test setup indicated a first natural frequency of 56 cps. No resonances were observed in this region, but several were found between 40 and 52 cps; however, due to the above mentioned shell mode excitation these were very difficult to pinpoint. Bandpass filter analysis is being performed to attempt to define the natural frequency and the associated mode shape.

It is of interest to note that a further refinement of the above mentioned dynamic tank model (which is presently being checked out) including the interaction between the fuel tank bottom and the oxidizer, predicts a frequency 10 cps lower than the earlier model.

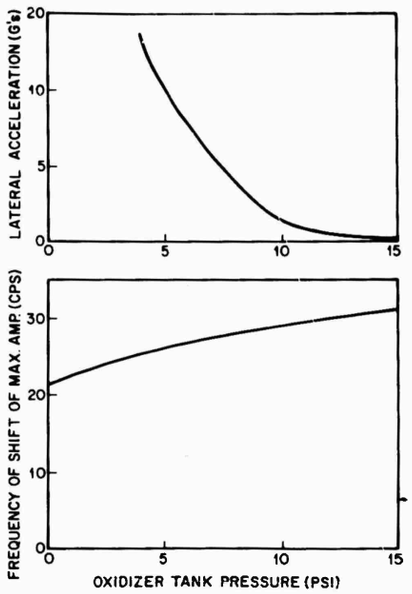

Fig. 9 - Shell mode characteristics

CONCLUDING REMARKS

A method of determining more accurately the dynamic behavior of liquid filled tanks using an elaborate theoretical model correlated with ground vibration test of a full scale tank and flight test data has been described. Preliminary data indicates that a further refinement of the tank model is necessary. The most obvious shortcoming of the present model is that the interaction between the fuel tank bottom and the oxidizer has not been taken into account. A model with this feature has been developed and is presently being checked out.

* * *

VIBRATIONAL ENERGY LOSSES AT JOINTS IN METAL STRUCTURES

Eric E. Ungar
Bolt, Beranek and Newman Inc.
Cambridge 38, Massachusetts

Experimental and theoretical results are discussed relating to the vibrational energy dissipation at riveted, bolted, and spot-welded joints between metal panels, beams, and supports. Some conclusions are drawn concerning the mechanisms responsible for this damping.

INTRODUCTION

Vibration engineers up to a few decades ago paid little attention to the damping of structures, and justifiably so. They knew that such damping essentially affects only the decay of free vibrations and the forced response of structures at resonance; free vibrations were seldom of consequence, and resonances could be avoided by proper design. More recently, however, engineers have been required to predict and to control the vibratory responses of extended structures to intense wide-band excitation, such as that from rocket noise. Here one usually cannot design practical structures whose resonances fall outside the excitation frequency range; and damping plays an important role in limiting the structural response. One must be able to estimate the damping in order to predict response; and of course, one also desires to understand the mechanisms responsible for damping in practical structures in order to be able to design configurations with favorable damping characteristics with the minimum weight or economic penalty.

Much useful information is available concerning the vibrational energy-dissipation properties of materials and homogeneous structures,[1,2] and concerning the design of highly damped structures incorporating viscoelastic (rubbery) materials.[3,4] The damping associated with slip at some simple structural joints has also been studied to some extent.[2,5-7] Very little work seems to have been done, however, on damping of the ubiquitous built-up structures (such as aircraft fuselages, which consist of numerous panels and reinforcing members joined together by various fastening means), particularly at frequencies above the fundamental resonances of the substructural panels.

The damping of a built-up structure is found to be much greater than that of a similar one-piece plate or shell; a one-piece structure may be made to ring like a gong when struck, whereas a built-up structure emits only a dull thud. Measurements indicate that, for example, one-piece aluminum

[1] B. J. Lazan, "Damping Properties of Materials and Material Composites," Applied Mechanics Reviews, 15, 81-88 (1962).

[2] B. J. Lazan and L. E. Goodman, "Material and Interface Damping," Chap. 36 of Shock and Vibration Handbook, Edited by C. M. Harris and C. E. Crede (McGraw-Hill Book Co., Inc., New York, 1961).

[3] J. E. Ruzicka, "Damping Structural Resonances Using Viscoelastic Shear-Damping Mechanisms," J. Eng. for Industry (Series B of Trans. ASME), 83, 403-424 (1961).

[4] E. E. Ungar, "Loss Factors of Viscoelastically Damped Beam Structures," J. Acoust. Soc. Am., 34, 1082-1089 (1962).

[5] L. E. Goodman, "A Review of Progress in Analysis of Interfacial Slip Damping," Sec. II of Structural Damping, Edited by J. E. Ruzicka, Am. Soc. Mech. Engrs., New York (1959).

[6] T. H. H. Pian, "Structural Damping of Simple Built-up Beam with Riveted Joints in Bending," J. Appl. Mech., 24, 35-38 (1957).

[7] L. E. Goodman and J. H. Klumpp, "Analysis of Slip Damping with Reference to Turbine Blade Vibration," J. Appl. Mech., 23, 421-429 (1956).

panels possess loss factors[8] of the order of 10^{-4}, whereas loss factors of the order of 10^{-2} were measured on a typical aircraft fuselage sections.[9,10] Since all-metal built-up structures differ from similar one-piece configurations only in that they incorporate joints, one is led to conclude that the damping observed in built-up structures must be associated primarily with their joints. (It has been shown that the addition of reinforcing beams to a panel increases the energy it loses to the surrounding medium as sound.[11] However, one finds that for typical aircraft structures in contact with air this increase is much too small to account for the observed damping differences between practical composite structures and one-piece shells or panels.)

In order to provide guidelines for designers and data for analysts (particularly those concerned with the newly developed energy methods[12,13] whose utility is at present limited to some extent by the unavailability of damping information) the U.S. Air Force is currently sponsoring a study aimed toward increasing our understanding of the dominant mechanisms responsible for the damping of structural joints, developing means for predicting such damping, and obtaining joints with increased damping.

The emphasis of this study is on joints that are structurally acceptable and that do not aggravate the usual joint strength problems, nor introduce new ones. (For example, little attention is paid to loose riveted joints, which are subject to fretting corrosion and fatigue.) Joints including such additions as gaskets or adhesive layers are not considered here because of the added complication and because some available theories[4] may suffice; and, since the purpose of designing damping into structures usually is the avoidance of large amplitudes, this study is primarily concerned with small amplitudes.

Some results of this study are described below, in the context of previous work.

RIVETED JOINTS IN BEAMS

Low Frequencies and Large Amplitudes; Nonlinear Behavior with Interfacial Slip

Pian and Hallowell[14] and Pian[6] analyzed the damping of I-beams with plates bolted to their flanges. The good agreement they obtained between their theoretical and experimental results shows that Coulomb (dry) friction between the flanges and cover plates is the dominant energy dissipation mechanism at the low frequency (quasi-static) and relatively high amplitude motions with which they were concerned. Goodman and Klumpp[7] studied the damping action of a cantilever composed of two identical leaves held together by a uniform pressure, a structure related to a built-up beam, as well as to a press-fit joint. They also dealt with quasi-static loading and large amplitudes, assumed energy losses to be due to Coulomb friction, and confirmed their assumption experimentally.

Goodman[5] has pointed out that the aforementioned cases involving Coulomb friction are special instances of a broader class of interfacial slip problems, in all of which the effective joint stiffness is amplitude dependent, the energy dissipated per cycle varies as the cube of the exciting force range, and there exists an optimum value of interface pressure for which the damping is maximum. (No slippage occurs

[8] Damping magnitudes throughout this paper are given in terms of the loss factor η, defined as the ratio of energy dissipated per cycle to 2π times the maximum energy stored during a cycle, for a system vibrating at steady state. The loss factor is a more general measure of damping than the more familiar damping ratio c/c_c since the former involves no implicit assumption concerning the damping mechanism or its linearity. For linear systems $\eta = 2c/c_c$, where c denotes the viscous damping coefficient, and c_c the critical damping coefficient.

[9] It should be noted that the damping of a panel or other substructure which is part of a larger structure cannot readily be measured. The usual methods reveal only the rate at which energy leaves the panel of interest, not its energy dissipation; much of the energy lost by the panel may be transmitted to other portions of the structure and be dissipated elsewhere.

[10] M. A. Heckl, R. H. Lyon, G. Maidanik, and E. E. Ungar, "New Approaches to Structural Vibration Analysis and Control," ASD-TDR-62-237 (Apr. 1962), AD-290-798.

[11] G. Maidanik, "Response of Ribbed Panels to Reverberant Acoustic Fields," J. Acoust. Soc. Am., 34, 809-826 (1962).

[12] R. H. Lyon, "An Energy Method for Prediction of Noise and Vibration Transmission," Shock, Vibration and Associated Environments Bulletin No. 33, Part II (Feb. 1964) p. 13.

[13] I. Dyer, "Response of Space Vehicle Structures to Rocket Engine Noise," Ch. 7 of Random Vibrations, Vol. 2, Edited by S. H. Crandall (The M.I.T. Press, Cambridge, Mass., 1963).

[14] T. H. H. Pian and F. C. Hallowell, Jr., "Structural Damping in a Simple Built-up Beam," Proc. First U.S. National Congress of Appl. Mech., ASME, New York (1952), pp. 97-102.

at very high interface pressures, hence no energy is dissipated. At very low pressures slip occurs readily, but the friction forces are low, so that again little energy is dissipated. Maximum energy dissipation occurs at an intermediate pressure, where both slip and friction forces are appreciable.)

In linear (viscously or viscoelastically damped) structures the stiffness and loss factor (or damping coefficient) are independent of amplitude, and the energy dissipated per cycle varies as the square of the amplitude. The previously discussed structures with joints in which Coulomb friction dominates thus behave nonlinearly. Such behavior has also been observed in full-scale aircraft structures at low frequencies and large amplitudes.[15]

Higher Frequencies; Observed Linear Behavior

Mead[16] measured the damping due to a cover plate riveted onto a flange of a partially cut-through I-beam and found it to behave linearly up to considerable amplitudes. Essentially linear behavior over a wide range of frequencies and amplitudes was also observed[10] on joints cut from the fuselage of a production aircraft. This linearity indicates, of course, that other than ideal Coulomb effects must dominate the damping of these joints.

The aforementioned experiments carried out on actual aircraft beams (stringers) with attached sections of skin, and on modifications of these structures, also provided some other results[10] which may help one understand something about the damping mechanisms involved:

1. Beam-and-skin samples with riveted and spot-welded connections, and with rivets replaced by well-tightened nuts and bolts, all gave very similar damping results. The important damping action in such joints is thus evidently not associated with the connectors themselves.

2. Removal of every other rivet had little effect on the observed damping. Further removal of every other of the remaining rivets produced a small increase in damping. Repetition of this process led to the point where a considerable increase in damping was observed when only a few rivets were left. This experiment provides further evidence that damping here is not associated with the connectors themselves or with their immediate vicinity; if it were, the observed damping would have been proportional to the total number of rivets.

3. Loosening of the rivets or the addition of lubricant at the beam-skin interface produced increases in damping, which were greater with looser rivets and less viscous lubricants. This, as well as the previous result, may perhaps be explained by an increase in some component of relative motion that increased looseness or lubrication permits. (The usual aircraft structural joints probably are made with interface pressures which are much greater than that which may result in very high damping; however, joints that are much looser than those in common use may be expected to be basically unacceptable for structural purposes.)

4. Beams with wider faces in contact with the skins provided greater damping. This result shows again that more of the beam face width is involved in energy dissipation than the area nearest the connectors.

SUPPORT JUNCTIONS

Theoretical Results for Some Postulated Damping Mechanisms

The damping of beams and plates attached at their ends or edges to rigid supporting structures has been studied by Mentel.[17] Although he was primarily concerned with supports incorporating viscoelastic inserts, he did present analyses of beams (and circular plates) with short portions of both ends (or all edges) inserted into slots and subject to Coulomb friction. His beam and plate analyses are analogous; for the sake of simplicity we shall discuss his work henceforth only in terms of beams.

Mentel considered the damping of end-supported beams to be produced by the axial (translational) relative motion between the beam ends and the supports, with the relative motion caused by the shortening of the distance between

[15] D. O. Fearnow, "Investigation of the Structural Damping of a Full-Scale Airplane Wing," NACA TN 2594 (Feb. 1962).

[16] D. J. Mead, "The Damping, Stiffness and Fatigue Properties of Joints and Configurations Representative of Aircraft Structures," WADC-University of Minnesota Conference on Acoustic Fatigue, Edited by W. J. Trapp and D. M. Forney, Jr.; WADC TR 59-676 (Mar. 1961), pp. 235-261.

[17] T. J. Mentel, "Vibrational Energy Dissipation at Structural Support Junctions," Sec. IV of Structural Damping, Edited by J. E. Ruzicka; Am. Soc. Mech. Engrs., New York (1959).

the beam ends that occurs as the beam is deflected; he also assumed the beam ends in contact with the supports to be rigid and the Coulomb friction forces to be uniformly distributed over the contact area. The amplitude and frequency dependences of damping implied by his analysis are discussed later, in conjunction with those implied by some other models of dissipation mechanisms.

In keeping with the slip-damping analyses described by Goodman,[5] we extended Mentel's work to take into account finite stiffness of the beam ends in contact with the support and the associated likelihood of the occurrence of slip over only a portion of the contact area. In addition, we carried out analyses that describe how the damping (or power dissipation) of a center-driven beam or narrow plate varies with amplitude and frequency, for the various damping mechanisms listed in Table 1 assumed as acting at the support junctions. The calculated amplitude dependences of power dissipation are given in Table 1, so that they may be compared with the experimental results presented below. The related frequency-dependences are strongly influenced by the beam resonances; their other properties are of less interest here and will be described elsewhere.

SOME EXPERIMENTAL RESULTS

In order to obtain a better understanding of the damping of end-supported beams we performed a number of experiments on narrow panels with their ends bolted to a rigid and massive jig, as shown in Fig. 1. In one set of experiments each test panel was driven at its center via an impedance head and the time average power supplied to the panel (equal, in

TABLE 1
Relation Between Energy U_d Dissipated per Cycle and Beam Deflection Amplitude Y, for Various Mechanisms Acting at Supports; $U_d \propto Y^n$

Energy Dissipation Mechanisms	Exponent n
I. Mechanisms associated with relative motion tangential to interface	
A. Coulomb friction	
1. Rigid beam ends, slipping fully[a]	2[b]
2. Elastic beam ends, slipping over part of contact area	4 to 6[c]
B. Shear of thin layer of asperities	
1. Perfectly plastic layer	2[b]
2. Work-hardening plastic layer	>2[b]
3. Viscoelastic layer	4
C. Viscous friction over entire interface	4
II. Mechanisms associated with rotation and relative motion normal to interface	
A. Coulomb friction associated with relative motion of asperities, motion normal to interface	1[b]
B. Compression of thin layer of asperities	
1. Viscoelastic layer	2
2. Perfectly Plastic layer	1 to 2[b]
C. Viscous friction associated with relative motion of asperities, motion normal to interface	2

[a]Corresponds to Mentel's Analysis.[17]
[b]Value shown applies above threshold amplitude for occurrence of mechanism.
[c]Depends on friction distribution.

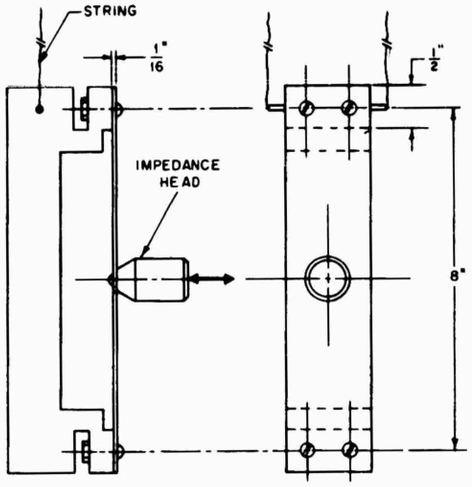

Fig. 1 - Arrangement used in support junction damping experiments

the steady state, to the dissipated power) was determined[18] as a function of frequency and amplitude. In a second set of experiments the rates of decay of free vibrations were measured after exciting the panel at one of its resonances and moving the driving system out of contact with the test panel. Although some experimental problems associated with the extremely small average power values we want to measure have not yet been fully resolved, the measurements we have obtained so far do provide some useful information.

Figure 2 shows a typical result plotted on linear scales, and Fig. 3 shows a logarithmic cross-plot of the same data. The driving point velocity is seen to remain proportional to driving force up to a quite sizeable velocity-amplitude; at amplitudes above the "nonlinearity threshold" this proportionality is no longer maintained. A discontinuity is observed at a certain amplitude, and nonlinear behavior continues at still higher amplitudes. The slope of a line fitted to the points of Fig. 3 that fall below the nonlinearity threshold is found to be 2.0; this and the previously noted velocity-force proportionality indicate that the system at small amplitudes indeed behaves linearly and as if it were viscously damped.

The discontinuity of the curves of Figs. 2 and 3 appears to be associated with the occurrence of gross slip, as indicated by the test panel deflections observed after driving the panel at various levels. After having been driven above the "discontinuity" level the panel was found to remain bowed (as if it had buckled due to axial forces acting at its ends); after having been driven below this level the panel was found to return to the initial flat configuration it had before the excitation was applied.

The slope of the line in Fig. 3 corresponds to the exponent to which Table 1 refers. Thus, this experimental result shows that those mechanisms for which the exponent differs markedly from 2.0 cannot dominate the damping behavior of this test panel below the nonlinearity threshold. Slopes of 2.0 were observed also for other modes and other panels at other frequencies and interface pressures, except that somewhat higher slopes (up to 2.5) were obtained for very low pressures. There appears to be a qualitative as well as a quantitative difference between the behavior of "tight" and "loose" joints; it seems likely that some mechanism with a higher associated exponent comes into play in looser joints in addition to the mechanism with exponent 2.0 which predominates in tight joints.

It was also found that for the range of interface pressures studied (0.1 to 12 in.-lb bolt torque, corresponding to about 2 to 240 lb force per screw[20]) the damping at a given frequency (or mode, allowing for the small shift in resonance frequencies produced by changes in joint pressure) and amplitude in the linear behavior region decreased monotonically as interface pressure was increased. Curves of damping versus interface pressure, however, were found to become flatter for higher values of pressure; that is, a given change in pressure had less effect at higher interface pressures.

[18] The impedance head provides two simultaneous signals: one proportional to acceleration, the other to force. Suitable instrumentation[19] then permits one to obtain a signal proportional to the instantaneous product of force and velocity (mechanical power) and the time-average of that signal.

[19] D. Noiseux, C. Dietrich, E. Eichler, and R. Lyon, "Random Vibration Studies of Coupled Structures in Electronic Equipments, Vol. II," Bolt Beranek and Newman Inc., Report No. 1061 (Oct. 1963). (To appear as ASD Technical Documentary Report.)

[20] Interface pressures were known in terms of bolt-torque. The torque-tension characteristics of the screw-nut-washer arrangements used were measured by means of a specially constructed jig. For the range of torques discussed here tension, and hence interface pressure, were found to be proportional to torque for all practical purposes.

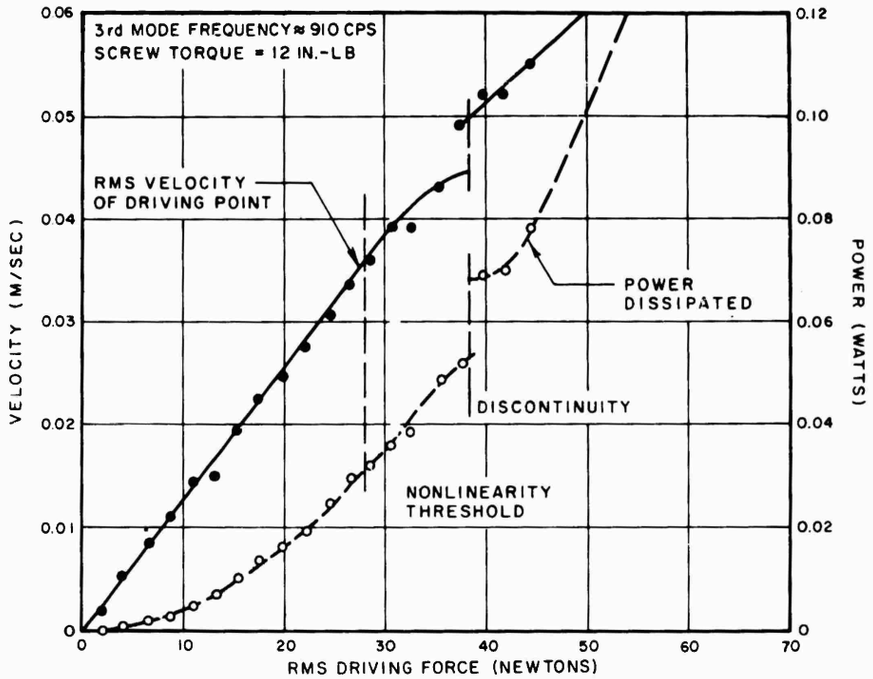

Fig. 2 - Typical amplitude effects measured on panel of Fig. 1

Analyses based on the assumption of elastically deforming beam ends slipping over part of the support contact area (in the axial direction) also indicate decreasing power dissipation with increasing friction force. They do not account for any flattening of the damping-vs-pressure curve, but the flattening observed might be due to the occurrence of a nonproportionality between pressure and friction force at higher pressures. The assumption of fully slipped rigid beam ends results in a predicted increase of power dissipation with interface pressure. This trend disagrees with the experimental observations, hence this energy dissipation model evidently is not applicable here.[21]

The results of a series of vibration decay measurements, however, seem to indicate that the energy dissipation mechanism dominant at low amplitudes is not associated with axial slip. The decay rates of test panels, mounted on jigs like that shown in Fig. 1, were measured for two configurations; in one configuration the panel was mounted as shown in the figure, in the other the panel was attached as a cantilever to only one side of the jig, facing away from the jig center. For damping mechanisms associated with axial slip one would expect to find the panel in the original configuration (attached at both ends) to be much more highly damped than the same panel mounted as a cantilever. But no great difference was observed; the loss factors of a given test panel in the two configurations were found to be roughly the same (and constant over all three or four modes of each configuration at which measurements were made). In some cases the loss factor per supported end was even found to be greater for the cantilever than for the two-support condition.

The loss factor values obtained from these decay measurements were found to exceed the values measured for a freely suspended panel by a factor of roughly 100. Great care was exercised in the experiment in order to eliminate spurious effects produced by the jig support, by the accelerometer used to sense the

[21] No relation between interface pressure and damping may be established for the other postulated mechanisms of Table 1, unless one introduces additional assumptions concerning the pressure-dependence of the various mechanisms. Since the results then are dominated by these assumptions, for the choice of which one has little basis, these results provide little information concerning the applicability of the postulated mechanisms.

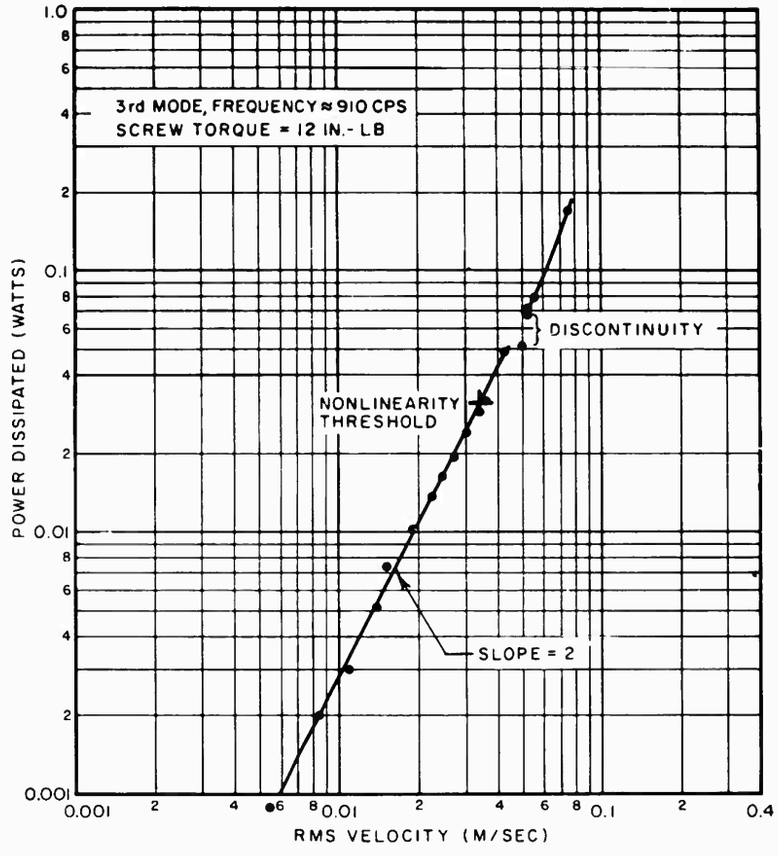

Fig. 3 - Power dissipated as function of amplitude for panel of Fig. 1

motion, and by the accelerometer cable. Hence, the previously described results cannot be ascribed to the dominance of material over joint damping, or to experimental errors, and evidently indeed describe the damping behavior of the joints investigated.

PLATES WITH REINFORCING BEAMS

The damping of plates due to joints between them and attached reinforcing beams or bulkheads should have some features in common with that of narrow panels attached to rigid supports, as described in the previous section, since the latter configuration may be visualized as a special case of the former (i.e., for rigid and massive reinforcing beams and for normal incidence of plate flexural waves on the beams). The previous results should thus have some bearing on the low-frequency behavior, say, of an aircraft panel bounded by stringers and bulkheads; however, the high frequency behavior may be expected to be affected also by the presence of plate waves with other than normal incidence and by the finite stiffness and mass of the reinforcements.

Absorption Coefficients of Structures Attached to Panels

The damping behavior of panels with attached reinforcements can probably be best described (or estimated) in terms of the absorption coefficient concept introduced by Heckl[10,22] in analogy to similar coefficients commonly used in acoustics. He reasoned that a beam-joint

[22] M. Heckl, "Measurements of Absorption Coefficients on Plates," J. Acoust. Soc. Am., 34, 803-808 (1962).

or other one-dimensional dissipative elements on a plate extract energy from flexural waves propagating along the plate (and randomly incident on the beam-joint) in a manner analogous to that in which an acoustically absorbent panel in a room extracts energy from sound waves travelling around the room (and impinging on the panel randomly).

From Heckl's analysis one finds that the effective loss factor η of a plate may be expressed as

$$\eta = \eta_o + \frac{\lambda \Sigma \gamma_i L_i}{\pi^2 S},$$

where γ_i denotes the absorption coefficient of the i^{th} dissipative plate boundary (or attachment) portion; L_i the length of this portion; η_o denotes the loss factor of the plate by itself (without dissipative boundaries or attachments); S the surface area of the plate; and λ the wavelength of bending waves on the plate.[23] The indicated summation is to be taken over all boundaries (and attachments).

The absorption coefficient γ_i is a dimensionless quantity, defined as the ratio of the power dissipated by the i^{th} boundary to the power (in the incoming waves) incident on it. The derivation of the above equation assumes that the wave field on the plate is diffuse, that the wavelength is considerably smaller than the mean free path ($\lambda << \pi S/\Sigma L_i$), that the boundary structures are several wavelengths long ($\lambda << L_i$), that the dissipative effects of the various absorbing boundaries and attachments add linearly (are proportional to length) and do not interact, and also that the absorption coefficients are independent of amplitude. Heckl[10,22] has demonstrated experimentally that these assumptions are valid for a diverse collection of boundary structures (at frequencies that are high enough for the wavelengths to satisfy the aforementioned restrictions) up to considerable amplitudes, and we have done the same for a variety of bolted-on beams.

The utility of the previously displayed equation is two-fold: (1) it shows how one may determine the absorption coefficient of a given boundary structure, perhaps in order to compile a catalog of these coefficients; and (2) it shows how one may predict the loss factor of a panel with given dimensions and boundary attachments from a knowledge of the pertinent absorption coefficients.

It would be most useful if one could compute the absorption coefficient of a given boundary structure from analytically derived results. Unfortunately, the details of the processes occurring at the interfaces are as yet insufficiently understood to permit meaningful analyses to be performed, except for the special cases of damping tapes or viscoelastic strips[10] which are of little interest here. For riveted or bolted joints one must, at present, be satisfied with empirical data, with some insight into the mechanisms involved, and with an appreciation of which parameters are most important.

In order to study the effects of various factors on the absorption coefficients of bolted-on beams we embarked on a series of experiments using a plate like Heckl's, as shown in Fig. 4. These experiments consisted of measurements of the loss factor η_o of the bare plate and of the loss factor η of the plate with various attached beams. We then could compute the loss factor contributions $\eta - \eta_o$ of the attached beams, and subsequently their absorption coefficients from their known total length L (the free plate edges having $\gamma_i = 0$). All loss factor measurements were made by observing vibration decay rates in third-octave bands, in order to avoid the effects of individual modes and at the same time retain some frequency resolution.

Our study shows that at the higher frequencies the loss factor contribution $\eta - \eta_o$ (which is proportional to the absorption coefficient) of an aluminum beam bolted onto a given aluminum plate, in general:

1. is proportional to total beam length (verifying the additive property of absorption coefficients);

2. is roughly proportional to the width of the beam-plate contact area;

3. increases with increasing beam stiffness;

4. appears to be little affected by interface pressure, particularly for pressures high enough to produce structurally acceptable joints;

5. shows peaks, when plotted against frequency, at frequencies where the bolt spacing corresponds to integral multiples of the half-wavelength $\lambda/2$ of bending waves on the plate (see Fig. 5); and

[23] λ may be computed from $\lambda \approx \sqrt{1.8\, h c_L / f}$, where h is the plate thickness, f is the frequency (cycles/unit time), and c_L is the velocity of longitudinal waves in the plate material. For steel or aluminum, $c_L \approx 2 \times 10^5$ in./sec.

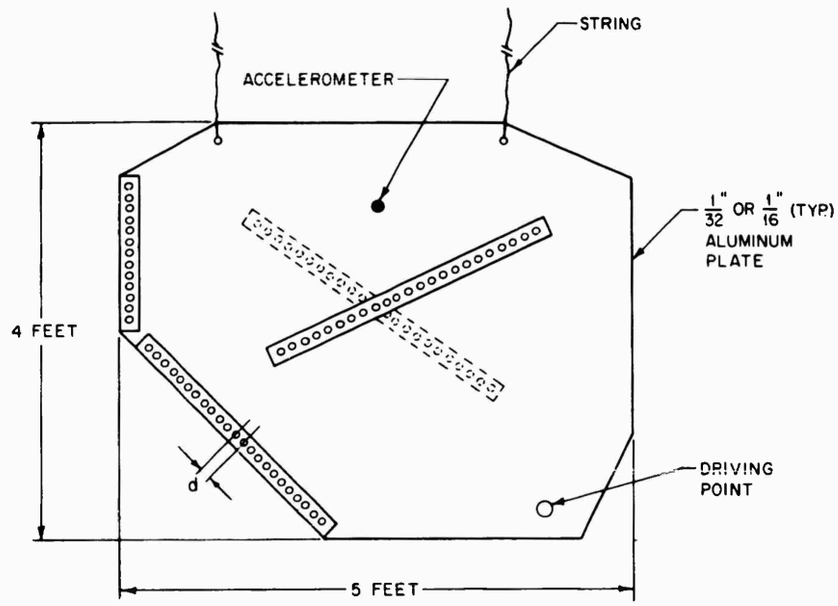

Fig. 4 - Plate used for absorption coefficient study

6. decreases markedly if the beam portions between bolts are prevented from contacting the plate (e.g., by use of washers inserted between beam and plate, placed on the bolts) or are forced in tight contact with the plate (e.g., by metal spacers clamped between beam and plate in the regions midway between the bolts).

At low frequencies the beams produce so little added damping that changes in their damping contribution produced by changes in the various parameters investigated could generally not be resolved by the experiment. However, there did appear to exist a relatively clear trend indicating that at low frequencies the effect of beam stiffness is the reverse of that observed at high frequencies.

The previously summarized results lead one to conclude tentatively that the damping of beams attached to plates:

1. is not associated with the connectors or the interface in the immediate vicinity of the connectors, particularly at the higher frequencies, and

2. probably occurs due to small-amplitude slapping or interface-squashing in the region between connectors.

Further investigations, including examination of the waveforms generated by small accelerometers attached at various positions along the beams while the plate is driven with a pure sinusoid, and stroboscopic observation of a beam-plate system made of rubber (to bring the phenomena of interest into lower frequency regions, where visible amplitudes can be obtained with available shakers), tend to confirm these conclusions.

CONCLUDING REMARKS

Considerable progress has been made toward understanding the mechanisms that dominate the damping of structures with bolted, riveted, or spot-welded joints, and toward providing means for estimating the damping of practical joined structures. Much work remains to be done, however, before such estimates can be made accurately and reliably for all significant structural combinations.

Results available to date indicate that the mechanism dominating the energy dissipation in built-up beams and similar structures vibrating at low frequencies and relatively large amplitudes may be described in terms of Coulomb friction and partial slippage at the interfaces. The low amplitude damping of edge-supported panels at low frequencies, and of end-supported beams at all frequencies, is probably dominated by (as yet not fully identified) mechanisms associated with normal or

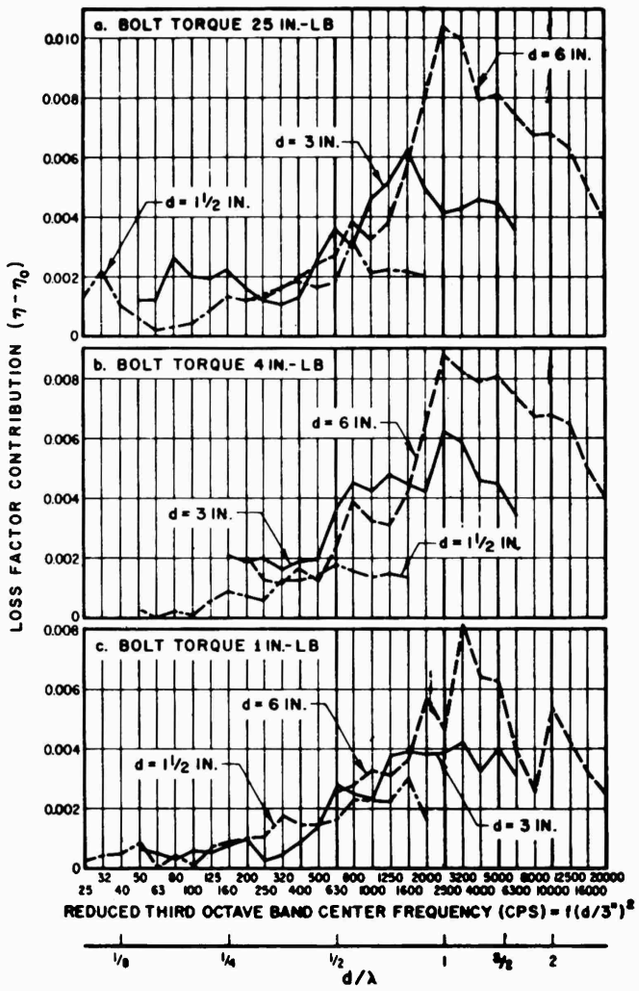

Fig. 5 - Effect of bolt spacing d on loss factor contribution; measured on arrangement shown in Fig. 4

rotational motion rather than with tangential slipping relative to the supports, but the aforementioned friction mechanism may also play some role. The damping of edge-supported or reinforced panels at high frequencies on the other hand, appears to be primarily due to slapping or squeezing occurring at regions of the interface not at or near the connectors.

Further work planned under the current program includes attempts at providing or extending analytical bases for some of the phenomena observed, as well as a number of experimental studies. The latter include investigations of the effects of interface surface roughness and cleanliness, and of judiciously placed drops of lubricants and dissipative materials. Also planned are experimental studies of multiple-row riveted and of continuously welded joints, and of simply implemented joint modifications that may improve damping.

Dr. Burgess (United Technology Center): A suggestion was made yesterday that damping could be improved in structures by simply putting a layer of damping tape between the two surfaces being riveted. What does your research show about this?

Dr. Ungar: Mead, of Southampton University has written a report which describes how to optimize the damping of overlapping joints by the insertion of a viscoelastic layer. However, if I understood the response yesterday correctly, the layer of tape was not inserted for damping purposes primarily, but it was inserted as an elastic connection between the surfaces in order to reduce the stress-raising effect of the rivets.

Mr. Forkois (NRL): Would you expect a reduction in the fatigue life by increasing these damping characteristics? Have you considered this at all in any of your tests?

Dr. Ungar: We have done no fatigue tests, but I feel that it stands to reason that some increase in the fatigue life can be obtained with an increase in damping because of the decrease in the overall response. If this is true, then the damping action occurs at those panel areas which have relatively low stresses under normal conditions. This would homogenize the stress distribution and I feel would increase the fatigue life.

Mr. Roberts (Aerospace Corp.): Even though you didn't mention it in your paper, do you have any experience with epoxy bonded joints?

Dr. Ungar: We have done some experimenting with epoxy bonded joints. Most epoxies are relatively rigid and have very little damping, and our experiments show that the damping of epoxy bonded joints is much less than that of the ordinary riveted joints.

* * *

Section 5
APPLICATION OF DATA TO DESIGN

DESIGN OF SPACE VEHICLE STRUCTURES FOR VIBRATION AND ACOUSTIC ENVIRONMENTS*

C. E. Lifer
Marshall Space Flight Center, NASA

The advances in design state-of-the-art for space vehicle structural vibrations have not kept pace with improvements in environment definition and testing. As vehicles become larger and more expensive, this gap must be eliminated. The need for a uniform design approach throughout the aerospace industry is presented and a proposed basis derived by the MSFC is explained.

Considerable attention and effort have been devoted during the past 10 years to the definition of space vehicle vibration and acoustic environments, and to the development of better test techniques and equipment. Instrumentation of test vehicles has grown tremendously in both the number and the range of measurements, and data acquisition systems have been improved in order to make the information more accurate and useful. The introduction and refinement of random testing equipment and procedures, the development of high-force shakers, and the increased recognition and use of acoustic testing have contributed to much more reliable space vehicles. Although there is still a wide variation in the approaches to vibration and acoustic testing, the need for these tests is now accepted by all aerospace manufacturers.

For the most part, however, efforts at optimizing design procedures for vibration and acoustic environments have been unsuccessful, and comparatively little has been accomplished in this area. There is still a widespread belief among designers and manufacturers that it is not possible to design for vibration, or that the only way to consider vibration and acoustic environments is to design for the static loads with an arbitrary factor applied to these loads to cover vibration, acoustics, and other mysterious unknown loads. The component or structure is simply tested (and often redesigned and retested) to determine its adequacy under the specification environments. It is true that this procedure usually will accomplish the end result of a satisfactory component or structure, but in many cases it will result in an overdesign or in a costly test and redesign effort.

At present there is wide variation in methods and philosophies of designing for vibration and acoustics in the aerospace industry. This state of confusion is the result of the varying experiences of manufacturers with different missile and space vehicle programs, and of the absence of a centralized controlling or monitoring agency to establish a recommended procedure which has been successfully demonstrated on several design programs. The two extremes of this variation are the total disregard of vibration loads in design and the very conservative analysis using maximum environmental levels and assumed response amplifications greater than those normally encountered in practice. The first extreme invariably requires much redesign and retesting before an acceptable product is achieved, while the latter usually produces an overweight or non-optimized design. The most desirable approach is one in which a design is based on vibratory and acoustic

*Invited paper.

loads of carefully selected probability of occurrence and based on the most thorough and accurate structural analysis possible, combined with developmental testing.

The assurance of required vehicle reliability through analysis and testing has become much more important because of the manned space flight program. At the same time, we must develop more efficient space vehicles in order to increase their payload weight capability. In order to satisfy both these requirements, design for vibration must be more accurate than it has been in the past. The technology of predicting structural response must be improved, and design procedures must be developed uniformly throughout the aerospace industry.

In order to define the reliability of a space vehicle, the reliabilities of its components must be known. If various components are designed and tested to criteria which are not compatible, or even similar, the definition of reliability of the whole system becomes impossible. Design procedures for static loads, thermal stresses, pressures, and wind loads are relatively uniform throughout the industry, but vibration and acoustics design have been left open to interpretation.

As an example, let us examine a large space vehicle now under development. The engine manufacturers do not believe in vibration load design, and since their contracts do not specifically require them to design for vibration, they use the cut-and-try method of building and testing. When vibration failures occur they merely beef up the failed part and continue testing. The first stage manufacturer is at the exact opposite pole, using a large force of dynamics analysis to calculate vibratory and acoustic forces for each component and substructure, and using very conservative load prediction techniques. The second stage manufacturer is somewhere in between the two extremes, performing limited analyses in support of design within his stress analysis section, analyzing only those items which look questionable from vibration standpoint, and using a much less conservative load prediction procedure than that of the first stage producer. The third stage is designed using still another approach to vibration and acoustic loads, and finally one payload design has as yet not considered vibration in the preliminary design analysis.

From the above information, how does one attempt to define system reliability from the vibration and acoustic aspect? The answer is that one cannot readily predict the reliability of this system design until extensive ground and flight tests have been completed. Furthermore, if the ground test specifications and procedures are not uniform and compatible, their results will be difficult to use in establishing reliability. Since design of new vehicles and their components for vibration and acoustics are based primarily on the environmental specifications, a uniform system design requires uniform specifications for all portions of that system. To further point out this problem, components and stages are often used on more than one vehicle system, and uniform design and test specifications and procedures for all systems would facilitate the selection and evaluation of these components for use on new vehicles.

The need for vibration testing of space vehicle structures and components prior to flight testing the system assembly became obvious as these vehicles grew more complex and costly, and extensive development and qualification tests are now accepted as integral parts of vehicle programs. In a similar manner, increasing complexity and cost of structural components and of test programs require good assurance before designs are released for manufacture that they will withstand their environmental vibration and acoustic conditions. This assurance can come from a proper consideration of these environments in the structural design, through analysis and development testing.

The vibration and acoustic environment conditions which are significant in design usually result from engine or stage static firings or system flight tests. The energy sources are: combustion and exhaust flow noise; turbopump vibrations; ignition, release, and cutoff dynamics; and, aerodynamic and buffeting pressures resulting from high-speed flight through the atmosphere. In addition to the conditions of static and flight tests, ground handling and transportation conditions should be covered in the environmental specifications. The sources of vibration energy are generally random in nature, but their mean level variation with frequency and time can be predicted with fairly good confidence.[1,2] The transfer characteristics of the vehicle structure modify the statistical nature of the environment in such a way that, at a typical structural section, the response

[1] R. H. Lyon and P. A. Francken, "A New Approach to The Estimation of Space Vehicle Vibration," Bolt, Beranek, and Newman, Inc., Report No. 815 (May 1962).

[2] I. Dyer, "Response of Structures to Rocket Noise," Chap. 7 of Random Vibration, Vol. 2, Edited by S. H. Crandall (The M. I. T. Press, Cambridge, Mass., 1963).

usually resembles several superposed sinusoids which have randomly varying amplitudes.

The dynamics analysts and the designers rely on the specification writers to describe the vibration and acoustics environment accurately and in sufficient detail to permit prediction of vibration loads. Some of the requirements of a good specification from the design viewpoint are described below:

1. The specification must be based on well defined and meaningful reliability values. These should be established considering vehicle or system mission, criticality of individual structures, and cost.

2. The specification must be in sufficient detail to cover the wide variation of environments which occurs between structures of different mass and geometry. It should also be specific as to whether the values listed are to be regarded as inputs or responses.

3. The definition of time or condition for which the environment applies should be included wherever possible, since vibration loads must be added to other time varying loads. Figure 1 illustrates this need.

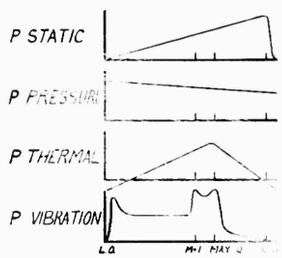

Fig. 1 - Flight time vs loads

4. The specification should be kept current so that it includes any effects of design changes, results of analyses and tests, etc. It should become increasingly accurate and detailed as more knowledge is obtained.

The effects of the vibration and acoustic environments which are important to a structural designer are the loads or stresses induced in materials and connections, and the displacements which result from these loads. The loads are response inertial loads which cannot be considered as static loads except at the point or section for which they are calculated. Similarly, the displacements must be defined with respect to points on a structure. Since the environment is basically random, the loads and displacements must be described in terms of probability of occurrence, and in terms of the contributing modal frequencies.

Assuming that the specifications have been perfected to the level or state described above, it remains for the designer and the dynamics analyst to achieve a structural design which is best suited to withstand the environments of that specification in conjunction with other conditions. The basic intent of this paper is to prescribe an organizational arrangement, and a functional procedure which will make the achievement of this end more probable and less costly in time and effort. An outline of this procedure is shown in Fig. 2.

In order to be most efficient, the consideration of vibration and acoustics must be included in the preliminary design or concept phase of structural development. The reason for this is quite well known to dynamics analysts who have had to recommend that a design be changed extensively in order to have better dynamic characteristics. Once a design concept has been studied from the normal aspects of weight, static strength, producibility, and the like, it is very difficult and costly to convince the designer, as well as management, of the necessity for changing the design, thus requiring restudy and reevaluation. During the preliminary phase, the configuration and material selection are most readily influenced, and parameter studies can yield valuable results. An illustration of this is shown in Fig. 3.

The preliminary design phase is an appropriate time to consider the use of materials and fabrication techniques which will improve the vibration and acoustic response characteristics of a structure. These practices and materials have been in existence for several years, yet their use is still resorted to only in problem areas where standard techniques have proved unsatisfactory. The usual practice is still to modify the equipment to take the structural response environment rather than design the structure to have a minimum environment. I submit that we are reaching the limits of the use of such a philosophy. This subject has been

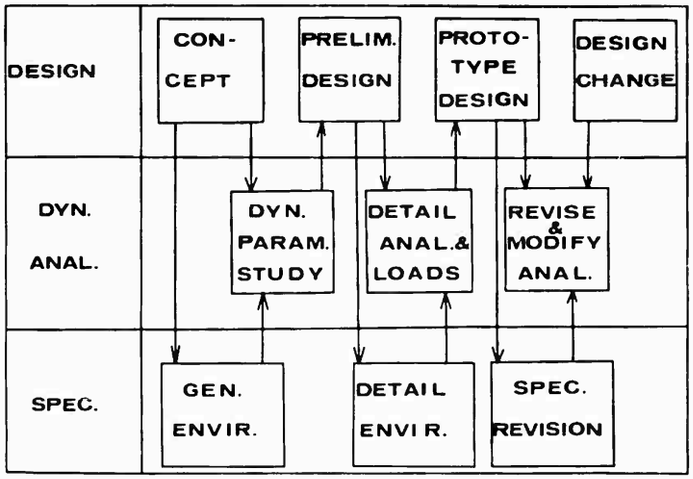

Fig. 2 - Dynamics support of design

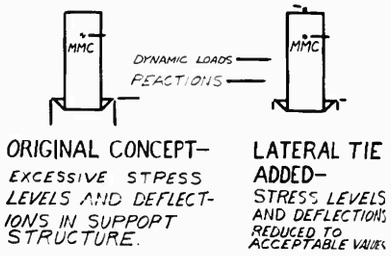

Fig. 3 - Concept analysis

treated extensively in Refs. 3 through 5, and the details will not be repeated here.

As an example of the applications of dynamics analysis to the preliminary design phase, let us take an imaginary payload structure and assume the mission of this payload, its maximum structural weight, exterior shell configuration, and vehicle location and interface definition are the only fixed or predetermined characteristics. It is known that certain components and equipment must be included in this payload, but their exact location and method of support are left to the designers. Working with the designer, the dynamics analyst can study possible configurations to compare their response to the vibration and acoustic excitations of the launch vehicle. If a particular internal component is sensitive to acoustic energy, methods of acoustic isolation such as those employed in submarines and oceanographic research vessels[6] may be employed in structural configuration. Arrangements of structure to de-tune or de-couple resonances can be studied analytically by making use of analog computers and small-scale dynamic model tests. Mountings of components which are sensitive to vibration may be studied to determine if grouped "cannister" mounting is superior to a dispersed mounting arrangement. In these studies, simple mathematical models are utilized in analysis, such as in Fig. 4.

Once the payload configuration and component locations have been established, the dynamics analyst can provide the designer with approximate vibration loads for components and structures for use in his preliminary design, and can tell him which components require vibration isolation mountings. An iterative process is then conducted, as the designer derives

[3] M. A. Hechl, R. H. Lyon, G. Maidanik, and E. E. Ungar, "New Methods of Understanding and Controlling Vibrations of Complex Structures," ASD-TN-61-122 (June 1963).

[4] E. G. Fischer and H. M. Forkois, "Theory of Equipment Design," Chap. 42, and "Practice of Equipment Design," Chap. 43 of Shock and Vibration Handbook, Vol. 3 (McGraw-Hill Book Co. Inc., New York, 1961).

[5] C. M. Harris, Editor, Handbook of Noise Control (McGraw-Hill Book Co. Inc., New York, 1957).

[6] I. P. Vatz and R. F. Williams, Jr., "Development of Noise Control Specifications for the Woods Hole Oceanographic Research Vessel," Edited by H. C. Herreshoff, New England Section, SNAME, Bethlehem Steel Co. (Oct. 1962).

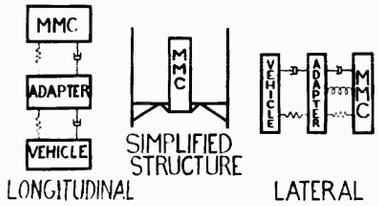

Fig. 4 - Preliminary dynamic model

structural details such as member sizes and materials and the dynamics analyst incorporates these in his study to provide more accurate loads and recommends changes. It follows naturally that as the stage of design progresses the analysis should become more and more detailed, i.e., the mathematical model of a structural system should include more mass-spring-damper elements, and sub-system studies should be made in order to provide detailed design information. Figure 5 illustrates a detailed analysis model.

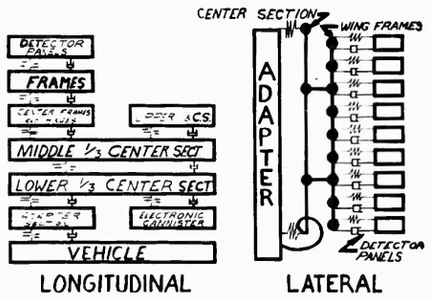

Fig. 5 - Detail dynamic models

Development tests provide valuable support to design and should be considered in any large structural development program. These tests may range from small scale model tests and tests of individual structural components through an exact replica of the system. Their purpose may be merely to provide response information (damping, and the like) about structural elements, or they may be used to select a design concept for the system. When used to supplement a thorough analysis, they permit accurate prediction of environmental response and more efficient structural design.

As was indicated previously, the support of final design is an extension and refinement of the preliminary design analysis work, making use of the results of development tests and, when possible, qualification and static firing tests. In the case of long-duration programs, designs may be improved as the result of static firing tests and flight tests. The environments, or the structural response, may be shown to be less severe than that predicted, and the need for weight savings may justify redesign for the actual environment.

One principle which should be kept in mind is that the accuracy of prediction techniques for environments and of the load calculation procedures does not warrant carrying the resulting accelerations, loads, or pressures to more than two or three decimal places. Admittedly, it is much more impressive (on the surface) to tell the designer to include an acoustic response stress of 11,976 psi in his design that it is to quote a figure of 12,000 psi, but a predicted acoustic level of 155 ± 2 db does not warrant such accuracy.

In order to accomplish the close and strong support of the designer, as was described above, it is necessary to have a strong dynamics analysis group consisting of engineers familiar with design as well as with vibrations and acoustics. The theory and methods of analysis are well established and are described quite adequately in the literature,[7-10] and can be learned by engineers with the above experience in a short while, so that with a small nucleus of dynamicists one can develop an effective analysis group in a matter of a few months. Figure 6 illustrates methods of analysis which are commonly used.

The possible organizations which may be used are diverse, but for most effective coordination one where dynamics analysis, stress analysis, and design are together under one organizational head is recommended. The most desirable are those arrangements which provide close teamwork with minimum organizational bottlenecks. When such organizational

[7] J. P. Den Hartog, Mechanical Vibrations, Fourth Edition (McGraw-Hill Book Co. Inc., New York, 1956).

[8] C. T. Morrow, Shock and Vibration Engineering, Vol. I (John Wiley and Sons, New York, 1963).

[9] H. H. Hubbard and J. C. Houbolt, "Vibration Induced by Acoustic Waves," Chap. 48 of Shock and Vibration Handbook, Vol. 3 (McGraw-Hill Book Co. Inc., New York, 1961).

[10] C. E. Crede, "Failure Resulting from Vibration," Chap. 5 of Random Vibration, Vol. 2, Edited by S. H. Crandall (The M. I. T. Press, Cambridge, Mass., 1963).

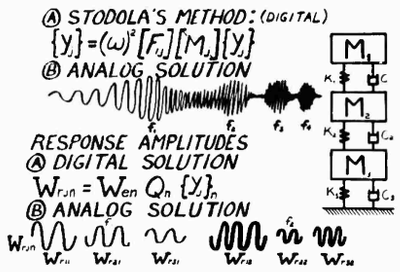

Fig. 6 - Analysis procedure

alignments as described above are not possible, an alternate arrangement would be for the dynamics analysis group to have drawing sign-off responsibility, just as the stress analysis group normally has. This does not insure the close support during the early design stage described previously, and must be supplemented by liaison activity. The effective utilization of development testing indicates the similar need for close organizational ties with a testing facility whose services would be available quickly to the analysis personnel. For a majority of these tests, a small facility would be sufficient, and large tests could be performed by other laboratories.

One of the major problems in designing for vibrations and acoustics is the selection of a "sigma level" for design, or a design factor for the levels given in the environmental specifications. Ideally, one would determine the expected number of cycles of each level of vibration and do detailed fatigue damage study to arrive at a design. This is not feasible economically, nor is it warranted by the accuracy of the specifications and load calculation procedures. It remains for the dynamics analyst, therefore, to select an optimum procedure for deriving design loads, pressure, and so on, from the specifications. This must be done considering the probability and confidence level of the specification environment, the required confidence in the vehicle design, and the manner in which the designer uses or treats the loads which are given him.

The environmental specifications derived by the Propulsion and Vehicle Engineering Laboratory at the Marshall Space Flight Center consist of acoustic specifications and random, sinusoidal sweep, and sinusoidal resonance dwell vibration specifications. In addition, shock test specifications are included. The sinusoidal resonance dwell levels have been determined to represent the optimum design vibration environment level, considering the confidence level requirements of man-rated vehicles and the design practices of contractors (as required by design criteria). The resulting design if felt to be near optimum, with an effective confidence level of 97.5 percent and a probability of 2.8 sigma for the predicted environments.

The procedure described above is not being specified as the optimum procedure, for use by all agencies because it has been shown to be perfect. Rather, it is being recommended in order to achieve some degree of compatibility in design in at least a segment of the industry. If all contractors on even one vehicle program utilize this procedure and experience similar results (hopefully they would be successful results), this could be used as a basis for deriving an improved procedure. It could be pointed to as an example of a complete system design with compatible, uniform consideration of vibration and acoustic environments.

I would like to recommend to the leaders in this field, both in government and industry, the formation of a representative working group to study the serious problem of structural design for vibration and acoustic environment. The specific areas of study would include the following:

1. What are the design practices which have been most successful in producing structures to withstand their environments?

2. In those successful practices, what was the relationship of design to specifications?

3. What was the statistical confidence in the specification environment?

4. What was the target confidence level in the successful design procedure?

5. Is the concept of uniform and compatible specifications feasible?

6. If compatible specifications is a possibility, what steps are needed to achieve this goal?

7. What research has been done, and what must be done in order to better define the optimum design procedure?

It is suggested that this working group consist of personnel from government agencies, universities, or independent laboratories. Representatives of industry and government could be requested to assist in exploring the problem areas. Should this working group derive

positive results, it should make them widely known over the entire engineering field.

With the application of the principles I have described above, and with careful study by a conscientious engineering working group, the art of designing structures for vibrations and acoustics can become a science.

* * *

SUMMARY OF DESIGN MARGIN EVALUATIONS CONDUCTED AT THE U. S. NAVAL MISSILE CENTER

C. V. Ryden
U.S. Naval Missile Center
Point Mugu, California

Incremental levels of environmental stresses are applied to missile systems to induce failures deliberately. It is assumed that those components which fail are the weakest link in the structure. Improvements to missile reliability on the basis of such test programs will be discussed.

INTRODUCTION

An interesting area in the application of environmental data is that of determining how environmental factors affect the reliability of missiles and other equipment. The Design Margin Evaluation (DME) is an environmental test technique used at the U.S. Naval Missile Center (NMC) in an attempt to determine this relationship by subjecting the test article to incremental levels of environmental intensity in an effort to determine the level (particularly shock and vibration) at which the device performs with satisfactory reliability and to determine which components fail under these environments. In other words the objectives of these tests are: (1) to determine design weaknesses in the missile; (2) to determine critical operating environmental parameters; (3) to establish a basis for estimating reliability under environmental conditions; and (4) to determine compatibility of the missile with operating environments.

This test technique has been used at NMC in connection with some of the air-to-air and air-to-surface missiles in the weight class from 300 to 1100 pounds. This technique, however, could be extended to any missile or in fact to any electronic or mechanical device, or any combination of the two.

This paper will discuss the principles of reliability and statistics as applied to the design of these tests and the results of three completed evaluations with comparison of these findings with later flight tests results.

DISCUSSION

The reliability of an equipment has been defined as its conditional probability of performing its function within specified performance limits at a given age for the period of time intended and under the operating stress conditions encountered.[1]

One of the most common parameters used to determine the reliability of a device is what is called the failure rate or its reciprocal mean time between failure (MTBF). It can be shown (Ref. 1) that the most general relationship between failure rate and reliability is given by the following equations:

$$\lambda(t) = -\frac{1}{R}\frac{dR}{dt}$$

or

$$R(t) = \exp\left(-\int_0^t \lambda(t)\,dt\right),$$

where

λ is the failure rate,

t is the time period during which the reliability is required, and

R is the reliability.

[1] I. Bazonsky, Reliability Theory and Practice (Prentice-Hall, Inc., Englewood Cliffs, New Jersey, 1961).

These equations apply no matter what the failure density function is.

In the case where λ is a constant, then the reliability function is exponential. This mathematically defines the case where failures occur strictly due to chance failures and at random intervals in time.

Besides the random or chance failures, equipment usually exhibits early failure during the early phase of its life, and wear-out type failure following its useful life.

The failure rates during the early failure and wear-out periods are usually greater than during the chance failure period. The high failure rate during the early failure period results from such things as substandard or weak parts, or improperly installed parts. This early failure period is sometimes called the "burn-in" or "de-bugging" period. Following the debugging period, as the substandard parts fail, the failure rate decreases, and reaches a minimum and more or less constant value. This period of life of the device, during which the failure rate is the lowest (giving the greatest reliability) is called the useful life of the device. During this period, the exponential failure distribution is a good approximation. As the components begin to reach the wear-out period, the failure rate starts to increase quite rapidly. A graph of failure rate as a function of age is shown in Fig. 1.

For the exponential function (Fig. 2), the reliability is given as a function of operating time which is the time measured from the start of any arbitrary time period during which reliable operation of the equipment is required. Therefore, so long as the failure rate (λ) is a constant, the exponential distribution is independent of component age. In other words, the reliability is the same for any time period of equal duration during any part of the useful life provided the failure rate is a constant. In addition to the exponential function there is another common failure distribution known as the normal distribution, shown in Fig. 3, together with associated reliability function. For the normal distribution the reliability is a function of operating life or age of the device in contrast to the exponential distribution which is not dependent on age.

The failure distribution, due to wear-out, usually follows a normal distribution. Therefore, as the equipment approaches the wear-out period, the normal distribution is then superimposed on the exponential failure distribution. The failures due to wear-out are added to the chance failures.

Providing then that the equipment is past the early failure phase and that the useful life period is many times the required operating period, the failures which occur during the useful life are strictly chance failures and follow the exponential distribution.

As expressed in the previous definition of the reliability of an equipment, two factors which affect the reliability of a device are the stress level at which the components operate, and the strength of the components. The failure rates of components change significantly even with small changes of stress level.

It is well known that both the operational environmental stress and component strengths are not discrete values but have distribution about some mean. Figure 4 shows a typical possibility of these distributions. The overlapping area under these distributions is

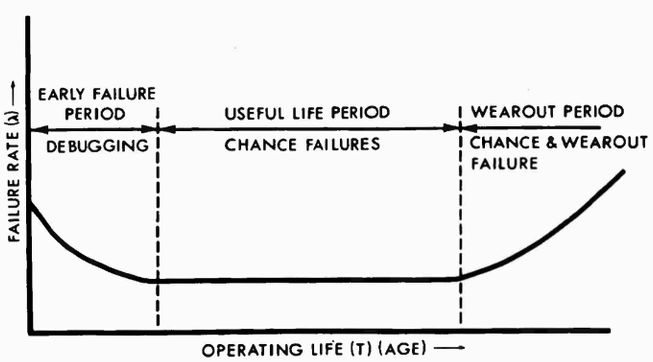

Fig. 1 - Failure rate vs operating life

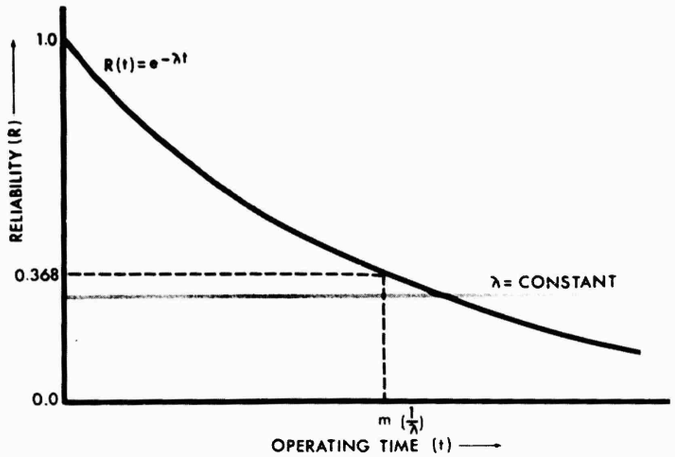

Fig. 2 - The exponential failure distribution

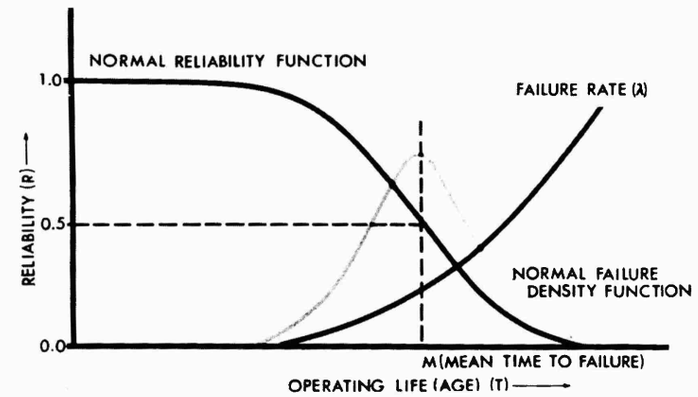

Fig. 3 - The Gaussian failure distribution

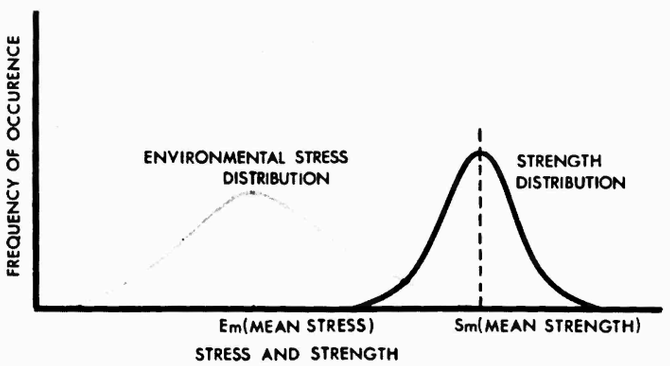

Fig. 4 - Distribution of environmental stress and component strength

proportional to the probability of failure. This overlapping area can be reduced by separating the mean stress and mean strength and/or making the distributions narrower. In other words, any combination of strengthening, quality control or mitigation that will spread the means and/or reduce the deviations of the distributions will reduce the overlapping area and result in a higher reliability.

The stress and strength referred to above, however, applies to a mixture or combination of parameters such as vibration, temperature, altitude, electrical, and so forth. With such a combination of stresses and strengths, statistical testing and analysis should be employed. Therefore, the device is subjected to various operating stresses at incremental levels; i.e., a factorial type experimental design with the various environmental stresses considered as the main factor of the experiment. During the DME, several levels of environmental stresses are applied to the missile sections; first, a level near the expected field level for tnat section, then twice and if necessary three or even four times this level, deliberately inducing failures into the components assuming that those components that fail, at least those that fail consistently, are the weakest links in the section. By observing the failure rate while being subjected to the various stress levels, one can obtain information on the influence of the various environmental factors on failure rate. The failure rate serves as a substitute for a measure of component strength. Also, regression analysis can be performed, using data obtained on degradation of missile performance during the various environmental tests.

An outline of a one-third replicate factorial experiment with missiles confounded is given as an example in Table 1. In this experiment three missiles are to be subjected to nine tests, one test at each level of three environments (temperature, altitude, and vibration). Each missile is to be tested to essentially the same duration and severity of environment.

The results from this experiment can be analyzed by standard analysis of variance and sequential test procedures. From the analysis of variance, Refs. 2 and 3, the direct effect of the four factors (vibration level, direction, temperature, and altitude), and the first order interaction effect of three of the factors (vibration level, direction, and temperature) can be determined.

In this type of experimental design, however, no information can be gained about the effect of the use of different missiles (missiles are confounded), the interaction of altitude with other factors, and all second order interactions. In other words, for example, by analysis it may not be possible to determine whether a change in failure rate is due to a variation in missiles or a third order interaction of vibration direction, altitude, and temperature.

In order to be able to determine the effect of all the interactions of the factors with a high order of significance in a design employing several factors, a large number of tests are required. In order to restrict the magnitude of the test program to practical limits, certain assumptions must be made based on past information and experience. It is usually reasonable to ignore some of the higher order interactions and perhaps the variations between missiles because these are found to be negligible; thus, permitting a test program of a practical size. In the event, however, that during the tests, higher order interactions are not found to be negligible and the test for significance yields little confidence because interactions of the factors are included in the residue in the analysis of variance, then additional tests can be conducted to give the required information and reduce the size of residue, and thus increase the significance and confidence in the test results. In other words a second one-third replicate, and if necessary, the full factorial design can be performed.

For many of the DME tests, conducted at NMC, shock and vibration have been considered the main environmental stress parameters. These tests have mainly included shock tests followed by random vibration tests simulating motor ignition shock followed by motor-induced vibration. Figure 5 shows a missile nose section attached to a shaker for longitudinal axis vibration. The missile or missile sections while being subjected to various levels of shock and vibration were operated and monitored.

A typical design for these tests is shown in Table 2. Seven missiles were used for this evaluation which consisted of 24 shock and 24 vibration tests. The sequence of the tests and the selection of the missiles for each test were determined from a table of random numbers. The levels for the shock and vibration tests were arrived at from results of several missile flight tests conducted at NMC. An estimated

[2] "Fundamentals of Analysis of Variance," J. Am. Soc. Quality Control, Vol. XIII, Nos. 2, 3, and 4 (Aug., Sept., and Oct. 1956).

[3] O. L. Davies, Design and Analysis of Industrial Experiments (Hafner Publishing Company, Newport, R.I., 1954).

TABLE 1
Test Sequence for Design Margin Evaluation

Vibration Direction	Altitude	Vibration Level								
		V_1			V_2			V_3		
		Temperature								
		T_1	T_2	T_3	T_1	T_2	T_3	T_1	T_2	T_3
Longitudinal	A_1	1				1				1
	A_2			2	2				2	
	A_3		3				3	3		
Normal	A_1			3	3				3	
	A_2		1				1	1		
	A_3	2				2				2
Lateral	A_1		2				2	2		
	A_2	3				3				3
	A_3			1	1				1	

A_1: Sea level
A_2: 15,000 feet altitude*
A_3: 50,000 feet altitude*
T_1: -40°F*
T_2: 75°F
T_3: 160°F*

V_1: First level vibration†
V_2: Second level vibration†
V_3: Third level vibration†
1, 2, and 3: Missile numbers. Testing sequence to be randomized.

*Subject to alternation based on analysis of operational environmental data.
†Levels of vibration and testing duration to be determined from analysis of operational environmental data. Vibration will consist of both random wave (simulating captive flight, motor burn, and free flight) and the sine wave sweep or narrow band random wave sweep (simulating the effect of high amplitude low frequency vibration induced during arrested landings and catapult launches).

TABLE 2
Chronological Sequence of Tests

Environmental Level	Longitudinal Shock	Lateral Plane #1 Shock	Lateral Plane #2 Shock	Longitudinal Vibration	Lateral Plane #1 Vibration	Lateral Plane #2 Vibration
1	12E 27F	2B 26E	14G 31C	5E 25D	4D 39D	1A 33E
2	15A 34F	3C 28G	16B 37B	13F 29A	6F 43A	7G 35G
3	21G 42G	8A 32D	19E 44B	18D 30B	9B 45C	11D 38
4	24G 46O	10C 41F	23B 47E	20F 36A	17C 48F	22A 40E

NOTE: 1) Letter refer to missiles.
2) Sequence of tests was taken from a table of random numbers.

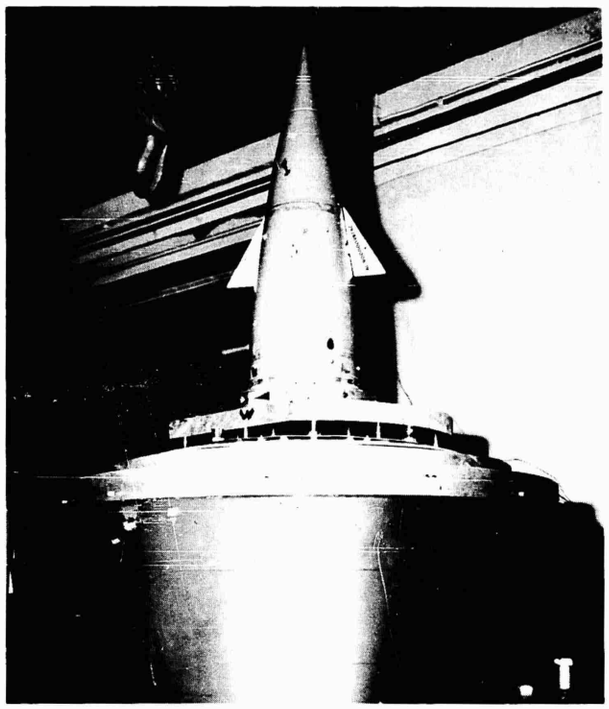

Fig. 5 - Missile nose section set up for longitudinal axis vibration

equivalent of the flight environment was chosen for the first level; the second, third, and fourth levels were made two, three, and four times the first level respectively.

During these tests a large number of failures occurred; a large percentage being in one particular component. Subsequent to these tests, flight tests were conducted using a revised model of this missile incorporating changes pointed out by the results of the environmental tests, and the results of the flight tests indicated an improvement in reliability (lower failure rate).

Table 3 shows another design in which three missiles were subjected to 54 tests at three levels of shock and vibration. The results of these tests indicated a high reliability and compared quite favorably with subsequent flight tests.

The results of these tests may be shown on graphs such as that shown in Fig. 6. This is a plot of failures versus use cycle for a particular reliability, in this case 95 percent, at several confidence levels as computed from the equation:

$$T = \frac{\tau \chi_{\alpha}^{2}(ar + 2)}{2 \ell n \frac{1}{P}}, \qquad \text{(Ref. 4)}$$

where

T is the total test time,

τ is the operation time,

χ_{α}^{2} is the chi squared value at risk level α,

r is the number of failures, and

P is the reliability.

This equation is based on the exponential failure distribution covered in detail in Refs. 1 and 5;

[4]Office of Naval Research, ONR Contract Nomr-2163(00).

[5]B. Epstein, "Test for the Validity of the Assumption That The Underlying Distribution of Life is Exponential," Technometrics (Feb. and May 1960).

TABLE 3
Sequence of Shock and Vibration Tests

Axis	Longitudinal			Vertical			Horizontal		
	S_1	S_2	S_3	S_1	S_2	S_3	S_1	S_2	S_3
V_1	1	2	3	10	11	12	19	20	21
V_2	4	5	6	13	14	15	22	23	24
V_3	7	8	9	16	17	18	25	26	27

NOTE: Each vibration test was preceded by a shock test.

S_1 - 75 g peak
S_2 - 150 g peak
S_3 - 225 g peak

V_1 - 9 g rms
V_2 - 18 g rms
V_3 - 27 g rms

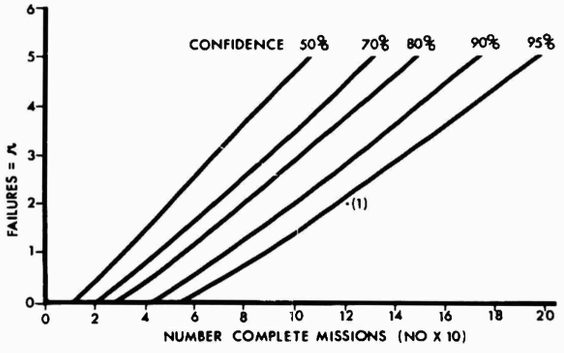

Fig. 6 - Number of failures vs number of missions for 95-percent reliability at several confidence levels; results of test

i.e., that the missile is being operated in the useful life phase (that failure rate is constant) and that the failures are chance failures. This equation also includes the fact that the number and duration of tests are limited and, therefore, the reliability must be expressed at a level of confidence. An example of this analysis follows: consider two failures (r) occurring during the tests, a total test time (T) of 360 seconds, an operational time (τ) of 3 seconds while being subjected to motor-induced shock and vibration. Then considering all shock and vibration tests, and assuming that the first level is equal to or exceeds the in-flight motor-induced environment, and noting that two failures occurred during these tests, it can be shown by the use of the above equation that the resulting reliability is at least 95 percent at the 95-percent confidence level, as indicated by the point marked (1) on Fig. 6.

Other DME tests have included low temperature-vibration and high or low temperature-vibration-altitude combined environments. Examples of these are shown in Table 4.

In conjunction with flight test data, laboratory transmissibility tests have been conducted. The objective of the transmissibility tests was to determine the transmissibility of shock and vibration from one section, primarily

TABLE 4
Sequence of Tests

Test	Axis	Level 1	Level 2	Level 3
Shock Room Temperature and Sea Level Altitude Condition	Longitudinal	1	10	19
	Vertical	2	11	20
	Horizontal	3	12	21
Vibration Room Temperature and Sea Level Altitude Condition	Longitudinal	4	13	22
	Vertical	5	14	23
	Horizontal	6	15	24
Vibration Low Temperature and Altitude Condition	Longitudinal	7	16	25
	Vertical	8	17	26
	Horizontal	9	18	27

NOTE: Shock

Level I	
Longitudinal	70 g peak 0.015 sec duration
Vertical and Horizontal	40 g peak 0.015 sec duration
Level II	
Longitudinal	140 g peak 0.015 sec duration
Vertical and Horizontal	80 g peak 0.015 sec duration
Level III	
Longitudinal	210 g peak 0.015 sec duration
Vertical and Horizontal	120 g peak 0.015 sec duration
Vibration	
Level I	7 g rms random noise for 60 sec
Level II	14 g rms random noise for 60 sec
Level III	21 g rms random noise for 60 sec

the motor section, to several locations at other points within the missile. This type of test together with mechanical impedance studies is useful when a missile structure is changed slightly or when a different motor is used with the missile.

The results of the tests referred to in the foregoing tables are given in more detail in Refs. 6-10. The reliability, indicated by these laboratory environmental tests compared closely to that indicated by subsequent missile flight tests. During several of the tests, weak areas were pointed out, and after these areas were strengthened, an increase in reliability was also demonstrated during subsequent missile flight tests.

It is felt that Design Margin Evaluation tests should be conducted as early as possible during the development phase of a missile, and that the results of these tests should be taken into consideration for possible design improvements, and also that design improvements should be continued until acceptable reliability and confidence have been demonstrated and that compatibility of the missile with operating environments have been determined.

[6] J. B. Overton, "Phase I of Design Margin Evaluation of Model XAAM-N-6a SPARROW III Missile," USNMC Technical Memorandum No. NMC-TM-60-61 (Nov. 18, 1960).

[7] J. B. Overton and P. R. Elam, "Phase II of Design Margin Evaluation of Model XAAM-N-6a SPARROW III Missile," USNMC Technical Memorandum No. NMC-TM-61-33 (June 15, 1961).

[8] P. R. Elam and R. G. Whitlock, "Phase III of Design Margin Evaluation of Model XAAM-N-6a SPARROW III Missile," USNMC Technical Memorandum No. NMC-TM-62-35 (Aug. 1, 1962).

[9] C. V. Ryden, "BULLPUP Transmissibility Design Margin Evaluation and Criterion for Missile-Engine Compatibility," USNMC Technical Memorandum No. NMC-TM-61-65 (Apr. 4, 1962).

[10] U.S. Naval Missile Center letter report to Bureau of Naval Weapons Ne144/nn, Serial 0351, of Aug. 15, 1962. Subject: WEPTASK No. RM-372P-086, BULLPUP ASM-N-7a (Maxson) Design Margin Evaluation Letter Report.

Mr. Himelblau(Nortronics): In one of your earlier slides, you indicated that reliability is a function, shall we say, of the mean environment, the variation in the environment, the mean strength, and the variation in the strength. Yet, in the rest of your paper you didn't talk about these factors. How do you reconcile that we would be able to determine the reliability without knowing each of these four functions?

Mr. Ryden: The slide showing the distribution of strength and stress is qualitative. It would be pretty hard to come up with actual detailed information on these factors, but it does show that as you increase the environmental stress towards the strain, you are increasing this overlapping area and increasing the possibility of failure.

Mr. Himelblau: I grant you that. It shows that you are going to increase the reliability and yet you talk about specific reliability numbers. It's hard for me to see how you get those reliability numbers without knowing those four variables. Did you determine the mean environment and the variation within that environment for those missions?

Mr. Ryden: The environmental level was an estimate of the equivalent flight level. In other words, we looked at several records of flight data.

Mr. Himelblau: Did you establish the mean level and the variation of the level?

Mr. Ryden: Yes, the mean values.

Mr. Himelblau: Well, how can you determine your reliability then, if you do have a variation in the flights and you just consider the means? You should know the standard deviation of that variation, shouldn't you?

Mr. Ryden: Well, we didn't -----

Mr. Himelblau: I grant that you can ignore it, but the reliability figure that you have for the one is not the same as the reliability figure for the other.

Mr. Ryden: You are limited in your flight test data, maybe you have data from five flights -----

Mr. Himelblau: Yes, but you said you ignored the variation.

Mr. Ryden: They were reasonably close to each other.

Mr. Himelblau: In other words, you make the assumption that the variation between flights is small compared to the mean value.

Mr. Ryden: Right, the standard deviation is small.

* * *

PANEL SESSION

THE USE OF ENVIRONMENTAL DATA IN DESIGN

Moderator: Dr. John C. Burgess, United Technology Center

Panelists: J. M. Brust, Nortronics
E. G. Fischer, Westinghouse
P. A. Franken, Bolt, Beranek, and Newman
J. T. Risse, Sandia Corp.

An edited version of the discussions which took place during this panel session follows. Not all comments are included since some were repetitions of statements that were made earlier.

INTRODUCTION BY THE MODERATOR

Design can be defined as the process by which shapes and sizes of various materials are chosen and integrated to provide a unit which performs a predetermined function. Although there is ample opportunity for demonstration of artistic talent, success in the engineering sense depends upon the unit performing its function satisfactorily over a prescribed lifetime. Since weight and cost are often important considerations, the materials involved must be used efficiently. This, in turn, requires an adequate stress analysis.

Stress analysis involves many facets, such as choice of methods of analysis, numerical techniques, and amount of simplification of the physical problem. A particularly important facet is the determination of the proper physical properties, including failure criteria, of the materials chosen for the design. Most important to the subject of the panel discussion on "The Use of Environmental Data in Design," however, is the facet often called simply "loads."

"Loads" is the term many engineers use to describe the complex of conditions in which the unit being designed must survive and must perform its function. It is thus a generalized synonym for "input conditions," or for "environmental data." These different terms are pertinent to this discussion, since they emphasize the problem of communications. They are usually used by separate groups of people having different technical backgrounds, all of whom are dealing, however, with the same basic problem. This problem, the use of environmental data in design, forms the subject of the panel session. Discussion of the panel session was directed to some extent by the four topics:

1. How Environmental Data Should be Presented;
2. How New Environmental Information Should Get to the Design Engineer;
3. How New Environmental Data Should Get Into Specifications; and
4. How Design Engineers Should Use Environmental Data.

The major points made by the panel members on these topics are:

1. Data can be presented in many different forms; thus any form can serve a useful function.
2. Data should be presented in the form which the particular design engineer can best use; thus the form of presentation depends upon the extent and type of the design engineer's background and experience.
3. Data, especially current data, most often get to the design engineer through

specialist groups; thus cooperation between design and specialist groups is necessary.

4. Data get rapidly into specifications only through people; thus responsibility for so doing must be assigned to specific personnel.

5. Design engineers must understand environmental data in order to use same; thus a system, including the manner of loads presentation, should be complicated only to the extent that the design engineer can visualize the response.

6. A good design engineer must have experience.

Following the introductory remarks by, and discussion among the panel members, audience participation was invited on each of the four topics in turn.

DISCUSSION

Mr. Schwartz of the U.S. Navy Marine Engineering Laboratory commented on work being done by his organization. "We are engaged in compiling an acoustic library of vibration data taken on nuclear submarines, destroyers, and other kinds of ship. The data are taken on ship service turbine generator sets, main propulsion systems, and items of this nature. Of course, most of the data are classified, but it is available to the Navy. If, for example, they wish to determine a specification level for a new turbine generator set, they can run through the compiled data to see how the vibration level has evolved for a series of turbine generator sets. Perhaps on this basis they can make a comparison."

Dr. Burgess asked, "In what form is this data?"

Mr. Schwartz said that it is digitized for storage on magnetic tape, but he was not sure how it was analyzed.

Dr. Burgess asked for any further comments or questions concerning how environmental data should be presented.

Mr. Fest of Aerospace Corporation questioned Dr. Franken concerning the presentation of data. "Would you accept an overall rms value from zero to 2000 cps as a definition of the environment? I don't think you would, but I think there should be some limit as to how wide you will go? How wide do you think we should go?"

Dr. Franken said that the answer to the question was, in part, yes. "Since we are talking about the use of environmental data for design, we could take an overall level from zero to 2000 cycles if the designer is only going to integrate from zero to 2 kc and talk about an overall level. I don't think that is very neat, however. I do think that third octaves are, in general, a very satisfactory compromise. They give you enough detail so that if something really sticks out you will see it. With full octaves you sometimes do not. On the other hand, if you go down to your 5- or 10-cycle bands, you will be there all day on each piece of data, as you know. As you saw in the summaries that Dr. Curtis presented a couple of days ago, you smear it out anyhow. I happen to favor third octaves. I think they are a reasonable compromise."

Mr. Gray of the STL said he didn't believe that data should be presented to designers. "I believe that the data should be presented to some sort of criterion group which will wring every bit of significant evidence out of it. If it is a spectral analysis, it should be a very narrow band spectral analysis. If they are transient data, they should, perhaps, include the raw data. This criterion group should in turn convert this to a specification. The specification should then be given to the designer. Typically, these data do not represent the missile or the aircraft under consideration. The data are gathered from other missiles and aircraft and, therefore, has to be interpreted. The job of interpretation is not with the equipment designer."

Dr. Burgess asked, "Aren't we doing that now?"

Mr. Gray said, "Yes, but the question concerned the form in which the data are to be presented to the designer."

Dr. Burgess continued, "Your point is that the form in which the data are now presented is satisfactory."

Mr. Gray said that this was correct as long as the data are presented to the people developing the criteria in the form which is the most explicit. He did not consider something like overall rms explicit.

Dr. Franken said that he didn't consider it explicit either. "I think, however, that we're agreeing that we want to work with the designer

as closely as we can and in his terms. If that's all that he is ever going to get out of the data, then I think we are cheating ourselves to give him them in some other form. We have to work on his terms. As Dr. Fisher said earlier, he is the one who is going to lose his job when this thing blows up. Let's work with him, in his terms, and educate him as much as we can."

Dr. Burgess said, "This is a very natural transition to the next question, how new environmental information should get to the design engineer. Are there any questions on this subject, or comments?"

Dr. Curtis of Hughes Aircraft Company said his comment pertained to both questions. "I tend to reinforce Mr. Gray with respect to dynamic data and with respect to the design of equipment rather than basic structure. I don't believe we should give environmental data or even try to define dynamic loads to the designer. This is partly because it is embarrassing when he comes back and asks us to interpret and analyze the designs against the loads that we have given him and we find ourselves unable to do so. I think, in a less facetious vein, that we should give him our best interpretation, as analysts, of a reasonably equivalent static load which appropriately accounts for frequency and effective mass effects. If we cannot do this, surely the designer cannot. We should give him a simple load of this kind, and tell him to design to the best of his experience in the field. When he has done this, he should come back and let us analyze to see how it responds to the best of our experience and capability. I believe we will save a lot of confusion that now arises when we give designers rather exotic design requirements that we do not understand ourselves."

Dr. Burgess asked, "Is it a part of your point that analysis is only effective if you have something to analyze?"

Dr. Curtis responded, "Yes, I think I could agree with that. I would also say that it is not the input which will make a design good or bad, it is the response. If we do not know what the response will be until after we have designed it, let's not burden the designer with trying to predict a response numerically. He can design it better by the seat of his pants; after it has been laid out and dimensioned, then let us go and analyze it."

Dr. Burgess asked if his basic comment suggested that information to get to the designer should be in the form of a specification of an equivalent static load?

Dr. Curtis said, "Either that or just say nothing. You see, there are certain circumstances, for instance, on missile or aircraft equipment, where there are maneuvering steady load factors to which he is capable of designing. He has a dynamic environment which presumably can be superimposed on top of that. I think if you just give him a steady load factor environment and he designs as he knows best to that one, 90 percent of the time he will meet both without even trying."

Mr. Risse agreed that information should get to the designer through the specialist groups, since, as was said, if anyone in the organization is able to do anything with the data, they should be. He also agreed with Dr. Franken that these specialists can get a feel quickly for what the designer is capable of doing with the information given him. The designer should be given what he can use, and only what he can use. The design really can not be checked until it is in existence. Mr. Risse emphasized that all organizations should be set up so that there can be personal contact and a meeting of the minds on what is needed and what can be used.

Dr. Burgess commented, "Perhaps we can say that the design environmental data should be complicated only to the extent that the design engineer can understand how to use it."

Mr. Mutter of the Boeing Company said, "We work very closely with our project people in the design of our vehicle. The project group, our stress group, and our dynamics group are tied together. We go through an iterative process in the design. We give preliminary design loads to the designers who make preliminary layouts and come back when they have to change thicknesses and so on. Working personally with the designers and the stress group, we check each and every design. Although it may take two or three iterative processes until they finally come up with an adequate design, we very seldom give them the basic environments or even the spec. We normally talk with them, get the preliminary design, do frequency calculations, compute responses, give them the loads, and so on until we get a satisfactory design."

Dr. Burgess commented on the obvious spirit of cooperation among the people in these groups.

Mr. Mutter agreed. "Our designers look upon us as specialists in the field. They feel they do not have the time to do it and that we can do a better job. We have very good cooperation within our organization in this respect."

Dr. Burgess asked whether his group has responsibility for the structural integrity.

Mr. Mutter answered, "We have responsibility for the dynamic aspects of the structural integrity. We supply all the dynamic loads information to a stress group which has to sign off the stress analysis on all the design items."

Mr. Houston of Norair pointed out that the maturity of a design in a modern missile is not evolutionary, but revolutionary. "We might find that the techniques that the designer uses emphasize the objective of the design. In other words he designs for the function, rather than for the environment. Unless he is designing shock mounts, or something like that, the subject of the operation is making the design work within a system. Now, the general technique in using standards in this design, or specifications that are modifications of standards is experience. The experienced designer designs it just as he did last time unless somebody tells him to make it a little better, a little stronger, or a little more useful for a specific task. Where you do not have experience is in a brand new task or with brand new people. They have to rely a lot more on the environmental laboratories and facilities to give them the information to be incorporated into a design from a dynamic standpoint. I do not think that we are talking about starting from scratch under any circumstances; we are talking about making one just like it was last time with slight changes."

Dr. Franken suggested that the central problem is failure criteria. "Mr. Lifer referred to it in his paper. He said that you take the environmental data and compare them with the failure criteria. Then you find out if you need shock isolation, or redesign, or what. Where do we get the failure criteria? In your firm with these experienced designers, where do they get failure criteria?"

Mr. Houston asked, "Failure criteria with respect to what?"

Dr. Franken replied, "I don't know. Design with respect to what? I would think the design would be with respect to some failure criterion in some fuzzy way. In other words, it works or it doesn't. If they are doing a good job of design, it means that it's not failing. Now, where does this success come from? I think it comes from tests and experience. How are we going to get this information and get it to the designer, if we have to get it to the designer, in some meaningful form? This is where we need the most work, not in refining our predictions, not in refining our descriptions, but in the description of the failure criteria."

Mr. Houston continued, "There are two types of failure that can be incorporated into a design. One of them is failure of a previous design, that the designer has to know about so that he can make corrections in his initial design. The other type of failure is the failure in the designer's product, in a laboratory operation. I do not believe that we are so naive as to say that the designer does not know about this, because he has to work with this type of information he is not that far away from his design."

Dr. Franken responded, "No, I don't believe we are naive, but it seems to me that both your types of failure are established and checked through laboratory and field tests. Ultimately, that's where you end up."

Mr. Brust interjected a comment. "Dr. Franken says that most of the time we get our failure criteria doing tests, and this is definitely the wrong way to go. If the dynamicist consulting with the design engineer becomes familiar with the functional aspects of the design, he will be in a position to try to determine the failure mechanism of the item under design. By understanding the specification the way he does and working with the designer, many times he can eliminate failures long before they ever get into test. Understanding the environment as he does and interpreting the environment to the designer, he can, with the designer, pretty well pick and choose and develop a design with components that have a good chance of passing a specification. Here we are talking about black boxes and hardware, not necessarily primary structures. It is only the cognizant type people who also have an understanding of the environment who should get on board with the designer. You can not make suggestions to these designers if you do not understand what they are trying to accomplish. You have to understand what that mechanism is going to do. You have to understand how his electronic devices operate. Obviously, this is where you have to lean on their shoulders, as well as they lean on yours, to have you interpret the specs for them."

Dr. Franken indicated that he seemed to be in the middle. "Dr. Curtis says you cannot analyze this very well, and I tend to agree with him. Mr. Brust says you can do it without tests. I just do not know where you get failure criteria."

Mr. Brust said that he did not say without tests, but a lot can be done before one gets to tests.

Dr. Franken agreed. "You should be using good design practice. I think the experience that Dr. Fischer refers to is extremely important. The heart of the matter here is that we need to get good seat-of-the-pants feel on how to use the data as best we can. Ultimately, our idea of when a thing malfunctions is based on the fact that it malfunctions. Mechanical relays are the only thing that I know that have been handled analytically."

Mr. Kirkley of the Martin Company wondered why Dr. Franken was questioning where the criteria come from to start with, since Dr. Franken is working in that particular field.

Dr. Franken responded, "I am saying that the only origin I know for these criteria are field and laboratory tests on similar items. When you go into a brand new item with a radically new design and a whole new suspension system internally and the like, you have got to get out and shake it, or rattle it, or roll it, or whatever."

Mr. Kirkley indicated that he thought Dr. Franken had been talking about design criteria, but Dr. Franken pointed out that he was talking about failure criteria.

Mr. Kirkley said, "I do not think that is quite in keeping with the subject we are discussing here. From the engineering standpoint, I think what the designer is going to do is design for a criterion presented in a specification. He is not going to go to tests-to-failure. If you get into a discussion regarding cost and quantity and units to be tested, and so forth, you will soon find out that you would go out of business trying to do this. What the designer is going to aim for is to meet that design criterion with a slight margin based on his experience. He eventually is going to get into a qualification test phase, which sometimes comes from the same spec document and sometimes from another one. When he meets these criteria, both he and his employer have met their obligations to the government, or whoever the prime contractor may be. One thing that I have found is that too many designers use the test as the design goal and they do not pay any attention whatsoever to the design criteria. Many of our tests do not simulate the conditions for which he should be designing. One good example of this is the acceleration factor. We cannot test to some of the accelerations that the missile sees. The designer designs for the test in this case, and I think it is erroneous. We are having quite a problem educationally in my own firm, trying to get people to realize that we should get away from the tests and look at the design criteria, think about them, and study them. Use the environments you are in, or relate them as if they could happen at the same time, and you will have the best product. You will be assured of meeting the test."

Dr. Franken offered a final comment on this question. "I think that failure criteria do enter in this way. The design criteria are established through negotiations, calculations, and crystal ball gazing, and the designer has to meet them. He still has to know whether the component, as he originally receives it, will meet the design criteria, or does he have to make a modification to the design. In some way he has to know what the safe levels of operation for his component are. Independent of the design criteria, he has got to have the failure criteria in the back of his mind. If you do not have that information somewhere in experience or documented, we are going to have problems when we get to the test just as you described."

Mr. Forkois of NRL commented, "Well, of course, there are excellent points in all the panel members' discussion. Mr. Brust indicated that other documents (other than specifications) should be made available which would help the designer. I'm strongly in favor of this. These could be in the form of design guides which synthesize not only good and fairly uncomplicated mathematical analyses, but also, the results of practical experience and basic philosophies which are so important in the design of reliable equipment. You cannot create designers overnight. You cannot take a young man out of school and start talking to him about what we have been discussing today, and expect him to design a missile structure. Even in the formulation of design guides, experienced and knowledgeable engineers and scientists are likely to have disagreements in basic philosophy.

"As a result of all the years that I have been attending symposia, I have come to the conclusion that the best designers can do, is to design an efficient structure, which means putting the weight of structural materials in the places where it will do the most good. But, how is this done? I think the answer is that the structure must be designed for stiffness and lightness — the lighter the structure is, the stiffer it will be and the stronger it will be. This implies high structural frequencies. This is the ultimate that can be accomplished with a given structural weight allocation. This method may not be a perfect answer but surely it will reduce significantly the number of design problems.

"The only other way to resolve our technical problems would be the invention or creation

of materials with infinite strength, zero weight, and last but not least, zero cost. In this way meetings of this kind could be rendered unnecessary."

Dr. Burgess said, "We have been talking on only two of the four subjects. That is why this has gone on as long as it has. Let's switch the compass for a moment to the third one, how new environmental data should get into specifications. The comment made on this by the panel was essentially that we should create a new document which is a source of such information, rather than continually changing the specification documents themselves. Are there any questions or comments specifically directed toward this subject?"

Mr. Root of Collins Radio Company commented, "I happen to work mostly in the vibration and shock areas. When you start talking about compiling the data in just these two areas, you are now talking about a library of books. I don't see how such a document is feasible. In other words, how do you get enough meaningful information in one location?"

Mr. Brust responded, "We don't necessarily have to compile the data from every system of the last 10 years. A committee that would work on a document of this sort could select representative weapons systems from the various types of missiles, and document only those. I do not really believe that this would be as voluminous as you describe. I personally feel that using something like 25 missile systems today would suffice to give us a generalized feeling for what the environments would be with ballistic type missiles, airborne missiles, polaris type weapons, and so on. As we increase our number of systems yearly, we can add one or two to this document, and I think we would stay pretty much up to date. Now, mind you, you do not need to use all systems because this is only a guide. My feeling regarding this document is that it is not intended to be the new specification for the new systems. The prime contractor will develop the detailed specifications. MIL STD 810 or our old MIL-E-5272 normally never were the final qualification test specs. In general, the prime contractor develops a new specification based on a detailed study of the mission profile and the details that go along with the system he is going to design. I think all of us could agree that to develop a general specification for a given type of system is almost an impossibility, without a tremendous amount of conservatism built into the spec."

Dr. Fischer offered a generalization regarding the presentation of data. "Some of the early textbooks I used were those written by Den Hartog and Timoshenko. If you look at these books, some of the early ones, they were essentially cookbooks. They gave case histories of a lot of failures, a lot of problems which showed great ingenuity in either recognizing the problem or solving a problem. Since those days, I think the tendency has been to generalize and use more mathematics. We are inclined to seek some kind of an organization whereby somebody, without exercising intelligence or experience, can somehow use the method and get the same results that these early experts did, apparently intuitively. I think this is the problem. No matter how many handbooks you write, it is still a question of getting it across to a person and having him use it with the tools he has available."

Mr. Mutter of the Boeing Company said that in compiling a list of the various environments of all of these vehicles, we have to be very careful in inserting these into a new specification. "I know in our particular vehicle we are extrapolating from one to another. You can take levels on one vehicle, but you have to consider the type of structure, the material properties, the weight of it, and so forth, when you are trying to extrapolate to another vehicle. You have to consider the external acoustic effects if the vibrations are primarily acoustically induced, and there are frequency shifts in your spectra. So, to interpret or extrapolate the environment realistically from one vehicle to another, you almost need to take a look at your drawings and see what type of structure you have, as compared to the type of structure you are anticipating in your new vehicle. I do not think you can take one vehicle 100 feet long and another 150 feet long and boost your environment accordingly. I think there's more to it than just a simple comparison of the environments."

Dr. Burgess interjected, "There's an interesting philosophical point that flows through our entire conversation. We seem to be trying to put the whole subject matter in such a form that we will not be needed, but what we are really finding out is that no matter how we put it, we are still going to be necessary."

Mr. Risse commented, "I am one of those who feels that the hardest environments to cope with are the induced environments. With induced environments, any hardware affects its own environment. I think that this basic fact means that a specification is, or should be, as individual as fingerprints. Gross generalizations of specifications may be well for guidance purposes, but guidance, in my mind, is not the

same thing as specifications. If you make what you call a specification very general in nature, it is no longer really a specification. A specification is the sort of thing that you use in a contractual sense, and it should be very specific. It may indeed be something that gives a lot of us difficulty because we try to pin it down before the fact. We cannot really tell what the specification should be ahead of time. As I think somebody said, the specification must be fluid, it must be a changing sort of thing, and must be negotiated constantly."

Mr. Eustace of the Martin Company said he would like to expand on a generality that had been mentioned several times. "I am in a position where I am between the specification writer and the designer, essentially supporting and assisting in the writing of specs and assisting the designer in conforming to these specifications. But I have a problem. Let us say that I know my specification exactly. For example, in shock, let us say it is 100 g for 5 milliseconds, or 15 g for 20 milliseconds, or something like that. How do I go to that designer and intelligently tell him how to design his system so that he will have confidence in me. When his system works with reservation, or maybe does not work, will he come back to me next time assured that I will give him a good answer? Our job is to help him and he recognizes that this is our function, but how do we help him. In this specific case of shock for example, what do we do? Do we arbitrarily take a pulse width and say that any time your pulse width is greater than 25 milliseconds, call that a static equivalent design load and design for that case, or should we take another approach?"

Mr. Risse referred to his previous remarks. "This is a personal sort of thing. You determine the best way to help him simply by sitting down with him and finding out how much he knows, how much he is capable of using."

Mr. Eustace continued, "Let us say he is a typical designer, one who is relatively inexperienced in the field of shock and vibration, and that he is relying entirely on me for guidance. He has no feel for the subject whatsoever, which is a situation that we constantly run into. He will rely completely on my statements. I am, in theory, a specialist. I am supposed to be the one who will give him this answer, but I am, in many instances, unable to give him an answer that will satisfy my own conscience."

Mr. Risse said he didn't see why. "It sounds to me as though in practice you are the designer. If you give guidance and it cannot be understood, maybe you do not have a designer."

Mr. Eustace explained that in his organization the design people are not asked to assume the responsibility for stress and dynamic support. "They are to come to us for assistance and our difficulty is in giving them the counsel which they require. We are the specialists and should be able to answer these questions. I have posed this question many times before at various meetings and have never been able to get a concrete answer."

Mr. Risse said the problem was very serious if the information cannot be boiled down to the best static equivalent load that the designer can understand.

Mr. Eustace asked, "What is a static equivalent load? This is a term that is bounced around a great deal and after 7 years working with designers, I still do not have an answer."

Mr. Risse said, "If you were talking about a shock, as you were a moment ago, then you calculate maximum response and give him that load as a static load."

Mr. Eustace asked whether we would honestly ask him to make that structure good for 150 g, or 1000 g, as the case may be.

Mr. Risse said he was not in a position to appreciate all the kinds of hardware that might exist. "I think that there are appropriate numbers for certain kinds of structures and they may not be the same for all structures. The peak response may not be appropriate for a yielding type of structure, if you can allow yielding as part of the normal function of a single shot operation. On a frangible or brittle material peak response may very well be the failure criterion you need to use. I think that you are in a position to help make the judgment as to what the failure criterion should be."

Mr. Eustace said he wanted to straighten the record out. "We do what we can in coming up with an intelligent design. We will work with the designer, study his design, and come up with a number. We decide on a certain thickness or chassis structure, or a certain amount of reinforcement, or what have you, and we come up with a design that probably will work. This is experience, but our stress people want design criteria. If we have 1000 g for 0.5 millisecond, certainly we are not going to ask for 1000 g statically on a complex structure. They laugh at us, and we realize this."

Mr. Risse did not think they should laugh for certain kinds of structures. Perhaps for other kinds of structures they should.

Dr. Franken commented, "I think you have hit on a point that should bother everyone here. Thank goodness your conscience is bothered. I think the point is the failure criterion. We do not know it and no one else does. We ought to be looking at the shock on similar pieces of equipment and determining what the shock spectrum is, if that is the form you want to put it in. Then we should find out if the shock spectrum for this particular piece that you are analyzing exceeds it, and if it does, you are in trouble."

Dr. Fischer said to Mr. Eustace, "Sometimes it is just a case of lucking out. There are other considerations more of an active performance nature which give you sizes and thicknesses and weight. To a large extent, with the environment and with the response, you look for problem areas. Most of the time it looks OK based on an ordinary yield point. If it gets a little close, you look a little harder, and perhaps if you visualize yielding as helping you, you design 20 percent beyond the yield point. Under other conditions such as resonance, you may try to introduce damping. Sometimes you go all the way and isolate the piece. I must admit that all we are doing is eliminating weaknesses. Having eliminated as many weaknesses as you can, you tend to approach what we call a one horse shay design; however, you still have not optimized the design. For years we have wound up with stronger, heavier structures, but they do not necessarily get off the ground. With that extra criterion that we have to get off the ground, we have to optimize. It is not what we have been doing."

Mr. Fest of the Aerospace Corporation felt that the big problem was that people try to use numbers in a quantitative, rather than a qualitative way. "We should not try so much to design to an environment, but rather we should tell the designer the things he should do and should not do when he designs a package. A booklet or pamphlet, or something with basic rules should be provided to show what to do and what not to do when you design a box. These rules will change with the level of the environment. The do's and don't's will change in going from a 5-g environment to a 50-g environment. Do not try to tell the designer he has a certain environment to meet, but tell him what he should do and what he should not do for this certain package."

CONCLUDING REMARKS BY THE PANEL

Dr. Franken: "Let me be very negative. I do not see any significant advancement to come about in the analysis and presentation of data. I would also go further and say, prediction of environmental broadband random data such as that which we have been talking about here will not be advanced significantly by the type of procedure for analysis and study that we are now pursuing. On the other side of the coin, I think the significant advancements that will come will make the data or predicted data more meaningful, more useful, more readily accessible, and a lot cheaper to get. I think this is true for the kind of data we have been talking about. It is true for the impedance measurement that we have also talked about earlier in the Symposium. I think we have to get away from the traditional approach and analyze, predict, and present our data in a more general and useful form."

Mr. Risse: "We have been all over the map here this afternoon. I am sure that we did not even dent a number of the aspects of these topics. One that distressed me a little was that we categorized specifications and we categorized designers pretty narrowly. In general, I do not see too much disagreement among us other than in detail and a matter of where particular techniques will work effectively and where they won't. I do take issue with Dr. Franken just a little in that if, for example, you broaden a set of impedance data, or smear it out, you can legislate yourself out of a solution of any kind."

Mr. Brust: "We dynamicists have a real obligation in terms of the cost effectiveness that our good friend Mr. McNamara is trying to achieve in this administration. The way we can do this is by knowing what type of specifications we have and by knowing what a specification really is. We have kicked around and narrowed down what a specification really looks like to the legal mind and what it looks like to the engineer's mind. The engineer develops the specification, knows the amount of safety factor he has developed in this spec. He knows what can happen to that specification when it is being used to beat a piece of hardware to death in the laboratory. If he is not there to recommend or make changes and add the information that he picks up during the early phases of a program and during the flight test phase, it costs a lot more. He must try to modify the requirements and to work with the customer. We find many times that we are expending literally thousands of dollars on programs, redesigning and retesting and again redesigning hardware to a specification that was originated much earlier with a good deal of conservatism. At that time conservatism was necessary because of the lack of information available. Unless we can make this

a team effort involving the customer, the contractor, the subcontractor, and others who want to operate on the specification, our military programs will continue to cost as they are costing. I think here is an area where we here can do a great deal to try to cut this down. Believe me, it is not an easy job to walk into a chief engineer's office and tell him that the spec we have is wrong; it is too high. Stop the heresy, so to speak, that is going on down in the laboratory. This is our problem, and people like ourselves have to continue to find a way that we can legally change specifications when we know that they must be changed. When you run a flight test and find that the rms g during a post-launch phase of a missile is only 0.5 g, and you are testing it in the laboratory to 10 g, something is wrong and you should continue to try to do something about it."

Dr. Fischer: "I would like to try to emphasize the positive a little bit. I think, generally speaking, that failures are due to things that could have been avoided. I will not call them blunders, and I will admit there is a lot of hindsight in saying a thing like that, but generally speaking, the failures are not due to a new phenomenon. In other words, the designer does need help and I think specifications are a big help. Perhaps they do not hit the mark exactly, but at least they point up the need for an analysis. It is amazing to me how often things are designed without an analysis. Similarly, a spec will point up the need for a test. It is amazing to me how a simple test like dropping something on the floor would have indicated an obvious point of weakness. Thirdly, I think when we do get around to helping the designer, there is a very simple measuring rod for telling whether you are doing any good or not. If you are helping him to the extent that you are assuming responsibility for the design, I think you can feel assured that you are doing some good. If you are just giving some advice, it can go in one ear and out the other. We have to assume responsibility in our approach to design problems."

* * *